

University of Southampton Research Repository ePrints Soton

Copyright © and Moral Rights for this thesis are retained by the author and/or other copyright owners. A copy can be downloaded for personal non-commercial research or study, without prior permission or charge. This thesis cannot be reproduced or quoted extensively from without first obtaining permission in writing from the copyright holder/s. The content must not be changed in any way or sold commercially in any format or medium without the formal permission of the copyright holders.

When referring to this work, full bibliographic details including the author, title, awarding institution and date of the thesis must be given e.g.

AUTHOR (year of submission) "Full thesis title", University of Southampton, name of the University School or Department, PhD Thesis, pagination

UNIVERSITY OF SOUTHAMPTON

Gamma Ray Astronomy in the Low Energy Range

By

E.P.A. Bailey

A thesis submitted for the degree of Doctor of Philosophy

Department of Physics
January 1979

CONTENTS

Abstract

Chapter 1	Introduction	1
1.1	Gamma Ray Astronomy	1
1.2	The Astrophysical Significance of Gamma Ray Astronomy	2
1.3	Mechanisms for Gamma Ray Production	4
1.3.1	Thermal Radiation Field	5
1.3.2	Inverse Compton Effect	6
1.3.3	Magnetobremstrahlung	6
1.3.4	Bremstrahlung	8
1.4	Astrophysical Sources of Gamma Rays	8
1.5	A Selection of the Observations of Known Gamma Ray Sources	9
1.5.1	Solar Observations	10
1.5.2	Supernovae and Supernova Remnants	11
1.5.3	Cygnus X-1	13
1.5.4	Cygnus X-2	14
1.5.5	Seyfert Galaxies	14
1.5.6	Centaurus A	16
1.5.7	Galactic Centre	17
1.5.8	The Diffuse Gamma Ray Flux	18
1.6	Gamma Ray Bursts	19
1.7	The Design of Gamma Ray Astronomy Experiments	23
1.8	The Objectives of the LEG 4 Experiment	25
Chapter 2	Techniques of Low Energy Gamma Ray Astronomy	27
2.1	Detector Design Considerations	27
2.2	Passive Collimation	28
2.3	Active Collimation	30
2.4	Anticollimation	32
2.5	Double Compton Telescopes	33
2.6	High Energy Resolution Detectors	35
2.7	Comparison of Different Detector Configurations	37

Chapter 3	Description of the LEG 4 Payload	41
	3.1 Description of the LEG 4 Experiment	41
	3.2 The Steering System	45
	3.3 In Flight Calibration of the Detectors	47
	3.4 Low Temperatures	47
	3.5 The Flight of LEG 4 and General Features of the Preliminary Data Analysis	48
Chapter 4	The Atmospheric Background and Gamma Ray Bursts	52
	4.1 The Conversion of Energy Loss Spectra to Photon Spectra	52
	4.2 Energy Loss Conversion Factors for the LEG 4 Experiment	59
	4.3 The Atmospheric Transition Curves	60
	4.4 The Atmospheric Gamma Ray Background	68
	4.5 The Search for a Gamma Ray Burst in the LEG 4 Data	74
Chapter 5	Analysis for Gamma Rays from the Crab Nebula Region	84
	5.1 The Method of Analysis for the Total Flux	84
	5.2 The Results of the Observations of the Crab Nebula by LEG 4	84
	5.3 The Method of Pulsar Phase Analysis	85
	5.4 The Results of the LEG 4 Observations of the Pulsar NP0532	89
Chapter 6	Discussion of the Results of the LEG 4 Experiment	95
	6.1 The Total Emission from the Crab Nebula	95
	6.2 Time Variability of the Crab Nebula	99
	6.3 Systematic Errors	102
	6.4 Source Confusion	106
	6.5 A Gamma Ray Burst	108
	6.6 The Pulsed Emission from the Crab Nebula Pulsar NP0532	108
	6.7 Theoretical Considerations	110

Chapter 7	The Milan-Southampton (MISO) Low Energy Gamma Ray Telescope	116
7.1	Introduction	116
7.2	The Basic Detector Design and Objectives	116
7.2.1	The Objectives	116
7.2.2	The Design	118
7.3	The Initial Assumptions of the Efficiency Program	121
7.4	General Outline of the Method of Solution	121
7.5	Optimisation of the Detector Design	127
7.6	Sources of Background	139
7.6.1	Atmospheric Gamma Ray Induced Background	139
7.6.2	Neutron Induced Background	140
7.6.3	Spallation	144
7.7	Preliminary Results of the MISO detector	144
Chapter 8	The Future of Gamma Ray Astronomy	149
8.1	Future Detectors	149
8.2	Gamma Ray Sources of Interest	156
8.3	An Anticollimated Double Compton Telescope	158
8.4	Summary	163
Appendix 1	The Thin Disc Approximation	165
References		173
Acknowledgements		188

UNIVERSITY OF SOUTHAMPTON

ABSTRACT

FACULTY OF SCIENCE

PHYSICS

DOCTOR OF PHILOSOPHY

GAMMA RAY ASTRONOMY IN THE LOW ENERGY RANGE

By Edward Peter Alexander Bailey

A low energy gamma ray telescope, and the results of its observations are described. The telescope consisted of four sodium iodide crystals, each of 120 cm^2 area, occulted by lead discs. Charged particles are rejected using scintillation, anti-coincidence shields.

The telescope was flown from Palestine, Texas in 1974. Gamma rays were observed from the Crab Nebula, the pulsar NPO532, and the atmospheric background. No evidence for a gamma ray burst was found, giving an upper limit of less than 5.8×10^3 bursts per year of intensity greater than $1.6 \times 10^{-6} \text{ ergs cm}^{-2}$.

Various types of existing, and planned, gamma ray detectors, and successful gamma ray observations are reviewed. Detailed calculations of the detection efficiency of a Double Compton telescope are presented and these results led to the development of the MISO low energy gamma ray telescope.

Preliminary calculations of the detection efficiency of an Anticollimated Double Compton telescope are presented, which suggest that further, more detailed investigation of this type of detector would prove fruitful.

Chapter 1 - Introduction

1.1 Gamma Ray Astronomy

The entire range of the cosmic gamma ray energy spectrum spans approximately sixteen orders of magnitude of energy from $\sim 10^5$ eV to 10^{21} eV. The development of experimental detection techniques in the range $\sim 10^5$ eV to 10^7 eV, a region where gamma ray lines are expected, is discussed in this thesis.

While this region offers considerable interest in astrophysical terms, as is discussed in the next section, it is in addition one which presents many experimental problems. The penetrability of matter by gamma rays enables examination of the earliest epochs of the Universe, yet it is this penetrability which causes problems in reducing unwanted background radiation from source measurements.

Advances in detector design have recently begun to fulfil the potential of gamma ray astronomy to be a powerful new tool for investigating the Universe.

The astrophysical implications of measurements in Gamma Ray Astronomy are discussed in the next section.

1.2 The Astrophysical Significance of Gamma Ray Astronomy

Gamma rays give an indication of the interactions which take place at a wide variety of astrophysical sites. For example, the interactions of electrons with fields (synchrotron), matter (bremsstrahlung), or radiation (inverse Compton effect), and gamma ray lines emitted by atomic nuclei. Observations of line emission in the celestial gamma ray spectrum, while still relatively scarce, have great potential to open a new, revealing window to the universe, as pointed out by Lingenfelter and Ramaty (1978). The future extension of our knowledge through celestial nuclear-line spectroscopy may match, or even surpass that already obtained by using atomic and molecular line emissions. This is because the greater penetrability of nuclear lines implies that they can be observed from

processes and regions from which other types can not.

Historically, although gamma ray lines from celestial sources were predicted by Morrison as early as 1958, the first discovery of cosmic X-rays came in 1962 (Giacconi et al.). In retrospect, Morrison (1966, 1967) reviewed the arguments as to why X-ray sources might have been expected to be more intense than gamma ray sources. The generally accepted reasoning is that all conceivable sources give rise to a differential intensity spectrum falling off strongly with increasing photon energy, resulting in the stronger X-ray fluxes being more easily detectable.

Currently, X-ray astronomy is providing an abundance of important results, possibly the most significant of which is the tentative evidence afforded by X-rays for the existence of black holes. One widely favoured candidate for a black hole is Cygnus X-1. The strongest argument in favour of it being a black hole is that Cygnus X-1 is a compact object and has a mass larger than that allowed for a neutron star or white dwarf. Evidence for the former feature is associated with the observation of very rapid time variability in X-rays, while evidence for the latter has been provided by a combination of various types of observations of the Cyg X-1 star system.

Eardley et al. (1978) have outlined the controversial arguments for and against the adoption of Cyg X-1 as a black hole.

While X-ray astronomy has flourished in terms of observational results in recent years, the development of gamma ray astronomy as a tool for probing the universe, has been greatly restricted by three main problems: high instrument background, extremely low fluxes, and the lack of a gamma ray telescope with good directionality, energy resolution and efficiency in the energy region 50 keV to 10 MeV.

Nevertheless, interest in gamma ray astronomy continues because gamma rays figure prominently in the predictions of many astrophysical theories, including those involving the quantum-mechanical decay of small, primordial black holes (Page and Hawking, 1976).

Grindlay (1978) and Schönfelder (1978) suggest that Seyfert galaxies may be responsible for the bump at MeV energies, if not the total diffuse cosmic gamma ray spectrum above 1 MeV. Seyfert galaxies are discussed more fully in sections 7.7 and 8.2.

The importance of a continued study of low energy gamma ray astronomy has been highlighted by the discovery by SAS-2 (Thompson et al., 1974 and

1977, Kniffen et al., 1975) and CoS-B (Bennett et al., 1977, Hermsen et al., 1977 and Masnou et al., 1977) of high energy ($E_\gamma > 30$ MeV) gamma ray sources. A number of the sources observed by CoS-B and SAS-2 have not yet been identified with low energy gamma ray or X-ray sources. It is of interest astrophysically to know whether these sources are really emitting at low energies, or whether they have a cut off at lower energies.

Bignami et al. (1978) have discussed the contribution of discrete sources to the galactic gamma ray emission on the basis of the recent observations of gamma ray sources by the CoS-B satellite. They show that, if the sources are uniformly distributed throughout the galaxy, they can account for at least 40% of the galactic gamma ray luminosity. Alternatively, the whole galactic luminosity can be due to discrete sources if their density within 5 Kpc of the galactic centre is substantially higher than in the outer regions of the galaxy.

By contrast to the higher energy CoS-B and SAS-2 sources, BL Lac objects have been observed up to 60 keV (Mushotsky et al., 1978), but not so far at higher energies extending up to low energy gamma rays. Again, it is a matter of astrophysical significance to determine whether or not these objects have a cut off in emission in X-rays, or whether they do emit in low energy gamma rays. BL-Lac objects are discussed more fully in section 8.2.

The discrete energies of gamma ray lines can identify specific nuclear processes at work in the cosmos. In addition, the width and possible frequency shift of gamma ray lines contains unique information on the emission site. For example, the conditions prevalent at neutron-star surfaces and black holes may be examined by measuring the gravitational red shift of gamma ray lines. More specifically, the following astrophysical subjects can be directly investigated using gamma ray astronomy (Chupp, 1975):

1. The site of nucleosynthesis.
2. The location of any discrete sources of cosmic rays.
3. The nature of exotic sources such as QSO's and Radio Galaxies.
4. The conditions in the Universe at an early cosmological epoch.
5. The possible existence of antimatter in the Universe.
6. The properties of the solar flare particle accelerating mechanism.
7. The nature of Gamma Ray Bursts.

Nearer to Earth, gamma ray line measurements have already shown their usefulness in lunar and solar observations. Spectrometers on Apollo lunar orbiters (Metzger et al.,1974) have provided global surveys of the moon's surface composition and demonstrated regions of anomalous enrichment of iron, radioactive potassium, thorium and uranium. The OSO-7 satellite carried detectors (Chupp,1973) which observed gamma ray line emission during the solar flares of 4 and 7 August 1972. For the first time it has been possible, using the intensities of these lines, to derive information on the acceleration time, energy spectrum and total number of energetic nuclei in the flare regions. The lines at 0.5, 2.2, 4.4 and 6.1 MeV are attributed to positron annihilation, neutron capture on hydrogen and de-excitation of excited states in C^{12} and O^{16} all resulting from nuclear reactions of flare-accelerated particles in the solar atmosphere. These results have provided new restrictions on models of the acceleration and escape of energetic particles in solar flares, as well as on the flare process in general (Ramaty et al.,1975).

High energy celestial gamma rays (over 30 MeV) which are attributed to neutral-pion decay, have figured in observations which have also placed important new constraints on the distribution of cosmic rays in the Galaxy (Fichtel et al.,1975).

One of the most recent comprehensive reviews of the general fields of X-ray and Gamma Ray astronomy has been given by Greisen (1971) and this gives a broad perspective of the astrophysical questions. Harwit (1973) and Chupp (1976) have produced books which are useful references at the advanced introductory level. Stecker (1975) and Fichtel (1977) have reviewed the recent experimental and theoretical work relating to Gamma Ray Astrophysics in general.

Having outlined the Astrophysical significance of Gamma Ray Astronomy, we need next to consider the emission mechanisms giving rise to the observed gamma rays, as in the next section.

1.3 Mechanisms for Gamma Ray Production

This section summarises the known gamma ray production mechanisms. For each mechanism, the relationship between the nature of the source

and any gamma rays that might be detected at the earth is discussed.

More detailed descriptions of the mechanisms can be found in the work of Heitler (1954), Fazio (1967), Lüst and Pinkau (1967), Boldt (1969), Ginzburg (1969), Stecker (1971), Greisen (1971), Ginzberg and Syrovatskii (1964), Ginzberg (1967), Shklovsky (1960) and Chupp (1976).

The majority of the production mechanisms of low energy gamma rays involve the interaction of electrons with radiation (inverse Compton effect) with fields (synchrotron), and matter (bremsstrahlung). In addition gamma rays emitted by atomic nuclei give gamma ray lines of characteristic energies.

1.3.1 Thermal Radiation Field

When an astrophysical object is sufficiently hot and has the characteristics of a black body (i.e. an optically thick source), then gamma rays may be emitted. The unshifted thermal photon number spectrum for a black body source is given by the Planck formula to be

$$\underline{N(E_\gamma)} = 9.9 \times 10^{40} \frac{E_\gamma^2}{\text{MeV}^2} \left\{ \exp(1.2 \times 10^{10} E_\gamma/T) - 1 \right\}^{-1}$$

(photons $\text{cm}^{-2} \text{s}^{-1} \text{MeV}^{-1}$)

where $N(E_\gamma)$ is the number of photons emitted from a unit area of a black body per second at temperature $T(\text{K})$, and E_γ is in MeV. The position of the maximum is given by Wien's law as $E_{\text{max}} (\text{MeV}) = 4.7 \times 10^{-10} T(\text{K})$. The average photon energy $E(\text{MeV}) = 2.3 \times 10^{-10} T(\text{K})$.

The temperature range required for gamma ray energy photons due to this mechanism is $10^8 \text{ K} < T < 10^{10} \text{ K}$. At the lower extreme, solar flares temperatures as high as this have been suggested to explain some hard X-ray bursts (Chubb et al., 1966), and at the upper extreme, such high temperatures are appropriate to the early history of a big bang Universe or to temperatures occurring in explosive cosmic sources. In the present epoch, a cosmological black body radiation spectrum would be strongly modified by the red shift.

1.3.2 Inverse Compton Effect

The scattering of a highly relativistic electron from a photon can raise the energy of the photon. If an electron spectrum in the form of a power law of index $-a$, interacts with a black body radiation field, then the spatial index of the resultant scattered photons is β , where $\beta = \frac{a+1}{2}$.

Electrons of energy $E = \gamma m_0 c^2$, scattering photons of energy E_0 , will on average, produce a scattered photon of energy

$$E_\gamma = \frac{4}{3} E_0 \gamma^2 \quad \text{for } E_0 \ll m_0 c^2$$

$$\text{or } E_\gamma \sim \gamma m_0 c^2 \sim E \quad \text{for } \gamma E_0 \gg m_0 c^2$$

where $\gamma = (1 - \frac{v^2}{c^2})^{-\frac{1}{2}}$, $m_0 c^2$ is the electron's rest energy, and v is the electron's velocity. Inverse Compton effects are thought to be responsible for the hard X-ray and low energy gamma ray flux of NGC4151 (Manchanda et al., 1978).

1.3.3. Magnetobremstrahlung

The Lorentz force ($\underline{F} = q(\underline{v} \times \underline{B})$) due to a magnetic field, accelerates a charged particle causing it to spiral around the magnetic field direction. According to classical theory, the electron must radiate electromagnetic energy, producing what is known as synchrotron radiation. Shklovsky (1970) has used this mechanism to explain the emission of the Crab Pulsar. This process has also been used to explain the emissions of the Crab Nebula at radio, optical and X-ray wavelengths (Cowsik et al., 1970), and the radio emission from Jupiter. For the situation when the pitch angle of an electron with respect to a magnetic field is zero, so that the electron's motion is along the field line, gamma radiation can be produced if the field line is curved (Sturrock, 1971). This is called curvature radiation, and has been used to predict the gamma ray spectrum from a neutron star in the form of a pulsar. For the case of curvature radiation from protons, which seems to be applicable to the

Crab Nebula, Sturrock (1971) gives the energy of the gamma rays produced in the proton zone as

$$E_{\gamma p \eta} = 10^{-87.4} B^3 R^{17/2} T^{-13/2} \eta^{-1/2} \text{ (eV)}$$

where the radius where the emission occurs is given by ηR . R is the neutron star radius, T is the pulsar period in seconds, and B is the surface dipole magnetic field. The quantity η is greater than one but is limited by the velocity of light radius. Using values for the Crab Nebula of $T = 10^{-1.5} \text{ s}$, $R = 10^6 \text{ cm}$ and $B = 10^{12} \text{ G}$, the expression shows that energies as high as 10^9 eV can be produced by this process.

For synchrotron radiation the characteristic frequency emitted by a single electron above which the emitted radiation is negligible is given by

$$\nu_s = \frac{3e}{4\pi m_0 c^2} \gamma^2 B_p \text{ (Hz)} \quad \text{(Ginzburg, 1969)}$$

where $\gamma = \frac{E}{m_0 c^2}$ is the Lorentz factor for the electron, B_p is the magnetic field (in G) normal to the electron's motion and the other quantities are standard notation. The frequency distribution of the emitted radiation is a discrete asymmetric distribution with a maximum of the envelope at $\nu_m \sim 0.29 \nu_s$. Thus the energy of the photon at the maximum of the distribution is $E_{\gamma \text{ max}} \simeq 5 \times 10^{-15} \gamma^2 B_p \text{ (MeV)}$. It can be seen that very energetic electrons or strong magnetic fields are needed to produce gamma ray photons in the MeV energy range.

It has been shown by Ginzburg (1969) that if the electron input spectrum is of the form $N(E) = K_e E^{-a} dE$ (electrons cm^{-3}), then the photon spectrum is of the form

$$\frac{dN}{dE_{\gamma}} = 3.27 \times 10^{-2} a(a) \text{ KeV} \frac{B}{R^2}^{(a+1)/2} \left\{ \frac{2.59 \times 10^{-2}}{E \text{ MeV}} \right\}^{(a+1)/2}$$

(photons $\text{cm}^{-2} \text{ s}^{-1} \text{ MeV}^{-1}$)

where the photons are emitted from electrons trapped in a random magnetic field in a spherical region diameter L , and a volume V at a distance R from the observer.

It is of interest to note that the relationship between the electron

spectral index and the photon spectral index is the same as for the Inverse Compton Scattering. This is because the synchrotron process can be regarded as the interaction of an electron with the "virtual" photons of the magnetic field with energy density $\rho_H = \frac{B^2}{8\pi}$ (Jones, 1965; Boldt, 1969; and Stecker, 1974).

1.3.4 Bremsstrahlung

In this mechanism, when a charged particle interacts with matter, it is deflected by interactions with the Coulomb fields of the electrons and protons and the resulting acceleration gives rise to radiation. The photons emitted by this process can have a range of energies from zero up to the energy of the initial electrons.

Non-thermal bremsstrahlung is emitted with the same index as the electrons if the electrons have a power law spectrum. Bremsstrahlung by fast protons incident on electrons at rest has been considered as a possible source of gamma rays by Boldt (1969), Hayakawa (1970) and Brown (1970). However, Jones (1971) has extended the calculations and finds that proton bremsstrahlung is unlikely to make a significant contribution to the galactic cosmic gamma ray spectrum above ~ 5 MeV.

If a plasma is sufficiently hot, electromagnetic radiation can be emitted with energies as high as the X-ray and Gamma Ray region. When the emitting volume is optically thick, the spectrum is given by the Planck law, i.e.

$$I(E_\gamma) \propto E_\gamma^2 \left\{ \exp\left(\frac{E_\gamma}{kT}\right) - 1 \right\}^{-1}$$

If the source is optically thin then thermal bremsstrahlung transitions are possible among the electrons and ions of the plasma.

1.4 Astrophysical Sources of Gamma Rays

The main sites where gamma rays source mechanisms may operate are summarised in Table 1.2 (from Chupp, 1976).

Of recent interest are the Seyfert galaxies such as NGC4151 and BL

Table 1.2 Astrophysical sites where gamma ray source mechanisms may operate

Sun (solar activity or quasi-continuous production)

Cosmic (point or localised sources)

Supernovae and their remnants

Neutron stars - pulsars

Flare stars

Galactic core and disk

Radio sources - QSOs - black holes

Cosmic (diffuse sources)

Continuous spectrum

Cosmological π^0 and $H(n, \gamma)D$

Low energy cosmic rays in galaxy

Planetary Atmospheres

Lacertae objects such as MK501 and MK421 for the reasons mentioned in sections 1.2 and 8.2. The present observational status of the presently known low energy gamma ray sources is reviewed briefly in the next section. Possible low energy gamma ray sources that may be investigated in the future are described in "The future of gamma ray astronomy" in chapter 9.

Results which are related to observations discussed in later chapters, such as gamma rays from the Crab Nebula and its pulsar NP0532, and the Seyfert galaxy NGC4151, are not discussed in as much detail in the next section, as later.

1.5 A selection of the observations of known gamma ray sources

There is still a paucity of results in the low energy gamma ray

region, due to the experimental difficulties. However, the existing results point towards the increasing involvement of low energy gamma ray observations in theoretical astrophysics. The following sections discuss a representative selection of the low energy gamma ray observations of known sources. Where relevant, observations in other energy regions are included.

First, the discovery of spectral gamma ray lines in solar flares is discussed. Then supernovae and supernovae remnants, followed by the galactic sources, Cygnus X-1, the Seyfert galaxies and their possible relationship with the diffuse gamma ray background occupy the subsequent section. Sections 1.5.7 and 1.5.8 contain a summary of the observations of Centaurus A and the Galactic, in particular in relation to gamma ray lines. Lastly, the diffuse gamma ray flux and gamma ray bursts are discussed in sections 1.5.9 and section 1.6.

1.5.1 Solar Observations

Until 1970 there was no conclusive evidence for either solar neutron or gamma ray fluxes. There were, instead, at least three highly disputed claims of observations of both solar neutrons and gamma rays, all in times of relatively low solar activity. None of these "possible" events had occurred at the same time as the optical phase of any flare. The result of Apparao et al.(1966) was determined during very quiet solar conditions. The result of Daniel et al.(1967) was made several hours before a subflare. Daniel's result was questioned by Holt (1967), because no neutron decay protons had been seen by the OGO-A satellite which was in orbit at the same time. Daniel has answered this criticism (1971) by using a revised measurement of the atmospheric neutron flux. In the case of gamma rays, Kondo and Nagase (1969) reported an 800% increase in the gamma ray flux (3 to 10 MeV) 10 min after a 1N flare and associated radio burst.

Hirasima et al.(1969) reported a solar gamma ray increase coincident with 1000 MHz radio burst. More recently, evidence for a gamma ray burst on May 14, 1972 has been reported by Koga et al.(1974), but it did not occur in coincidence with any major solar event nor with the cosmic gamma ray burst on the same date (Strong et al.,1974).

Future satellite experiments may determine whether these events

are truly of solar origin. The current evidence for gamma rays associated with solar flares was obtained during the August 4th and 7th events of 1972 with the OSO-7 satellite (Chupp et al., 1973, 1974). Line emission at 0.51, 2.2, 4.4 and 6.2 MeV and continuum emission extending up to about 7 MeV were reported. In the August 4th event, the 0.51, 2.2, 4.4 and 6.2 MeV lines were of strengths 6.3×10^{-2} , 2.8×10^{-1} , 3×10^{-2} , and 3×10^{-2} photons $\text{cm}^{-2} \text{s}^{-1}$ at 1 AU, respectively. The strengths in the August 7th event were approximately a factor of 2 lower.

These lines are due to positron annihilation, neutron capture by protons and de-excitation of excited States of C and O (e.g., Ramaty, Kozlovsky, and Lingenfelter, 1975). Electron Bremsstrahlung could account for a large part of the continuum, at least up to energies of several MeV (Suri et al., 1975). A more recent theoretical treatment is that of Ramaty, Kozlovsky and Suri (1977).

Ramaty et al. (1975) have reviewed in detail the expected fluxes of gamma rays for different parent solar cosmic ray spectral shapes. However, these calculations assume that all nuclear phenomena in the solar atmosphere arise from non-thermal nuclear reactions and that the thermonuclear processes in flares are of no significance. Despite this, Chupp (1976) has pointed out that our experimental knowledge is sufficiently limited that some role for the thermonuclear reactions, such as ${}^2\text{H}(d,n){}^3\text{He}$, cannot be ruled out.

1.5.2 Supernovae and Supernova Remnants

Any successful measurements of gamma ray line fluxes from supernova remnants are important because they could provide direct verification of theories of nucleosynthesis (Chupp, 1976).

Haymes et al. (1968) made a search for nuclear lines below 1.5 MeV from the Crab Nebula using a large area NaI spectrometer in an active collimator, but only upper limit fluxes for the predicted lines were obtained. Jacobson (1968) made the first observation of the Crab Nebula using a high resolution solid-state gamma ray spectrometer. The detector was essentially a 4.6 cm^3 cooled Ge(Li) spectrometer in an active CsI(Tl)

anticoincidence shield, also acting as a collimator with an opening angle of $0.775 S_r$ (9° half-angle), and was effective for gamma rays less than 300 keV. This experiment gave tentative evidence for a line at 224 keV, however, Jacobson (1968) has pointed out that this might be due to local neutron background activation in the Ge(Li) spectrometer. Other more recent measurements on the Crab Nebula in the low energy gamma ray region are discussed more fully in later chapters.

The OSO-7 experiment of Chupp et al. (1974 b) has searched for gamma rays from a supernova remnant associated with the pulsar 0833-45, known as the Gum Nebula. Gamma ray lines are expected at several energies from this remnant, for example ^{28}Si (1.78 MeV), ^{12}C (4.43 MeV), and ^{16}O (6.13 MeV). No evidence for lines has yet been found.

Leventhal et al. (1977) conducted a search of Nova Cygni 1975, and Nova Serpentis 1970 for gamma ray lines. They used a balloon borne telescope with a large-volume lithium-drifted germanium detector as the central element, covering the energy range 100 keV to 5 MeV. No lines were detected from the novae, even though their experiment had a sensitivity relevant to current theories of explosive nucleosynthesis, and an energy resolution better than 5 keV.

To calculate the flux predicted due to Nova Cygni 1975, Leventhal et al. used the calculations of Truran (1975), which predicted that the flux at the earth in the 1275 keV ^{22}Na line produced by a nova event would be

$$\phi = \frac{8 \times 10^{-3} \exp(-t/3.8)}{R^2} \text{ photons cm}^{-2} \text{ s}^{-1}$$

where R is the distance to the nova in kiloparsecs and t is the time since the nova in years. They then took the distance to Nova Cygni 1975 to be 1.5 Kpc (Gallagher and Ney, 1976) to predict a flux in 1976 May, of 3×10^{-3} photons $\text{cm}^{-2} \text{ s}^{-1}$. This compared with their 2σ upper limit of only 1×10^{-3} photons $\text{cm}^{-2} \text{ s}^{-1}$. A similar calculation for Nova Serpentis yielded a predicted flux of 2×10^{-3} photons $\text{cm}^{-2} \text{ s}^{-1}$, compared with their experimental upper limit of 1.1×10^{-3} photons $\text{cm}^{-2} \text{ s}^{-1}$.

These results provide significant constraint on the theoretical parameters. As mentioned by Leventhal et al., the formula quoted has a multiplicative coefficient which is proportional to the product of two poorly known factors. One is the total mass ejected from the star in the nova explosion, and measurements on this for Nova Cygni are

provided by Gallagher and Ney (1976). The second is the enhancement of mass-22 nuclei in the ejected material relative to solar system abundance, and is calculated using theoretical hydrodynamic modelling of nova explosions. More recent hydrodynamic modelling of nova explosions (Starrfield, 1976) has produced numerical factors which are more consistent with the results of Leventhal et al.

The OSO-7 satellite (Chupp et al., 1974 b) was in operation when the Type I Supernova was discovered on 1972, May 13, in NGC 253, with a magnitude of 8.5 (Kowal, 1972) - although the time of its maximum magnitude may have been May 6th or earlier (I AU circular 2421). A Type I Sn had also occurred previously in 1895 in the irregular dwarf galaxy NGC 5253 (Sargent et al. 1974). The distance to NGC 5253 is of the order 3.5 Mpc (Sersic et al., 1972), and consequently Chupp (1976) has remarked that gamma ray lines could be predicted from this supernova at about 1/6th of the intensity predicted by Clayton et al. (1965) for the Crab Nebula. Nevertheless, a search for lines at 0.51 MeV, the ^{56}Co line at 0.847 MeV, and at 2.2 MeV before and after the optical maximum, has so far found no evidence for them. Because Clayton et al. (1969) have suggested that there might be significant Compton broadening of the spectral lines, Chupp et al. (1974 b) also searched their OSO-7 data for an enhanced continuum over the range 350 keV to 1 MeV. They used as a reference, the previous X-ray flux limits set by Ulmer et al. (1974) and by Canizares et al. (1974). However, no such enhancement was found.

1.5.3 Cygnus X-1

Cygnus X-1 is part of a close binary system with the star HDE 226868. The expected 5.6 day period has been found in X-rays by Holt et al. (1976) Cygnus X-1 is a source of great interest because evidence exists which leads to the controversial suggestion that it is a black hole. The controversial arguments for and against it being a black hole are discussed by Eardley et al. (1978). Among them it may be briefly mentioned that the mass of the secondary is supposed to be too great for a white dwarf or neutron star (Bolton, 1972), and that the rapid time variations observed suggest a very compact object.

Thorne and Price (1975) and Oda (1977) have produced models for the

X-ray emission in terms of an accretion disc.

Cygnus X-1 exhibits variability from milliseconds (Rothschild et al., 1974) to months (Parsignault et al., 1975). Cygnus X-1 has been observed in low energy gamma rays by Baker et al. (1973), but Mandrou et al. (1977) only obtained upper limits below the flux measurements of Baker et al. These observations might be at variance, although they could be reconciled by regarding Cygnus X-1 as variable, having a "low" state and a "high" state. Alternatively, the higher flux of Baker et al. may be, in fact, due to the presence of Cygnus X-3 in the field of view. The photon spectrum of Cygnus X-1 is shown in diagram 1.1.

1.5.4 Cygnus X-2

Ariel 5 shows evidence for an 11.17 day period (Holt et al., 1976) and large variations in spectra have been found in the 10 - 100 keV range by Ulmer et al. (1974) in this source.

Dean et al. (1973) found a definite flux from Cygnus X-2 for energies greater than 0.8 MeV, but, by contrast, Lovett et al. (1973) place upper limits at lower levels in the 1-10 MeV range.

1.5.5 Seyfert Galaxies

The Seyfert galaxy NGC 4151 has been observed in hard X-rays by Baity et al. (1975) using OSO-7, Auriemma et al. (1978), and Paciesas et al. (1977). The original detection of X-ray emission from NGC 4151 (Gursky et al., 1971) raised many questions concerning the connection between the Seyfert phenomenon and X-ray emission. In order to answer some of these questions, Tananbaum et al. (1978) have analysed the Uhuru data, and, interestingly, have found significant flaring activity from NGC 4151 with as much as a factor of 10 increase in intensity on a time scale possibly as short as 730 seconds. This variability suggests a compact object. Observations of Seyfert galaxies are important in relation to determining their contribution to the diffuse X and gamma ray background (Tananbaum et al., 1978 and Schönfelder, 1978).

Photons $\text{cm}^{-2} \text{s}^{-1} \text{Mev}^{-1}$

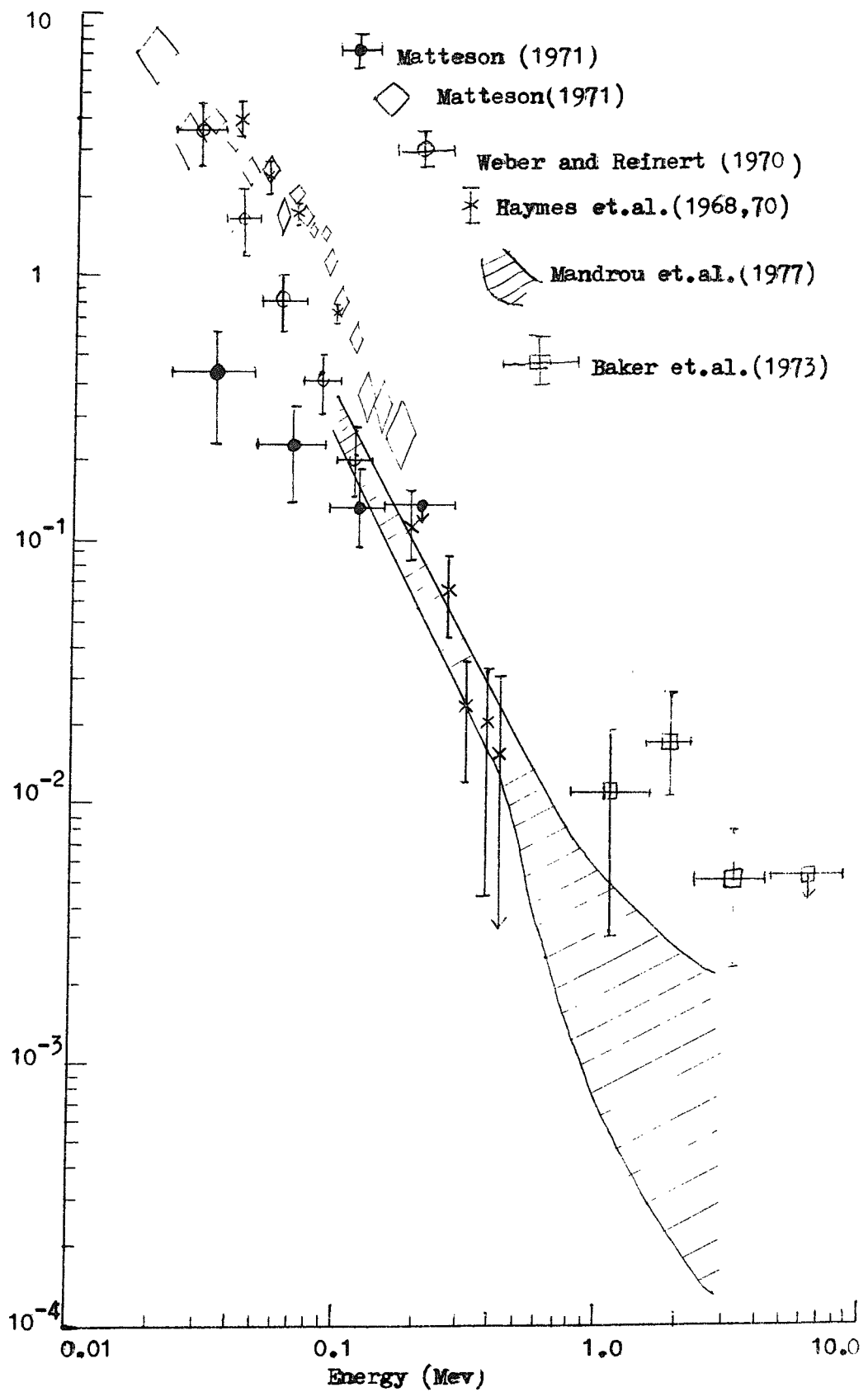


Diagram 1.1 The photon spectrum of Cygnus X-1
(From Martin , 1978)

NGC 4151 has been observed in the low energy gamma ray region by the Southampton-Milan telescope described in a later chapter (Di Cocco et al., 1977) and by Schönfelder (1978). Schönfelder suggests that galaxies of the same type as NGC 4151 could explain at least the bump at MeV energies, if not the total diffuse cosmic gamma ray spectrum above 1 MeV. Grindlay (1978) is in agreement with Schönfelder that the diffuse background spectrum at hard X-ray and gamma ray energies can be accounted for by Seyfert galaxies.

The COS-B observations of NGC 4151 should be evaluated in the near future, enabling a more precise evaluation of the spectral index above 3 MeV.

Elvis et al. (1978) report the X-ray observations of 13 Seyfert galaxies detected by the Ariel V satellite and they discuss the inverse Compton process in Seyfert galaxies.

1.5.6 Centaurus A

Hall et al. (1975) have claimed the first detection of gamma ray spectral lines from an extragalactic source, the radiogalaxy Centaurus A and its optical counterpart NGC 5128. The lines are at energies 1.6 MeV and 4.5 MeV, and have strengths $(3.4 \pm 1.0 \times 10^{-3})$ and $(9.9 \pm 3.0) \times 10^{-4}$ photons $\text{cm}^{-2} \text{s}^{-1}$ respectively. These lines are presumed to be due either to low energy cosmic rays interacting with the interstellar medium of NGC 5128, or to nucleosynthesis in the galaxy itself.

Although the lines were detected in the April 1974 measurements, they were not detected in previous measurements in 1968. This discrepancy has been suggested to be evidence for variability, consistent with the variability observed in microwaves by Kellerman (1974) and in X-rays by Davison et al. (1975) and Winckler and White (1975).

Hall et al. (1975) suggest that the 4.5 MeV line is due to de-excitation radiation of carbon-12. However, three different models have been proposed for the 1.6 MeV line. The 1.6 MeV line is fairly broad (22% FWHM), however, Hall et al. point out that an intrinsically unbroadened line cannot be ruled out because the energy resolution of their experiment was only 11% at this energy. One possibility is that it is a single line which may be Doppler broadened. This suggests that the observed line is due to de-excitation radiation from Ne^{20} . The 22%

width suggests that the neon nuclei would have characteristic energies 22 MeV/nucleon. They may therefore be classified as low energy cosmic rays. The interactions between the low energy cosmic ray nuclei and the particles comprising the interstellar medium in the source region would serve to excite the nuclei.

A second model proposes that the broadening is the result of the blending of several narrow gamma ray lines from 10 MeV/n cosmic ray nuclei and from excited interstellar nuclei. Lines of energies 1.37 MeV, 1.63 MeV and 1.78 MeV can be produced by the nuclides Mg^{24} , Ne^{20} , and Si^{28} respectively. All three are relatively abundant in cosmic rays as observed at the earth. Unlike the Galactic Centre observations of Haymes et al. (1975), however, no 511 keV line was detected from Cen A by Hall et al. (Their 2σ upper limit to a 511 keV line was 8.4×10^{-4} photons $cm^{-2} sec^{-1}$). Since positrons are expected on the basis of a cosmic ray origin from the nuclear gamma rays, through pion decay and radioisotope formation, this makes the cosmic ray origin doubtful.

A third possibility is that the lines are due to excited nuclei being synthesised in the source. Variability may be associated with explosive events within the galaxy.

Hall et al. also detected the continuum emission from Cen A and found that a good fit to the spectrum was $(0.86 \pm 0.17)E^{-1.9 \pm 0.04}$ photons $cm^{-2} s^{-1} keV$.

Centaurus A is the closest radiogalaxy. The intense emissions of radio, optical, and X-ray energy from Cen A and the optical galaxy NGC 5128 that it surrounds, attest to the high density of energetic electrons in the source. The presence of these electrons suggests the presence of a large flux of energetic nuclei. Excited nuclei radiate gamma ray spectral lines in the energy interval extending from X-rays to ~ 10 MeV. Detection of nuclear gamma rays gives unique information on the existence, composition and intensity of high energy nuclei in the galaxy.

Because the models of the emission of Cen A depend on the line widths and the extent of any variability observed, this source merits further experimental investigation, particularly with the use of high energy resolution solid state detectors.

1.5.7 Galactic Centre

A line at 500 keV from the direction of the Galactic Centre was

reported by Johnson et al. (1972) and Johnson and Haymes (1973). However, a more recent measurement (Haymes et al., 1975) places this line at 530 ± 11 keV, and in addition presents evidence for a gamma ray line at 4.6 ± 0.1 MeV, also from the Galactic Centre. The 4.6 MeV line is attributed to excitation of the first excited state of ^{12}C at 4.43 MeV. The line at around 500 keV, is still rather controversial as regards its physical origins.

Fishman and Clayton (1972) have interpreted the line as being caused by the decay of an excited state of ^7Li at 478 keV, while Kozlovsky and Ramaty (1974) have proposed a mechanism for the 478 ^7Li line involving $\alpha - \alpha$ reactions. Yet another production process proposed is that of 0.51 MeV photons being gravitationally red-shifted as they leave neutron stars (Guthrie and Tadamaru, 1973). Finally Leventhal (1973 a) has put forward an explanation for the line involving a combination of positron annihilation in the interstellar medium at 0.51 MeV, and the instrument resolution of 15% of the Rice experiments, being folded together with the net result of a shift of the 0.51 MeV peak close to the 480 keV line indicated by the experiment.

1.5.8 The Diffuse Gamma Ray Flux

Measurements of the spectral shape of the cosmic diffuse gamma ray energy distribution, in the energy region 1 to 30 MeV, have important theoretical implications for cosmology. Morrison (1958) suggested the mechanisms that would probably be most important for X and gamma ray production. The theories have more recently been reviewed by Silk (1970, 1973), Pal (1973), Stecker (1974) and Horstman et al. (1975).

Mechanisms for producing the continuous radiation include synchrotron radiation, electron bremsstrahlung, inverse Compton scattering of cosmic ray electrons by starlight and by the 2.7 K blackbody radiation, and decays of π^0 - mesons produced by cosmic ray interactions with matter and by matter-antimatter annihilations. More specifically, Stecker (1969) and Stecker, Morgan and Bredekamp (1971) have emphasised that gamma rays produced in early cosmological epochs would be highly redshifted and that this would produce a bump in the cosmic diffuse gamma ray energy distribution about 1 MeV. Rocchia et al. (1976) suggested that instead of a bump, a dip should be expected below about 1 MeV caused by gamma ray selective

absorption at the source.

Several authors (Golenetskii et al., 1971; Pal, 1973; Daniel and Lavakare, 1975; and Horstman et al., 1975) have emphasised the importance of observing the correct cosmic diffuse gamma ray energy flux undistorted by measurement. A major problem is that the cosmic diffuse radiation is considered to be isotropic in space and constant in time. Consequently it is not possible to use variations in direction or in time to isolate the gamma rays, as is possible from a directional source. The observer has to subtract every background, measured and calculated, to leave a remaining flux, unexplained in any other way, that is called the cosmic diffuse gamma ray flux.

Induced activity is one source of unwanted background. The delayed counts from induced activity in inorganic crystals such as NaI is a serious problem in the energy range 1 to 30 MeV (Dyer and Morfill, 1971; Dyer, Engel and Queenby, 1972; Fishman, 1972; Trombka et al. 1977). Spacecraft have a particular problem with induced activity due to bombardment by cosmic ray particles and protons trapped in the radiation belt. For this reason, the original measurements of Vette et al. (1970) and Trombka et al. (1973) obtained on Apollo 17 results are now limited to 1 - 10 MeV and have been lowered significantly (Trombka et al. 1977).

The recent results of White et al. (1977) and Schönfelder et al. (1977) have been achieved using versions of double Compton telescopes, which are particularly suited for such measurements. Unfortunately, balloon experiments need to use the atmospheric growth curves to calculate the contribution from the diffuse flux.

The main body of results are shown in a graph in a later chapter when the LEG experimental results are discussed.

Improvements can still be made to measurements in the low energy gamma ray region to enable more accurate restrictions in the theoretical parameters used in explaining the shape of the cosmic diffuse gamma ray spectrum.

1.6 Gamma Ray Bursts

The discovery of gamma ray bursts by Klebesadel, Strong and Olson (1973) heralded the start of a new impetus in X and gamma ray astronomy. Considerable efforts have since been made to understand the nature of these bursts, although, as yet, no final consensus of opinion exists

about the burst mechanism, as mentioned by Grindlay et al.(1978).

The events were originally called gamma ray bursts since the Vela satellite detectors used by Klebesadel et al.(1973) were sensitive in the range 0.2 - 1.5 MeV. However, Lewin (1977) points out that gamma ray bursts could equally well be called X-ray bursts, since a large portion of the energy in the bursts is emitted in the X-ray region below 100 keV (Klebesadel and Strong, 1976). For this reason, low energy gamma ray astronomy has a rather limited role to play in the science of gamma ray bursts. Despite this, future detectors may have a sensitivity to be able to search for possible gamma ray lines in burst spectra. Any such lines would have important consequences for burst emission mechanisms.

A significant advance in the study of gamma ray bursts, came when Grindlay et al.(1976) discovered bursts from a source in the globular cluster NGC6624 in December 1975. Previously, there had been no convincing temporal or spatial correlation of a burst with any known celestial processes or objects (Cline and Desai, 1976). Subsequently, in 1976, a further 19 X-ray burst sources were discovered, mostly by SAS-3 and OSO-8 (Lewin, 1977). The total number now known is in excess of 30, being strung along the galactic equator, with the majority of them located within about 35° of the galactic centre (Lewin, 1977). Two of them have been identified with sources in globular clusters (Grindlay et al., 1976; Liller et al.1977; Clark et al.1977; Forman et al. 1976; and Li et al.1977). Another three have a high probability of being associated with faint blue stars (McClintock,1977; Grindlay, 1978; Davidsen, 1975; Bond, 1977). Although a number of burst sources have been identified with sources of steady emission, no steady emission has been observed from at least two sources (Lewin,1977).

Typical features of bursts are:

Peak intensities $\sim 10^{-8}$ to $\sim 10^{-7}$ erg cm⁻² s⁻¹ ;

Rise times of less than a few seconds;

Durations of a few seconds to a few minutes;

Many burst sources produce bursts recurring at approximately regular intervals of from hours to days;

In most bursts, the lower energy flux persists longer than the higher energy flux.

As regards recurrence, the most regular burst intervals have been observed from MXB 1659-29, varying between 2.0 to 2.6 h during October 1976. Interestingly, MXB.1659-29, as well as being very "regular",

does not emit a detectable flux of "steady" X-rays (Lewin, 1976, 1977). By contrast, MXB 1837 + 05, (Swank, 1976; Li, 1976, 1977) and MXB 1735 - 44 (Lewin, 1977) are examples of highly irregular burst sources, with intervals varying from ~ 1 h to ~ 2 d. As pointed out by Lewin (1977), the limitations of present day experiments have a tendency to make it appear that most burst sources have intervals from hours to days. Future detectors may be able to determine whether this is a true state of affairs, or whether longer burst intervals (weeks, months, years) are also typical for X and gamma ray burst sources.

Bursts from a particular source, tend to have characteristic profiles, but not always. For example, MXB 1743 - 29 produced eight bursts at approximately 35 h intervals which each showed two, and sometimes three, distinct peaks at energies above 6 keV (Lewin, 1976). MXB 81735-44 produces bursts which are typically narrow, only lasting 4 to 6 s (Lewin, 1977), while MXB 1636-53 and MXB 1728-34 produce bursts with fast initial decays of the order of a few seconds, followed by long gradual decays at low energies (Hoffman, 1976, 1977). By contrast, the bursts from MXB 1837 + 05 show great variation which may be related to the irregularities in the burst intervals (Li et al., 1977). MXB 1728-34 normally has a characteristic burst profile with intervals varying from 4 to 8 h (Hoffman 1976, 1977), but a very different behaviour was observed for a while in July 1977 observations (IAU. Circ. No.3078, 1977). Other variations in burst profiles from sources are reviewed by Lewin (1977).

A burst usually undergoes significant spectral changes in its short life, with the spectrum typically softening during the burst decay. However, spectral hardening has been observed in the decay of bursts from one source, MXB 1820-30 (Grindlay, 1976; Clark, 1976). Spectral hardening during the rise of a burst is fairly common (Lewin, 1977).

An important quantity in relation to testing nuclear-flash models of X-ray bursts is the ratio of time-averaged luminosity of the steady emission to that of the burst emission. This varies from $\lesssim 2$ for the rapid burster MXB 1730-335 (Lewin, 1976) to ~ 250 (Hoffman et al., 1977). Thermonuclear flashes might be expected to exhibit characteristic structure in the 1-10 MeV region, which is one reason for studying gamma ray bursts in low energy gamma rays.

The rapid burster MXB 1730-335 is significantly different in character to all other burst sources, sometimes producing up to 4,000 bursts a day. No steady emission has been observed from this source (Ulmer et al., 1977;

Liller et al, 1977; Kleinmann et al., 1976).

If the differentiation of class of gamma ray bursts and X-ray bursts of Lewin (1977) is accepted, then there are interesting comparisons to be made. For example, X-ray burst sources cluster along the galactic equator while gamma ray burst sources do not. X-ray bursts are repetitive on time scales of hours to days, whereas gamma ray bursts are not. The spectra of X-ray bursts are much softer than those of gamma ray bursts. The total flux density of a gamma ray burst is typically around 2 orders of magnitude higher than that of an X-ray burst. Lewin, 1977, remarks that because gamma ray bursts are not recurrent, unlike X-ray bursts, then gamma ray bursts cannot be the high energy tails of normal X-ray bursts produced by nearby burst sources. Nevertheless, some associations between gamma and X-ray bursts can be found (Evans et al., 1976). For example, a gamma ray burst observed by Apollo 16 (from galactic latitude $\sim -46^\circ$) exhibits a triple-peaked time structure (Metzger et al., 1974) which is rather similar to the structure in bursts from MXB 1743-29 (Lewin, 1976).

The theoretical models for X-ray burst sources can be separated, broadly speaking, into two categories (Lewin, 1977). One is the concept of instabilities in the accretion of matter onto a compact object (white dwarf, neutron star or black hole). The second is the idea of thermonuclear flashes in matter accreted onto the surface of a neutron star.

However, there are notable exceptions which fall into neither category mentioned by Lewin, although the following two examples may be mainly intended as models for and/or predictions for the harder gamma ray bursts. The model of Sofia and Horn (1974) suggests that cosmic gamma ray bursts may be produced by collisions of chunks of antimatter of mass $\sim 10^{15}g$ with normal stars. Another model is that of Page and Hawking (1976) who have examined the possibilities of detecting hard gamma rays produced by the quantum mechanical decay (evaporation) of small black holes created by inhomogeneities in the early universe. The details of the evaporation process will depend on unknown nuclear characteristics, but the Hagedorn (1965) statistical bootstrap model has given some quantitative predictions for high energy gamma rays (200 to 1000 MeV). Based on this model, Weekes and Porter (1977) have used separated atmospheric Cerenkov detectors to set an upper limit for primordial black hole explosions in the galaxy at 0.04 events/pc³-year.

Most of the remaining theories recently proposed have been reviewed by Lewin, 1977. In addition it is worth mentioning the recent paper of Grindlay (1978) which outlines a theoretical model which purports to explain the observed phenomena comprehensively. This is based on a

mechanism in which massive ($\sim 10 - 100 M_{\odot}$) black holes, from massive stars and the cores of disrupted globular clusters undergo supercritical spherical accretion in interstellar clouds.

An upper limit for the frequency of gamma ray bursts determined by the LEG 4 experiment is discussed in section 4.5.

Having reviewed the observational status of low energy gamma ray astronomy and its context in relation to other energy ranges, it now follows that some of the major limitations on the design of gamma rays should be outlined. These are discussed in the next section.

1.7 The Design of Gamma Ray Astronomy Experiments

In this section the basic limitations and requirements of a design of a gamma ray telescope are discussed. The various solutions, tried in the past by various experimenters, to the problems of designing low energy gamma ray telescopes are described in the next chapter. The design of a gamma ray telescope depends on the objectives of the experiment. For example, the observation of gamma ray flux from point sources (pulsed and unpulsed), observation of gamma ray lines, gamma ray bursts, and the diffuse gamma ray background.

In relation to the LEG 4 experiment, let us first consider the requirements of a detector to observe a gamma ray flux from a source. In general a detector will see a net background counting rate, $dB(E)/dE$ (cts $s^{-1} MeV^{-1}$), where E is the energy loss in the gamma ray detector that would correspond to some channel number equivalent to a full energy loss by a gamma ray of energy E . The limiting gamma-ray flux that can be measured from a source in the direction θ, ϕ , is then given by (Chupp, 1976):

$$F_{\min} \leq \frac{n}{s(E, \theta, \phi)} \sqrt{\frac{2 dB(E)/dE \cdot \Delta E}{T_{\text{obs}}}} \quad (1.7.1)$$

where ΔE is the FWHM energy resolution of the instrument at energy E , T_{obs} is the observing time of the measurement and $S(E, \theta, \phi)$ is the sensitivity of the detector for a photon of energy E entering the detector from the source in the direction (θ, ϕ) . The definition

of sensitivity used in this equation is the full energy efficiency at energy E times the effective area the detector presents in the direction (θ, ϕ) . For inorganic scintillators or solid state detectors the full energy efficiency is the probability that the full energy of the photon is lost in the crystal. n is effectively the number of standard deviations of the background fluctuations that corresponds to a detectable signal. It is usually taken to be 2 or 3. The equation 1.7.1 assumes that the background is also measured for the time T_{obs} .

It can be seen that to increase the accuracy of the detector one major requirement is to reduce the background as much as possible. Chupp (1976) has reviewed the major sources of background in gamma ray detectors, including atmospheric and diffuse cosmic gamma rays, atmospheric neutrons, intrinsic radioactivity of detector material, and spallation.

Other parameters of interest in designing gamma ray telescopes are: angular resolution, energy resolution, minimum detectable flux (or a highest sensitivity), and time resolution.

If we have an observable flux from a source of F (photons $\text{cm}^{-2} \text{s}^{-1}$) where $F \geq F_{\text{min}}$, then the signal-to-noise ratio of the measurement is the observed signal counts ($F \cdot S(E) \cdot T_{\text{obs}}$) divided by the fluctuation in the background counts $\sqrt{C_B \cdot T_{\text{obs}}}$ giving

$$\frac{S}{N} = \frac{F \cdot S \cdot T_{\text{obs}}}{\sqrt{C_B \cdot T_{\text{obs}}}} = F \cdot S \sqrt{\frac{T_{\text{obs}}}{C_B}} \quad (17.2)$$

The objective of any experiment is to maximise this ratio. In addition, the background C_B must be reasonably constant in order not to mimic a true gamma ray source.

The finest spatial or angular resolution attainable at energies of the order of 1 MeV can only be ~ 1 degree. This is a limit due to the instrument techniques currently available, which are limited by the high penetrability of gamma rays in this energy region.

For both alkali halide scintillators and solid state detectors, high energy resolution is possible for gamma ray spectroscopy. Alkali halide detectors, if NaI is used, are capable of resolutions (FWHM) of $\frac{\Delta E_\gamma}{E_\gamma} \approx 7\%$ at the standard energy, 662 keV, varying with photon energy $\propto E_\gamma^{-1/2}$. By contrast, the highest energy resolution measurement that can be achieved with cooled Ge(Li) solid state detectors is $\gtrsim 1$ keV and is limited by electronic noise. Consequently, the fractional energy resolution

$\text{FWHM} \propto E_{\gamma}^{-1} + K^1 E_{\gamma}^{-\frac{1}{2}}$ and is a considerable improvement over the alkali halide scintillators at all energies.

It may be found in the future, that in the majority of cases of astrophysical importance, gamma-ray line widths may be much wider than the resolution achievable by solid state detectors. For example, consider inelastic proton scattering on ^{12}C , in a low density gas, giving a 4.43 MeV line. Then it is possible that the line width due to the Doppler effect of a distribution of carbon velocities will be ~ 100 keV. This is given approximately by $\Delta E_{\gamma} \cong \frac{4v}{c} E_{\gamma}^0$, where ΔE_{γ} is the original gamma ray energy from the interaction, and v is the order of the maximum velocity of the nuclei involved in the interaction (Chupp, 1976). A more accurate expression incorporating the angle of emission of the excited nucleus has been calculated by Meneguzzi and Reeves (1973).

For the supposed 4.43 MeV line of width 100 keV, it would be sufficient to use NaI(Tl) which has a line width of ~ 130 keV at 4.43 MeV, whereas a typical solid state detector would have a line width of ~ 3 keV at the same energy. The LEG 4 experiment used NaI crystals because it was not designed specifically to observe gamma ray lines. However, any gamma ray lines detected would have given an observable feature, despite the lower energy resolution of LEG4 than solid state detectors, the sensitive area possible with LEG 4 experiment being a compensating factor in the sensitivity of this detector. If any features had been detected by LEG 4, then this would have merited further investigation by solid state detectors.

Taking into account the aforesaid basic limitations on detector design, the LEG 4 experiment was designed by the Southampton University Gamma Ray Astronomy Group. First, the basic objectives of the LEG 4 experiment are outlined in the next section.

1.8 The Objectives of the LEG 4 Experiment

The LEG 4 experiment was the latest in a series of successively improved low energy gamma ray telescopes. Earlier detectors in the series have been described by Lovett (1973). An earlier anticoincidence system, the LEG 2 experiment, had detected what appeared to be a large excess above the extrapolated X-ray spectrum from the Crab Nebula in the 1 to 10 MeV range (Baker et al., 1973). Because the results had a low

statistical significance, it was decided that an improved detector, concentrating during its flight solely upon the Crab Nebula source, would provide either an astrophysically interesting confirmation of the previous result, or the opposite. The opposite result would also be interesting, implying a possible time variability of the Crab Nebula, although due to the low significance of the previous result, this would be a less likely alternative.

The LEG 4 experiment was designed to incorporate the following improved features over the LEG 2 experiment for observing the Crab Nebula:

- four times the sensitive area
- up to ten times the time exposure to the Crab Nebula in favourable wind conditions
- two pairs of detectors in opposite phase as regards being "ON" or "OFF" the source to cancel out transient background effects
- temperature stabilisation of Gain Factors, using thermostatically controlled heaters
- digital transmission and storage of data, as opposed to the previous Analogue methods, to enable faster and more comprehensive data analysis using computers.

A by-product of the proposed increased exposure time to the Crab Nebula was that the statistics would be improved sufficiently to enable a search for the pulsar NP0532 in the Crab Nebula in the 1 to 10 MeV range.

That the experiment should have been able to detect both the pulsed and unpulsed components of the gamma ray emission from the Crab Nebula simultaneously, was especially significant experimentally and astrophysically. Experimentally, because it had not been done before for gamma rays from the Crab Nebula in the 1 -10 MeV region. Astrophysically, because if an excess was found to exist in the unpulsed component, the measurements should have demonstrated the degree of association, if at all, of the pulsar NP0532 with this excess.

An interesting result in the relation to the pulsar NP0532 was that of Hillier et al.(1970). This had indicated a very hard spectrum which if verified would have implied that the pulsing star was the major energy source for the whole nebula (Orwig, 1971). However, Kurfess (1971) has suggested that this result may have been high due to a calibration error.

The next chapter describes past and present designs of gamma ray telescopes and their limitations. Consideration of these alternative designs led to the construction of the LEG 4 telescope which is described in detail in chapter 3.

Chapter 2 - Techniques of Low Energy Gamma Ray Astronomy

2.1 Detector Design Considerations

This chapter deals with the variety of methods currently available for detecting low energy gamma rays from Cosmic Sources. Detectors may be balloon based, or satellite borne. Ground based detectors cannot be used in the low energy gamma ray range due to the attenuation of the atmosphere. Balloon based detectors have negligible atmospheric attenuation, but are limited in their time exposure, although recent transatlantic balloon flights have extended the time exposures possible (Delury, 1976 and Auriemma et al., 1978) up to the order of a week. Satellite experiments can produce even longer time exposures, but have the disadvantage of much greater expense. In addition, the background count rate depends on the orbit of the satellite.

It may be desired to observe the cosmic diffuse background, or discrete cosmic sources (pulsed and unpulsed), or gamma ray lines (either from discrete sources or from the background), or gamma ray bursts and other transient phenomena.

Transient phenomena and pulsed radiation measurements require good time resolution. For example, to observe the Crab Nebula pulsar, timing accuracy of the order 1 m sec is required, whereas for the longer duration (up to 22 sec) gamma ray bursts, 0.5 sec might be regarded as sufficient. However, any fine time structure of the burst would require a greater accuracy to be observable.

Gamma ray lines may be detected by detectors without particularly good energy resolution (such as NaI detectors) because the line will still show as a feature superimposed on the background and/or source spectrum. However, solid state detectors (such as Ge(Li) detectors) with better energy resolution may observe the finer structure of any detectable lines.

The unequivocal identification of gamma ray sources with X-ray and radio sources requires an angular resolution better than 1° . But at present the best angular resolution is only of the order of 2 or 3° in the low energy gamma ray region. For example COS-B (Hermsen et al., 1977) has detected new X-ray sources within the angular resolution of previous experimental measurements which purported to have observed the Crab Nebula

in low energy gamma rays. This particular problem is discussed further in chapter 6.

In the energy range 1 to 10 MeV, the Compton Interaction is the most important interaction of gamma rays with matter, and is more efficient for higher Z material (Evans, 1955).

In order to maximise the sensitivity of the detector, and to detect cosmic point sources, a method of collimation and/or background subtraction is required. Early attempts to fulfil this requirement used a mainly passively shielded detector using brass or lead as the shield. A typical example is described in the following section.

2.2. Passive Collimation

An example of this type of system is the LEG 1 detector of the Southampton group (Lovett, 1973). Diagram 2.1 shows the detector arrangement.

The central crystal was a sodium iodide crystal, Thallium activated, 12.4 cm in diameter by 5.1 cm deep, directly encased in 0.6 cm of NE102A scintillation plastic. Both crystal and plastic were viewed by a single 12.7 cm, 54 AVP photomultiplier tube, with pulse shape discrimination used to distinguish between the two-an arrangement known as a phoswich.

The passive shield was made of lead with an average thickness of 5 cm in the line of sight from the centre of the crystal. The lead contained a small amount of antimony for good casting and mechanical properties and a thin brass liner was used in the bore for mechanical strength.

Totally enclosing the lead shield was a layer of boron-loaded wax, containing 0.3 gm cm^{-2} of Boron Carbide (B₄C) in approximately the same quantity of wax. This layer absorbed thermal neutrons with a better than 99.9% efficiency in the reaction $\text{B}^{10} + \text{n} \rightarrow \text{Li}^7 + \alpha$ with a cross section of 4000 barns. This was, in turn, enclosed by an outer anti-coincidence shield which consisted of a box of 0.6 cm thick NE102A scintillation plastic viewed by eight 5 cm photomultiplier tubes, mounted on the corners.

The angular resolution was found to be 8° HWHM, and this was not strongly dependent on energy.

However, the lead shielding on LEG 1 was found to have actually

Passively shielded detector (Lovett, 1973)

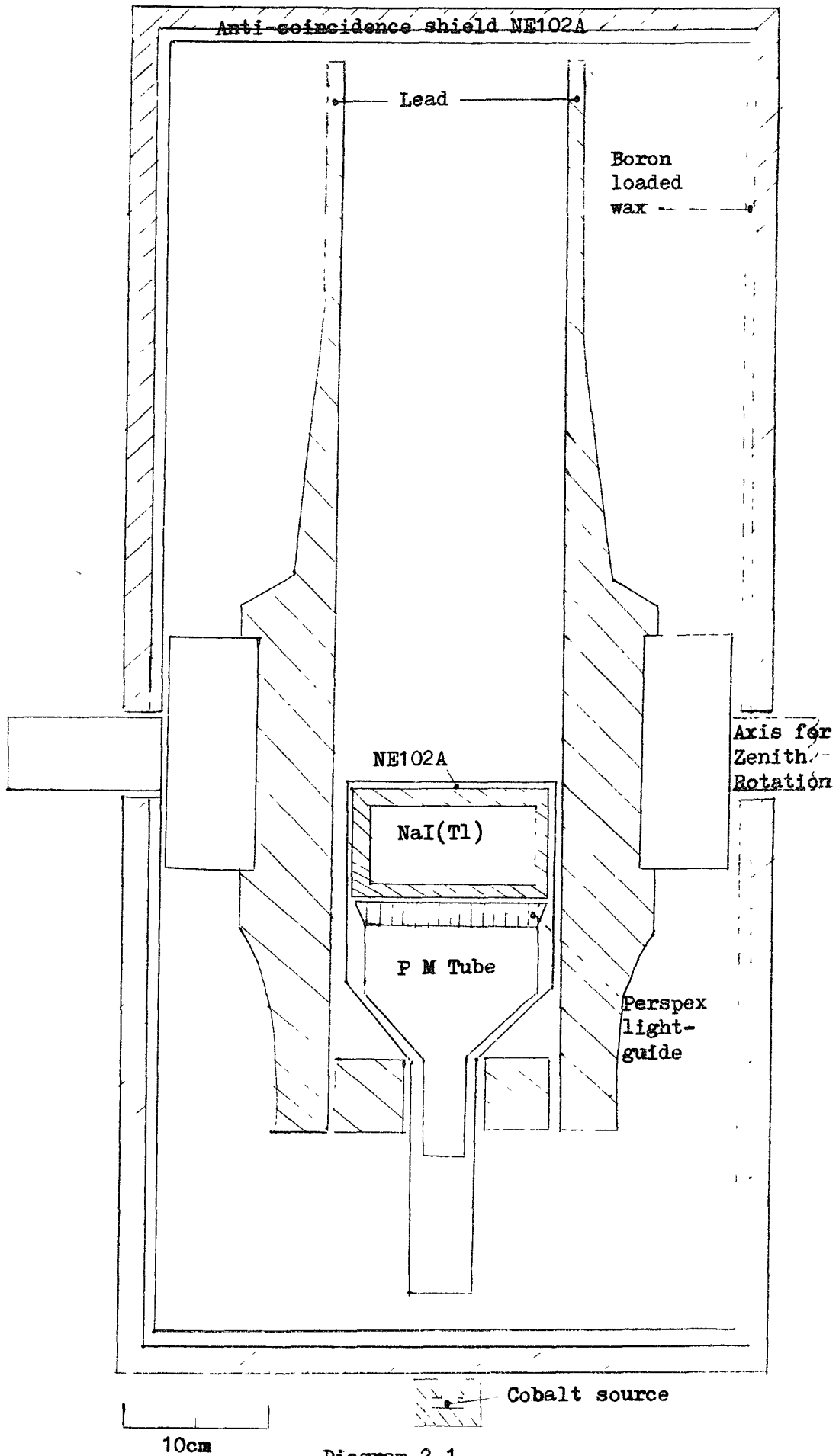


Diagram 2.1

increased the background count rate when compared with the flight of the central detector crystal without the shield. In addition, the phoswich veto system produced doubts as to whether it was rejecting genuine events as well as unwanted background events. Such an increase in counting rate due to lead shielding was also observed by Vette (1962), Jones (1961), Clark, Lewin and Smith (1968).

The problems of passive shielding gave rise to the concept of active shielding, some practical applications of which are described in the following section.

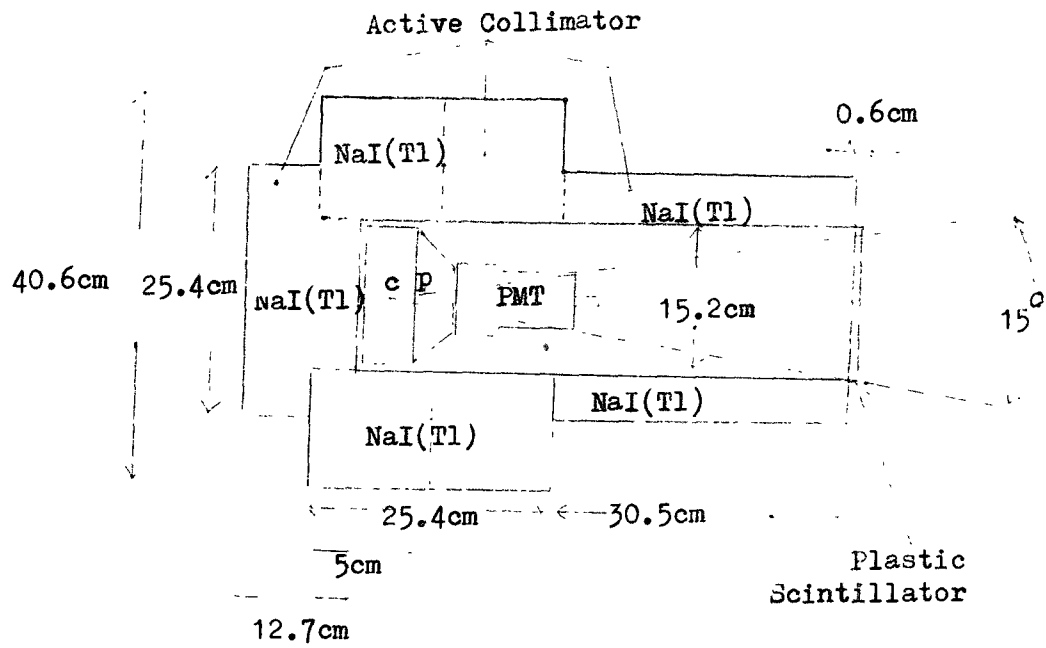
2.3 Active Collimation

Gruber et al. (1974 and 1977) used an actively shielded detector. The detector consisted basically of a 10 cm diameter by 7.6 cm thick NaI(Tl) scintillator, surrounded by a four-piece cup shaped CsI(Na) collimator with average 6.35 cm thickness. A 1 cm thick plastic shield across the aperture extended charged particle shielding to 4π . A 5 inch photomultiplier tube viewed the central detector through 7.6 cm thick by 10 cm diameter section of shield. Discrimination of shield from detector events in this "phoswich" unit was efficiently made through measurement of pulse rise times. The aperture width of 50 degrees FWHM was nearly constant with energy, but rather large. Only below 400 keV was the collimation highly effective.

Gruber investigated the background spectrum and claimed to have seen both the Crab Nebula unpulsed and pulsed emissions. However, the poor directionality of the detector leaves room for uncertainty as to whether or not only the Crab Nebula was observed.

Another actively shielded detector is that of Walraven et al. (1975) which detected the pulsed and unpulsed flux of the Crab Nebula in the region 0.1 to 1.5 MeV. Their detector basically comprised of a central NaI(Tl) crystal of 182 cm² sensitive area and 5 cm thick as in diagram 2.2.

By contrast to the larger sensitive area, balloon-borne experiments of Gruber et al. and Walraven et al., Carpenter et al. used a smaller area satellite experiment with the advantage of increased time exposure. The actively shielded detector of Carpenter et al. comprised a central CsI(Na) crystal of area 8 cm², and 4 cm thick, shielded by CsI, which detected the



c.... NaI(Tl)

p.... Hollow, thin-wall light pipe

Actively Collimated Gamma-Ray Detector

Diagram 2.2

Crab Nebula in the energy range 26 keV to 1.2 MeV.

The problem with active shielding is that above approximately 1 MeV, it tends to veto an increasing proportion of events because the secondary photons and electrons have enough energy to escape from a first interaction in the central crystal, and interact in the active shield.

In addition, large quantities of alkali halide scintillation material is being used in the shield rather than in the central detector of the source gamma rays.

An alternative is to use the alkali halide material to increase the sensitive area of the central detector, for detecting the source and admit the presence of the background to some extent. This approach is incorporated in the principle of anti-collimated detectors, which are discussed in the next section.

2.4 Anticollimation

An early example of this type of system is that of the Bristol Group (Adams et al., 1969; Daju et al., 1970). The LEG 4 anticollimated system is described in later chapters. Lovett (1973) describes the earlier LEG 2 system. A more recent system is that of Mandrou et al. (1976 and 1977). Their detector has observed the Crab Nebula total spectrum up to about 4 MeV, and consists of an $80 \text{ cm}^2 \times 2.5 \text{ cm}$ thick CsI crystal in an NaI well, 5 cm thick. A lead shutter 8 cm thick by 12 cm diameter, cut into two half cylinders, is placed at a distance of 57 cm from the detector, where it subtends an angle of 10.5 degrees about the axis of the detector. The two halves of the cylinder are first separated for 10 minutes to observe the source, then closed for 10 minutes to accumulate a background only spectrum, and so on for the entire flight. A separate flight, not observing a source, showed that no false excesses are produced by the shutter itself in the 80 keV-10MeV range.

Another shutter-occluder detector for balloon flights is that of Forrest et al. (1975). It will be of interest to see the future development of such detectors.

By contrast, the desire to obtain an improved gamma ray signature has led to the parallel development of other systems based on the

Double-Compton principle. By time-of-flight, energy ratio, and angular considerations, a double Compton telescope has a much higher probability of distinguishing between gamma ray, or neutron induced events in the detector than the previous detectors described. Double Compton telescope systems are described in the next section.

2.5 Double Compton Telescopes

Schönfelder et al.(1977) have constructed a Compton telescope and White et al.(1977) have constructed a variation on the same principle. Schönfelder's detector consists of two plastic scintillator blocks with a vertical spacing of 12. m. The dimensions of the upper detector are 15 cm x 15 cm x 15 cm; and of the lower one, 60 cm x 60cm x 15 cm. Both detectors are surrounded by thin anticoincidence shields of plastic scintillator to reject charged particles. A gamma ray is identified by a first Compton collision in the upper detector and a second one in the lower detector. This sequence is confirmed by a time-of-flight measurement. An event is recorded when the time of flight of the scattered gamma ray has a value of between about 0 to 9 ns. Within this interval the time-of-flight distribution is measured in steps of 1.3 ns. For each event the pulse heights E_e' and E_e'' in the upper and lower scintillators are measured. From their values, the energy and direction of the incoming gamma ray can then be found. The telescope has an acceptance cone of 26 degrees half-width at half maximum between 1.5 and 2 MeV, 23 degrees between 2 and 3 MeV, of 18 degrees between 3 and 5 MeV, and 14 degrees between 5 and 10 MeV. The energy resolution is 40 per cent FWHM at 2.75 MeV. The effective geometrical area for vertical incidence is zero below 1 MeV, increases to 1.6 cm² at 1.5 to 2 MeV, has a maximum of 2.6 cm² at 3-5 MeV and drops to 2.2 cm² at 5 - 10 MeV. With this detector, Schönfelder et al(1977) measured the atmospheric background, the diffuse cosmic background, and the zenith variation of the atmospheric background. In addition, they claim upper limits to the Crab Nebula total flux which are at variance with the results of Gruber et al.(1977) and the LBG 2 and LBG 4 experiments (as discussed in a later chapter).

A schematic diagram of the UCR double Compton scatter telescope of White et al.(1977) which was used to measure cosmic diffuse gamma rays, is shown in diagram 2.3. The incident gamma ray, γ , scatters from an

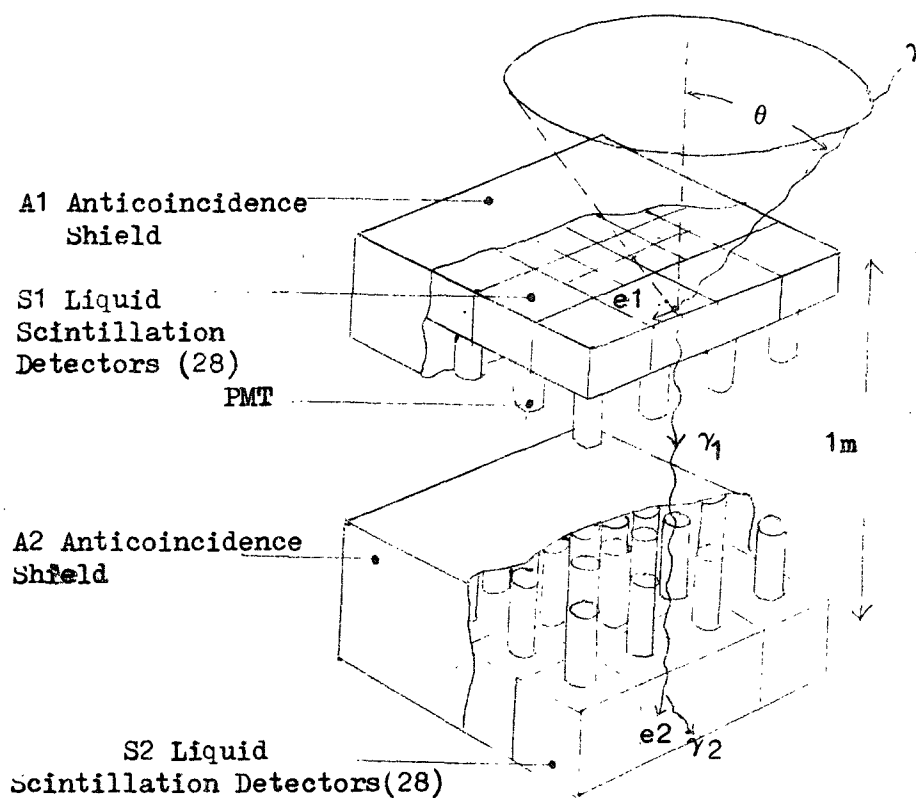


Diagram 2.3

A sketch of the double Compton scatter gamma-ray telescope. A gamma-ray incident on scintillator S1 scatters through an angle θ from an electron $e1$, continues on as γ_1 to scintillator S2, scatters from electron $e2$, and continues on as γ_2 . Two cells vertically one above the other are 'vertical' cells. Two cells displaced relative to the vertical are 'cross' cells.

electron, e_1 , at angle θ to the incident direction in the liquid scintillator, S1, continues on as γ_1 to a second liquid scintillator, S2, where it may be entirely absorbed in S2 or escape with part or all of its energy. The dimensions of S1 and S2 are 100 cm x 100 cm x 12.5 cm and 100 cm x 100 cm x 20 cm, respectively. Each tank of liquid scintillator is divided into 28 cells for better angular resolution. The outside cells are 25 cm x 25 cm, and the inside cells 12.5 cm x 12.5 cm, and each cell is viewed by a separate photomultiplier. Each scintillator tank S1 and S2, with its 28 photomultipliers is completely surrounded by a plastic scintillator 0.6 cm thick to prevent any charged particle from entering or leaving S1 or S2. Gamma rays are separated from neutrons by time-of-flight between S1 and S2. White et al.(1977) also used their detector to set upper limits to a number of point sources from the galactic anti-centre region. Schönfelder et al. are developing an improved version of their telescope, which is described in chapter 8.

For the detection of gamma ray lines, better energy resolution may be required than can be catered for by alkali-halide detectors. Consequently, high energy resolution detectors have been recently developed which use special cryogenically cooled materials. These detectors are described in the next section.

2.6 High Energy Resolution Detectors

Leventhal et al.(1977) flew a high energy resolution detector which found evidence for a line feature from the Crab Nebula at 400 ± 1 keV. Their telescope consisted of a single Ge(Li) crystal about 6.3 cm in height and about 4.7 cm in diameter with an active volume of about 92 cm³. Diagram 2.4 shows the telescope design schematically. The Ge(Li) temperature is typically 85 k. Surrounding the central detector are 184 Kg of active NaI in three sections. The effective entrance aperture of the collimator increases slowly with energy from 11 degrees FWHM at 50 keV to 13 degrees FWHM at 1.33 MeV. The energy resolution of the individual sections of the shield was about 20 per cent at 0.662 MeV. The energy resolution of the Ge(li) pulses below 2 MeV was 3.4 keV FWHM.

Another example of a high energy resolution detector is the one planned for the HEAO-C mission. HEAO-C will be the first long-term

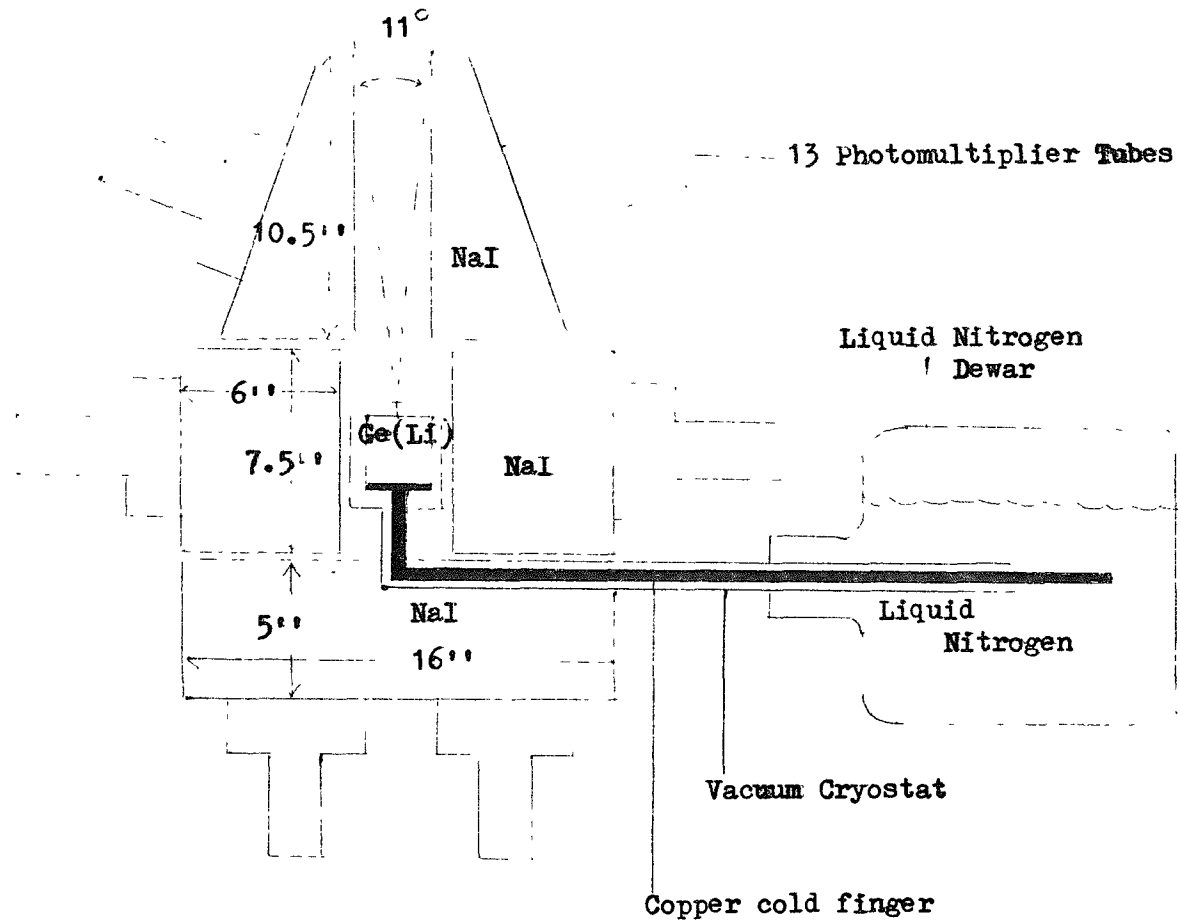


Diagram 2.4 Solid state detector

space mission using a high energy resolution spectrometer; a cooled solid state detector. The detector comprises four cooled Ge(Li) spectrometers, each of volume 60 cm^3 with an overall effective area of 64 cm^2 . These are contained in a CsI(Na) anticoincidence shield collimator. The angular resolution of the CsI(Na) well collimator is $\sim 30^\circ$ FWHM at $\sim 1 \text{ MeV}$ and the energy resolution is $\leq 2.5 \text{ keV}$ FWHM.

Cryogenic cooling is required to maintain the resolution capability of the Ge(Li) unit. To achieve this, a two-stage sublimation system using solid methane and ammonia, is used during flight. Liquid N_2 is used to stabilise the coolants prior to launch. As an alternative to Ge(Li) cells, Jacobson (1975) has pointed out that intrinsic Ge cells could be used. The advantage of intrinsic Ge is that it does not need to be cooled before launch, only during operation. This results in some simplification of pre-launch activities.

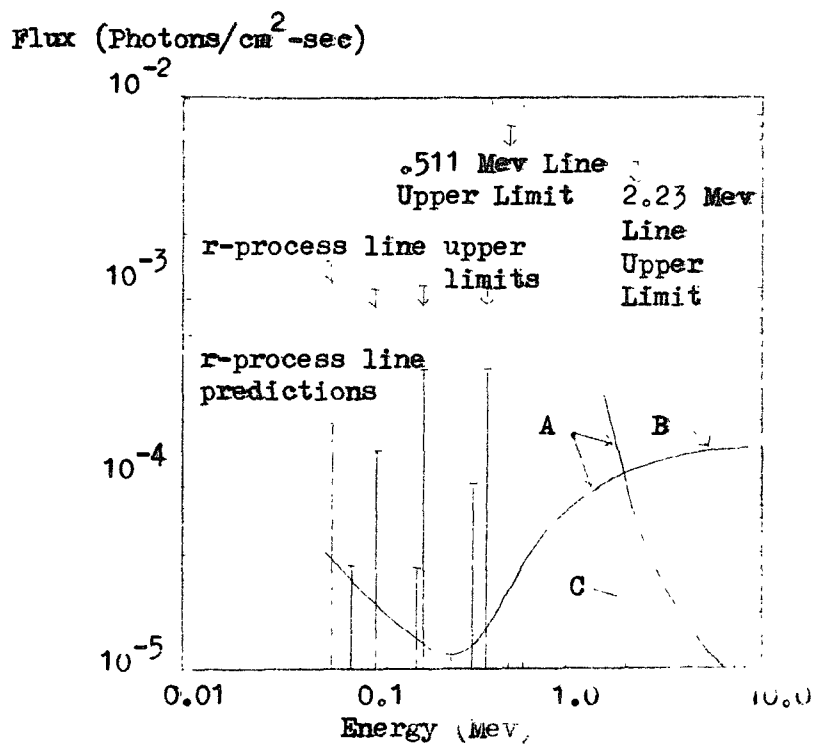
The electronic system enables the four Ge(Li) cells to operate as a single large total absorption spectrometer, and as a pair spectrometer. An estimate of the expected flux sensitivity of the HEAO-C spectrometer is shown in diagram 2.5. The solid curve gives the expected 3σ flux sensitivity for two operating modes of the instrument (Jacobson et al. 1975). The predicted fluxes of several r-process lines from the Crab Nebula are also shown for comparison as well as some upper limits to the r-process lines determined by an experiment of Jacobson (1968).

2.7 Comparison of Different Detector Configurations

Any comparisons drawn between detector configurations remain somewhat subjective without a more detailed computer analysis of each type of detector. However, some comments can be made which have a range of general applicability.

New designs are continually being introduced. Two of these, an active anticollimator system (Morfill and Pieper, 1974) and a Compton coincidence detector within a semi-active shield, will be described in later chapters.

Lovett (1973) has made detailed calculations comparing actively shielded detectors with unshielded anticollimated detectors. The sensitivity as a function of weight of scintillator and weight of



- A.... Detector Sensitivity Threshold
- B.... Anticoincidence Mode
- C.... Pair Spectrometer Mode

The estimated line flux sensitivity for the HEAO-C GeLi spectrometer compared to the predicted r-process line limits (From A.Metzger, 1973)

Diagram 2.5

occluding blocks is calculated by Lovett for the 1 to 10 MeV region. Shielded systems fare relatively poorly in the calculation. Shielded detectors improve relatively at higher weights, but it would seem that very heavy and expensive detectors would be needed before the advantage is definite.

An unshielded system has the advantage of simplicity. Shielded systems in general have a complicated anisotropic response function to background radiations which themselves are anisotropic. Unshielded detectors can achieve the same sensitivity as actively shielded systems using less of the expensive scintillator material. A disadvantage of unshielded detectors is the high background count rate. The source flux is now a relatively small fraction of the total count rate (about 0.06% for $30,000 \text{ cm}^2$ pf crystal). This means that the consistency of the count rate has to be very good to avoid systematic errors, which in turn means careful monitoring of count rate changes due to altitude variation and temperature effects on the gain. By contrast, shielded detectors have a much higher source to background ratio for the same statistical significance and therefore larger percentage changes in the background can be accommodated.

However, another factor in favour of anti-collimation, is that the detector axis can be left pointing at the source of interest while accumulating background and source flux data. Shielded detectors need to move off the source direction to measure background for a period, and then back to the source for a source period. This change of attitude of the detector may in itself change the detector background, as was noted by Lovett (1973) with the LEG 1 experiment. In addition, time is wasted steering away from the source, and then afterwards relocating it.

Purely passive shielding seems to have the twin problems of increased weight of detector and increased background count rate, as mentioned in section 2.2.

Compton telescopes are not designed especially for gamma ray line astronomy. This is because the angular and energy resolution is poor. For example, for a design by Herzo et al.(1975), Monte Carlo calculations suggested an energy resolution of 50% FWHM, angular resolution $15^\circ \rightarrow 17^\circ$ FWHM and sensitivity of 280 cm^2 . These figures of angular resolution and sensitivities are also easily attainable with collimated scintillators. However, the Compton telescope is still attractive because the coincidence requirement dramatically reduces the background counting rate of the telescope - background is one of the major limitations of collimated instruments. The Compton telescope of Herzo et al.(1975) has been

estimated to be capable of attaining a 2σ flux sensitivity of 8×10^{-5} photons $\text{cm}^{-2} \text{s}^{-1}$ at 2.2 MeV for an observation time of ~ 65000 s ($\sim 19\text{h}$).

Schönfelder et al.(1973) and White et al(1973) have used Compton telescopes to measure the atmospheric and diffuse gamma ray flux, for which measurements Compton telescopes would appear to be very suitable.

A problem with Compton telescopes is that a serious background can result from neutron interactions that simulate true gamma ray coincidence events. White and Schönfelder (1975), have estimated that neutron interactions could produce as much as 50% of the apparent gamma ray events in the instruments flown by Schönfelder et al.(1973) and Herzo et al.(1975).

Ge(Li) spectrometers have good energy resolution, but have problems in that they need to be cryogenically cooled and need to reduce the background count rate low enough to produce signal to noise ratios comparable to other detectors. The semiconductor crystals cannot be manufactured as large as NaI crystals to date, and have a volume of typically $\lesssim 150 \text{ cm}^3$. Research is continuing into alternative materials to Ge(Li), such as CdTe, GaAs, HgI_2 (Bertoline and Coche, 1968; Pehl,1977).

After investigation of the relative merits of the other systems available at the time, it was concluded that the anticollimation system provided a cost-effective solution to the problem of background subtraction in cosmic point source measurements. This system was chosen for a detailed test of its capabilities and the basic experimental configuration is described in the next chapter.

Chapter 3 - Description of the LEG 4 Payload

3.1 Description of the LEG 4 Experiment

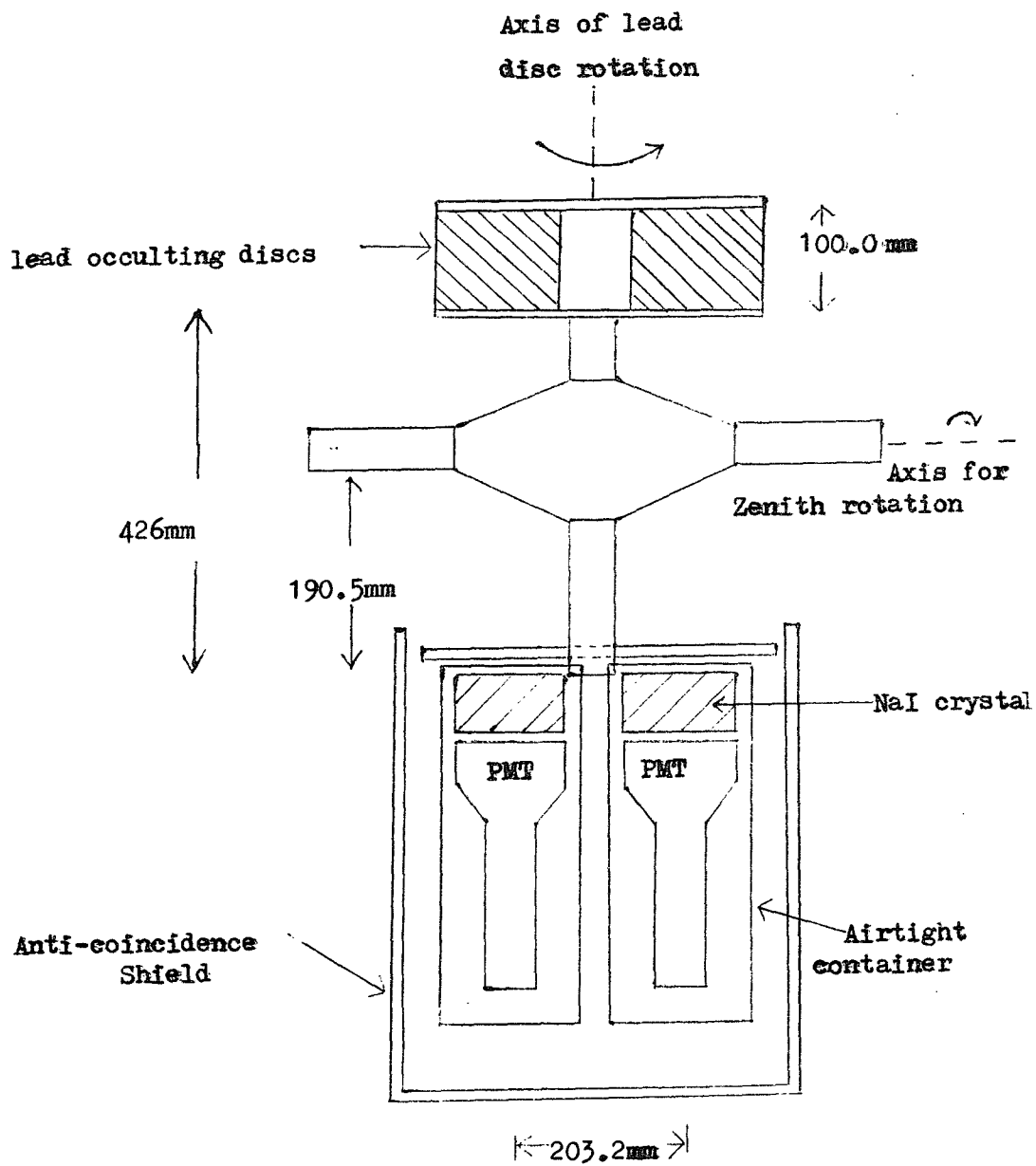
The LEG 4 experiment was the latest in a series of experiments aimed at producing an improved low energy gamma ray telescope. The first three experiments are described by Lovett (1973). The LEG 4 anticollimated low energy gamma ray telescope was designed to be sensitive in the energy range 0.66 to 10 MeV, and to observe the pulsed and unpulsed flux of gamma rays from the Crab Nebula. The orientation of the detector axis was varied using an alt-azimuth mount.

Schematic diagrams of the LEG 4 experiment are shown in diagrams 3.1, 3.2, 3.3, and 3.4.

Four Sodium Iodide crystals (12 cm diameter by 5 cm depth) were each mounted with their photomultiplier tubes inside airtight aluminium cans. The dynode chains of the photomultipliers were encapsulated in Sylgard 184 silicone resin, as an extra precaution against a leak in the cans which would cause voltage breakdown at the low pressures at balloon altitudes. The four aluminium cans were placed inside a five sided plastic anticoincidence counter to reject charged particles.

Above the four detector crystals, two lead discs were placed, each 10 cm thick. The discs could be rotated so that first one pair of crystals would be occulted from a source along the vertical axis of the detector (while the other pair of crystals was unocculted); then next the other pair of crystals would be occulted. The discs had a slightly larger diameter than the crystals, so as to completely occult a 5 degree radius area of the sky.

The 10 cm thickness of the lead occulting discs was chosen after consideration of the total linear attenuation coefficients of gamma rays in lead. Over the energy range 0.5 MeV to 10.0 MeV, the percentage of gamma rays that have not interacted after traversing 10 cms of lead, is $2 \times 10^{-7}\%$ for 0.5 MeV photons, reaching a maximum of 0.7% at about 2.6 MeV, and then decreasing again to 0.25% at 10 MeV. By comparison, for 5 cms thick of lead, the figures are $0.5 \times 10^{-2}\%$ at 0.5 MeV, reaching a maximum of 8% at 2.6 MeV, and decreasing again to 0.5% for 10.0 MeV photons. It may be seen that less than one per cent of the source flux is unaffected by interaction in the lead discs in the 0.5 to 10 MeV



Side elevation of LEG4 Detector System

Diagram 3.1

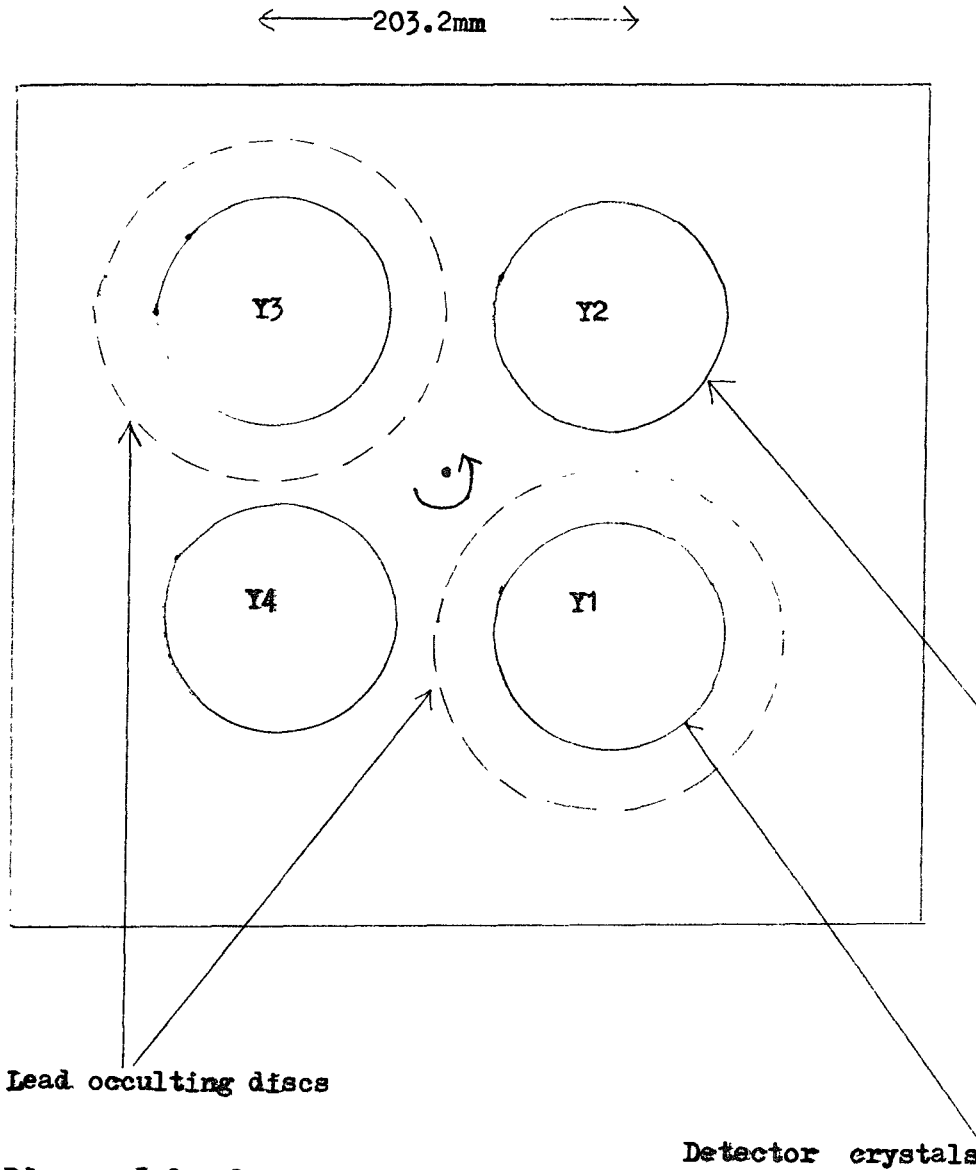


Diagram 3.2 Plan View of LEG4 Detector System

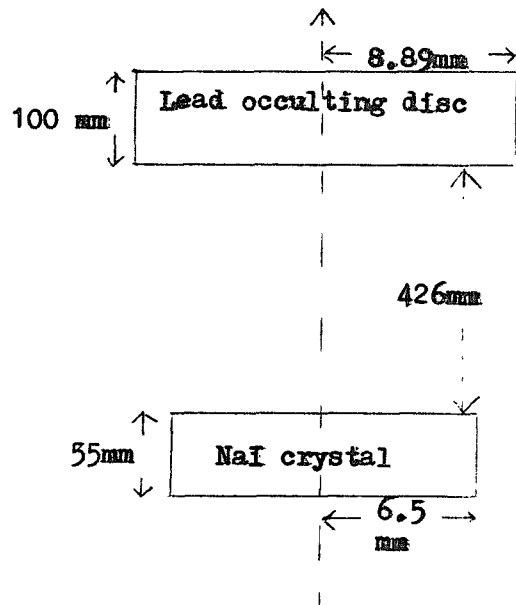


Diagram 3.3 Side elevation, crystal and lead disc dimensions.

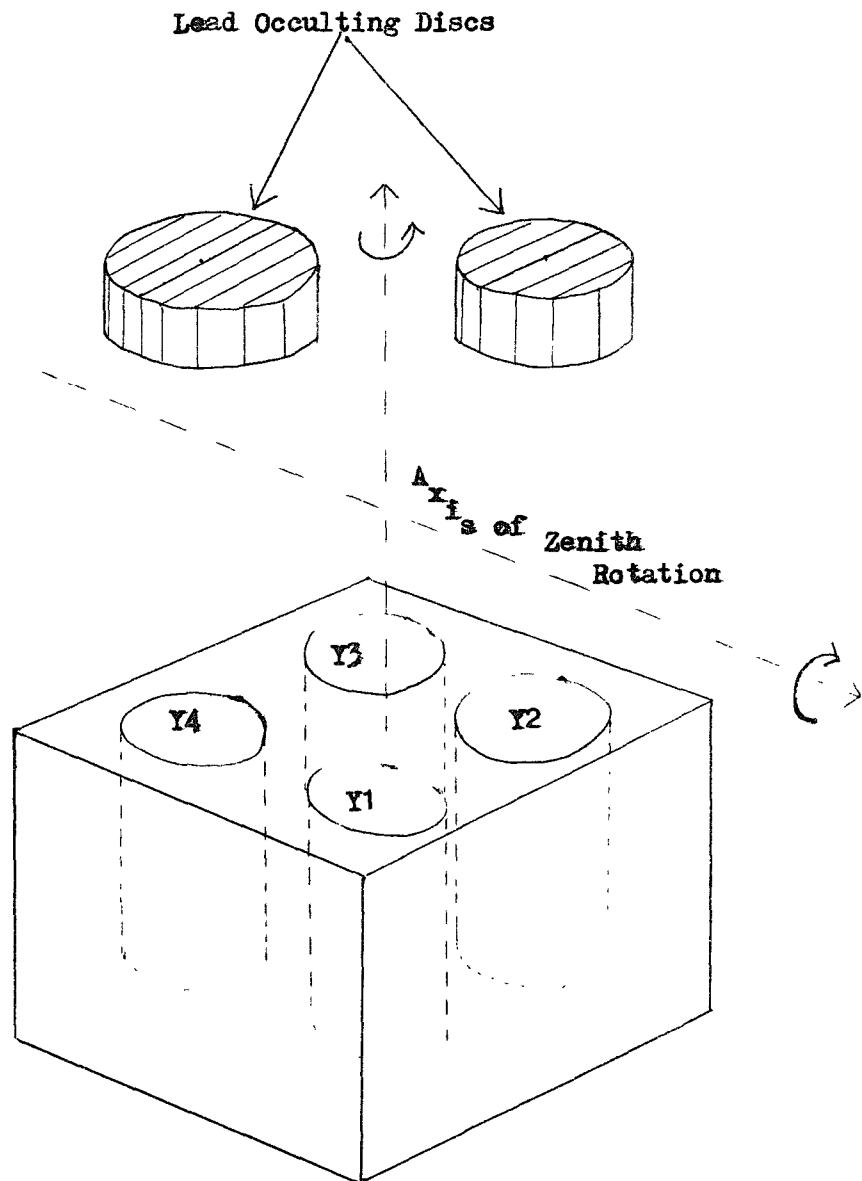


Diagram 3.4 LHC 4 Detector

energy range. In fact, the percentage of unoccluded source continues to decrease, from its maximum at around 2.6 MeV, up to 100 MeV at least.

A more accurate approach to the extent of the attenuation of gamma rays in lead is to consider the shape of the incident spectrum of gamma rays and the Compton interaction. Many photons that interact are not completely absorbed, but remain in the beam as photons of lower energy, having lost some energy in Compton collisions. This "build up" effect is particularly important at the lower end of the spectrum. These considerations were incorporated in the calculations of Lovett (1973). The results of his calculations for the attenuation of gamma rays in lead allowing for Compton scattering for an input spectrum of $E^{-1.5}$ photons $(\text{cm}^{-2}\text{-sec-MeV})^{-1}$ can be seen in diagram 3.5. When this build up factor is taken into account, the shielding factor is seen to be better than 100, where the shielding factor is defined to be the ratio of the number of photons in the energy range, detected from a given direction in the absence of the shield, to the number detected with the shield in place.

The consideration of the interaction probability of the incident gamma ray spectrum in the NaI crystals is similar to that for the lead discs. The consideration of the efficiency of detection of gamma rays in NaI crystals is treated in detail in section 4.1 and 4.2 as regards the conversion from the measured data to the original photon spectrum. The detection efficiency over the energy range 0.5 to 10 MeV varies from 30% to 70% where the efficiency at an incident energy E has been taken as the reciprocal of the energy loss conversion factors as defined in section 4.2. These figures were found for photon spectra of the form $E^{-1.4}$ to $E^{-2.3}$ which includes generally accepted spectral indices for the atmospheric gamma ray background spectrum and the Crab Nebula low energy gamma ray spectrum.

3.2 The Steering System

The whole experimental package could be rotated to different azimuth and zenith angles. The experiment was steered in azimuth using a reaction wheel system. The package rotated in the opposite direction to that of the reaction wheel due to conservation of angular momentum.

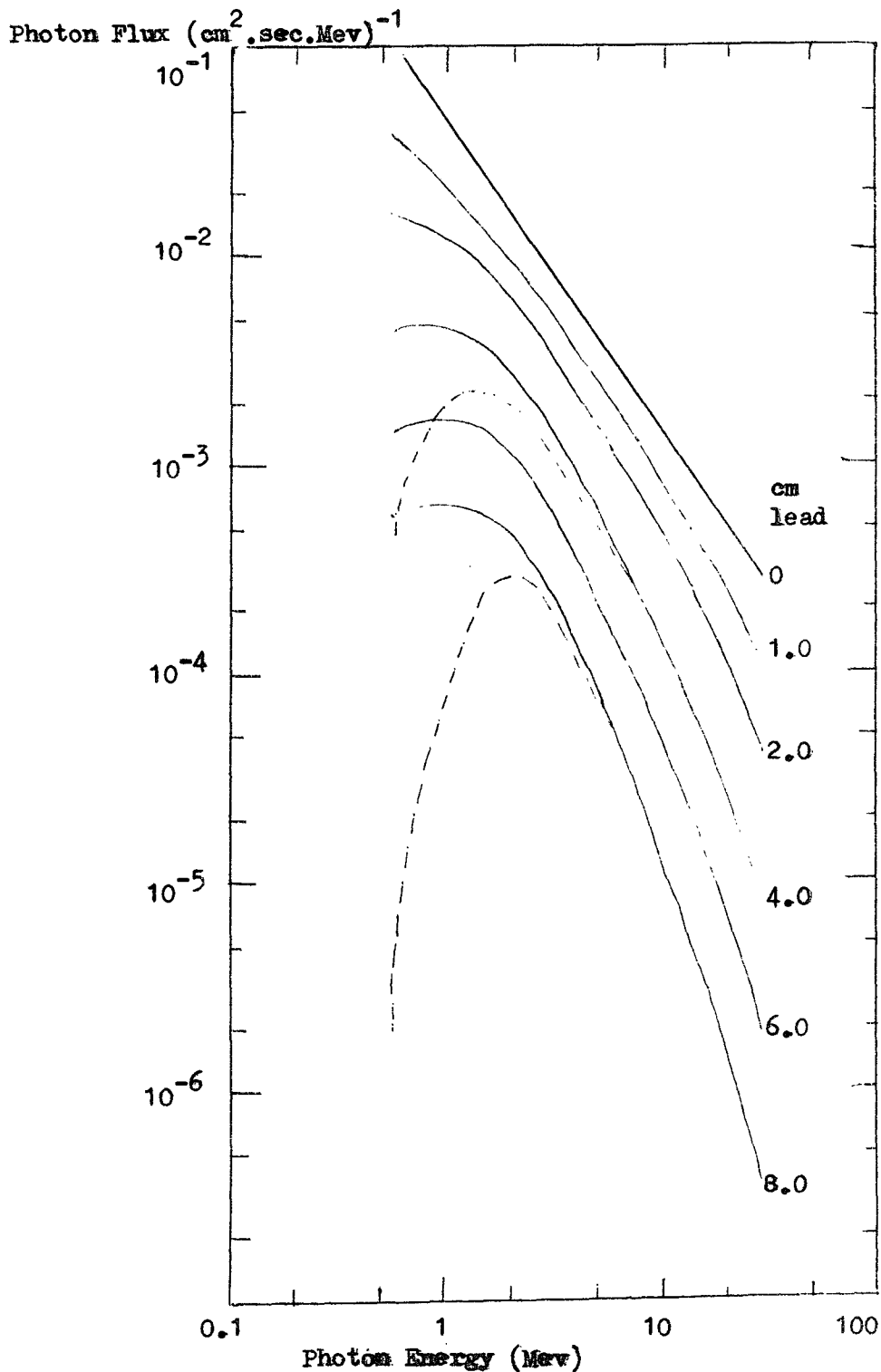


Diagram 3.5 Attenuation of Gamma Rays in lead, allowing for Compton Scattering for an input spectrum of $E^{-1.5}$ Photons/($\text{cm}^2 \text{ sec Mev}$) (Lovett, 1973)

— Photon flux at various depths in lead, allowing for absorption by pair production and photo-electric effect, and for scattering by Compton effect. - - - Shows the flux that has had no interaction i.e. the flux obtained using the total attenuation coefficients.

The azimuth of the payload was determined using a two-axis magnetometer system, which gives an absolute pointing accuracy at float altitude within one degree. The magnetometer outputs were calibrated against azimuthal angle on the ground before flight. Corrections for magnetic north with respect to true north, and for magnetic field line variations with varying balloon longitude during flight were incorporated in the determination of the true azimuthal angle.

The Crab Nebula was successfully tracked for three hours until just after transit. Steering control was lost when the control of the flight had to be transferred to the downrange station because the balloon had been carried over the radio horizon by unusually strong winds.

3.3 In Flight Calibration of the Detectors

To monitor gain changes during the flight of LEG 4, a Yttrium 88 source was placed 40 cm below the crystals of the 4 detectors. Yt 88 produces photon energies of 0.898, 1.836 and 2.76 MeV. The number of photons per 100 disintegrations of these energies are 91.5, 99.5 and 0.5 respectively. The relatively abundant 0.898 and 1.836 MeV peaks were used for in-flight energy calibration of the detectors. The total count rate above 0.66 MeV produced by the Yt 88 source was 18 per cent of the background count rate at float altitude of the balloons, for each detector. This meant that the calibration source gave clearly discernible peaks in 5 minute samples of data taken from the period when the balloon was at float altitude.

Just before the flight, the lower energy discrimination level of the four detectors was set at 0.66 MeV, using a Cs¹³⁷ source.

3.4 Low Temperatures

During ascent, the ambient air temperature can fall to below -50°C and at float altitude is approximately -30°C . Before the flight the detector was tested for normal operation using the thermal vacuum testing facility at Palestine, Texas. The experimental payload was

insulated with 100 mm thick expanded polystyrene. Electronic components were chosen to maintain their specification in the range -30°C to $+50^{\circ}\text{C}$ and gearboxes and bearings were packed with low temperature grease.

Because of the known gain-temperature characteristics of the detectors, it was decided that additional temperature control was needed to stabilise gain changes. Diagram 3.6 shows a temperature-gain graph typical for each detector inside its airtight container. The system was allowed time to stabilize for each reading at each temperature recorded, to avoid thermal lag giving innaccurate results. It can be seen from diagram 3.6 that a change in temperature, from $+20^{\circ}\text{C}$ to -20°C , causes a large change in gain. Such gain changes become difficult to compensate for accurately in post-flight data analysis. In addition, if the lower energy discrimination level is set at 0.662 MeV, then a drop in temperature to -20°C would mean that the lower discrimination level could effectively shift by as much as 0.15 MeV.

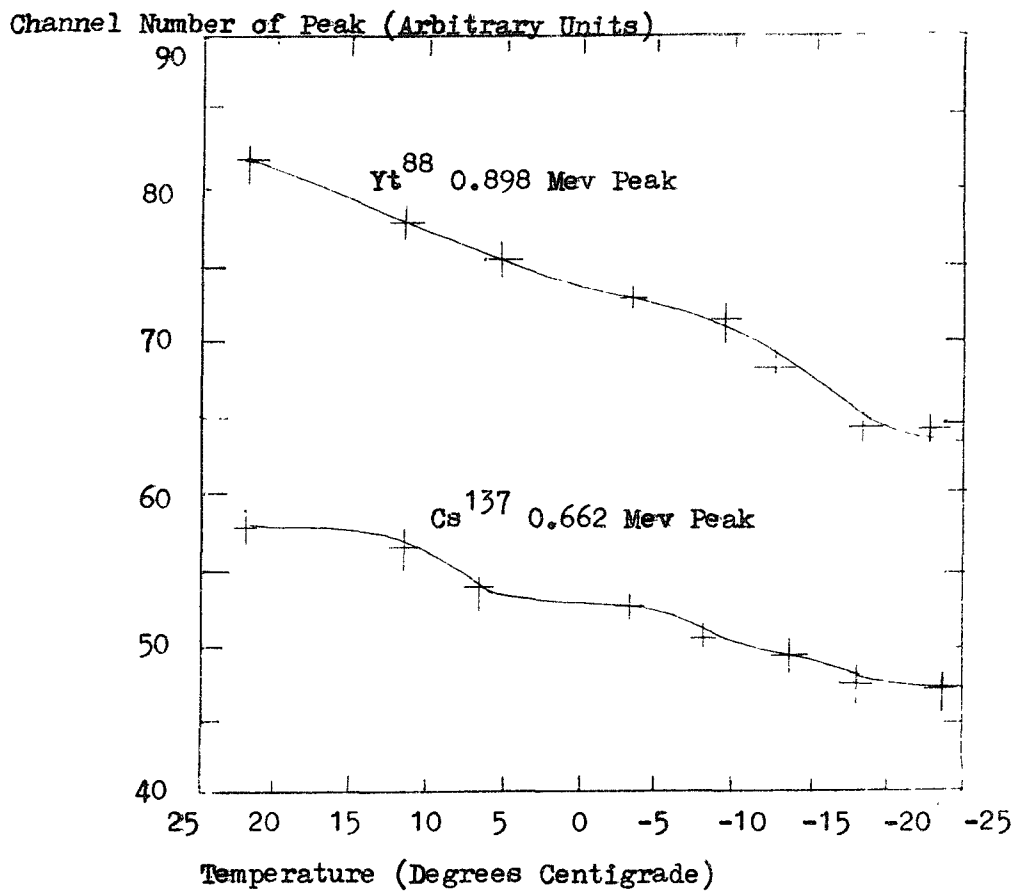
The required temperature control was achieved using thermostatically controlled heaters wrapped around each detector can.

3.5 The Flight of LEG 4 and General Features of the Preliminary Data Analysis

The LEG 4 experiment was launched from Palestine, Texas on 17th July, 1974 at 10.38 GMT. It reached a float altitude of 3.2 mb, and continued at this altitude for six hours from 13.30 GMT. At 16.000 GMT steering control was transferred from Palestine to the downrange station at Midland. Unfortunately, steering control was lost here, so no useful data could be extracted after 16.00 GMT. In addition, it was not possible to synchronise the timing of the data taken before the control transfer with the timing of the data taken after the control transfer. Consequently, no significant contribution to the pulsar data analysis could be obtained from the data taken after the control transfer.

During the flight, the occulting discs were moved to give, alternately, successive occultation and non-occultation periods of approximately 5 minutes duration each. The movement between each position took about 15 seconds. Table 3.1 gives additional information about the position of the balloon during the flight.

The flight was dedicated to the observation of the Crab Nebula.



Gain Variations with Temperature of Y2 Detector
(Y1, Y3, Y4 Detectors similar)

Diagram 3.6

Table 3.1 - Latitude, Longitude and Altitude of Balloon During
LEG 4 Flight (during data collection)

Time GMT Hours, Mins	Latitude Degrees and Minutes	Longitude Degrees and Minutes	Altitude K ft.
10.49	31° 49'	95° 43'	10
11.00	31° 51'	95° 47'	20
11.11	31° 52'	95° 50'	30
11.20	31° 52'	95° 52'	40
11.28	31° 52'	95° 54'	50
11.39	31° 52'	95° 58'	60
11.55	31° 52'	96° 06'	70
12.06	31° 51'	96° 13'	80
12.17	31° 51'	96° 20'	90
12.29	31° 50.5'	96° 32'	100
12.36	31° 51.5'	96° 38'	106
12.43	31° 52'	96° 41'	110
12.56	31° 50.8'	96° 50'	120
13.30	31° 50.5'	97° 23'	126.4
13.45	31° 47'	97° 52'	125.8
14.00	31° 45'	98° 10'	125.2
14.15	31° 42.5'	98° 30'	125.4
14.30	31° 42'	98° 54'	125.6
14.45	31° 38'	99° 01'	125.6
15.00	31° 37'	99° 25'	125.2
15.30	31° 35'	100° 37'	125.7
16.00	31° 40'	101° 08'	126.3

Several thermistors were placed at strategic points in the payload, for example on the detectors, inside the electronics package, etc. These showed no anomalous behaviour. The thermistor on the detectors showed a ramping up and down of temperature between 8°C and 15°C, the time between successive variations in temperature being about 40 minutes. This ramping shows that the thermostatically controlled detector heaters were working. Due to thermal lag, the actual temperature variations of the crystals and tubes within their airtight containers will have been smaller than the 8°C to 15°C range just outside the containers. The subsequent data analysis showed a gain drop consistent with the temperature of the detectors and the pre-flight temperature tests mentioned in the previous section.

Some problems were experienced, initially, in reading the data tapes. After a four month delay to find the cause, it was found that incorrect placing of the longitudinal parity check on the magnetic data tapes was the source of the problem. This was overcome by reconstructing the data tapes in the correct format using the facilities of the Royal Aircraft Establishment, Farnborough.

The data was transmitted in a digital form, and recorded on magnetic tape, although some of the data was also recorded in an analogue form as a back up procedure.

Chapter 4 - The Atmospheric Background and Gamma Ray Bursts

4.1 The Conversion of Energy Loss Spectra to Photon Spectra

In gamma ray astronomy in the 1-10 MeV range, there is a basic problem in converting the measured data back into the original photon spectrum incident upon the detectors. This problem occurs because the energy lost by a photon which interacts in the detector crystal is not strictly proportional to the energy of the photon.

A photon incident upon a scintillation crystal may or may not interact. The probability of interaction depends upon the energy of the photon, the dimensions of the crystal, and the crystal material. If the photon does interact, it can interact by several different types of reaction. In the energy range 1 to 10 MeV of incident gamma rays, the most probable types of reaction in NaI crystals are:

- 1) The photoelectric effect;
- 2) The Compton effect;
- 3) Pair production.

Consequently, photons of one energy incident upon the crystal will give different pulse heights from the photomultiplier viewing the crystal, according to the various interaction probabilities. The shape of this pulse-height spectrum or energy loss spectrum depends on the initial energies of the photon (E_0), and consequently upon the incident photon spectrum.

In practice, no unique, exact solution for the incident photon spectrum can be obtained by deduction from the energy loss spectrum. Instead of setting up numerous equations, and solving them exactly, one has to assume the shape of the incident photon spectrum. The assumption is generally based upon previous experience related to an extrapolation of other measurements and/or from experience of energy loss spectra obtained for various detectors.

In the energy range of interest on LEG 4, (1-10 MeV), the incident photon spectrum of the Crab Nebula was assumed to be a power law spectrum with index -2.3 and the atmospheric background was assumed to be a power law with index -1.4.

The predicted energy loss spectrum was then calculated using the assumed photon spectrum. If this calculated energy loss spectrum was

in close agreement with the experimental data, the assumed photon spectrum was then taken as correct. If not, a new photon spectrum was assumed. Sharp features, such as gamma ray lines, require a different treatment. However, if the energy loss spectrum is smooth, then there is no reason to suppose that there are any pronounced features.

To find the factors necessary to convert an experimental energy loss spectrum to an incident photon spectrum, accurate energy loss spectra are needed for incident gamma rays of different energies. These spectra depend on the size and shape of the detector. One can calibrate the detector with different sources of monoenergetic gamma rays, but there are very few readily available sources of gamma rays in the 1 to 10 MeV range for use in the laboratory. A proton Van de Graaf accelerator can be used to initiate various (p, γ) reactions which can produce gamma rays up to around 17 MeV, depending on the target material. Some typical interactions are briefly outlined in Table 4.1. An alternative approach is to use the data acquired by other experimenters who have used detectors of a similar size and shape. It was decided to use this latter alternative. The data of Berger and Seltzer (1972) was used. This data was previously used by Lovett (1973), but di Cocco (1976) has re-evaluated the conversion factors with much greater accuracy. The results of Lovett (1973) and G. di Cocco (private communication) are compared in the next section.

Berger and Seltzer modelled the response of sodium iodide detectors with a Monte Carlo computer program. The accuracy of their program was verified by comparisons with experimental results at energies up to 20 MeV.

They made a systematic tabulation of the response functions for 3 inch by 3 inch detectors irradiated with broad parallel beams of gamma rays, with energies between 100 keV and 20 MeV. Their results were given in a parameterized form which made it easy to interpolate between the tabulated values with respect to incident gamma ray energy. They found that 3 inch by 3 inch detectors are effectively "omnidirectional" in the sense that the shape of the response function depends very little on the direction of the incident gamma ray beam. Therefore, the tabulated data may be applied reliably to other source geometries, for example, to the case of a detector exposed to an isotropic gamma ray flux. However, the factors were scaled appropriately to take account of the increased depth of the crystals used in the LEG 4 detector.

A linear interpolation of the parameters between the energies

Table 4.1 - Some Interactions to Produce Gamma Rays

The following interactions can be initiated using the 6 MV Van de Graaff Accelerator at Harwell, England.

<u>Proton Energy</u>	<u>Interaction</u>	<u>Gamma Ray Energy</u>
1.64 MeV	$^{19}\text{F}(p, \alpha \gamma)^{16}\text{O}$	6.13 MeV (some 6.91 and 7.11 MeV)
445 keV	$^7\text{Li}(p, \gamma)^8\text{Be}$	17.64 MeV
1.5 MeV	$^{15}\text{N}(p, \alpha \gamma)^{12}\text{C}$	4.43 MeV

Note that the nitrogen target for this third interaction is a 90 per cent N^{15} gas target at about 1 atmosphere pressure.

An additional type of interaction useful for investigating the effect of neutrons on a detector is:

Various proton energies $\rightarrow ^7\text{Li}(p,n)^7\text{Be} \rightarrow$ neutrons of various energies

tabulated by Berger and Seltzer was used in the program developed by G. di Cocco. The program generated the energy loss spectra for incident photon energies in steps of 25 keV up to 1.2 MeV, and in steps of 100 keV from 1.2 to 20 MeV. The general form of the spectra (diagrams 4.1 and 4.2 from S.J. Martin, 1978, private communication) is similar to those generated by Berger and Seltzer which are shown in diagram 4.3

To find the conversion factors from the energy loss spectra to the incident photon spectra it is necessary to assume the shape of the incident photon spectrum. For the LEG 4 experiment, power law spectra were assumed of the form $\frac{dN}{dE} = KE^{-\alpha}$, where $\frac{dN}{dE}$ is the incident photon energy, K is a constant, E is the incident photon energy, and α is the incident photon spectral index. Although Berger and Seltzer found that the shape of the energy loss spectra changed little between the cases of broad parallel beams and omnidirectional beams, incident upon the crystal, the total efficiency does change by a significant amount. These differences were also tabulated by Berger and Seltzer and were incorporated in the program.

For the analysis of the LEG 4 experiment, energy loss conversion factors were calculated by the program. The conversion factors were defined as follows:

In the program the energy loss spectrum was split up into a number, n, of narrow energy loss bands. Let the relative intensity of counts in the i th band of the energy loss spectrum denoted by E loss i, due to an initial photon energy of energy E₀, be I(E₀, E loss i).

Then

$$I(E_0, E \text{ loss } i) = \frac{\text{The relative number of counts in the band } E \text{ loss } i}{\text{The total number of counts in the whole energy loss spectrum due to photons of energy } E_0}$$

Thus if N(E_j) photons of energy E_j are incident upon the crystal (N(E_j) may be of the form $KE^{-\alpha}$, for example), then a total number of N(E_j)e_T(E_j) interact in some way in the crystal, where e_T is the total efficiency. Of these, a number given by

$$\frac{dN}{dE}(E_j, E \text{ loss } i) = N(E_j).e_T(E_j).I(E_j, E \text{ loss } i) \dots 1,$$

lose an energy of E loss i in the crystal, and hence this is the number of counts in the energy loss spectrum that have lost an energy E loss i,

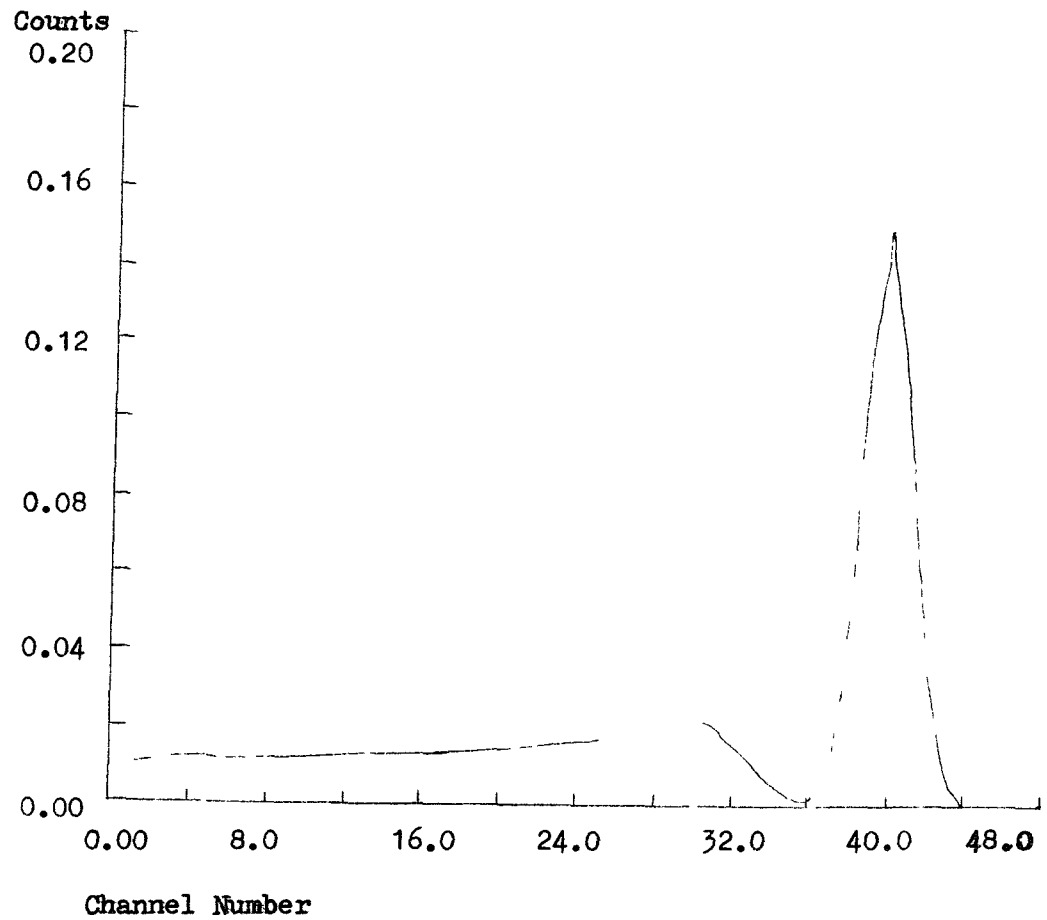


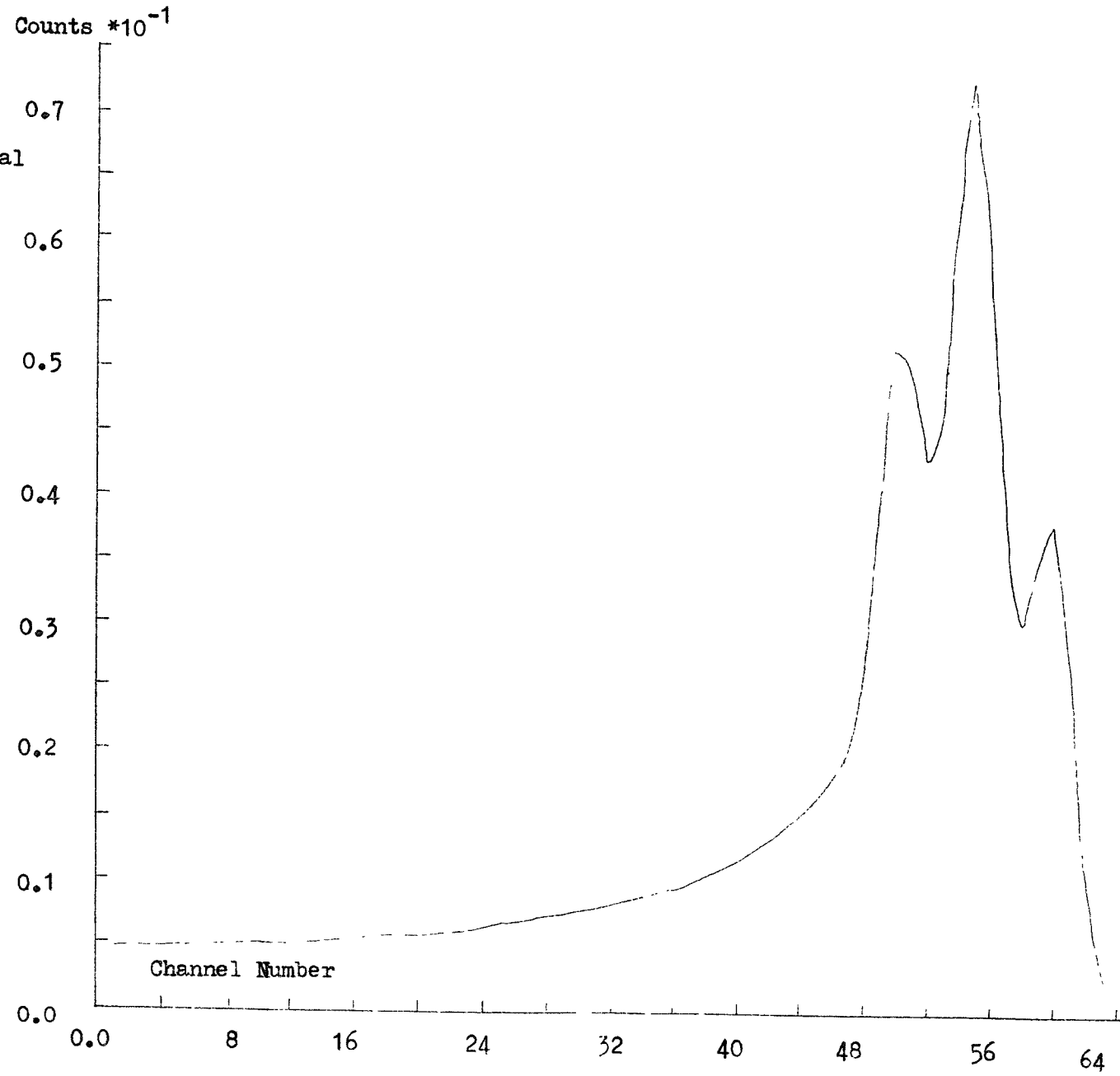
Diagram 4.1

Energy Loss Spectrum in 3" by 3" NaI crystal.

1.0 Mev Photons

Diagram 4.2

Energy Loss Spectrum
in 3" by 3" NaI crystal
6.0 Mev Photons



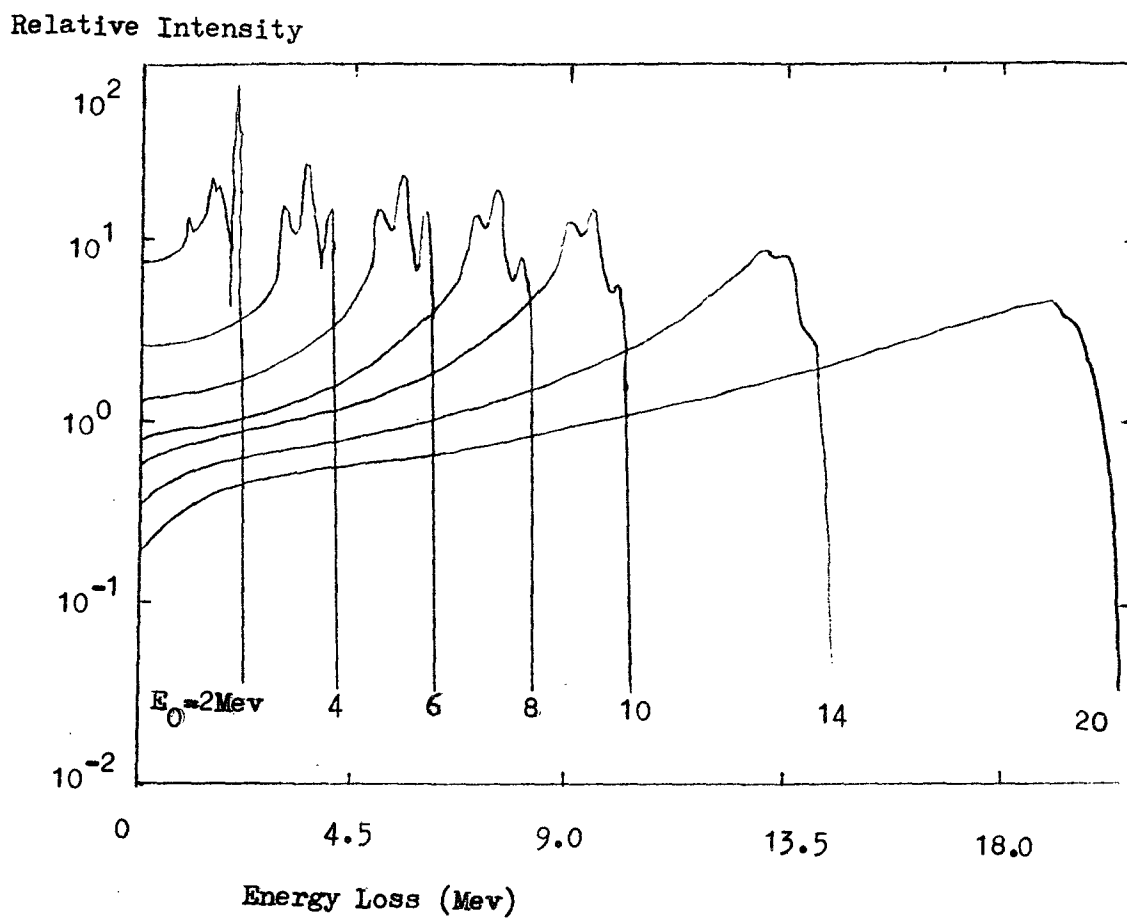


Diagram 4.3 Broad Parallel Beam Energy Loss Spectra for a 3" by 3" cylindrical NaI crystal generated by a Monte Carlo program by Berger and Seltzer (1972)

due to one band of incident photon energy, centred upon E_j .

To obtain the sum of the count contributions at a point E loss i on the energy loss spectrum due to all the photon energies E_j , $j=1$ to infinity, we sum up all the expressions like equation 1 until the contributions from higher and higher energies become so small as to be negligible.

Then the net number of counts at a point E loss i on the energy loss spectrum, due to the whole incident photon spectrum is given by

$$\frac{dN}{dE} (E \text{ loss } i) = \sum_{j=1}^{\text{effective infinity}} \frac{dN}{dE} (E_j, E \text{ loss } i)$$

Therefore

$$\frac{dN}{dE} (E \text{ loss } i) = \sum_{j=1}^{\text{effective infinity}} N(E_j) \cdot e_T(E_j) \cdot I(E_j, E \text{ loss } i) \dots (2)$$

Then it can be seen that $\frac{dN}{dE}$ photons of energy E_j around a narrow band dE wide, gives $\frac{dN}{dE} (E \text{ loss } i)$ counts at a point E loss i corresponding to the photopeak on the energy loss spectrum. Thus to convert from $\frac{dN}{dE} (E \text{ loss } i)$, which is the primary observational data, to $\frac{dN}{dE}$ of the original incident photon spectrum, we can use a conversion factor, R , where

$$R(E_j) = \frac{\frac{dN}{dE} (\text{photon})}{\frac{dN}{dE} (E \text{ loss})}$$

The energy loss conversion factors, R , were found for several different spectral indices, as described in the next section.

4.2 Energy Loss Conversion Factors for the LEG 4 Experiment

In the program, energy loss spectral data were only available for incident photon energies of 0.1 to 20 MeV. However, photons of higher energies than 20 MeV will contribute counts in the energy loss spectrum

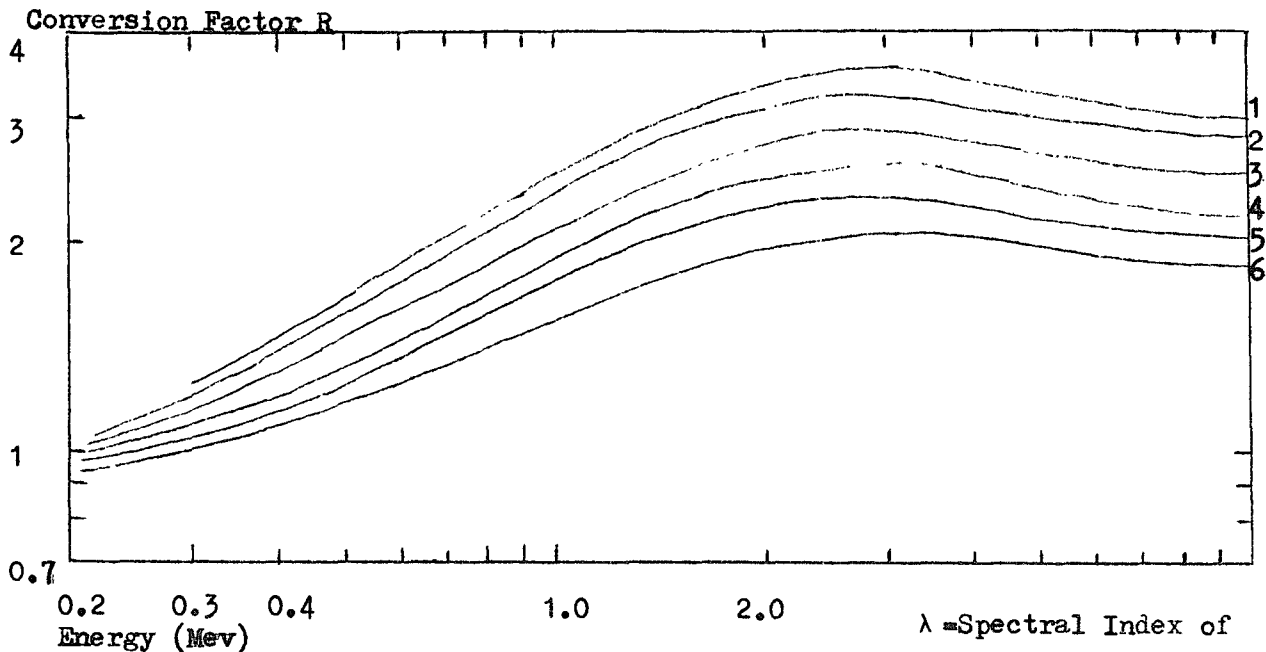
at lower energies than 20 MeV. To ensure that this contribution to the count rate due to higher energies than 20 MeV has a negligible effect on the accuracy of the conversion factors, only the conversion factors for the range 0.1 to 10 MeV were taken as accurate. This procedure is only applicable if the incident photons have a negative spectral index, giving decreasing photon numbers with increasing energy.

To find the variation of the factors, spectral indices of 1.5, 2.0, and 2.5 were used for both omnidirectional and broad parallel beams, for a 3 inch by 3 inch crystal. The omnidirectional case for $\alpha = 1.4$ was calculated to be used for the atmospheric gamma ray background. In addition, the program was run with a value of $\alpha = 2.3$, for use with the LEG 4 data obtained during the observation of the Crab Nebula. The results are shown in diagrams 4.4 to 4.5. In diagrams 4.5 and 4.6, the results of the latest work are compared with the conversion factors previously used for a similar detector to that of LEG 4 by Lovett (1973). Lovett used much wider energy bins for his summation of the spectrum. These bins were of the order 1 to 2 MeV wide. The latest results use bin-widths of only 0.025 to 0.1 MeV, and consequently should be far more reliable and accurate. In addition Lovett used the energy loss spectra of Berger and Seltzer in the form of idealised, hand-drawn graphs. The latest results were the numerically interpolated parameters calculated using a computer program, and for this additional reason the latest results should be far more accurate.

Nevertheless, the difference in conversion factors is at most a factor of about 1.5, within the limits of error quoted by R. Lovett for his approximations.

4.3 The Atmospheric Transition Curves

The atmospheric transition curves for the LEG 4 detectors are shown in diagrams 4.7 and 4.8. In addition the altitude of the balloon as a function of time is shown in diagram 4.9, and the count rate as a function of altitude, is shown in diagram 4.10. These count rates include the contribution from the Yttrium 88 in-flight gamma ray calibration source. Pre-flight tests showed that the Yttrium 88



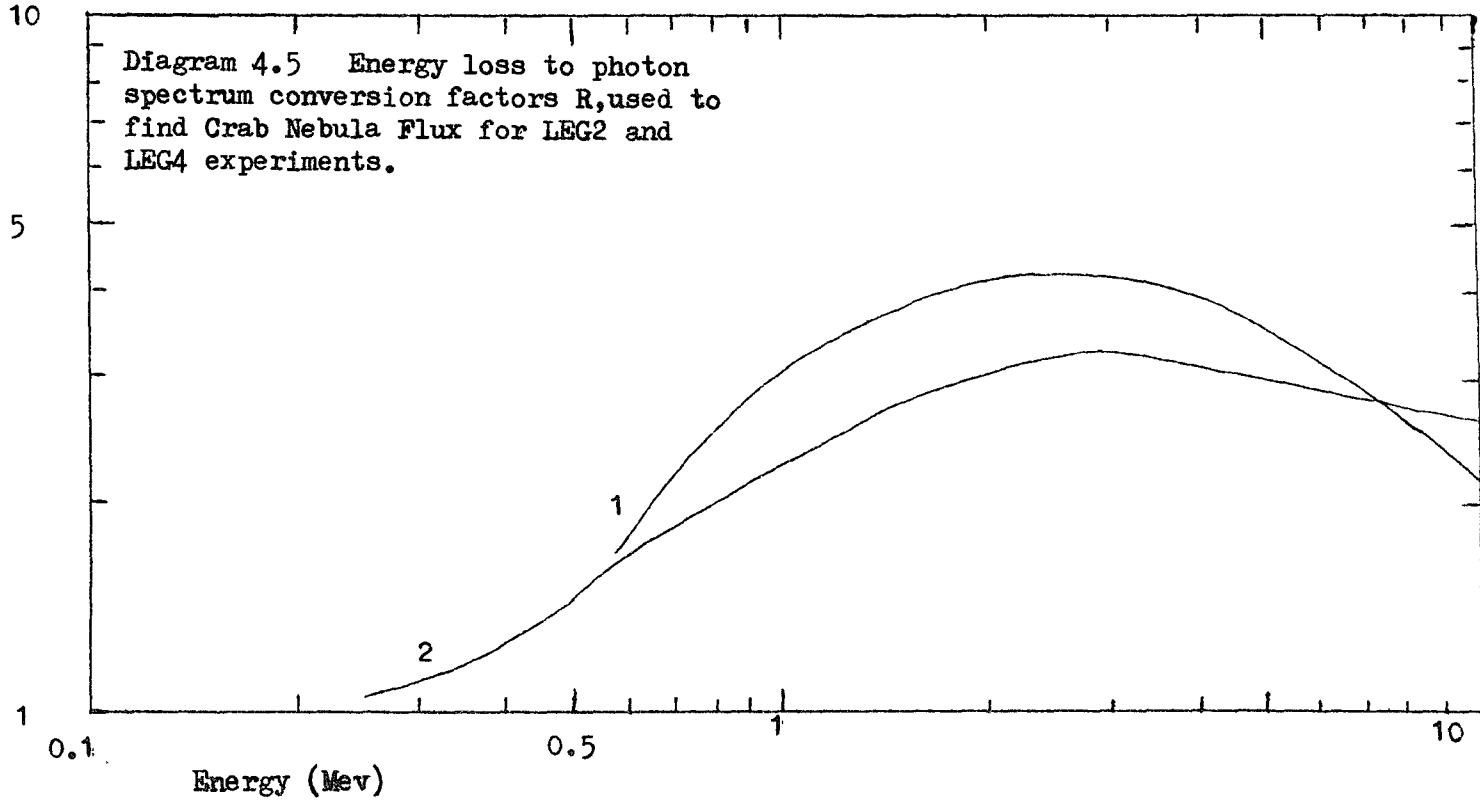
Omnidirectional Flux { $\lambda=2.5$...1
 { $\lambda=2.0$...2
 { $\lambda=1.5$...3

 Broad Parallel Beam { $\lambda=2.5$...4
 { $\lambda=2.0$...5
 { $\lambda=1.5$...6

λ = Spectral Index of Incident Photons

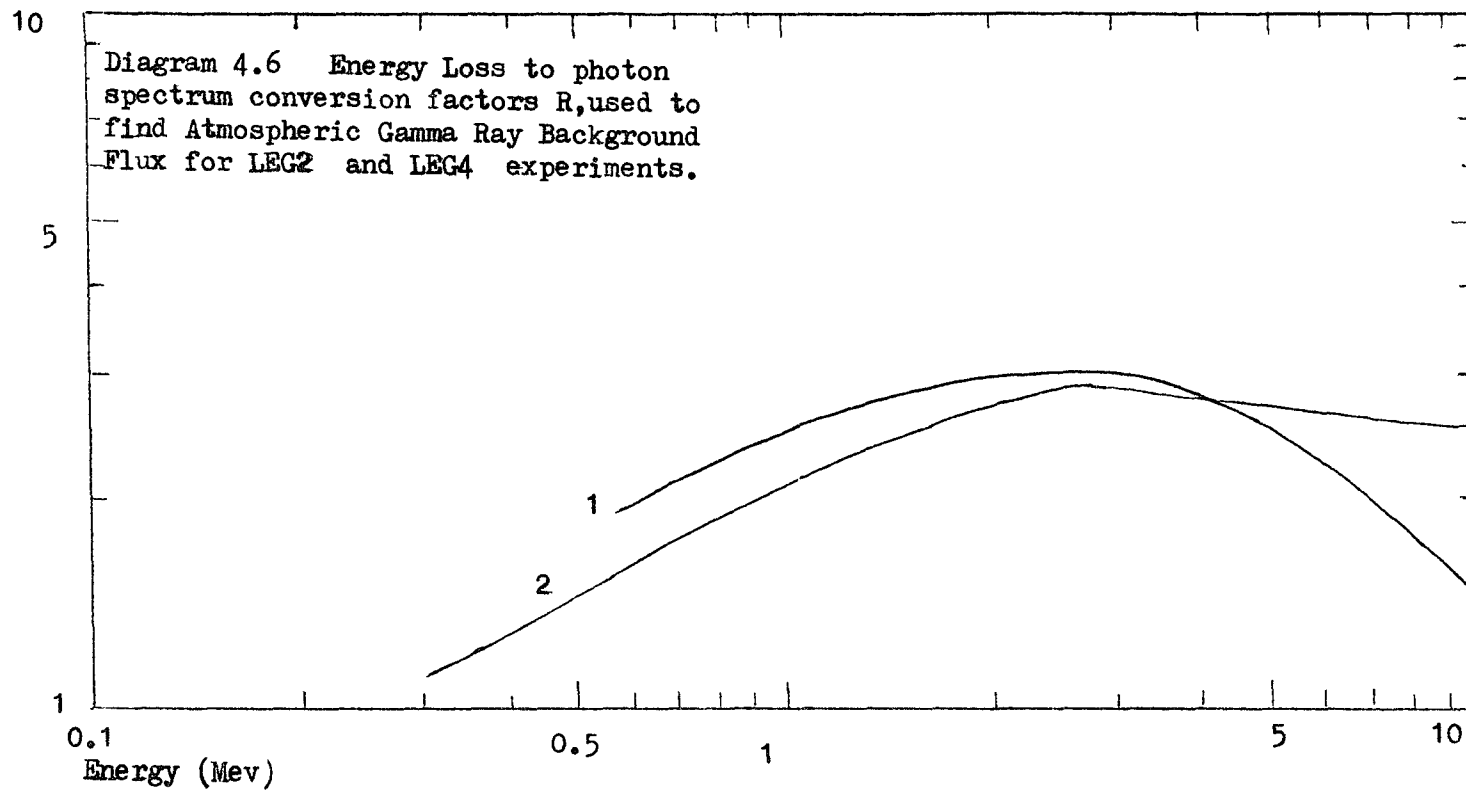
Diagram 4.4

Conversion Factor R



- 1.... Results of Lovett (1973) for an E^{-2} photon a spectrum.
- 2.... Present Results for a broad parallel $E^{-2.29}$ photon spectrum.

Conversion Factor R



- 1.... Results of Lovett (1973) for an $E^{-1.5}$ photon spectrum.
- 2.... Present Results for an omnidirectional $E^{-1.39}$ photon spectrum.

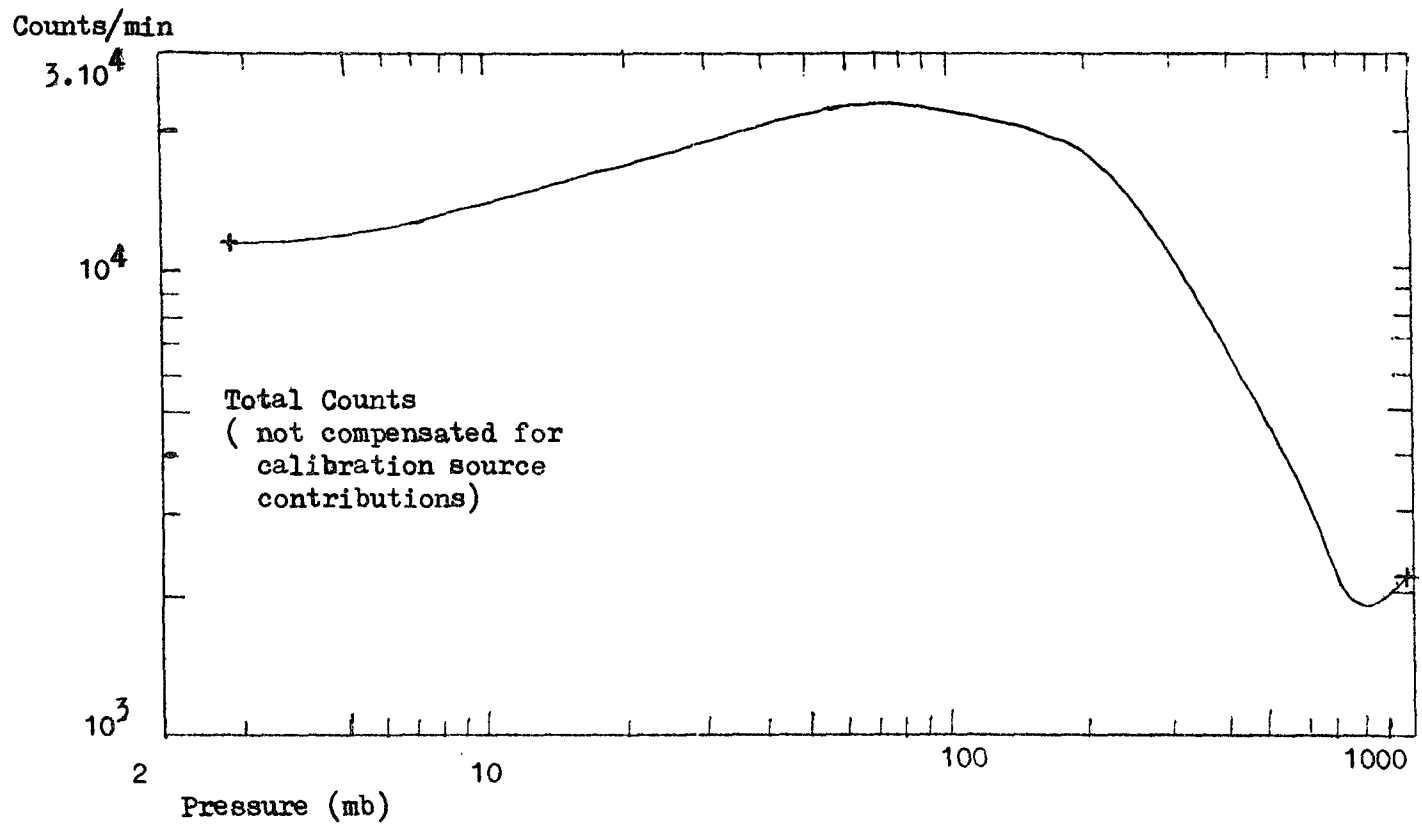
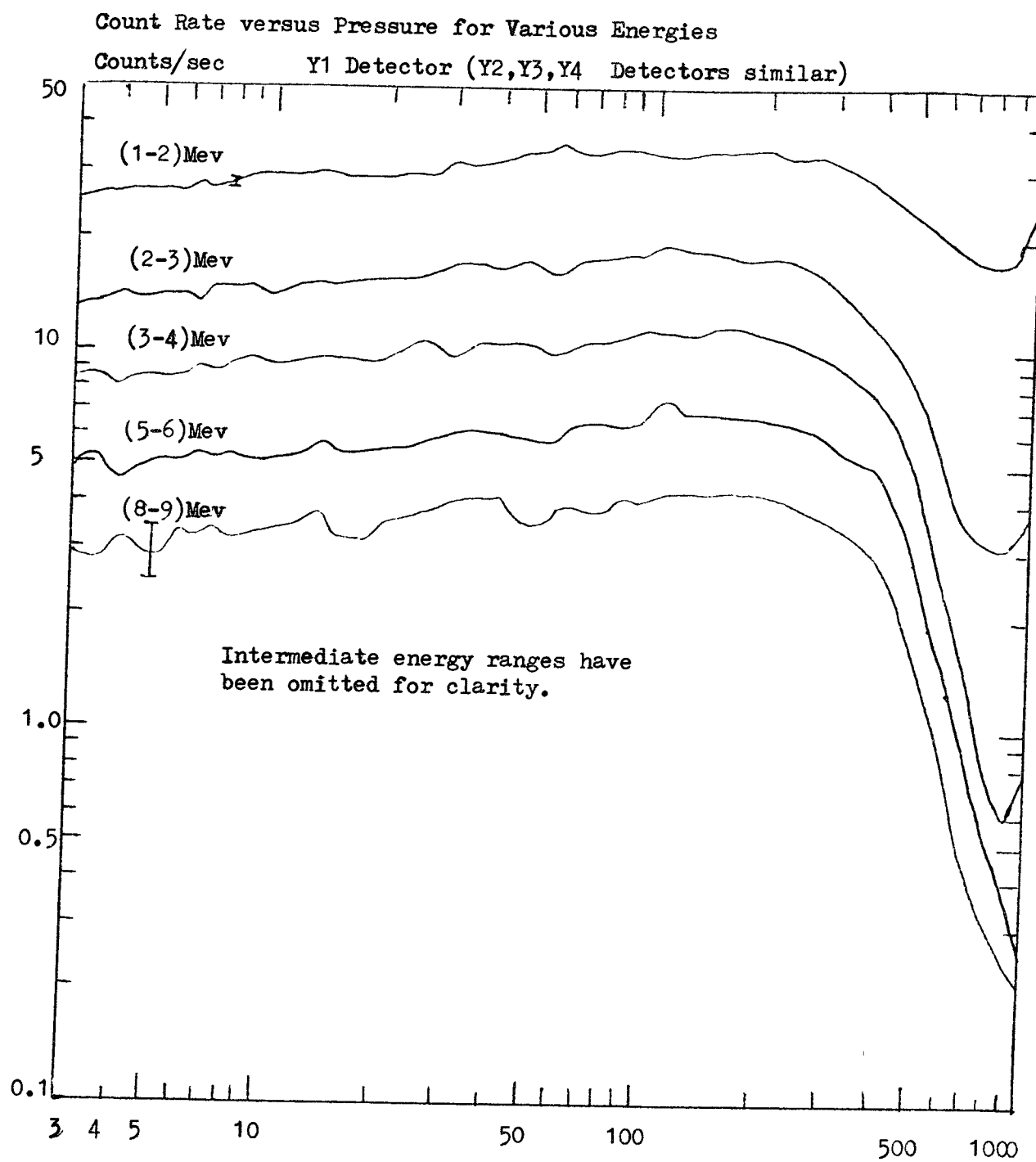
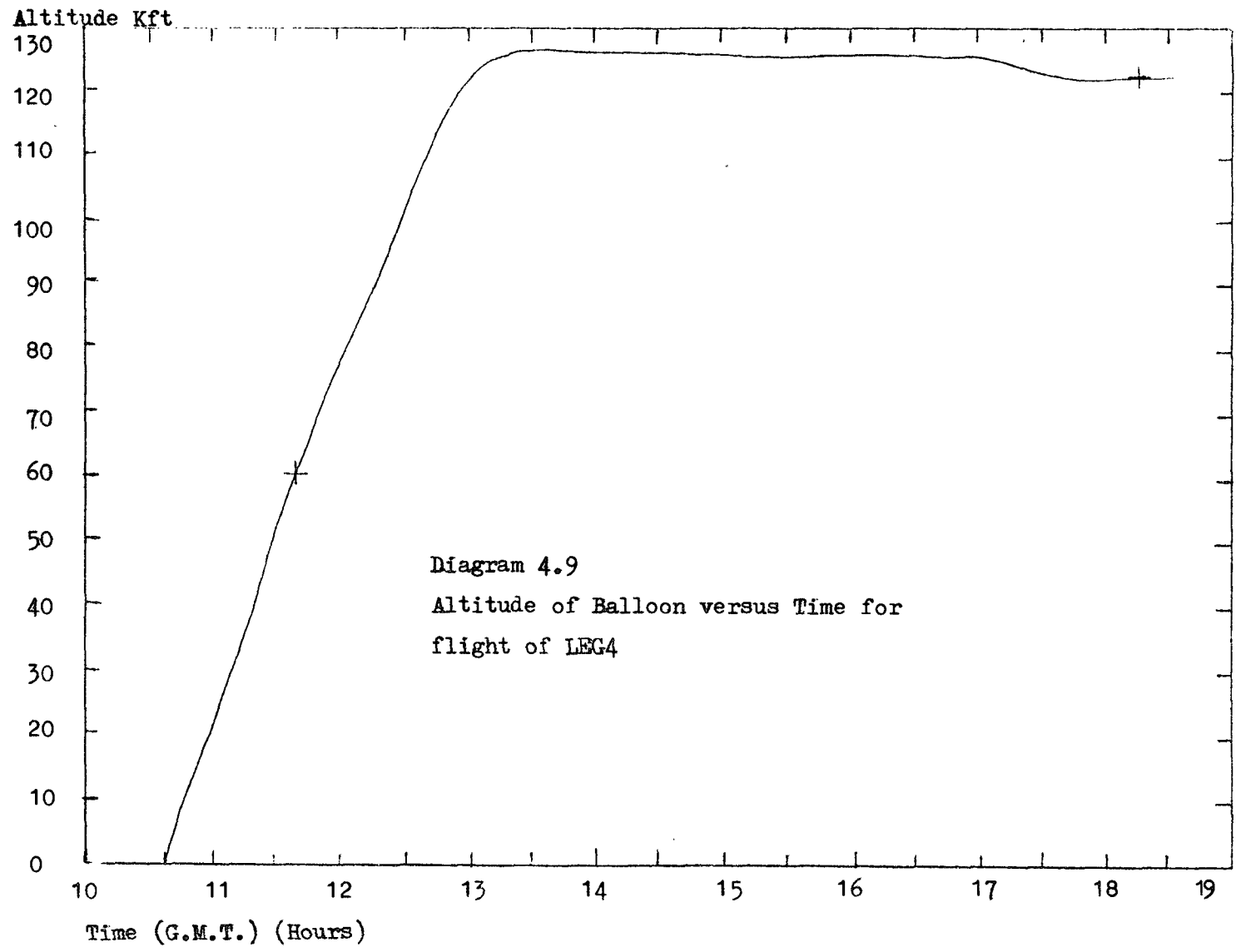


Diagram 4.7 Counts/min versus pressure for Y1 Detector. (other 3 detectors similar)

Diagram 4.8





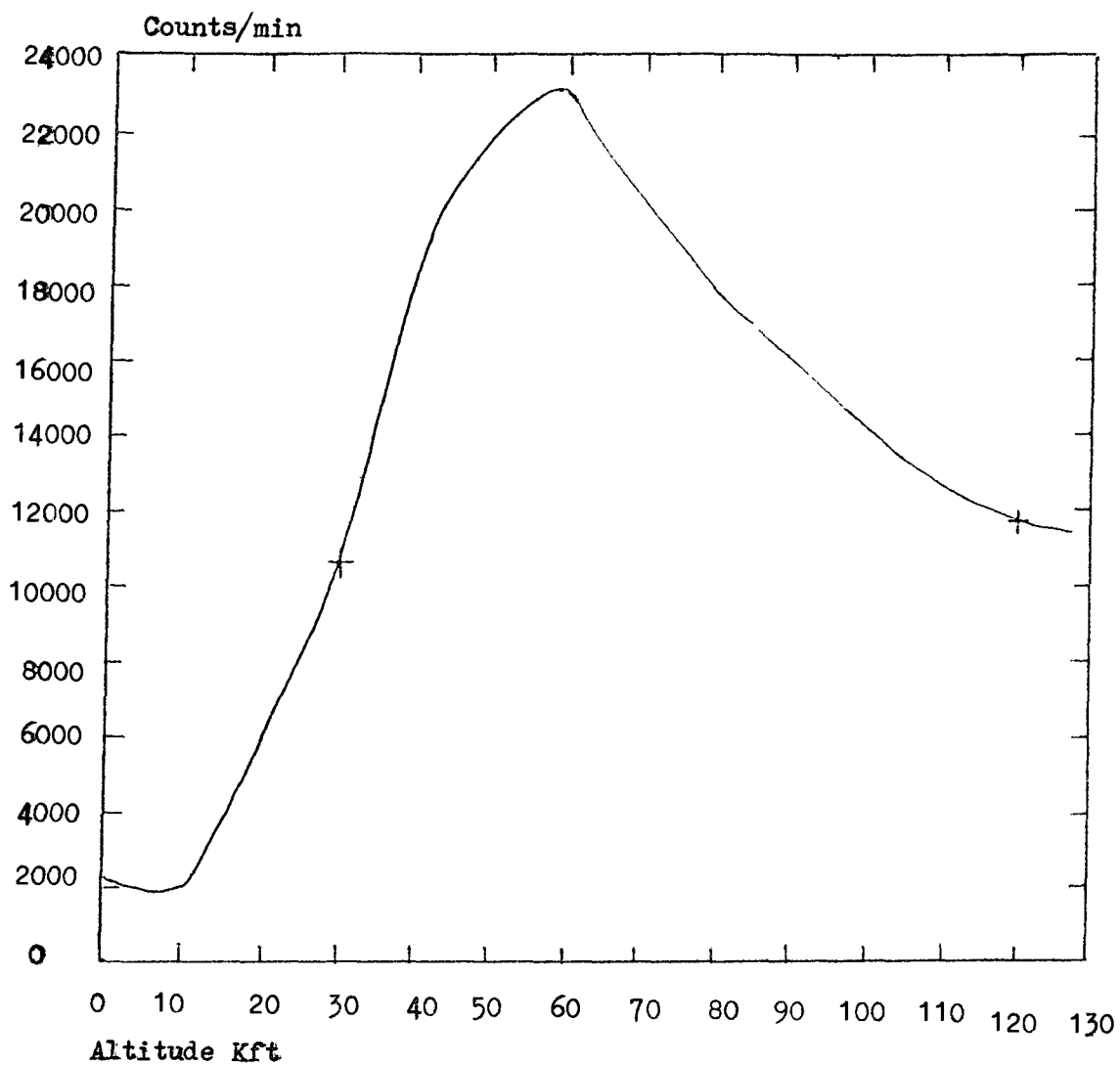


Diagram 4.10

Counts/min versus Altitude Y1 Detector (Other 3
detectors similar

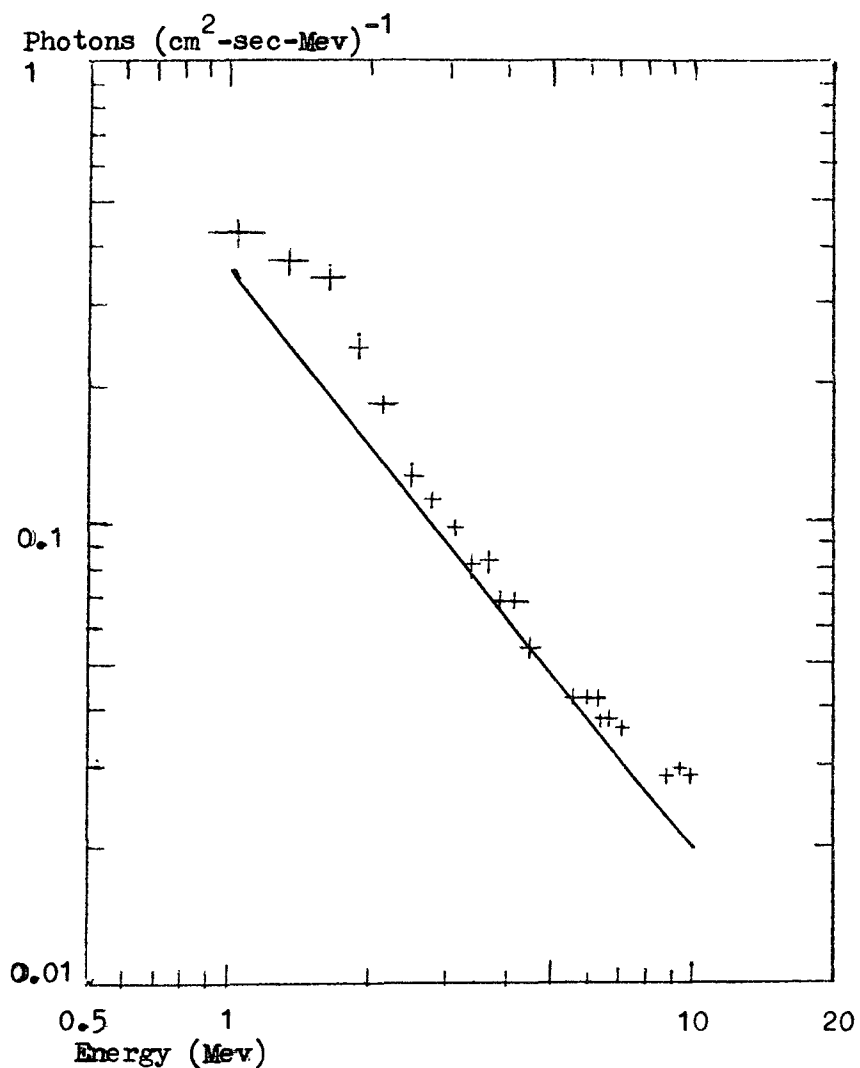
produced a count rate of 30 per second for all energies above 0.66 MeV in each of the 4 detectors. The Yttrium 88 should not affect the spectrum for energies greater than approximately 1.9 MeV, because its highest significant energy is around 1.836 MeV.

The main features of the graphs of count rates versus pressure can be interpreted as follows. The observed gamma rays are secondary photons resulting from cosmic ray interactions. There is an exponential decrease with increasing depth of the number of primary cosmic ray interactions, and hence the number of first generation electrons and photons produced also decreases exponentially. An electromagnetic cascade then results. Early on in the cascade, the high energy photons and electrons interact mainly through bremsstrahlung and pair production, resulting in many lower energy electrons and photons. In such a way, the photon flux increases with depth up to the so-called Pfofzer maximum. Below this Pfofzer maximum, because the energies of the particles are lower, energy absorptive-type interactions become more dominant, and the cascade gradually fades exponentially. At greater depths than 800 mb the photon flux again increases due to natural radio-activity from the earth. A more detailed discussion of the background flux is given by Ling (1874).

The results agree with those of other experimenters. (Lovett, 1973).

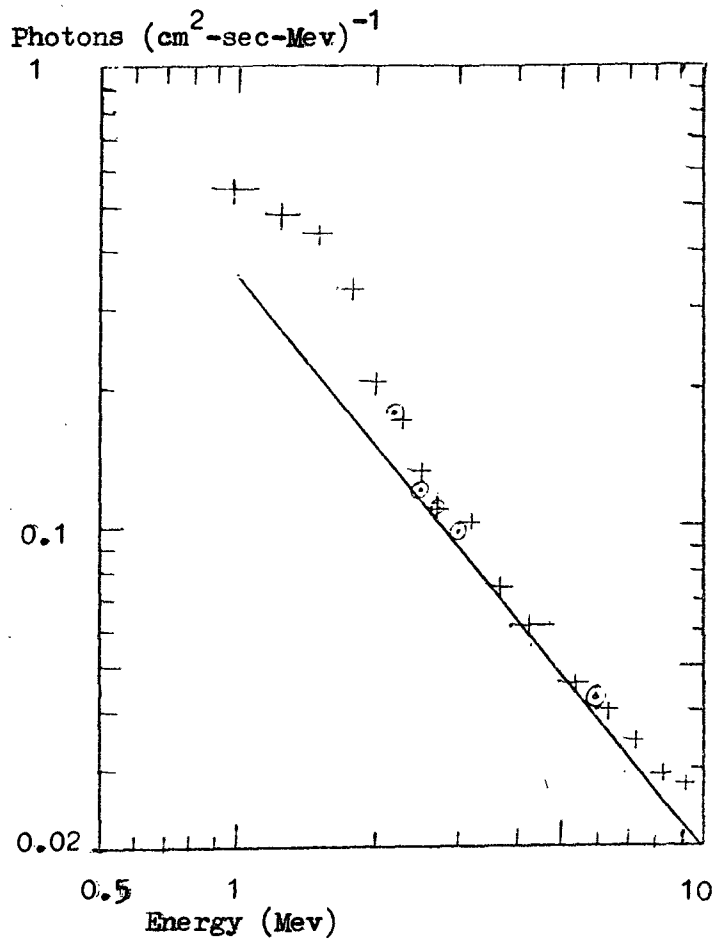
4.4 The Atmospheric Gamma Ray Background

It may be noted in diagram 4.8, a graph of count rate with pressure for different energies, that the counting rates for the different energy channels are approximately parallel above the Pfofzer maximum. This is evidence that the shape of the energy loss spectrum does not change significantly above the Pfofzer maximum. The resulting energy loss spectrum obtained in the LEG 4 flight at a depth of 3.2 gm cm^{-2} is shown in diagrams 4.11 and 4.12. For comparison, the results of other experimenters are shown in diagram 4.13. The energy loss spectrum is shown for all 3 detectors together and for Y4 detectors alone. In addition, portions of data used to find the pulsar flux were used to find the atmospheric flux as a check of the analysis procedures for those aspects of the data. The effect of the Yttrium 88 in-flight calibration source can be clearly seen up to about 1.8 MeV, as expected.



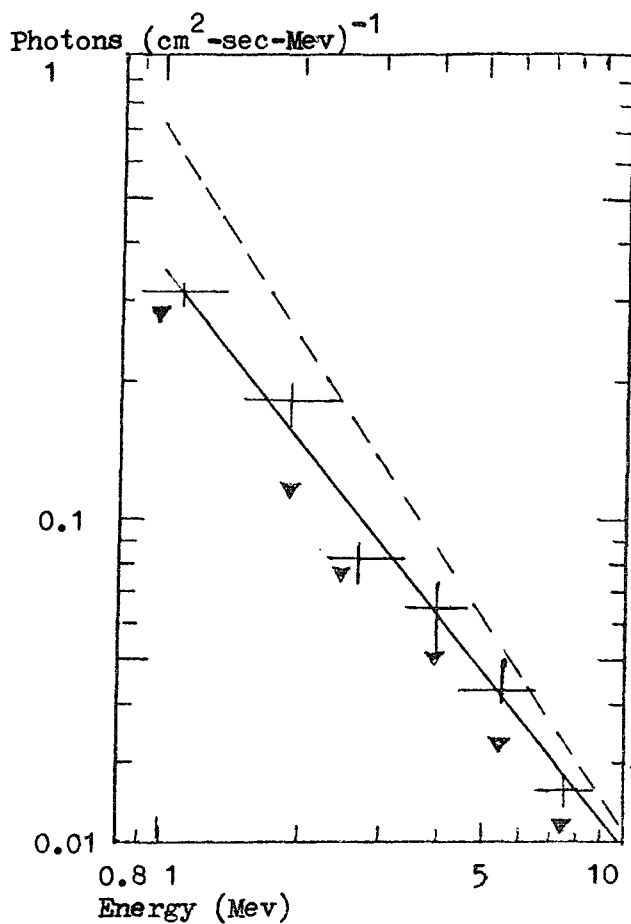
The crosses are the background flux obtained from the background periods used in the analysis to find the total flux from the Crab Nebula. The line is the best fit line to the results of Lovett (1973).

Diagram 4.11 Energy Loss Spectrum for the Atmospheric Background, including the contribution from the Yt^{88} calibration source, using the data from the Y1, Y3, Y4 detectors, at 3.2 g cm^{-2} .



Crosses are the atmospheric background flux obtained using the data of the Y4 detector only. Y1, Y3 similar. The line is the best fit line to the results of Lovett (1973). The circles are the flux obtained using the data of the Y1, Y3, Y4 detectors which was used in the analysis for the pulsed flux from the Crab Nebula.

Diagram 4.12 Energy Loss Spectrum for the Atmospheric Background, including the contribution from the Yt^{88} calibration source, at 3.2 g cm^{-2} .



Crosses.....LEG2 experiment ,Lovett (1973),normalised
from 13 g cm^{-2} .

Triangles.....Peterson,Matteson,Pelling,1972,normalised
from 3.5 g cm^{-2} .

Solid line.....Best fit line to the results of Lovett (1973)

Dashed line.....Best fit line to a selection of other
results (Orford,1973,private communication)

Diagram 4.13 Energy Loss Spectrum for the Atmospheric
Background at 3.2 g cm^{-2} .

Different results have been compared by being normalised to 3.2 gm cm^{-2} from the depths at which their experiments were actually conducted. This normalisation uses a depth dependence formula of:

$$\frac{N_1}{N_2} = \left(\frac{x_1}{x_2} \right)^{0.4}, \quad \text{where } N_i \text{ is the count rate at}$$

atmospheric depth of x_i . The energy loss spectrum has been treated such that it has been normalised to that for an isotropic flux crossing 1 cm^2 using a so-called omnidirectional factor G_0 , which is the effective area of the detector for an assumed isotropic flux. This was calculated by using the formula:

$$G_0 = \frac{\pi D l}{4} \left(1 + \frac{D}{2l} \right) \text{ cm}^2, \quad \text{where } D \text{ is the diameter, and}$$

l the depth of the crystal. For each detector in the LEG 4 experiment G_0 is 110 cm^2 . As can be seen, comparison with the best fit line of Lovett's results from the LEG 2 flight shows a very close correlation. This is to be expected, especially since the LEG 4 detectors were very similar to the LEG 2 detectors.

Using the conversion factors described in the previous section, the photon energy spectrum can be derived from the energy loss spectrum. The photon energy spectrum of the atmospheric background at 3.2 gm cm^{-2} is shown in diagram 4.14. It should be noted that the energy loss to photon energy conversion factors used for LEG 4 are more accurate than those used by Lovett. The new conversion factors are generally a factor of not more than 1.5 larger than the old factors. Consequently, despite the recalculation of the conversion factors, the spectrum is still in good agreement with other experimenters results. As in the energy loss spectrum, a slight excess over the smooth spectrum is to be seen at energies less than about 1.8 MeV. This, as expected, should have been due to the Yttrium 88 in-flight calibration source. It may be noted, diagram 4.13, that Peterson's results (Peterson, Pelling, Matteson, 1972) were also obtained at the location of Palestine, as were Lovett's LEG 2 results and these latest LEG 4 results.

It was observed during the analysis, that when the charged particle shield around the detectors had been switched off in flight as a test, that no significant reduction in count rate took place. This evidence indicates that this shield was not functioning. A similar test by

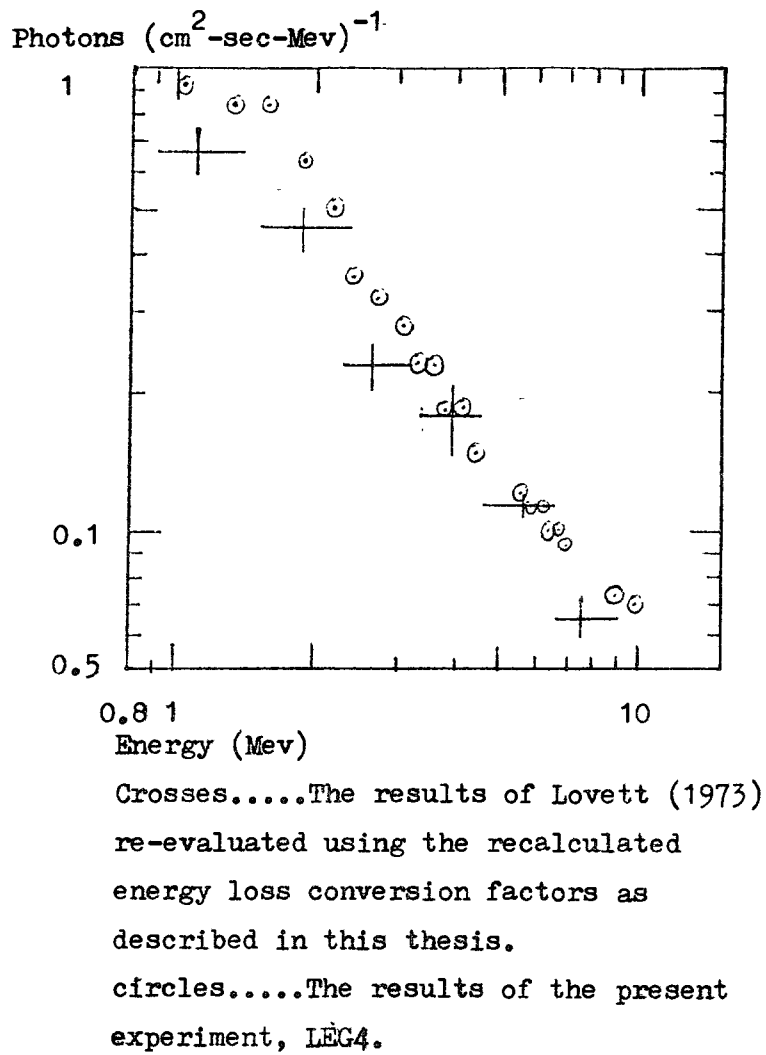


Diagram 4.14 The Photon Energy Spectrum
of the Atmospheric Background at 3.2 g cm^{-2} .

R. Lovett on the LEG 2 data appeared to show that the exactly similar charged particle shield was working on LEG 2, because it produced, approximately, a 30 per cent reduction in count rate when switched on. So, strictly speaking, the LEG 4 results for the photon energy spectrum of the atmospheric background should be reduced by about 30 per cent, due to the presence of charged particles. Taking this reduction into account, the agreement between the LEG 4 experiment and the LEG 2 experiment can be seen to be close.

It is of interest to compare the LEG 4 and LEG 2 experimental results with those of other experimenters, as shown in diagram 4.15. Noting that 4π steradians = the total solid angle, the results of the LEG 4 and LEG 2 experiments may be divided by the appropriate factor for comparison with the other results. An additional compensating factor to take into account is that the LEG 4 and LEG 2 results are presented at a depth of 3.2 g cm^{-2} , whereas the other results are presented at a depth of 3.5 g cm^{-2} .

It is of interest to examine the observations of Schönfelder et al. (1977) of the diffuse cosmic gamma ray flux in relation to the atmospheric gamma ray background (diagrams 4.16 and 4.17).

Although LEG 2 and LEG 4 experiments were not designed to measure the atmospheric and cosmic diffuse background, the results here may have a useful part to play in future such measurements by giving estimates of the background count rate in future detector systems.

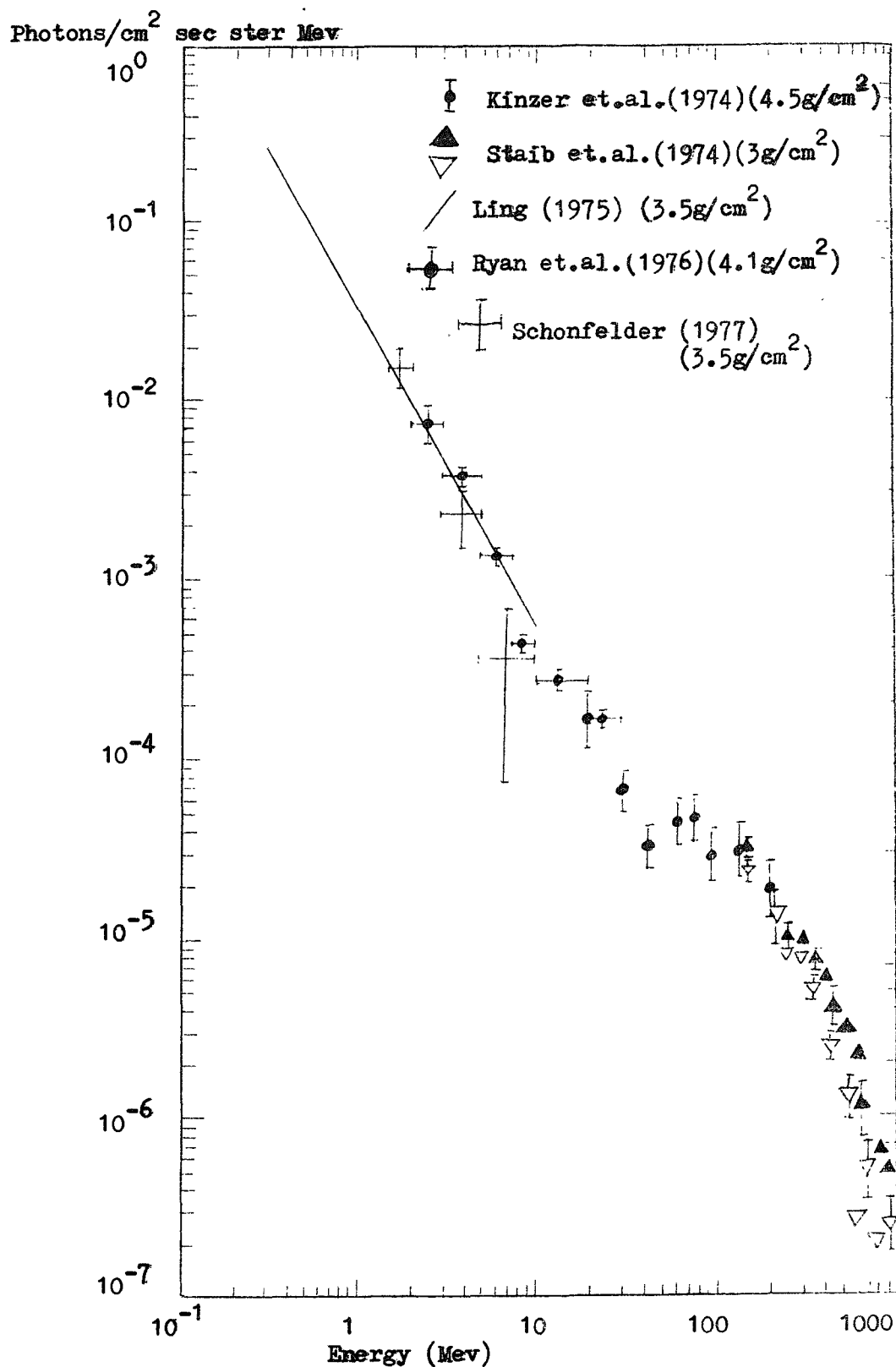
The results of the LEG 4 background measurements serve as a good check of the energy calibration, and the energy loss to photon spectrum conversion factors, used in the analysis of the Crab Nebula and Pulsar data.

Although the LEG 4 experiment could not measure zenith angle variations in the background, it is of interest to note the results of Schönfelder (1975), the semi-empirical model of Ling (1975), and the theoretical model of Schönfelder (1977), as in diagram 4.18.

4.5 The Search for a Gamma Ray Burst in the LEG 4 Data

Because the discovery of gamma ray bursts was first published in 1973 (Klebesadal, Strong and Olsen, 1973), the LEG 4 experiment was not designed to detect gamma ray bursts. However, with the publication of

Diagram 4.15



Total Gamma Ray spectrum (atmospheric and cosmic) at atmospheric depth 3.5g/cm². Measurements that were performed at depth t (g/cm²) were multiplied by $3.5/t$ in order to make them comparable.

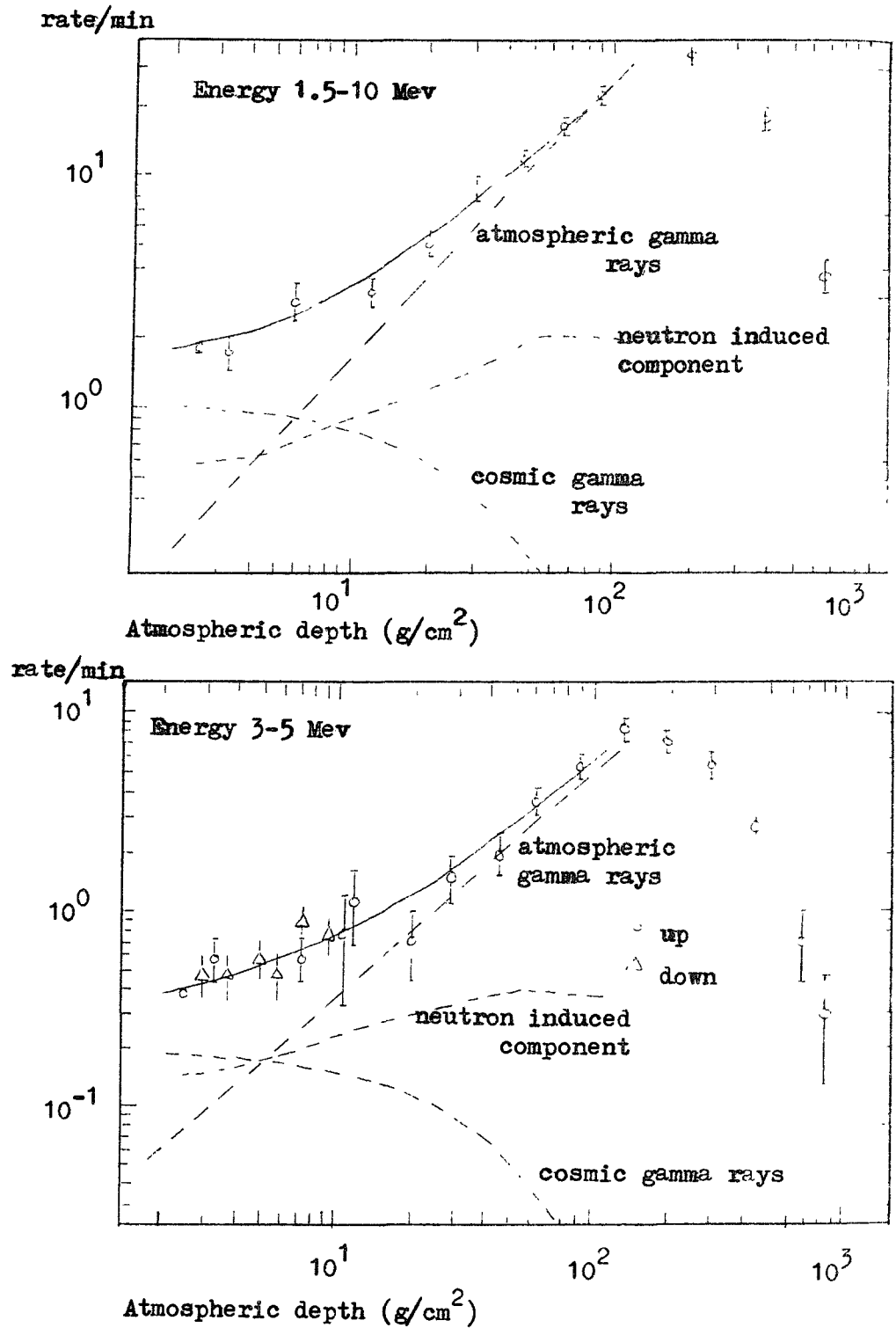
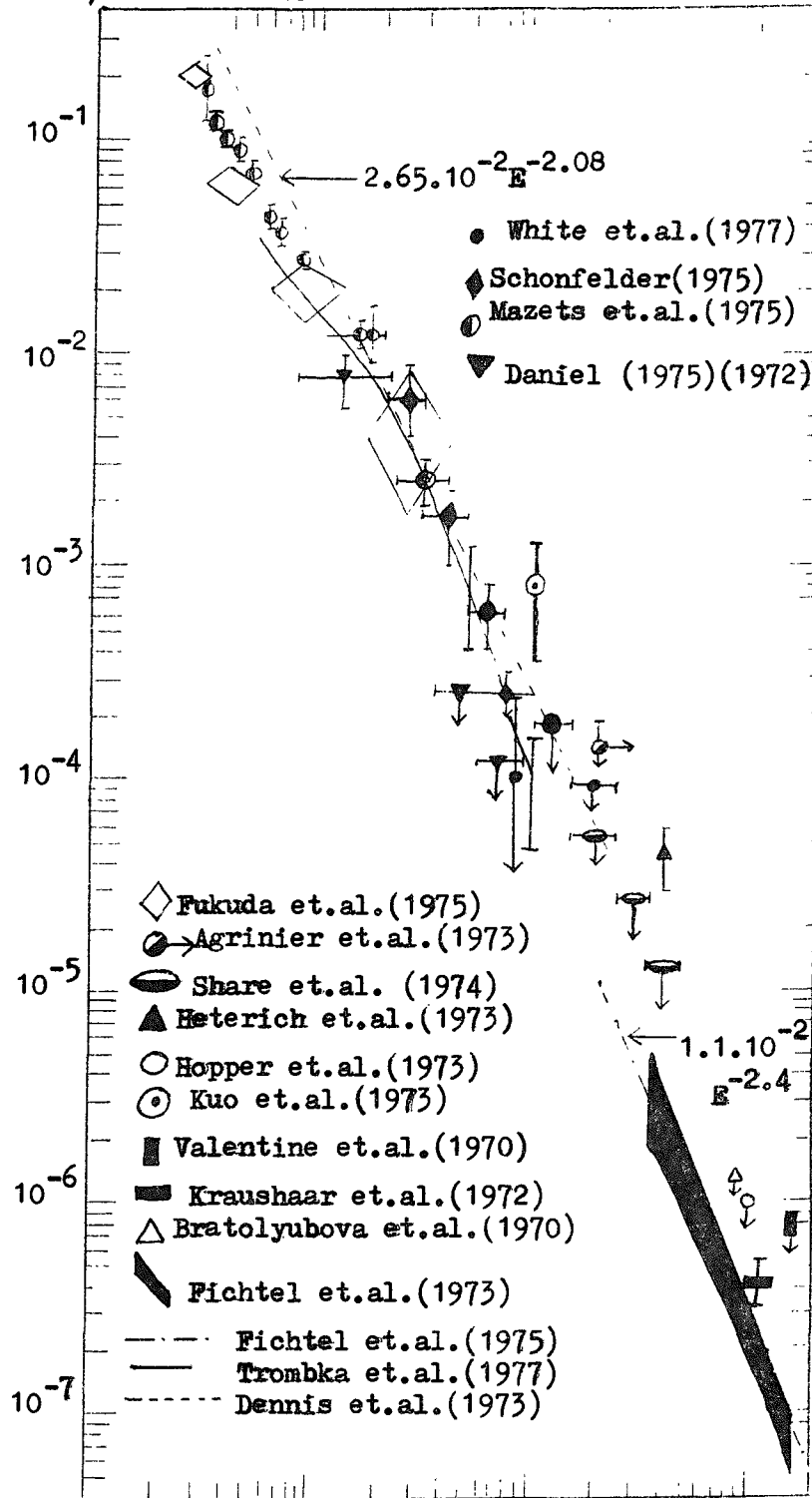


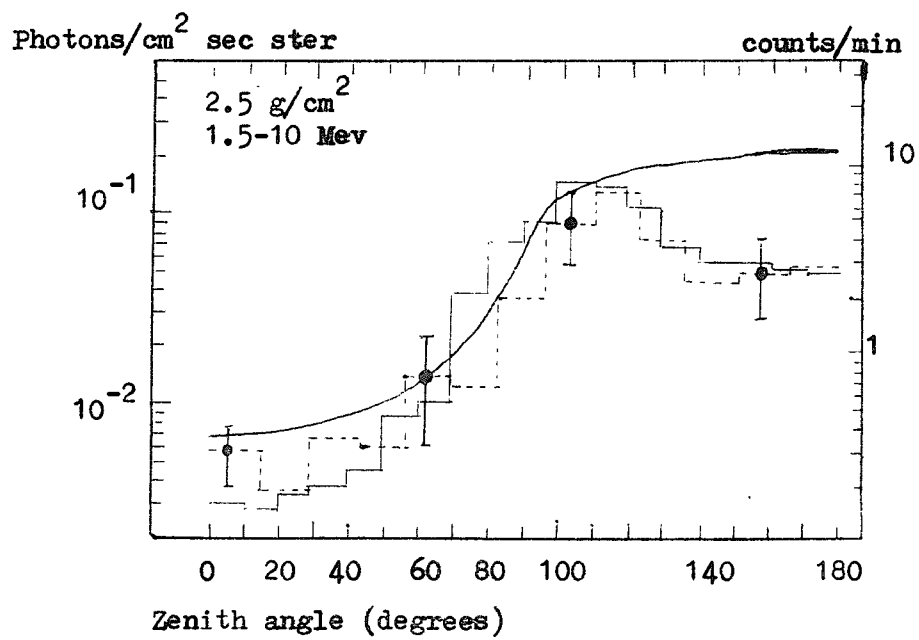
Diagram 4.16 Growth curves of the counting rate (from Schonfelder et.al., 1977)

Photons/cm² s ster Mev



Gamma Ray Energy (Mev)

The cosmic diffuse flux of gamma rays.
Diagram 4.17



—●— Schonfelder et.al. (1977)

— Ling (1975)

— Schonfelder (1976)

Zenith angle distribution of atmospheric gamma rays
(from Schonfelder et.al 1977)

Diagram 4.18

observations of gamma ray bursts, it was realised after the flight that a search of the data for a gamma ray burst might prove fruitful. In addition the gamma ray energy spectrum of gamma ray bursts was not well known and so a gamma ray burst detected by LEG 4 would have provided valuable spectral information.

A first burst search looked at each of the four detectors individually but with no energy discrimination. In other words, the total count rate for gamma rays of energies greater than about 0.66 MeV was investigated. From the limited results published at the time of the first burst search program (late 1974), it could be seen that typical bursts were of duration 10 seconds or less. Consequently, it was decided to use 5 second and 1 second sampling intervals to search the data for a possible gamma ray burst. One possible criterion for searching for gamma ray bursts is the method used for the LEG 4 data, as follows.

For the data of each detector, the number of counts in 5 seconds, N was compared with the counts of the previous 5 seconds, N_p , in such a way that if the magnitude of the quantity S , given by $S = (N - N_p) / (N_p)^{\frac{1}{2}}$ exceeded 2, then the magnitude of S , whether positive or negative, the time it occurred, and the detector in which it occurred was recorded.

It can be seen that S should record either sudden increases or decreases in count rate. The reasoning behind investigating the detectors separately was that a true gamma ray burst would be expected in all four detectors at once unless, of course, the burst had come from the Crab Nebula, in which case only the two detectors which were unoccluded at the time would register the burst.

At the same time as the 5 second sampling, in addition, the counts in one second, N_1 , were compared with the average of the previous 5 seconds, $\frac{N_5}{5}$, such that

$$S = \left(N_1 - \frac{N_5}{5} \right) / \frac{N_5}{5}^{\frac{1}{2}}$$

Again, if S was greater than 2, the magnitude and time of occurrence of this value of S , and the detector number was recorded.

Several apparent gamma ray bursts, selected by this first program, turned out to be due to synchronisation loss in the PCM telemetry system. These were easily identified by examination of the data block times.

A second, more detailed burst search program split the energies of the gamma rays into ranges of 0.898 to 2.0 MeV, 2.0 to 4.0 MeV, and 4.0 to 12.0 MeV. Because the energy discrimination system for the Y2

detector was found to be faulty, this detector was not used, and only the remaining three were analysed. In addition, the telemetry system was capable of registering the energy of only about one half of the gamma rays recorded (timing data being available for all the gamma rays recorded). This meant that the energy-discriminated counts had a greater statistical uncertainty than the total counts.

To create a statistically smoother picture, the new search program compared the number of counts in one time bin, N_1 , with the counts in the previous 40 time bins, N_{40} . So the quantity, S , was now generated by the equation:

$$S = (N_1 - N_{40}/40)/(N_{40}/40)^{\frac{1}{2}}$$

The length of the bin was set at the values:

0.125 seconds

0.25 seconds

0.375 seconds

1.0 seconds

5.0 seconds

and 10.0 seconds

to give varying time resolutions for different durations of a possible gamma ray burst. The value of S was then calculated for each time resolution value, for each detector, for each energy, and for all three detectors together, and for the first two energy ranges together, i.e. 0.898 to 4.0 MeV.

This more detailed analysis failed to reveal any significant features. Consequently, it was concluded that no gamma ray burst had been observed. One aspect of significance that arose out of the search program, however, was that it was noticed that there appeared to be some small correlation between the occurrence of some slightly significant features and the times when the lead occulting discs were moved during the flight. It was concluded that these features represented electromagnetic interference from the paddle motors when they were switched on. As a result, all data around each time the motors were on, was subsequently ignored for the Crab Nebula and Pulsar analyses.

From the larger volume of results on gamma ray bursts, published since the first and second gamma ray burst search programs, the null result can be placed in the context of the probability that the LEG 4 experiment could have detected a gamma ray burst. A description of

other results and theories on gamma ray bursts has been given in section 1.6.

Approximately 6 hours of the LEG 4 data was available for analysis for gamma ray bursts. The instrument has already been described in chapter 3. An important feature with respect to the detection of gamma ray bursts is that LEG 4 comprised 4 relatively large unshielded detectors. The 4 detectors had 2 separate HT supplies, one for each pair. This meant that most spurious events could be eliminated by the condition that corresponding increases and decreases in count rate occurred in more than one detector at a time.

Assuming a burst spectrum similar to that of the 27th April 1972 event detected by Apollo 16 (Matteson et al.1974) as being typical, and a burst duration of 1 second, then a gamma ray burst giving an excess greater than 3σ in the LEG 4 experiment for energies greater than 0.66 MeV, would have had a time integrated flux density, S , greater than 1.6×10^{-6} ergs/cm². No candidate burst event was found in the entire data. Consequently, the LEG 4 experiment places an upper limit of 5.8×10^3 bursts per year, N , of time integrated flux density, S , greater than 1.6×10^{-6} ergs/cm² for energies greater than 0.66 MeV. This upper limit and the results of some other experiments in the log N - log S distribution are shown in diagram 4.19.

It can be seen that the LEG 4 upper limit is very similar to those of Cline et al.1976 and Johnson et al.(1976), and is consistent with the other experimental results. Also shown in diagram 4.19 are the size distributions of indices of 0.5, 1.0 and 1.5. The number index is expected to depend upon the spatial distribution of sources, as discussed by Fishman et al.(1978). The integral size distribution above 10^{-4} ergs cm⁻² follows an $s^{-1.5}$ law, suggesting an isotropic, extragalactic distribution of the sources. However, for events with an energy less than 10^{-4} ergs cm⁻², the observed distribution appears to flatten out and the choice of number index ($\alpha = 0.5, 1.0$ or 1.5) in this region is less clear.

The LEG 4 upper limit lies above all 3 predicted size distributions and so it does not discriminate between the three. However, future flights of similar unshielded anti-collimated detectors, although basically designed for cosmic point source measurements, may be able to place further constraints on the theoretical size distribution of gamma ray burst sources with flights of longer duration. The extra duration could be achieved with the use of a Transatlantic balloon facility,

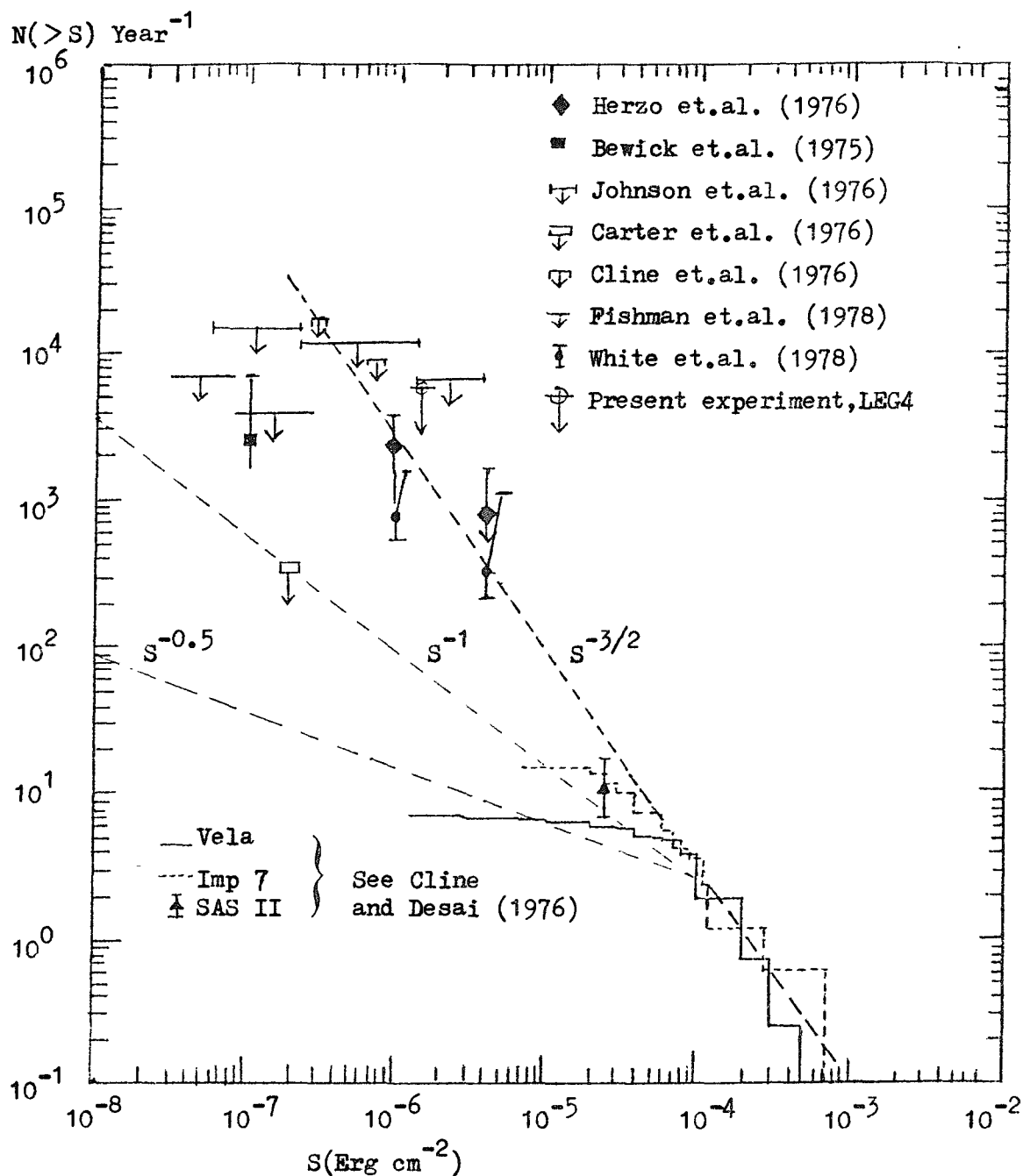


Diagram 4.19 The size distribution of gamma ray bursts.

as used by Carter et al.(1976), or by a satellite mounted experiment.

Chapter 5 - Analysis for Gamma Rays from the Crab Nebula Region

5.1 The Method of Analysis for the Total Flux

During the period of observation, the telescope axis was directed continuously at the Crab Nebula for three hours. Approximately once every 5 minutes the two lead occulting discs were rotated through 90 degrees about the telescope axis. In this way, each detector was first exposed to the source, and then shielded from the source for equal periods of 5 minutes. The difference between the number of counts accumulated during a period of exposure (ON state) and that during an equal occulted period (OFF state), should be due to the source.

In the case that the source is sometimes incompletely occulted during the "OFF" states, due to steering off-axis, the effective area of exposure was calculated every 0.5 seconds, as a function of the altitude data.

In order to avoid spurious variations due to electromagnetic noise pick up from the motors which rotated the discs, sections of data, within 10 seconds earlier or later than each motor switch-on command, were not used in the analysis.

Two data sets were recorded. One set contained the integral number of counts, the second set contained the spectral information, and comprised half the number of counts of the first set.

5.2 The Results of the Observations of the Crab Nebula by LEG 4

In the analysis, it was observed that one of the four detectors, the "Y2" detector, exhibited large fluctuations in count rate within any particular energy interval, although the total count rate (all energies) remained consistent with the smooth variations of the remaining three detectors (Y1, Y3, Y4).

Consequently, it was decided that the energy discrimination system for the Y2 detector was unreliable, and the Y2 detector was subsequently disregarded in the analysis. However, it may be noted in passing that the total counts in Y2 showed a positive excess consistent with a source

in the Crab Nebula.

When control was handed over from Palestine to the downrange station at Midland, steering control was lost. Consequently, no useful data on the Crab Nebula could be obtained from the Midland station. Timing data existed for the Midland Data, but the absolute phase was not related to the previous data recorded at Palestine. Because the length of the Midland data was less than that recorded at Palestine, only the Palestine data was analysed for the Crab Nebula and its Pulsar.

The results for the Crab Nebula flux are shown in Table 5.1. It may be noted that the Y1, Y3 and Y4 detectors were used for all energy ranges in the table, except the first (0.4 to 0.9) MeV range, for which Y4 had too high a threshold. Consequently, all ranges have a factor NEA, of 1575.25 seconds, except for the first range which has a factor of 1,005.7 seconds, where NEA is the time of exposure times the effective area factor.

In addition, the flux values of the LEG 2 experiment of R. Lovett (see Baker, Lovett, Orford, 1973) have been re-evaluated, using the improved energy loss to photon energy conversion factors described in the previous chapter (see table 5.2).

Many other energy bin sizes were tried, but no really significant features, suggesting gamma ray lines, were found.

The results of the total (all energy ranges together) excess counts for each of the 3 detectors analysed are shown in table 5.3. It may be noted that Y4 has a larger number of background counts than Y1 and Y3. This is because the portion of data used for the Y4 detector was slightly longer than the Y1 and Y3 detectors, which were in the "opposite phase" to Y4 as regards being occulted or non-occulted from the Crab.

The results are plotted and discussed in the next chapter in relation to the NPO532 pulsar results and the results of other experimenters.

Having given the results of the analysis for the total flux from the Crab Nebula region, the analysis and results for the pulsar NPO532 are discussed in the next two sections.

5.3 The Method of Pulsar Phase Analysis

The timing was provided by a crystal clock at the balloon launch station at Palestine. This clock was nominally accurate to 1 part in 10^7 , and it was synchronized with the WWV clock at Boulder, Colorado, at

Table 5.1 Gamma Rays from the Crab Nebula

Area A of each crystal = 132.75 cm²

Energy (MeV)	0.4 - 0.9	0.9 - 2.3	2.3 - 3.7	3.7 - 5.2	5.2 - 8.0	8.0 - 9.4
Em	0.57	1.3	2.9	4.4	6.3	8.6
Background counts (C _B)	122,790	260,988	83,026	49,602	65,477	25,159
Excess counts (C _S)	467 (+)	366 (+)	566 (+)	466 (+)	319 (+)	175 (-)
Energy Interval (DE)(MeV)	0.5	1.4	1.4	1.5	2.8	1.4
Energy loss to Photon Energy Conversion Factor R	1.64	2.65	3.3	3.1	2.8	-
Atmospheric Attenuation Correction Factor B	1.3	1.2	1.12	1.1	1.08	-
Time of Exposure x Effective Area Compensation Factor NEA (seconds)	1,005.7	1,575.25	1,575.25	1,575.25	1,575.25	1,575.25
$\frac{dN}{dE} = \frac{RBC_s}{(DE)(NEA)(A)}$ (photons/(sec-cm ² -MeV))	1.55 x 10 ⁻²	3.88 x 10 ⁻³	6.96 x 10 ⁻³	5.34 x 10 ⁻³	1.64 x 10 ⁻³	
\pm error $\frac{(2xC_S)^{\frac{1}{2}}}{C_B} \times \frac{dN}{dE}$	$\pm 1.6 \times 10^{-2}$	$\pm 7.8 \times 10^{-3}$	$\pm 5.24 \times 10^{-3}$	$\pm 3.54 \times 10^{-3}$	$\pm 1.71 \times 10^{-3}$	

Table 5.2 LEG 2 Results Re-evaluated, Using Improved Energy Loss Conversion Factors, for the Crab Nebula

Energy Range (MeV)	(0.92 to 2.0)	(2.0 to 5.89)	(5.89 to 10.6)
Energy E_m (MeV)	1.36	4.10	7.9
Old value, Energy loss to Photon Energy Conversion Factor, R_0 (R. Lovett)	3.8	4.1	2.9
New Value, R_N	2.7	3.1	2.75
New Value of Flux = Old Flux $\times \frac{R_N}{R_0}$ (photons/(sec-cm ² -MeV))	1.07×10^{-2} $\pm 0.92 \times 10^{-2}$	3.2×10^{-3} $\pm 1.06 \times 10^{-3}$	1.7×10^{-3} $\pm 1.32 \times 10^{-3}$

Table 5.3 - Background and Excess Counts for Crab Nebula (All Energies)
from LEG 4 Experiment (Individual detectors)

	Y1 Detector	Y3 Detector	Y4 Detector	Y1, Y3, Y4 Detectors together
Unocculted Periods Counts CON	741,142	719,193	846,457	2,306,792
Occult Periods Counts COFF	740,191	716,100	844,585	2,300,876
Excess Counts = CS = CON-COFF	951	3,093	1,872	5,916
$(\text{COFF})^{\frac{1}{2}} = \text{SIG}$	860	846	919	1,517
$\frac{\text{CS}}{\text{SIG}}$	1.11	3.7	2.04	3.9

the beginning of the flight. The timing of the arrival of a gamma ray was known to $\pm 0.8 \times 10^{-3}$ seconds. This was limited by the bit rate.

The main feature of this type of analysis is that it is not worth looking for the period due to poor statistics. Instead, the phase and period is assumed, and is taken to be the same as that of the optical and/or radio emissions. Because this analysis involves the accumulation of gamma ray arrival times into time bins of the same phase relative to the pulsar, some errors in the pulse shape might be accumulatively produced. However, detailed investigation showed that no such errors were introduced to any significance.

The period data for the Crab Nebula pulsar, NPO532, was kindly supplied by Dr. J. Rankin of Cornell University, U.S.A. His program took into account a number of effects on the pulsar period at the balloon including Doppler effects produced by :(i) velocity of the earth relative to the source, composed of the earth's rotation about its own axis, the earth's orbital motion about the sun, and the relative velocity of the sun and the source; and (ii) the velocity of the balloon relative to the earth's surface, while being propelled by the prevailing winds.

A full discussion of the correction factors required for the period of the Crab Nebula as seen at the earth is given by Orwig (1971). The periods used are shown in table 5.4.

5.4 The Results of the LEG 4 Observations of the Pulsar NPO532

Significant peaks in the pulse profile, in phase with the pulsar NPO532, were found in the analysis. However, these results were obtained using all four detectors, for all counts at all energies, above about 0.4 MeV. The pulse profiles for these results are shown in diagrams 5.5 and 5.6, for 16 time bins per period and 32 time bins per period, respectively. Of these total counts, the counts from the Y2 detector had to be rejected when the analysis split up the counts into energy ranges. This is because the energy discrimination system of the Y2 detector was not functioning correctly. In addition, the telemetry system only recorded the energy of approximately half the counts for which it recorded timing data. Consequently, the significance of the peaks, once energy discrimination conditions had been imposed on the analysis, was greatly reduced, due to the reduced statistics, as shown

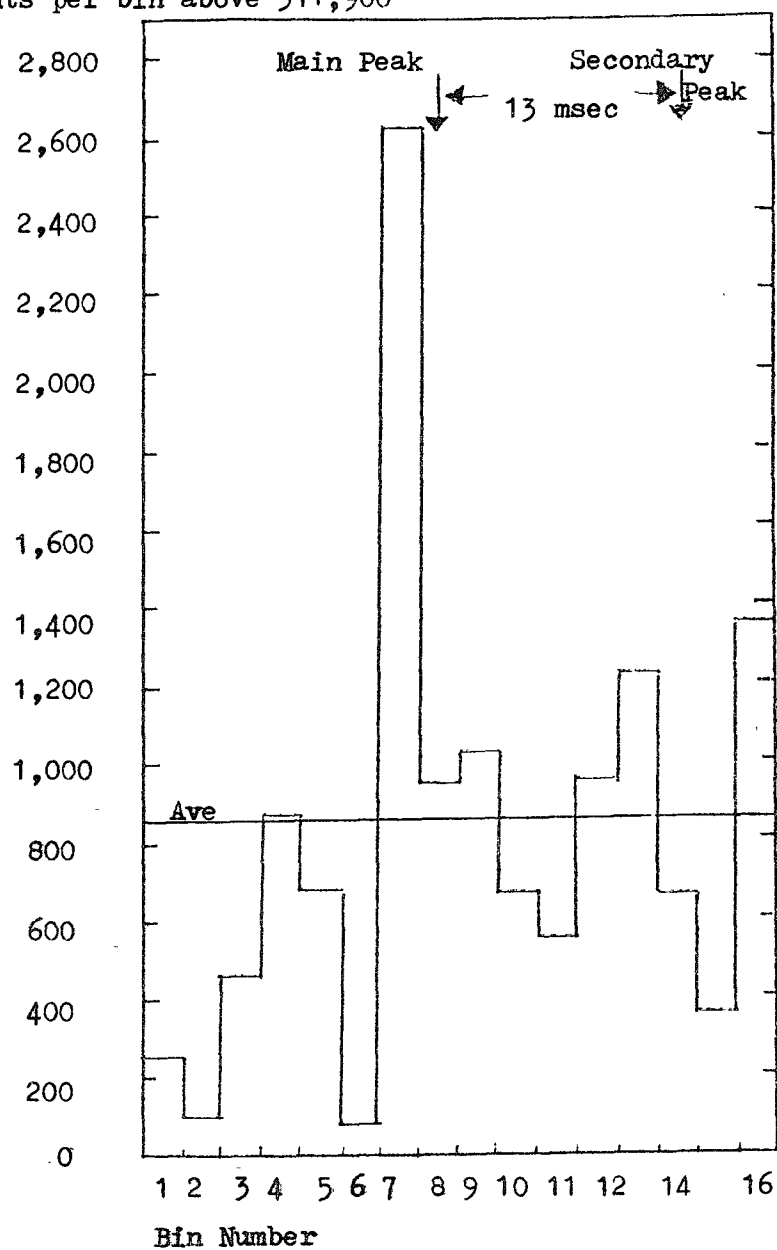
Table 5.4 Crab Pulsar Periods for Duration of LEG IV Balloon Flight on 17.7.74
 (As kindly supplied by Dr. J. Rankin, Cornell Univ., USA)

UTC Time	Sidereal Time	Barycentric Period (seconds)	On Board Period (seconds)	On Board Frequency (Hertz)	Lag (Usec)	Latitude (Degrees)	Height (Meters)	Longitude (Degrees)
12 30	1 43 15.1	0.0331666854	0.0331649826	30.152284746	27017.2	31 50	32317	96 38
13 30	2 40 24.9	0.0331666869	0.0331649886	30.152279309	19985.7	31 50	38415	97 23
14 30	3 37 26.8	0.0331666884	0.0331649963	30.152272323	13679.5	31 42	38567	98 10
15 30	4 27 48.6	0.0331666900	0.0331650041	30.152265246	8361.8	31 35	38323	100 37
16 30	5 20 50.5	0.0331666915	0.0331650129	30.152257212	3778.4	31. 45	38323	102 24
17 30	6 15 .3	0.0331666930	0.0331650220	30.152248926	65.3	31 56	37592	103 54
18 30	7 8 26.2	0.0331666945	0.0331650306	30.152241152	30360.5	32 6	37500	105 35

The "On board" period is the period at the Balloon, at the Latitude, Longitude and Height given.

The "LAG" is the time elapsed after the UTC time when the optical main pulse occurs.

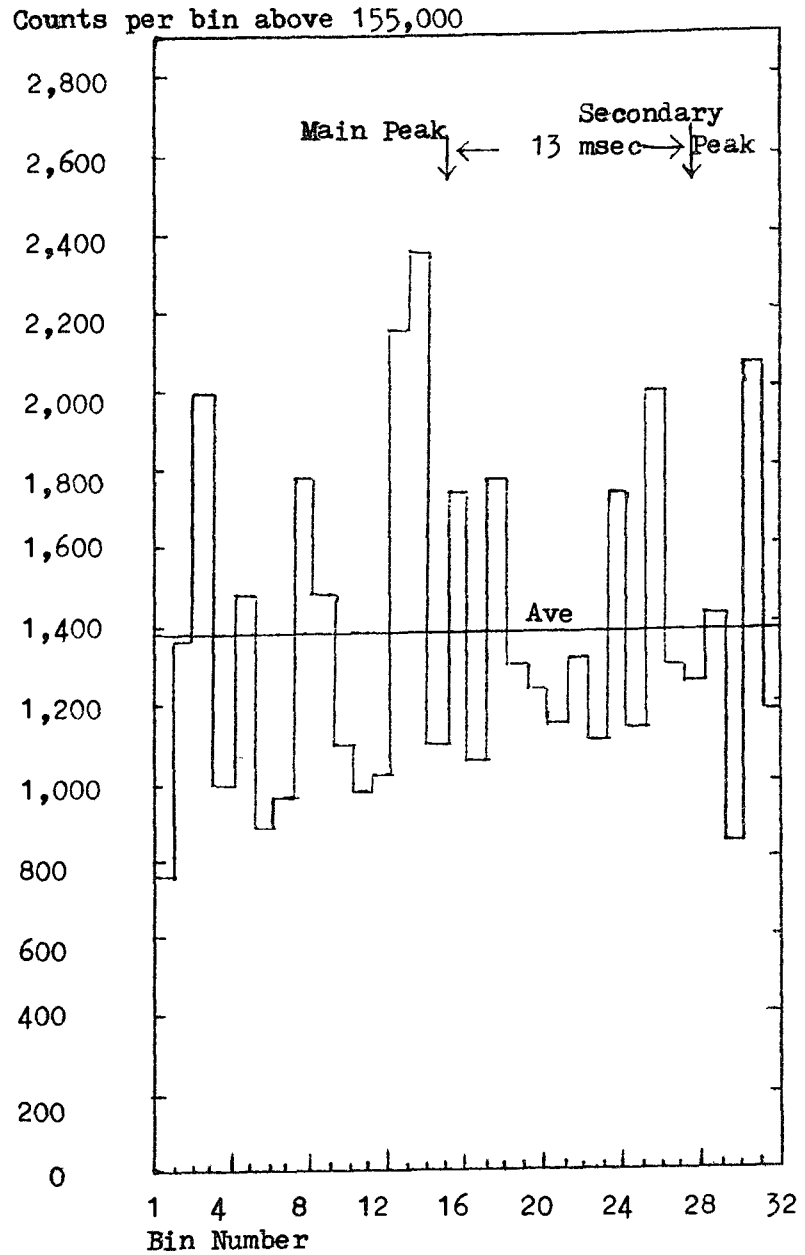
Counts per bin above 311,900



Ave line is average of all 16 bins

Diagram 5.5 Phase Histogram of NP0532

Total counts LEG4 experiment.



Ave line is the average of all 32 bins.

Diagram 5.6 Phase Histogram of NP0532

Total Counts LEG4 experiment.

in diagram 5.7. The exposure factor for these results was $2.37 \times 10^6 \text{ s} - \text{cm}^2$.

Comparison of the absolute phases of the optical main and secondary peaks of NP 0532 with the peaks in the phase histograms obtained from the LEG 4 data show that they coincide within the timing resolution of the experiment.

Many different energy bin sizes were tried, in a search for any possible pulsed gamma ray lines, but no significant features were found. The pulsar flux results are shown graphically and discussed in relation to the results of other experimenters in the next chapter.

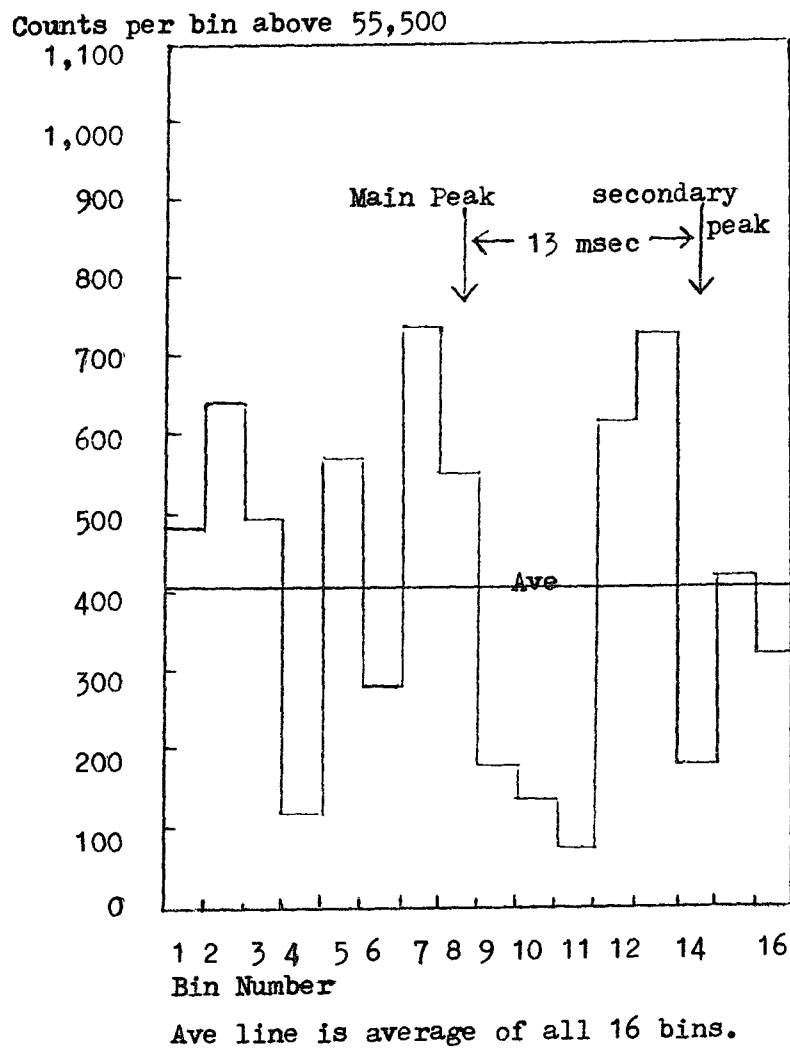


Diagram 5.7 Phase Histogram of NPO532
(0.898-15.0)MeV Range Y1, Y3, Y4 Detectors.
Exposure Factor $2.37 \cdot 10^6$ s-cm²

Chapter 6 - Discussion of the Results of the LEG 4 Experiment

6.1 The Total Emission from the Crab Nebula

The results of the LEG 4 experiment for the gamma ray emission from the Crab Nebula and those of other experimenters, are shown in diagram 6.1. It may be noted that the statistical error bars are rather large. However, the points suggest tentative evidence for an excess over the best fit power law extrapolation from the results of other experimenters at lower and higher energies. The experiments of Baker et al.(1973) and Gruber (1974) show agreement with the LEG 4 experiment. Some points of Walraven et al.(1975) are also high, but with large statistical errors, and these points were considered by Walraven et al. to be consistent with the power law extrapolation. Consequently, the results of Walraven et al. are omitted from diagram 6.1 for clarity.

By contrast, several other experiments have given results which can only be interpreted as consistent with the power law. These include those of Schönfelder et al.(1975), Kinzer et al.(1973), and more recently Mandrou et al.(1977) and Wilson et al.(1976). The results of Mandrou et al.(1977) are upper limits extending from 100 keV to 5 MeV, consistent with the power law, and so are omitted from diagram 6.1 for greater clarity. The results of Kinzer et al. may be considered to be at a higher energy than the energy range of the suspected "excess".

It is of interest to observe that although the experiment of Leventhal et al(1977) detected the Crab Nebula radiation only in the range 0.1 to 1 MeV, several of their higher energy points approaching 1 MeV are higher than the extrapolated spectrum giving a suggestion of an excess.

For energies greater than 10 MeV the gamma ray results of Parker et al.(1973), Wilson et al.(1976), Kniffen et al.(1974), and McBreen et al.(1973) are consistent with a power law extrapolation from the low energy X-ray region.

There appears to be a variation between the experimental results in the 1-10 MeV range. A number of factors could be causing such a variation, as described in the following sections.

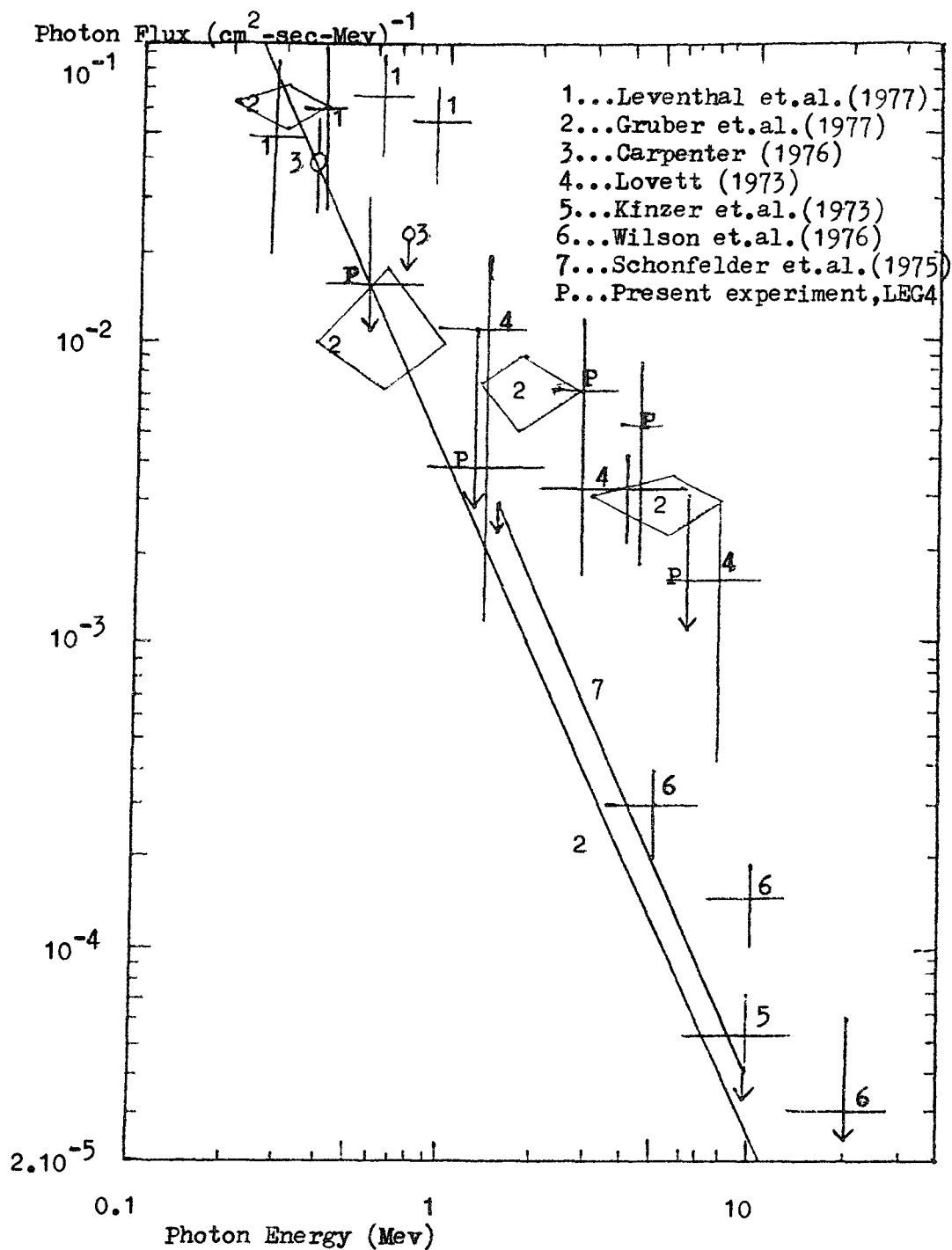


Diagram 6.1 Differential Gamma-Ray Spectrum of
 The Crab Nebula

6.2 Time Variability of the Crab Nebula

This factor is difficult to eliminate conclusively, if at all, because of its definition. However, it can be rendered more or less likely by comparison with emission at other energies, or by comparison with the pulsed flux from the Crab Pulsar, NPO532. Even so, although rather unlikely, there is a possibility that any variability is mainly restricted to just the 1-10 MeV region in the unpulsed flux.

Let us first examine results in other ranges around the time of the 8th August 1971 measurements of Gruber et al. The higher energy observations of Parker et al.(1973), which include sensitivity downward to 20 MeV, were made in part on September 24th 1971, and in part on October 2nd, 1971, close in time to those of Gruber. Parker's flux reported at a 2.6σ confidence level, is consistent with the $E^{-1.2}$ power law for X-ray energy flux. Therefore the flat 1-10 MeV spectrum observed by Gruber must have had a very sharp cut off, or the flux must have declined greatly by September 24th. Since the flux level changed significantly by the May 1973 results of Walraven et al., a radiating region smaller than the optical Crab Nebula is implied (Gruber and Ling, 1977), for which the pulsar or the nearby wisps are likely candidates. Activity in the wisps has been associated with the pulsar timing "glitch" of September 20th 1970 (Scargle and Pacini, 1971). Boclet et al.(1972), and Laros, Matteson, and Pelling (1973), have reported negative results for changes in pulsed or total emission at 20 - 200 keV from observations made a few days before and after this event. However, Fazio et al. (1972) report observable levels of $\sim 10^{-14}$ eV flux following (with a ~ 60 day delay) "glitches" on September 29th 1969, August 1st 1971, and October 25th 1971. Greisen et al.(1975) reported a definite decline of the pulsed flux between observations on October 6th 1971 and July 23rd 1973, and a possible decline of the steady (nonpulsed flux). The ~ 100 MHz pulsed radio flux showed, between 1971 and 1974, great variability and a general decline by a factor of 2-3 (Rankin, Payne and Campbell, 1974). In addition the radio emission shows great variability from pulse to pulse by as much as a factor of 10^3 (Heiles, Campbell, and Rankin, 1970; Drake, 1971; Argyle and Gower, 1972). Forman et al.(1974) have also observed variability in the Crab pulsar flux. They point out that there is an irregular, rapidly varying component, or that there are large fluctuations (factors of 2 or 3) in the 33 ms pulsed X-ray emission of the Crab on a time scale of several

tenths of a second or less. Helmken (1975) has observed evidence for a substructure at the phase position of the optical interpulse in 10^{11} - 10^{13} eV gamma rays. The variability in the $> 10^{11}$ eV flux from NPO 532 found by Grindlay et al. (1976) is consistent with the existence of a periodic flux which is variable in either its phase or intensity on the time scale of months.

By contrast, Ricker et al. (1975) have found evidence for variability at X-ray energies on a time scale of hours, and this agrees with the time scale of variations at radio frequencies observed by Schönhardt (1971). Gruber and Ling (1977) suggest a link between the apparent variability of the total flux and the "glitch" associated variability of the pulsed flux. They suggest that simultaneous total and pulsed flux measurements might show a time correlation which would indicate origin in the pulsar environment. LEG 4 is the only result in which a measurement of both the pulsed and total flux of the Crab Nebula region has been taken, at the same time, in the 1-10 MeV region, and this result appears to show that there is no corresponding large excess in the pulsed flux to coincide with the total excess in the 1-10 MeV region. Although the error bars are large, a large simultaneous excess in the pulsed fraction can be ruled out with a fair degree of confidence, because it would have shown up very clearly in the LEG 4 experiment.

Table 6.1 shows the dates of the principal observations of the Crab Total Flux in the 1-10 MeV region, and comments on the general character of the results. The fact that the periods of phase variability from radio through to very high ($> 10^{11}$ eV) energies may occur on a time scale comparable with the timing irregularities of NPO 532 suggest that changes in the neutron star rotation rate are involved (Grindlay et al. 1975). These could be induced by changes in the neutron star geology (Ruderman, 1969) or, alternatively, by particle release from the magnetosphere (Scargle and Pacini, 1971). In either case, small changes in the pulsar magnetic field geometry might be expected.

Roberts and Sturrock (1973) have proposed the existence of a dense ($\sim 4 \text{ gm cm}^{-3}$) accretion belt synchronously orbiting the pulsar at a distance of 150 Km. The material on the surface of this belt could possibly be excited to produce the observed radiation by nuclear line emission or bremsstrahlung.

Whether or not the tentative evidence for variability can be accepted, the possibility of systematic errors in the LEG 4 experiment need to be discussed. This discussion follows in the next sections.

Table 6.1 Time Variability of Crab Total Flux - Principal Results
in 1-10 MeV Region

<u>Name/s of Experimenters</u>	<u>Date of Experiment</u>	<u>Angular Resolution</u>	<u>Comments Regarding Excess</u>
Gruber et al.	8th Aug.1971	50° FWHM	Shows an excess in 1-10 MeV region
Baker et al.(LEG 2) (Southampton Group)	23rd Sept.1972	Occulting blocks subtend $\pm 7^\circ$ at detector	Shows an excess in 1-10 MeV region, but large error bars
Walraven et al.	15th May, 1973	13° FWHM	Some high points but overall statistically inconsistent with a clear excess in (1-10) MeV region
Schönfelder et al.	11th July 1974	26° FWHM(1.5 to 2 MeV) 23° FWHM(2 to 3 MeV) 18° FWHM(3 to 5 MeV) 14° FWHM(5 to 10 MeV)	Inconsistent with an excess
Bailey et al.(LEG 4) (Southampton Group)	17th July,1974	Occulting blocks subtend $\pm 7^\circ$ at detector	Shows an excess in 1-10 MeV region, but large error bars
Mandrou et al.	9th July,1975	Occulting blocks subtend $\pm 10^\circ$ at detector	Consistent with power law but only covers 0.1 to 4 MeV range
Leventhal et al.	10-11th May 1976	11° FWHM at 50 keV 13° FWHM at 1.33 MeV	Some high points near 1 MeV, but lower energy spectrum consistent with power law. No points observed greater than 1 MeV

6.3 Systematic Errors

In discussing the results of the observations of the Crab Nebula by LEG 4, consideration is needed of the possible sources of systematic error.

The analysis for the total flux of the Crab Nebula could give falsely increased or decreased results due to the following systematic errors:

- (i) The slight change in position of the two lead discs from source to background periods might, in itself, give rise to a change in the count rate.
- (ii) The source may really be all or partly due to another source being occulted by the diagonally opposite disc.
- (iii) Electromagnetic noise might be picked up on the telemetry or electronics system and might increase or reduce the effective source.
- (iv) Azimuth or zenith variations of the background count rate combined with the occultation of different areas of the sky, by the occulting paddles not occulting the source, could produce an increase or decrease in count rate.
- (v) There may be more than one source of interest within the opening angle of the telescope.
- (vi) The steering monitoring system might have been malfunctioning, resulting in either the wrong source, or no source, or a combination, being observed.
- (vii) Variations in the detector background count rate might cause problems.

In relation to (i), we need to investigate the dimensions of the discs and the crystals. The lead discs subtend between them an average solid angle of 0.1 steradian at a crystal face. In other words, less than 1 per cent of the total solid angle. This solid angle changes by less than 5 per cent when the lead paddles are moved to the other alternative position. This results in a net change to the total solid angle of 0.05 per cent of the total solid angle. In an isotropic background flux this would cause a change in count rate of 0.05 per cent, assuming that the lead paddles were 100 per cent efficient at stopping gamma rays.

For a 0.05 per cent change in count rate to have a 2 standard deviation significance, the total number of counts observed must be of the order 8×10^6 . At the rate observed by the three detectors, Y1, Y3 and Y4 used in analysis, this would need approximately 4 hours observation for each of the 3 detectors. In fact, in this analysis only about 2 hours of data was used for each detector. We can see that any effect would consequently only be small.

With reference to the second point, it has been checked that during the flight that no other sources were in the regions swept through by the diagonally occulting disc.

The third point concerning electromagnetic noise pick-up, can be safely eliminated as a possibility. This is because it was checked that no particular "triplet", of 2 background and one source period, predominantly caused an excess. In addition, on a shorter time scale, the programmes run to search for a gamma ray burst found no significant increases or decreases above the mean count rate.

Zenith variations producing a source or antisource can be ruled out. As mentioned in relation to point (i) about the change in subtended angle of the lead discs, any such background variation effects would be of the order less than 0.05 per cent of the count rate. In addition, because the steering of the experiment used an azimuth-zenith mount, then 2 detectors Y4 and Y1, would have seen a larger (or smaller, depending on the case) excess than Y2 and Y3, if such a zenith background variation effect were present. Such an effect was not found in the analysis.

By similar reasoning, it is unlikely that any azimuthal background variation effects were present. During the period of observation of the Crab Nebula used in the subsequent analysis, the zenith angle varied between approximately 38.8 degrees and 12.8 degrees, while the azimuth angle varied from about 96 degrees to 133 degrees.

The fifth possibility, that of an unknown source being present within the opening angle of the telescope, is one that is difficult to eliminate conclusively. It is a possibility that can only be resolved by the use of much higher angular resolution gamma ray telescopes, with better directional steering capabilities.

As regards whether the steering was malfunctioning, it is rendered unlikely in that the so-called occulted periods of the detectors did not give rise to any significant peaks in the analysis for gamma rays for the pulsar NP0532 in the Crab Nebula, whereas the so-called unocculted periods did give rise to a 3 standard deviation excess

consistent with the period of NPO532. This strongly suggests that the lead discs were indeed occulting the correct Crab Nebula source, and hence, that the steering was functioning as expected.

The seventh point concerns variations in the detector background count rate produced by, for example, gain changes due to temperature variations of the detectors and/or electronics systems, altitude variations of the balloon, loss of power due to the gradual run-down of the batteries, or a combination of these causes.

Let us assume that the general change in background rate is linear with time, over the period of observation of the Crab Nebula. The source (ON) periods intersperse the background (OFF) periods. For each "triplet" the background averaging procedure already described will adequately avoid any generation of a false source.

Let us now suppose that the change in background count rate is not linear. Consider diagram 6.2 a. In this diagram the background is schematically portrayed as following a convex curve in time, and it is assumed that there is no source contribution. Suppose period "3" is a source period (i.e. a period when the crystal was exposed to a supposed source). Because the average of periods 2 and 4 falls below the count for 3, a false "source" has been found. However, if instead of periods 2, 3 and 4 we had chosen periods 1, 2 and 3 then we would also have found a positive excess. Yet in an analysis, 2 would have been a background (occulted) period, not a source period. In other words, for such a convex variation, it does not matter which set of periods are chosen as source or background periods, a positive excess is always found. However, with a true source contribution, as shown in diagram 6.2 b, this is not so. If the periods are taken in the alternative "wrong" manner, i.e. the source and background periods are interchanged, then we would have obtained a negative difference. This gives a simple way to check whether a positive difference in the analysis is due to a true source, or due only to a background variation. An analysis was run on the computer with the source and background periods interchanged, and a negative difference was found, indicating that a true source flux had been found. Of course, this reasoning depends upon the time scale of the background rate changes being relatively long compared with the five minute observation periods. This was so on the LEG 4 experiment.

Evidence that the positive excess found for the Crab Nebula is not a result of the instrument itself, comes from the previous LEG 2 experiment (see R. Lovett, thesis). The LEG 2 experiment had similar

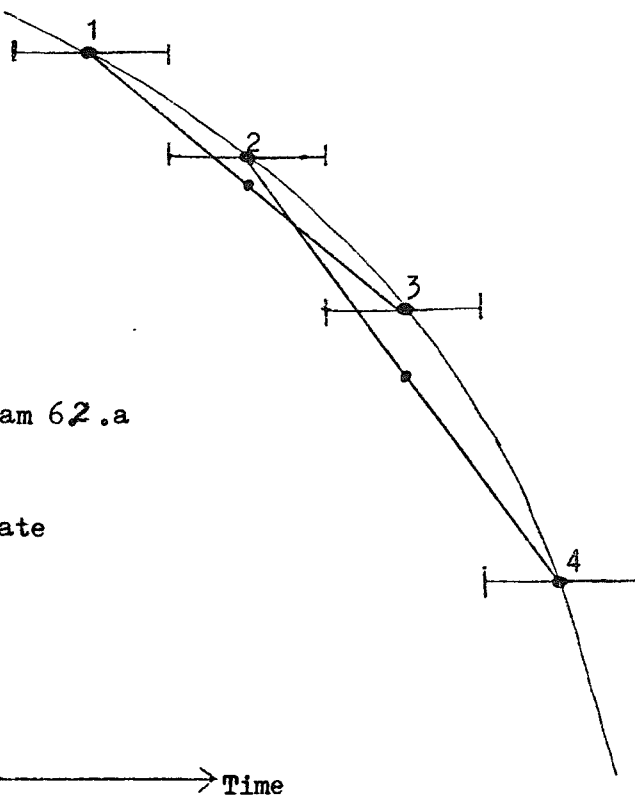


Diagram 62.a

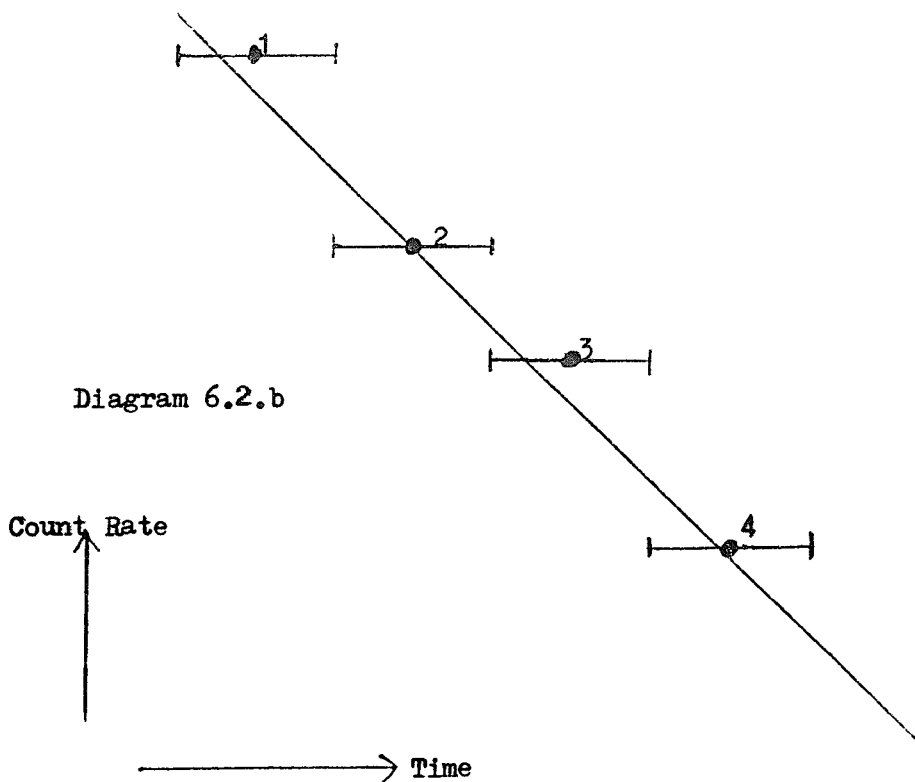


Diagram 62.b

dimensions and used the same anticoincidence method that was used by the LEG 4 experiment. Lovett reports that positive excesses were found for Cygnus X-1 and the Crab Nebula but that null results were obtained for the Perseus X1 and Cygnus X2 regions, (where such results were not unexpected from other observations). A purely instrumental effect would have been expected to generate "false" sources for whatever region of the sky was observed.

Additional evidence that the excess found by LEG 2 and LEG 4 is not a false excess due to this type of anticollimated detector, is furnished by the fact that the detector of Gruber and Ling, which also detected an excess, was based upon the completely different principle of active shielding, as described in section 2.3. Consequently, it seems unlikely that any excess is due to the type of detector used.

The possibility of source confusion is discussed in more detail in the next section.

6.4 Source Confusion

Because of the difficulty of obtaining good angular resolution for low energy gamma ray detectors, source confusion can be a problem in this energy range. One way of checking whether or not source confusion has occurred is to compare measurements with measurements in other ranges. Another way is to compare the angular resolutions and results of different detectors used in approximately the same energy range, for observing the same source.

The angular resolution figures given in table 6.1 show that in comparing the Baker et al. and the LEG 4 results with the others, source confusion is less likely using LEG 2 and LEG 4 than with the other detectors, because of better angular resolution. Consequently, it seems improbable that source confusion can explain the difference between the various low energy gamma ray observations.

However, time variability of nearby sources is a possibility. This would require that such a time variable source was within the field of view of all the detectors mentioned in table 6.1. It is of interest to remark that at least one long-term X-ray transient, A0535+26, has been observed near the Crab (e.g. Rosenberg et al. 1975). A recurrence of this source after 6 months has been reported (Joss, 1975).

Assuming this recurrence to have been periodic at the time of the measurements of Gruber, Baker (LEG 2) and LEG 4, then this possibility cannot be ruled out. However, the low result of Schönfelder just 6 days before the LEG 4 flight would indicate that such a source would have had to have flared up rather quickly. In fact, A0535+26, was observed by Rosenberg et al. to be just detectable on April 13th, 1975, and during the 16 days of observation, it was seen to brighten to nearly twice the Crab's intensity (in the 3-7 keV range). Their observations showed a factor of 10 increase in count rate in the 8 days between April 21st and April 29th, 1975. The source was seen to vary with a period of 103.83s, and has a very flat spectrum in the 3-7 keV range. Kaluzienskii et al. (1975) observed the decay of A0535+26 in the 3-6 keV range. It was first observed by them on April 29th, 1975, with an intensity \sim 15% more intense than the Crab, at which level it remained for approximately one week. The source then decayed with an e-folding time of \sim 19 d. These timescales of intensity increase or decrease are of the order required to explain the low result of Schönfelder et al. only 6 days before the results of the LEG 4 experiment (see table 6.1). Alternatively, Schönfelder et al. may have badly estimated the background as the Crab Nebula scanned through the aperture of their double Compton telescope. Additional support for strong variability, is lent by the OSO-7 satellite results of Canizares et al. (1976) who observed that A0535+26 was a factor of up to 6 times as intense as the Crab Nebula in the 20 keV region on 13th May, 1975.

The LEG 4 data was not analysed for the 104 s period of A0535+26, because the statistics of the low count rate of the 1-10 MeV range of gamma rays require the period to be known exactly at the time when the data was taken, for any reasonable source strength to be detected. At the time of the LEG 4 experiment the period of A0535+26 was not known accurately enough for an analysis. However, Gruber et al. (1977) analysed their experiment which extended to lower energies, for the 103.83s pulsation. But they found no evidence for its detection. However, Gruber's result was a long time before the observation of A0535+26 in mid-1975, and consequently, the period of A0535 may have evolved considerably in the meantime, particularly considering the short time scale of its rapid rise and decline in intensity.

Additional information on A0535 is given by Ricketts et al. (1975), Kaluzienskii (1975), and Coe et al. (1975) who showed that the spectrum of A0535+36 above 10 keV falls steeply.

From the observed characteristics of A0535+26, it may be seen that a transient source close to the Crab cannot be ruled out as being responsible for the variation in the low energy observations, although bearing in mind the angular resolutions and the steepening spectrum of A0535+26 in particular, this possibility appears relatively unlikely.

At energies > 100 MeV, COS-B has observed three sources near the Crab Nebula (Hermsen et al. 1977). These are CG 176-7, CG 189+1, and CG 195+4. CG 195+4 has also been observed by SAS-2 (Kniffen et al. 1975). However, at these energies, all three sources are less intense than the Crab Nebula. Assuming that they are less intense than the Crab Nebula in the low energy gamma ray region as well, then it may be seen that these sources cannot be the source of the large excess seen by LEG 4, unless these sources are themselves highly variable in nature.

In addition, each of these sources are outside the opening angles of the LEG 4 and LEG 2 experiments.

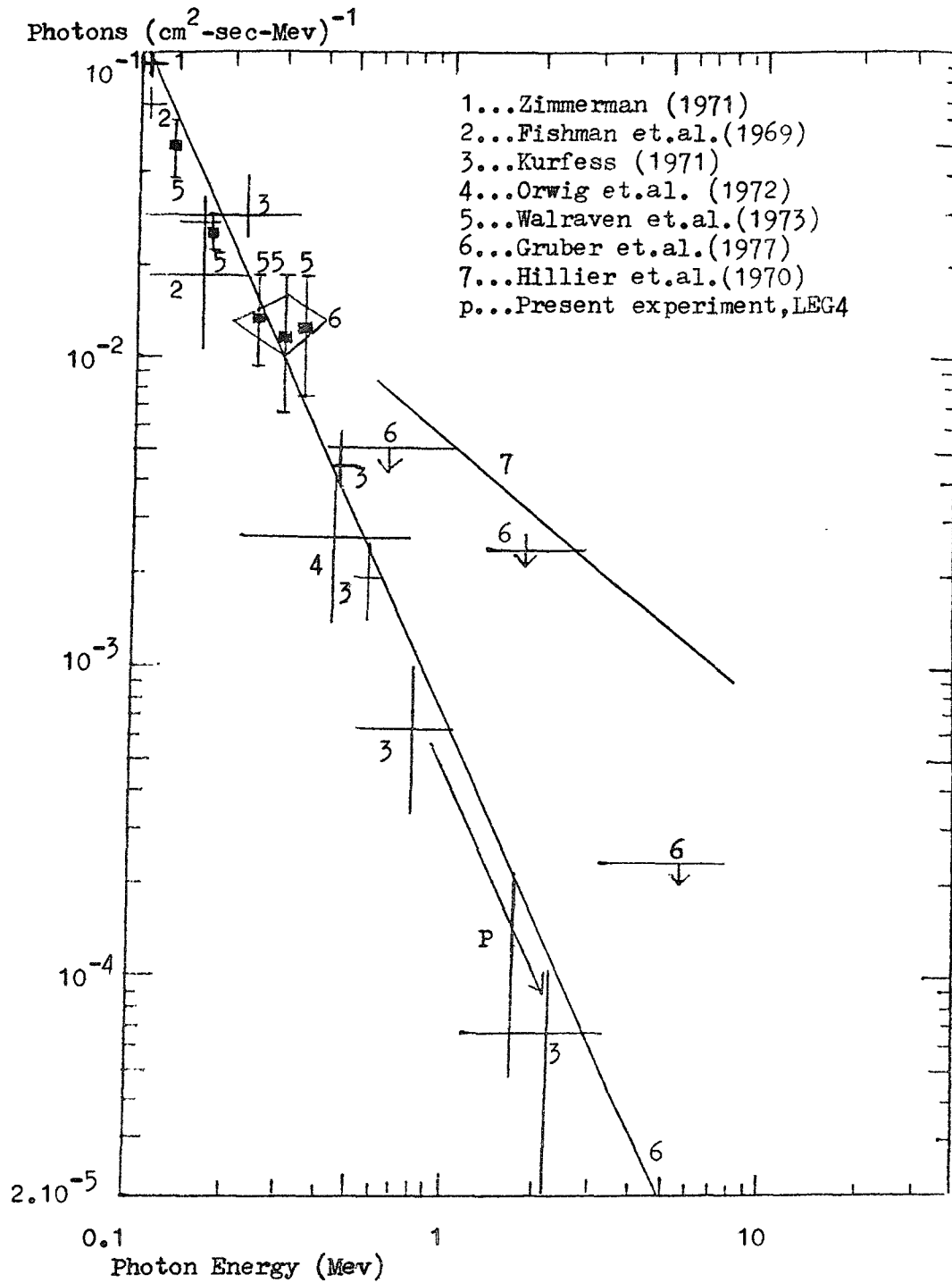
6.5 A Gamma Ray Burst

The possibility that a gamma ray burst caused the excess has been eliminated from the LEG 2 and LEG 4 experiments by the analysis procedures described in chapter 5. It appears that Gruber has not yet considered the possibility of a gamma ray burst. However, if all the source excess had occurred within one short time interval, he would probably have noticed it. In addition, his published graph of count rate versus time of observation of the Crab Nebula, during his drift scan procedure, showed no sudden variations.

However, taking the three experiments together, and the fact that it would have to have been a recurrent, very hard gamma ray burst which appears inconsistent with other data (see section 1.6), it seems rather unlikely that gamma ray bursts were responsible for the excesses.

6.6 The Pulsed Emission from the Crab Nebula Pulsar NP 0532

The results of this experiment for the pulsed emission from NP 0532 are shown in diagrams 6.3 and 6.4, together with the relevant results of



Line '6' is $0.0007(E/1\text{Mev})^{-1.2} \text{ Mev } (\text{cm}^2\text{-s-Mev})^{-1}$
 (Gruber,1977)

Diagram 6.3 Differential Gamma-Ray Spectrum of
 NPO532 Pulsar.

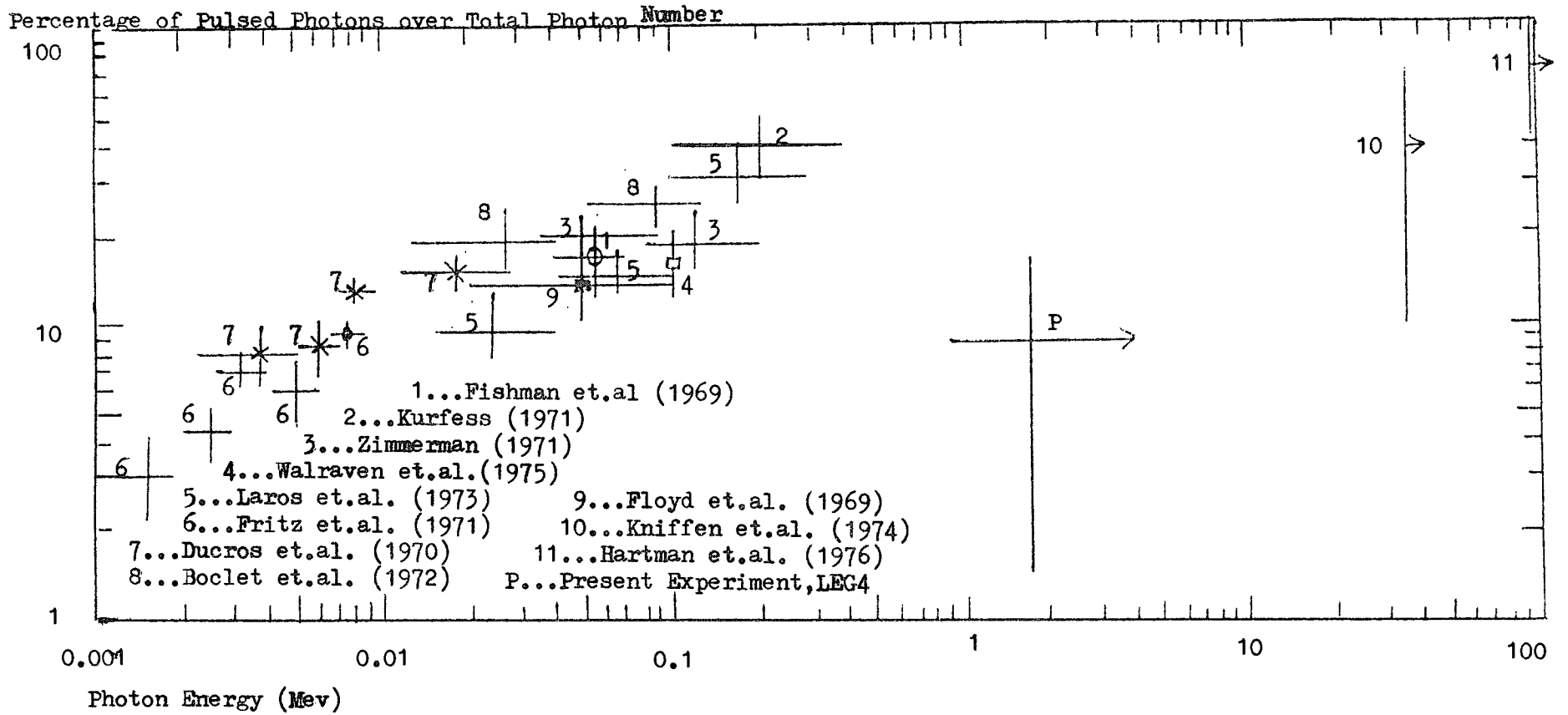


Diagram 6.4 Pulsed Portion as a function of Photon Energy

other experimenters.

Because the statistical uncertainty of the LEG 4 result is rather large, this point is probably best considered an upper limit. The flux was calculated by taking the excess counts in time bins 7 and 13 in diagram 5.7 over the average of the remaining 14 time bins. Despite the statistical uncertainty, the result as shown in diagram 6.3 gives a definite indication that if the pulsed emission had contained a 1 to 10 MeV excess, as may be the case for the total flux, then the LEG 4 experiment would have seen the pulsar to a far greater statistical significance. So the present data indicates no corresponding excess in the pulsed radiation. The point plotted in diagram 6.3 appears to be consistent with an extrapolation between other results. The exception is the high result of the Bristol Group (Hillier et al. 1970). However, ~~Kurfess~~ (1971) has suggested that this result may have been high due to a calibration error.

A search in various energy intervals for evidence of pulsed gamma ray lines in the pulsar spectrum, revealed no evidence for such features. For comparison with the total emission spectrum, the pulsed over total photon percentage is plotted together with other results in Diagram 6.4. Again, the LEG 4 result is possibly best regarded as an upper limit, assuming that the total flux points obtained by LEG 4 are valid. The low value of the LEG 4 point reflects the high points obtained for the total Crab emission in the 1-10 MeV range. Interestingly, no other experiments have detected the total and pulsed emission simultaneously, to date, in the 1-10 MeV region. Experiments, such as the Milan-Southampton (MISO) telescope, which flew in 1977 and is still being analysed, may be able to produce further interesting results in this energy range - particularly in relation to the Crab Nebula. A preliminary result of the MISO experiment, seems to indicate a high flux for the Crab Nebula total spectrum integrated over energies greater than about 1 MeV. The pulsar data is still being analysed.

The statistical significance is not great enough to quote a main to secondary peak ratio. Nevertheless, the pulse shape, as shown in diagrams 5.5 to 5.7, is consistent with the pulse shape of NP 0532 seen by other experimenters in this energy range. Share (1973) has reviewed the X and gamma ray observations of the NP0532 and in particular he has compared the light pulse shapes found for different photon energies. There is not sufficiently accurate data available to draw firm conclusions about the pulse shape, but there appears to be evidence that the pulse

shape varies significantly from 100 keV to 1 GeV. For example, the height of the main and secondary peaks are approximately the same in the results of Kurfess in the 100 to 400 keV range. By contrast, the secondary peak is conspicuous by its absence in the results of Albats et al. (1972) in the range 10 to 30 MeV. As pointed out by Share, it is clear that the sensitivity of gamma ray detectors requires about an order of magnitude improvement in order to permit detailed studies of the Crab pulsar.

Having discussed the experimental measurements of the pulsed and unpulsed gamma ray from the Crab Nebula, the next section reviews the astrophysical implications of these results.

6.7 Theoretical Considerations

A variety of models for the Crab Nebula and its pulsar, NPO532, have been proposed. There appears to be gathering evidence, through tentative associations of time variability, of a closer association between the pulsar NPO532 and the unpulsed flux from the Crab Nebula, for X ray energies and above. Indeed, some models of the total unpulsed emission invoke the pulsar as a necessary energy source (Apparao, 1973).

The two mechanisms commonly proposed for the production of X and low energy gamma rays in sources are the synchrotron process and emission by a hot gas. These two mechanisms have each been proposed for the Crab Nebula. The synchrotron process has tended to find most favour in the past. This is because of the observed polarisation of the X rays and also the power law nature of the observed spectrum (Apparao, 1973). By contrast, Sartori and Morrison (1967) have reasoned that the power law form of spectrum can be produced by a superposition of thermal emission from plasmas with two or more temperatures.

Maraschi and Treves (1973) have made detailed calculations using the concepts of synchrotron radiation and Compton scattering to explain the origin of the gamma ray emission from the Crab Nebula and NPO532. They suggest that synchrotron radiation may explain both fluxes, and that Compton scattering may contribute significantly to the pulsed flux above 100 MeV and to the continuous flux above

1 GeV. They then suppose that, if the variations of the continuous flux observed at 10^{11} eV by Fazio et al. (1972) are real, then the synchrotron process is favoured and variations should also be observable at low gamma ray energy, but not in the X-ray band.

Theories of nucleosynthesis in supernovae suggest that radioactive debris may be present in the Crab. Clayton and Craddock (1965) and Clayton et al. (1969) predicted on the basis of the Californium hypothesis, that gamma ray spectral lines exist in the Crab Nebula's radiation at energies between soft X rays and approximately 10 MeV. Line fluxes that were at most 1×10^{-4} photons $\text{cm}^{-2} \text{s}^{-1}$ were predicted by them. However, no gamma ray lines from the Crab Nebula have yet been detected, except a 4σ observation of Leventhal et al. (1977). Leventhal et al. report evidence for the presence of a line feature at 400 ± 1 keV from the Crab Nebula, of flux $(2.24 \pm 0.65) \times 10^{-3}$ photons $\text{cm}^{-2} \text{s}^{-1}$, and suggest that this is the positron annihilation line (511 keV) redshifted by the gravitational field of the neutron star. However, a later experiment by Ling et al. (1977) using an equally sensitive detector, failed to find this line. This again may be evidence for time variability of emission from the Crab Nebula at hard X-ray to low energy gamma ray energies.

Although the line fluxes predicted by Clayton et al. are an order of magnitude lower than the extrapolated X-ray spectrum, the possibility of lines, excited in some way, being the source of the tentatively proposed variable 1-10 MeV excess from the Crab Nebula - or some other nearby unresolved source, cannot be ruled out.

If the excess has a maximum somewhere between 1 and 10 MeV, and a rapid fall off outside this interval, as suggested by experiments outside this energy range, then such a sharp feature is not characteristic of the spectra of the standard continuum emission mechanisms, such as synchrotron radiation, thermal or non-thermal bremsstrahlung or inverse Compton radiation. Gruber (1974) has calculated fits of these spectra to the excess under the assumption of a monoenergetic electron distribution which maximises their spectral sharpness, but as he points out, these show unacceptable chi squares of about 6 per degrees of freedom. Physical arguments can be raised against these models, because, for any of them, a nearby monoenergetic electron population, as required, is quite unlikely. The lifetime of the 10^{15} eV electrons necessary for the synchrotron model would be only a few years and a single, recent injection would have to be postulated in order to avoid evolutionary broadening of the electron



energies (Gruber, 1974).

Two other mechanisms which have greater spectral sharpness are black-body emission and nuclear line emission. However, Gruber calculates that a black-body of temperature 3 MeV, or $T = 3 \times 10^{10}$ degrees, must have a radius of one centimetre at the distance of the Crab to produce the observed flux. This seems unlikely.

As already mentioned, the calculations of Clayton and Craddock (1965) for the present radioactive decay lines to be expected on the basis of the r-process (Burbidge et al. 1957) are factors of 100 to 10,000 in strength below the observed excess, and the principal lines mentioned do not extend higher than 1.8 MeV. Thus remnant radioactivity is also unlikely to cause the 1-10 MeV excess.

A possibility that remains is gamma ray emission following collisional excitation of matter (Gruber 1974). Because of the wide energy band of the excess, a number of lines must be involved, or some sort of spectral broadening, such as Doppler spreading or Compton scattering operating on a small number of lines. The deuteron-formation line at 2.236 MeV, already observed in solar flares (Chupp et al. 1973) would be a natural candidate. For this possibility, there must exist within the nebula some region with a density sufficient to support the observed emission, with a flux pervading the region to collisionally excite the matter. Gruber (1974) has made calculations to estimate the density of such a region required to explain the observed excess. He finds that the calculated mass density and kinetic energy density of such a region are inconsistent with two regions considered - the nebula at large and the pulsar magnetosphere out to the speed of light cylinder. However, a third region, the dense equatorial ring which has been postulated to surround the neutron star at a radius of about 150 km (Roberts and Sturrock, 1973) remains a possibility. Substantial Compton scattering would account for the lack of spectral features so far observed.

The source of the plasma, for collisional excitation of the matter in the belt must be the surface of the neutron star. The nature of the pumping mechanism to eject this plasma has not been worked out (Roberts and Sturrock, 1973).

Another theory of interest is that of Cocke (1975). He has considered the production of power-law spectra and the evolution of cosmic synchrotron sources, and applied his calculations, in particular, to the Crab Nebula. His model consists of an interior region (region A), surrounding the

pulsar, where hydromagnetic activity is observed, and where Fermi acceleration is believed to occur. This region is surrounded by a larger region B (the rest of the nebula), where there is no Fermi acceleration, and the dominant loss processes are synchrotron losses for optical and X-ray electrons, and adiabatic expansion and diffusion losses for radio electrons. Cocke argues that the observed synchrotron spectrum is too complicated to be fitted well by the conventional model of Shklovsky (1966), with only one break in the spectrum at low energy X-rays, and that his dual model is in good accord with the observed spectrum and with certain other characteristics of the nebula. Cocke's interpretation is that there is also a break in the spectrum at around 1 to 10 MeV. This proposed additional break is interesting for low energy gamma ray measurements. However, Cocke's model does not explain a 1-10 MeV excess, because the spectrum is presumed by him to be fitted by single power law between the breaks from low energy X-rays to around 1-10 MeV, and then another single power law up to high energies. Nevertheless, his theory may be capable of adaptation to fit a 1-10 MeV excess.

The previous theories mentioned, have been presumed to have to explain an excess solely in the 1-10 MeV region, which implies a relatively sharp feature. However, a nearby transient source would not be necessarily restricted to having such a large excess in only the 1-10 MeV region, thus enabling its spectrum to be fitted by the more conventional models such as synchrotron processes, for example, A0535+26 as discussed in section 6.2.

An alternative is the nuclear de-excitation radiation model of Roberts and Sturrock (1973), where the radiation originates in a condensed region much smaller than the nebula, for example the proposed accretion ring in synchronous orbit around the pulsar (Roberts and Sturrock, 1973).

If the concept of transient sources is accepted, then there exist many theories of such transient X and gamma ray phenomenon, as discussed in section 1.6.

Now let us consider the pulsar NP0532 itself in more detail. One important experimental parameter is to measure accurately the phase of the main pulse at gamma ray energies to determine if there is any shift from the optical and X-ray positions, as might be expected if the one originates near the surface of the neutron star and the other at the speed-of-light cylinder (Maraschi L. and Treves A., 1973). There is some evidence of a shift in the LEG 4 data (see diagrams 5.5 to 5.7) although this is probably a result of poor statistics.

As regards the experimental implications for theories of the pulsar NPO532, the most striking feature of the Crab Pulsar, in the 10^4 to 10^9 eV range, is the transition from a predominantly unpulsed flux at lower energies to a predominantly pulsed flux at higher energies (Fichtel, 1977). Although the data is still uncertain, we may draw a few conclusions. The pulsed and unpulsed emission mechanisms clearly have a different energy dependence, which is understood, qualitatively at least, by a model in which the pulsed emission comes from synchrotron radiation near the pulsar, while the unpulsed component comes from regions of lesser magnetic field strength, probably by a combination of scattering of electrons and interaction of high-energy protons and the ambient gas.

Shortly after the discovery of the first pulsars, Gold (1968, 1969) produced a model of a rapidly spinning neutron star with a strong surface magnetic field ($\sim 10^{12}$ gauss) and a co-rotating magnetosphere. Using this basic model, Shklovsky (1970) has pointed out that the synchrotron emission from a source of relativistic particles can explain the pulsar spectral emission features.

A number of theories to explain the Crab Pulsar emissions have since been formulated, but these are mainly variations on the theme of a neutron star at the core. Many of the earlier theories have been reviewed by Apparao (1973). Some more recent theories include those of Massaro and Salvati (1977), Michel (1978), Salvati and Massaro (1978), Hinata (1977, 1978), Hardee (1977), Cheng and Ruderman (1977) and Roberts and Sturrock (1973).

Of these, Hinata (1977, 1978) deduces the momentum distribution of relativistic particles near the Crab pulsar from the observed X and gamma ray spectra ($10^3 \sim 10^9$ eV). Cheng and Ruderman's model (1977), predicts that electron-positron pair production in the Crab pulsar outer magnetosphere at the "outer gap", 3×10^7 cm from the neutron star, is the source of pulses at all observed energies. The model gives optical and X-ray pulses from inverse Compton scattering of radio photons by e^+ and e^- particles, and this Compton boosting is predicted to only be significant in the faster pulsars similar to the Crab, because of the much weaker magnetic fields near the light cylinder in much slower pulsars.

Hardee (1977) explains the phase difference between radio and gamma ray pulses at $> 10^{11}$ eV found by Grindlay et al. (1976) as being due to magnetic field configuration and aberration effects.

Salvati and Massaro (1978), and Massaro and Salvati (1977) have

developed a model specifically calculated for gamma ray emission from the pulsar PSR 0833-45, but they point out that their model can be applied to most pulsars. This is as opposed to earlier ideas which were tailored solely to the Crab pulsar and were based on inverse Compton scattering. Their model, by contrast, assumes that the primary particles are accelerated close to the star surface and then injected along the open field lines, which cause them to emit curvature radiation.

It appears, then, that explanations of the emissions from the Crab pulsar, NPO 532 are found more easily than for the tentatively proposed 1-10 MeV excess in the total flux from the Nebula. Nevertheless, many models of the pulsar are inextricably bound up with models of the total emission, and so consequently, a 1-10 MeV excess, if confirmed, may have important consequences for such theories.

Having examined the results using the anticollimated LEG 4 detector, it is recognised that many of the major astrophysical questions associated with low energy gamma ray astronomy can not be conclusively answered with detectors of such low sensitivity.

Consequently, the Southampton group considered improved designs of detectors. The resulting design chosen for experimental investigation is the MISO Low Energy Gamma Ray Telescope. This experiment is described in the next chapter, together with a description of the computer calculation of the theoretical predicted efficiency of the central detector.

Chapter 7 - The Milan-Southampton (MISO) Low Energy Gamma Ray Telescope

7.1 Introduction

The LEG 4 detector, while giving interesting results, was still relatively insensitive. Consequently, a new detector design was proposed and constructed jointly by the Southampton and Milan University groups. This detector first flew from Palestine, Texas on 22nd and 23rd May, 1977.

This chapter mainly deals with the computer program developed to optimise the detection efficiency of the central part of the detector. Once this program had been used to demonstrate the feasibility of the detector as regards its basic sensitivity, the Milan University group introduced additional refinements to produce a more comprehensive program to deal with all the modes of operation of the instrument of interest. However, all the essential aspects of the efficiency calculation are included in this chapter.

The telescope is described by Maccagni et al.(1974), and the details of the tests of the detector, particularly for neutron-induced background effects, are described by S.J. Martin (1978).

The next section describes the overall features of the detector and the original objectives behind its conception.

7.2 The Basic Detector Design and Objectives

7.2.1 The Objectives

The inception of the development of this detector was prompted by the relative insensitivity of previous detectors in the low energy gamma ray range. A problem in designing telescopes for gamma ray astronomy in the 1-10 MeV region is the effect of the low photon absorption cross-section and the fact that the nature of the detection processes makes it difficult to obtain a good intrinsic angular resolution.

Passive Collimation has had problems due to the build up of low-energy gamma rays in the shielding due to a variety of mechanisms (Lovett, 1973). Active collimation, to obtain the sensitivity required, needs to use large crystal detectors. These are rather expensive for larger-aperture applications, making it an uneconomic proposition to provide the shielding thickness necessary. In addition, there may also be a problem with the anticoincidence counting rates at float altitudes because of the length of the light pulse from the crystal, due to the large volume of scintillator.

Anticollimation has the advantage of simplicity. At the time of the original conception of the MISO telescope, the anticollimation method was considered to be rather difficult to develop for a very high sensitivity application. This view has been subsequently re-examined as is mentioned in the next chapter.

Double Compton time of flight techniques are very good for observations of the diffuse cosmic gamma-ray flux, but have severe limitations for observation of point sources due to poor directionality and low efficiency.

As an attempt to improve upon past techniques, the Milan-Southampton collaboration set out to investigate the merits of a Compton coincidence detector with a semi-active shield.

One objective of low energy gamma ray astronomy is to extend the spectral information about known X-ray sources to higher energies, in order to facilitate discrimination between various theories of source emission mechanisms. In order for a low energy gamma ray telescope to be able to detect a reasonable number of sources, then extrapolating the spectra of known X-ray sources to higher energies suggests that the instrument should be able to detect a source flux of the order of 10^{-3} photons/cm²s $E > 1\text{MeV}$. In addition, the angular resolution needs to be adequate to avoid source confusion, and the energy resolution good to permit the detection of possible nuclear gamma ray lines. The MISO detector was designed to obtain a good gamma ray signature by the coincidence requirement between the upper and lower detector crystals. In addition, this coincidence condition gives some directionality from the bi-dimensional analysis of the energies deposited in S1 and S2.

The next section discusses the basic design of the MISO detector, which aimed at achieving the objectives set out in this section.

7.2.2 The Design

The detector is shown schematically in figure 7.1. Two scintillation counters S1 and S2 comprise the central detector. These are completely surrounded by a plastic anticoincidence counter A1, and separated by an independent anticoincidence counter A3. The final design chose the detector S1 to be composed of liquid scintillator NE 311, and the detector S2 to be a large NaI(Tl) crystal. The diameter of each counter is approximately 27 cm, the depth is 10 cm and the separation is about 3 cm.

An incident gamma ray, along the axis of the detector, first arrives at the detector S1, where it has a certain probability of undergoing a Compton interaction. Having been scattered, the photon then has a finite probability of emerging from S1 and then interacting again in S2. The coincidence of a pulse from S1 and S2 indicates a Compton scattering interaction. The anticoincidence jacket A1 is used to veto charged particles which lose energy in S1 and/or S2. To indicate whether the "particle" detected by S2 was charged or neutral, the A3 counter is used.

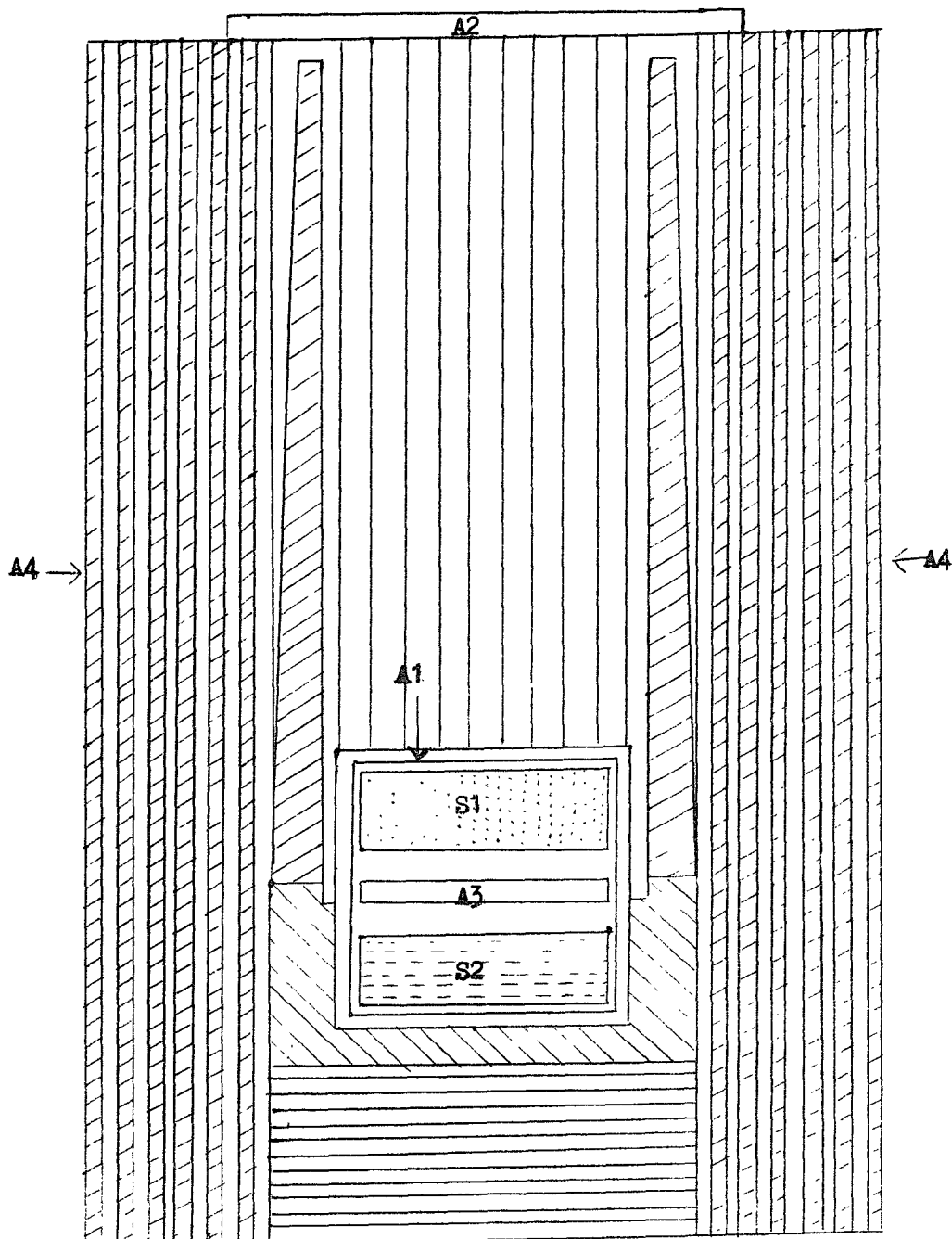
The lead/plastic scintillator sandwich A4 and A5, containing six radiation lengths of lead interspersed with six thin plastic scintillators is used to shield the central detector system from atmospheric gamma rays.

The thin plastic scintillator A2, by its operation, effectively eliminates the background effects caused by the entry of charged particles through the aperture of the telescope. Co axial angular directionality ($\sim 10^\circ$) for gamma rays in the range of interest is provided by the slatted lead collimator situated inside the semi-active shield. The shielding effect is improved by this collimator by increasing the radiation lengths to twelve, through which the atmospheric gamma rays have to travel before reaching the central detector.

A jacket, containing a mixture of boron, tungsten, and lithium (chosen for their high neutron absorption cross-sections) set in a wax moderator, surrounds the lower half of the central detector to act as a neutron shield. This shield is relatively efficient ($> 90\%$ up to thermal and epithermal neutron energies (up to ~ 600 eV)).

The logic condition for a pulse to be accepted, is given by the complete Compton coincidence signature: $S1.S2.(A1 + A2 + A3 + A4 + A5)$.

Features which improve the sensitivity of the telescope are: the intrinsic directionality of the system, and reduction of neutron effects, off-axis gamma rays, and spallation events by bi-dimensional analysis of



- | | | |
|--|--|---|
|  Pb |  A5 |  Plastic |
|  NE 311 | |  Mixture of compounds with high epithermal neutron cross sections. |
|  NaI (Tl) | | |

Diagram 7.1

the energies deposited in S1 and S2. It may be noted that the Compton coincidence system has some intrinsic directionality even without shielding. Directionality can be further improved by examining the energy deposited in the two scintillation material regions S1 and S2, which is dependent on the direction of the incoming photon. By this means, distinction can be made between photons incident from on and off axis, because if we assume that the photon undergoes an initial Compton interaction in S1, and that all the remaining energy is absorbed in S2, the apparent angle of Compton scattering is given by:

$$\cos \phi = 1 - \frac{m_0 c^2}{E_1} + \frac{m_0 c^2}{E_1 + E_2}$$

where m_0 is the electron rest mass, and E_1 and E_2 are the energies deposited in S1 and S2 respectively.

Typically, coincidences induced by spallation and neutrons, for example those resulting in β -decay in one element which emit a gamma ray photon in the direction of the other S element, will not deposit this energy in the same way as on-axis photons.

The coincidence system can study gamma ray energy deposits in the range ~ 0.18 MeV to ~ 20 MeV, because the lower thresholds on the liquid and sodium iodide detectors are 25 keV and 150 keV respectively. In order to maximise the on-axis detection efficiency for gamma rays with energy close to 1 MeV, the thickness of the liquid scintillator was chosen for an optimum value.

The telescope has an intrinsic angular resolution of about 14° FWHM in zenith, which is reduced in the azimuth plane to 3.2° FWHM by the use of a slatted collimator. The gamma and X-ray events are timed to an accuracy of 0.75 n sec.

In designing the telescope, several parameters of the detector geometry are variables which require careful choice in order to produce optimisation of the response of the instrument. A computer program was devised to investigate the theoretical detection efficiency of the central detector for various thicknesses and separations of the two elements S1 and S2. The basic elements of this program are described in the following two sections. A complete listing and description of the program is available from the library of the Southampton University astronomy group.

7.3 The Initial Assumptions of the Efficiency Program

The basic objective of the program was to find the theoretical efficiency of the central detector arrangement of the Compton coincidence system shown in diagram 7.2, for detection of gamma rays in the region of 1 to 10 MeV. The efficiency was defined as:

The number of gamma rays causing scintillations in both blocks

Total number of gamma rays incident

Initially, a simplified model was assumed as an approximation to ascertain the feasibility of the system as a relatively efficient gamma ray telescope. The Milan University group then replaced the initial simplified assumptions with more comprehensive calculations.

The original assumptions involved were the following:

1. It was assumed that gamma rays were initially incident along the detector axis, as in diagram 7.2.
2. The total attenuation coefficient was used to find the probability that a gamma ray has reached distance x into the element S1 without having undergone any interaction. At this distance, x , into S1, it is assumed to undergo a Compton interaction.
3. The gamma rays are assumed to be unpolarised.

Most of the basic physics can be derived from a standard text such as Evans (1955).

7.4 General Outline of the Method of Solution

In designing the detector, it was wished to determine the best dimensions, materials and geometries of the arrangement to maximise the source detection efficiency, and to reject the background gamma rays, in order to observe cosmic sources.

Consequently, the computer program was designed to find the various probabilities that a gamma-ray would interact at a particular location within either S1 or S2; for a particular incident gamma ray energy, E_γ ; distance d between S1 and S2; and depths w_1 and w_2 , of S1 and S2 respectively.

The expression obtained can then be used to find the efficiency for particular E_γ , d , w_1 and w_2 , and graphs of the results can then be

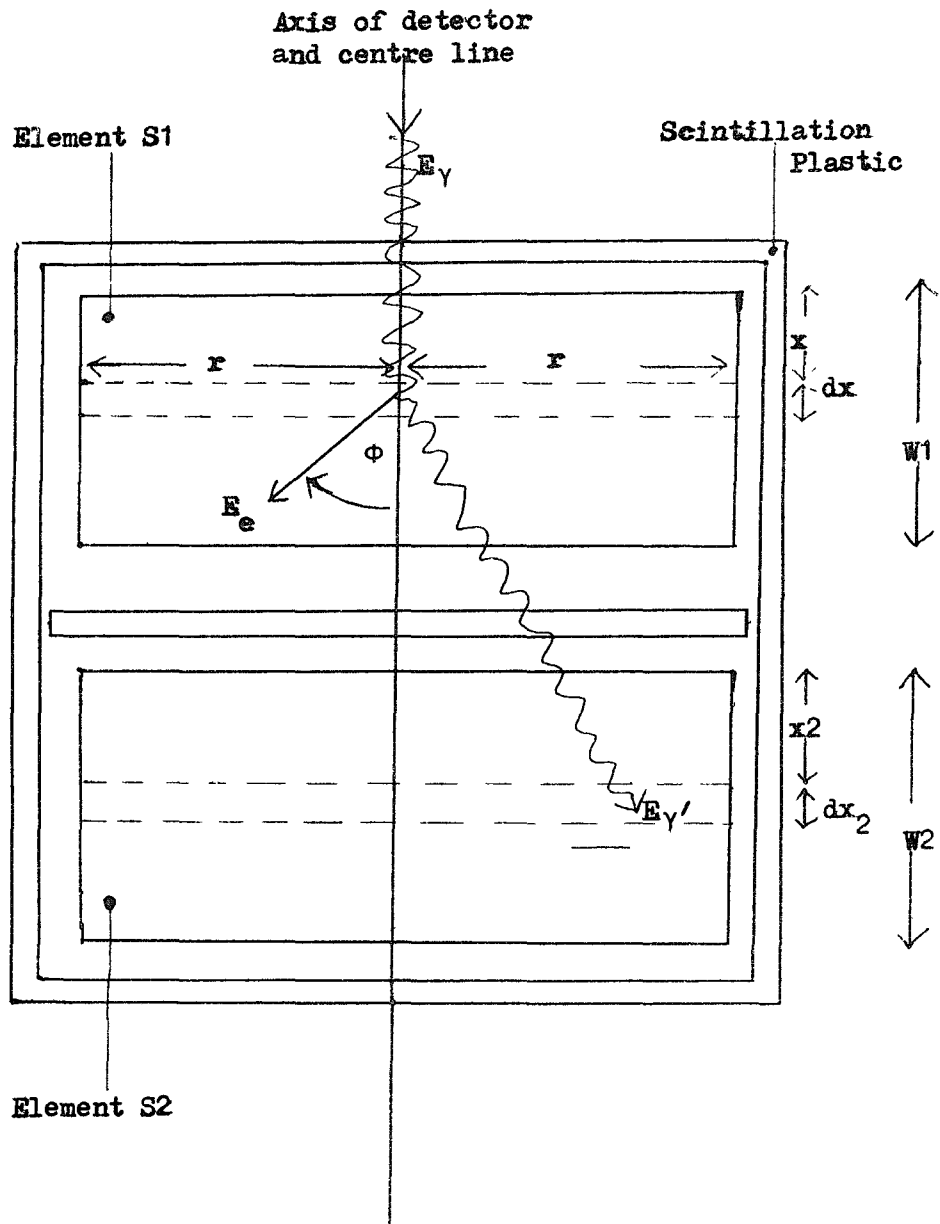


Diagram 7.2 Central Detector General Arrangement

examined for the optimum values.

The efficiency η can be expressed as the product of various probabilities, i.e.:

$$\eta = P_1 \cdot P_2 \cdot P_3 \cdot P_4 \cdot P_5 \cdot P_6 \cdot P_7 = \prod_{i=1}^{i=7} P_i$$

= the number of gamma rays causing scintillation in both S1 and S2 and not vetoed by the anticoincidence system, divided by the total number of gamma rays incident upon the detector.

The probabilities can be briefly described as follows:

- P_1 = The probability of a gamma ray arriving a distance x into S1 (i.e. the probability of not interacting before reaching x).
- P_2 = The probability of a Compton interaction at x into S1 giving energies E_e , E_γ' at x in S1, where E_e is the energy of the electron after the Compton interaction, and E_γ' is the energy of the gamma ray after the Compton interaction.
- P_3 = The probability of the gamma ray escaping from S1, i.e. the probability that the gamma ray does not interact again in S1 in the remaining distance ($w_1 - x$).
- P_4 = The probability that the electron of energy E_e , does not arrive in the scintillation plastic, and hence register in the anticoincidence counter and falsely veto the event.
- P_5 = The probability that the scattered gamma ray of energy E_γ' , reaches S2, once it has left S1.
- P_6 = The probability that the scattered gamma ray of energy E_γ' , interacts in S2 at distance x_2 .
- P_7 = The probability that the scattered gamma ray doesn't interact in the scintillation plastic and hence be falsely vetoed by the anticoincidence counter.

As a first approximation, it was assumed that if the gamma ray reached the top face of S2, then it always interacts, i.e. $P_6 = 1$.

In addition, it was assumed that the scattered gamma ray doesn't interact in the scintillation plastic at all, i.e. $P_7 = 1$.

In brief, $P_1 = e^{-\mu_0 x}$, where $\mu_0 =$ the total linear attenuation coefficient for various values of photon energy, $h\nu$, and Z values of the materials (Davison and Evans, 1952; White, G.R., 1952; White G.R., 1952; Latter and Kahn H., 1949; and Fano U. and Davisson and Evans, 1952; Evans, 1955).

P_2 and P_5 are combined in the expression, using the Klein Nishina formula:

$$P_2 P_5 = \int_{T=0}^{T_{\theta m}/T \max} K.A.B^2 dT \quad (7.1)$$

where K is a constant dependent on the material used in S1; T is the energy of the struck electron;

$$A = \left(\frac{\nu'}{\nu_0} \right)^2 \left(\frac{\nu_0}{\nu'} + \frac{\nu'}{\nu_0} - \sin \theta \right)$$

where θ and ϕ are the scattering angles as in diagram 7.3, $h\nu_0$ is the initial photon energy; $h\nu'$ is the scattered photon energy;

$$B = \left\{ \frac{(1+\alpha)^2 - \alpha^2 \cos^2 \phi}{(1+\alpha)^2 - \alpha(2+\alpha) \cos^2 \phi} \right\}^2, \text{ where } \alpha = \frac{h\nu_0}{m_0 c^2}$$

where $m_0 c^2$ is the rest mass energy of an electron.

For the Compton interaction, the scattering angle θ , places a limit on the maximum transfer of energy to the electron, T_{\max} . In addition, the scattering angles θ and ϕ are related to the electron energy T .

In order for the photon, scattered at angle θ , to reach the second element S2, it can be seen from diagram 7.4 that θ must be less than θ_{\max} , where θ_{\max} is given by

$$\tan \theta_{\max} = \frac{r}{d + (w_1 - x)}$$

a limit on T , so that $\theta < \theta_m$, is equivalent to the condition $T < T_{\theta m}$,

Diagram 7.3

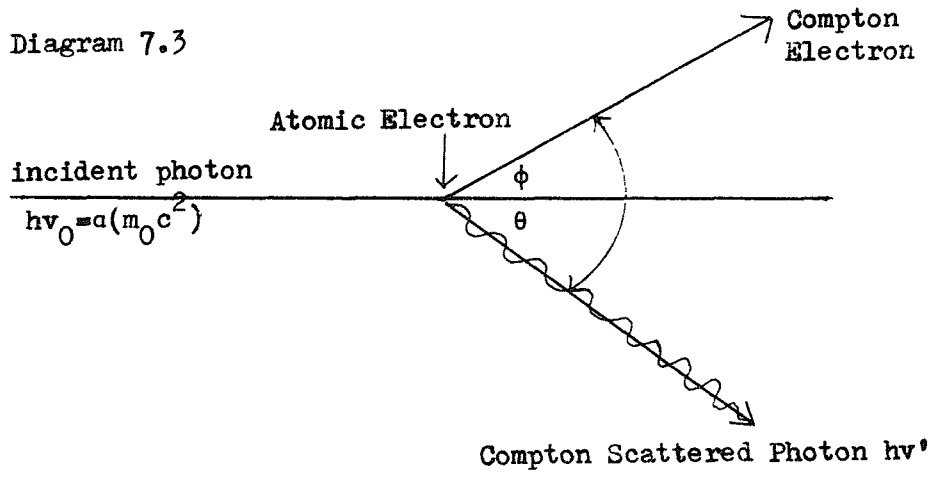


Diagram 7.4

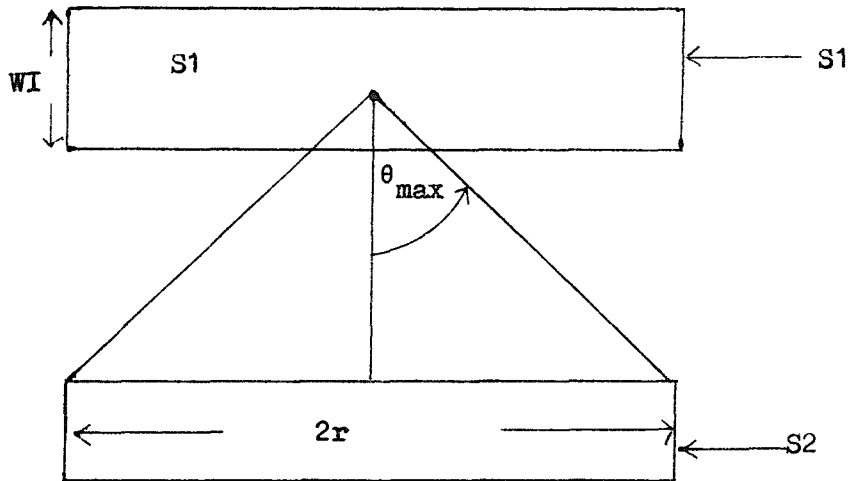
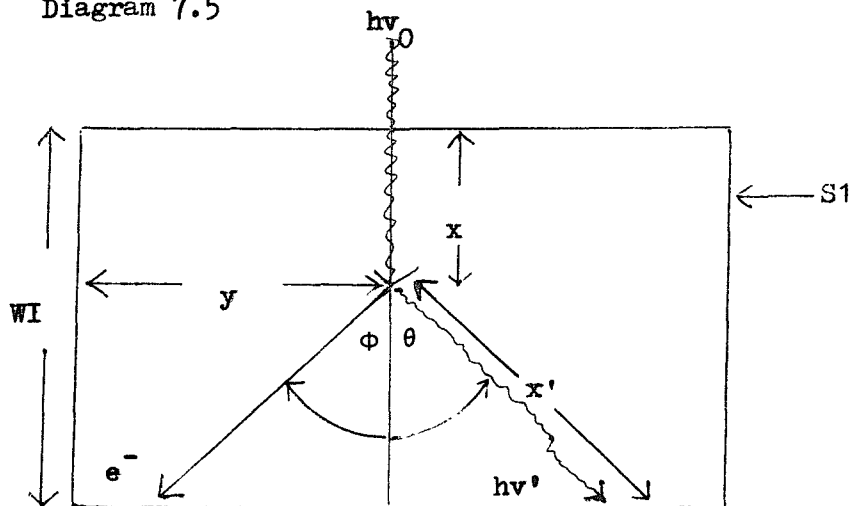


Diagram 7.5



where

$$T_{\theta m} = h\nu_0 - \frac{m_0 c^2}{1 - \cos \theta_m + \frac{1}{\alpha}}$$

So by limiting the integral of equation 7.1 to $T_{\theta m}$, or T_{\max} , whichever is the smallest, the two probabilities P_1 and P_5 are incorporated together.

In fact, equation 7.1 before integration, represents the probability that the photon is scattered at angle θ , the electron at angle ϕ , with energies according to $h\nu' = h\nu_0 - T$, where T lies between T and $T+dt$. Integrating over T gives the total probability for all scattered photon energies provided they are scattered at angles such that they will reach the second crystal S_2 .

$P_3 = e^{-\mu_0(w_1-x)\cos\theta}$, where μ_0 is the total attenuation coefficient for the new scattered energy $h\nu'$, and $(w_1-x)\cos\theta = x'$ is the distance the scattered photon has to traverse before emerging from S_1 (as in diagram 7.5).

P_4 was obtained using figures for the attenuation of electrons obtained by C. di Martinis (1972).

The equation for the overall efficiency was integrated numerically using the Gaussian method of integration (Conte). This method involves a considerable saving in computer time over the more traditional Trapezoidal, Romberg, or Simpson's Rule, methods, for a comparable accuracy, where analytic expressions for the variables exist.

Various checks for internal consistency within the program can be made. The major one being that the total probability of interacting at all should equal the sum of:

- a) the probability of interacting in S_2 with any interaction other than the Compton interaction (e.g. by pair production, photoelectric effect).
- b) the probability of interacting twice or more times in S_1 with the Compton interaction.
- c) the probability of a Compton interaction with a scattering angle outside the range to reach S_2 .
- d) the probability that the electrons are scattered with energy $T < T_{\min}$, so that they are not detected.
- e) the original detection efficiency calculated by the program.

The results of the program, including those of the more detailed treatment by the University of Milan, are described in brief in the next section.

7.5 Optimisation of the Detector Design

The sensitivity of the telescope depends not only on the quality of the shielding system, but also on the detailed design of the central detector.

A number of parameters can be varied in the program, for various cases of interest. Variations of the following parameters were investigated.

- E_0 - the initial incident gamma ray energy
- w_1 - the thickness of the top element, S1
- d - distance between the elements S1 and S2
- T_{min} - the lower discrimination level of the electrons produced by Compton interactions
- R - radius of the top element S1
- DISC - the upper discrimination level in the upper element, S1, which is in turn a function of the lower discrimination level in the bottom element S2.

In explanation of the use of DISC, we have the equation

$h\nu_0 - T = h\nu'$, where $h\nu_0 = E_0$ = the energy of the incident gamma ray; T is the energy of the scattered electron; and $h\nu'$ is the energy of the scattered gamma ray. Then, if $h\nu' > DISC$, therefore $T < (E_0 - DISC)$, and the largest value of T , $(E_0 - DISC)$, sets the upper limit on the integration over dT in the upper element, S1, for Compton interactions.

The reason for DISC, is to determine the directionality of a gamma ray which has interacted in S1 and S2. The energy of the scattered gamma ray is related to its angle of scatter, and hence its initial incident direction, as mentioned previously. To relate the directionality of the gamma rays to the discrimination levels in the lower element S2, a second program was run to find the relationships between E_0 , θ (scattering angle of the gamma ray), T (energy of scattered electron), $h\nu'$ (Energy of scattered photon), and the ratio $\frac{h\nu'}{T}$, for the Compton interaction.

Some results of this program are shown in figures 7.13 and 7.14.

Additional parameters that can be investigated are the depth and radius of the lower element S2. Some sample curves obtained from this program are presented in diagrams 7.6 to 7.12, and some sample curves from the results of the Milan University group are shown in diagrams 7.15 to 7.20.

In diagrams 7.7 and 7.15, the gamma detection efficiency of the Compton coincidence system, is shown for several values of the separation distance d between the detectors S1 and S2, for photon incidence along the axis. In the calculations for 7.15, the S1 detector was assumed to be made from NE 102A, but this should be a good approximation for the actual material used, NE311. These graphs show that the detection efficiency increases as the elements are placed closer together. However, decreasing the separation also affects the background counting rate. Detailed computations of the point-source sensitivity as a function of d have shown that, for the extremes of energy, the point source sensitivity is nearly independent of the detector separation.

The detection efficiency as a function of gamma ray energy, for several thicknesses of the S1 detector is shown in figures 7.7 and 7.16. From these, it can be seen that at lower energies, it is generally better to have a relatively thin S1 counter. As a means of obtaining a good compromise over the energy range of interest, it is probably best to maximise the integral number of counts in the desired energy band (e.g. 0.5 to 20 MeV). The results of this procedure can be seen in diagram 7.18. It can be seen that a maximum sensitivity should be attained using a detector thickness of about 10 cm.

The diagrams 7.7 and 7.16 give the values of the detection efficiency averaged over the whole area of the S1 detector. By contrast, diagram 7.17 gives an idea of the variation of the detection efficiency for different arrival positions of gamma rays on the surface of the S1 element. Figures 7.16, 7.17, 7.18 were obtained assuming a detection efficiency in the S2 unit (NaI) of nearly 100% and separation distance between the two elements $d = 0$.

Because the pulse heights of the signals from both the S1 and S2 elements are telemetered, suspected non gamma ray events can be rejected in the subsequent data analysis. Given that the total energy deposited in both the S1 and S2 detectors is E_γ , then from the equations of the

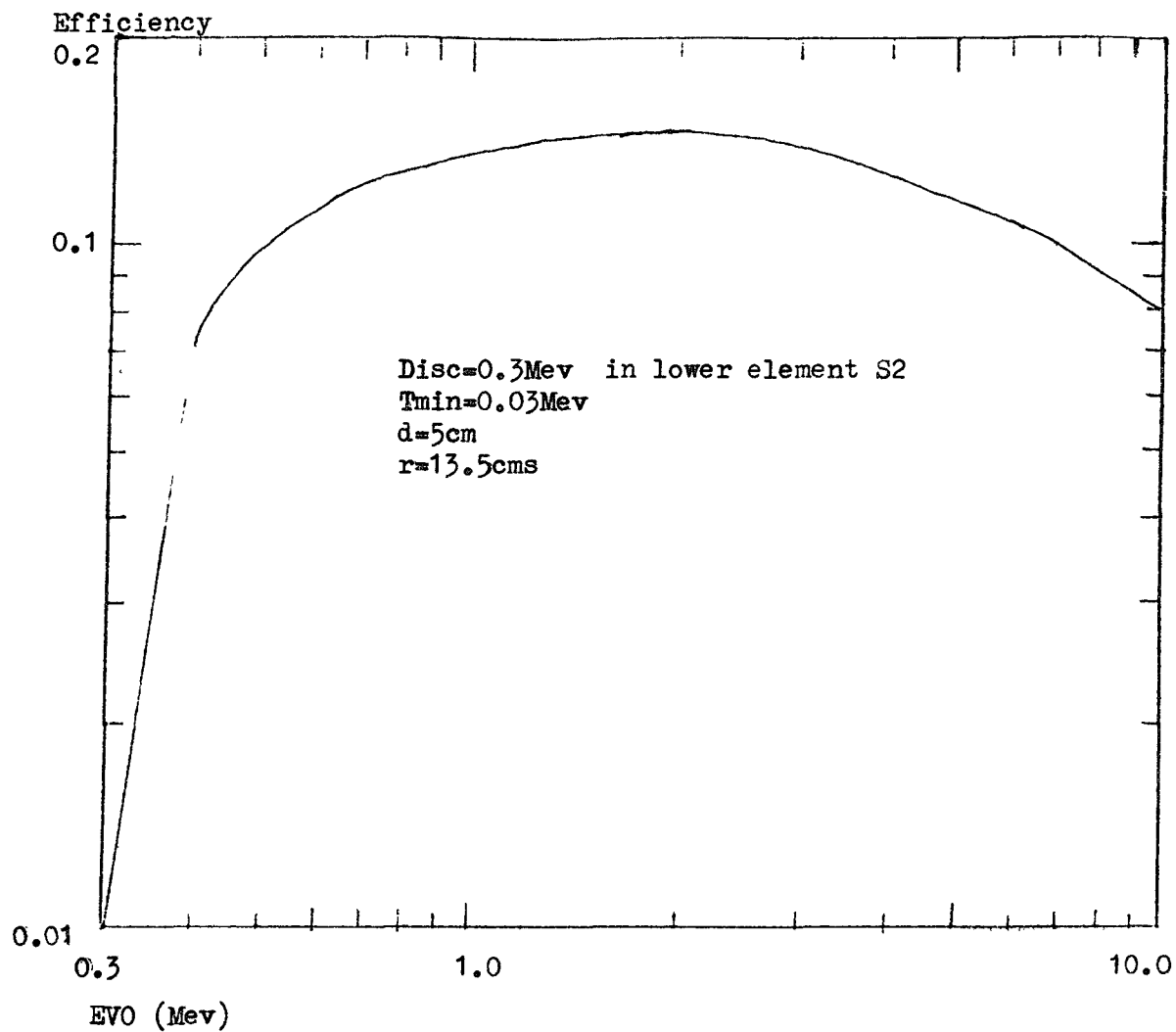


Diagram 7.6 Efficiency versus Photon Energy for 12.0gms
Thickness of upper element S1

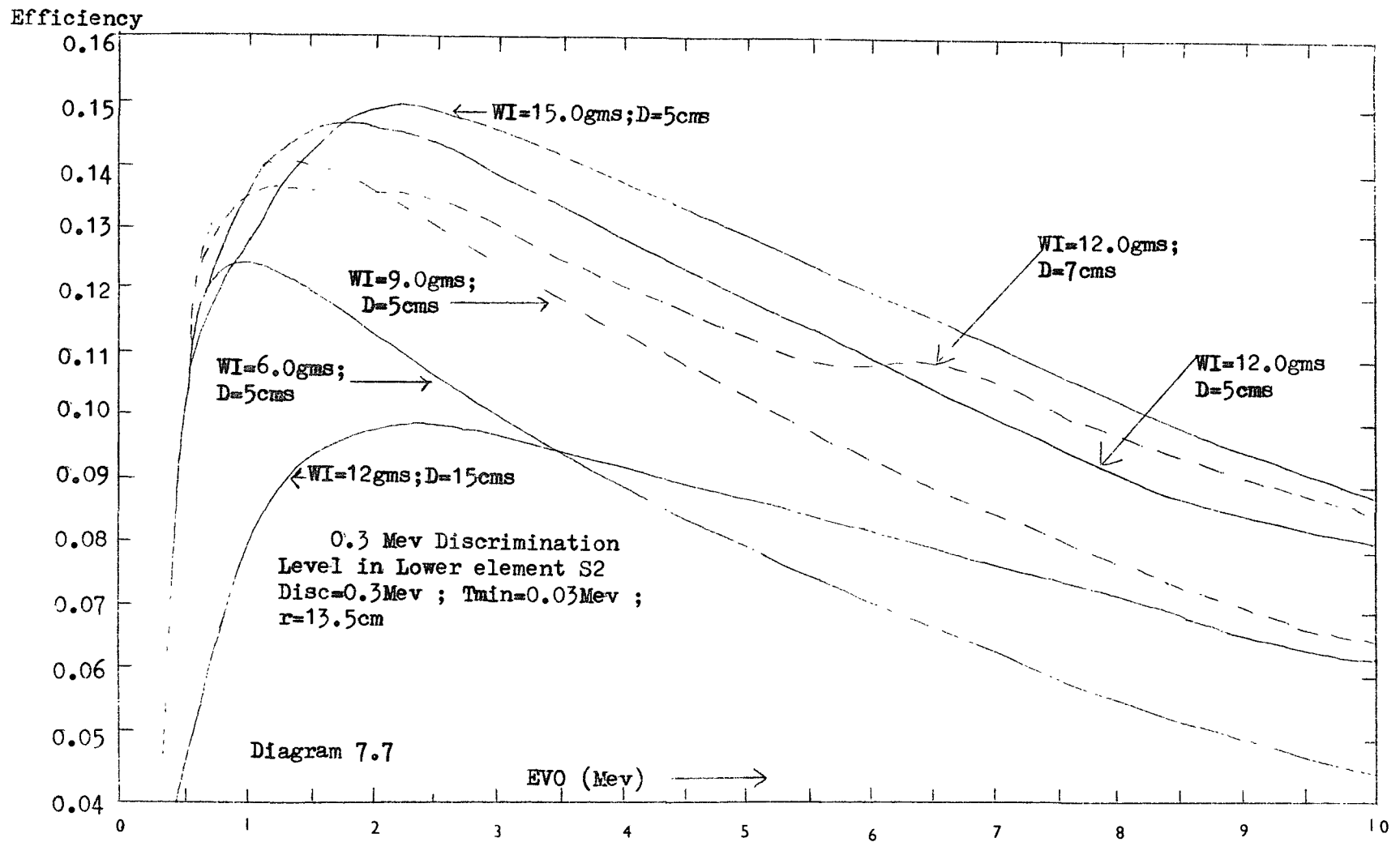


Diagram 7.9

Efficiency

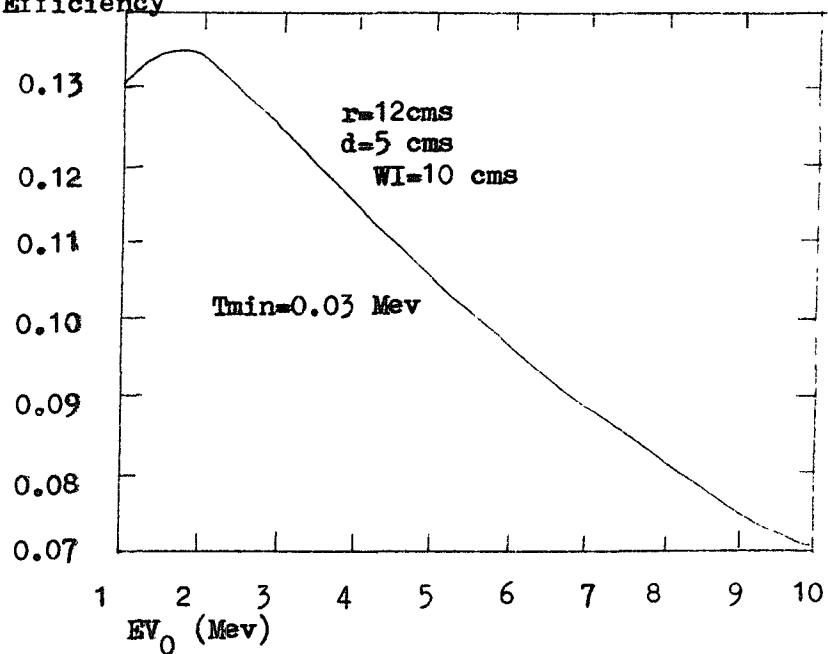


Diagram 7.8

Efficiency

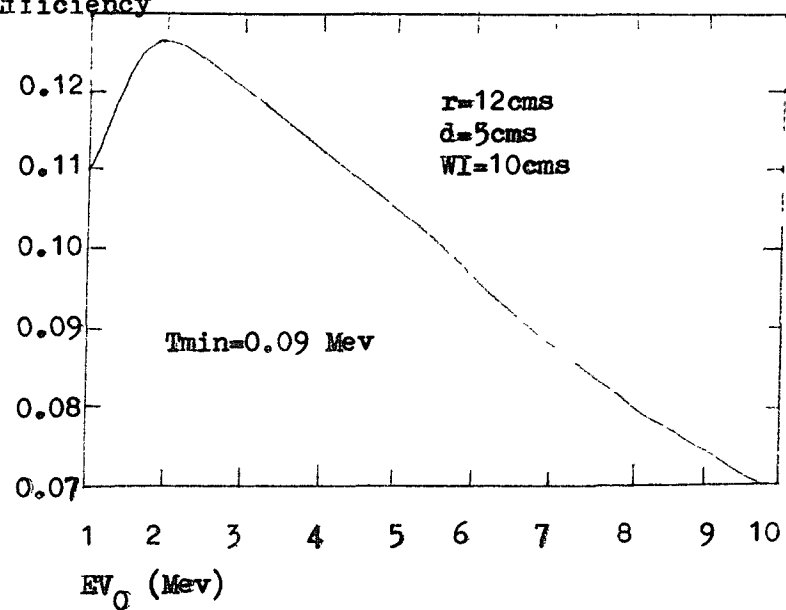


Diagram 7.11

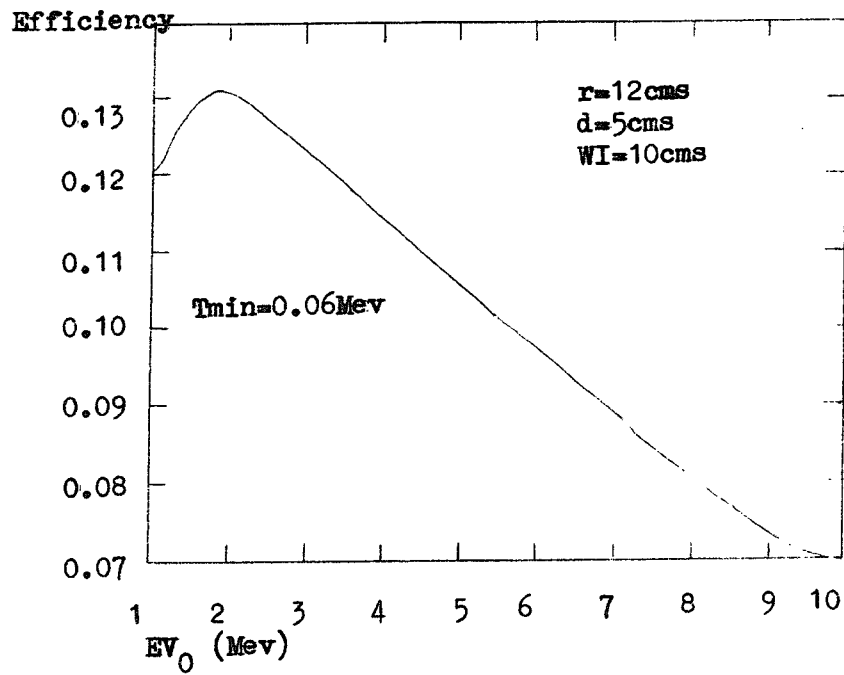


Diagram 7.10

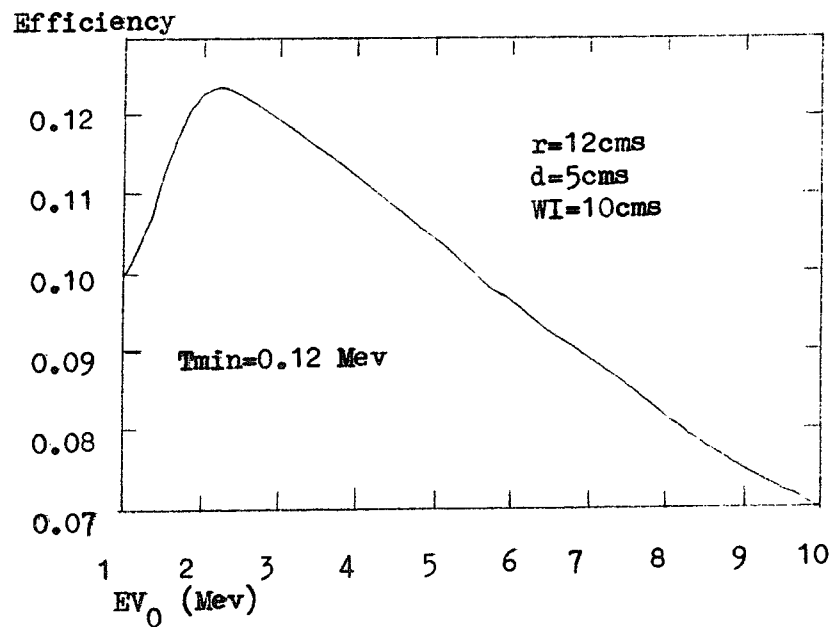
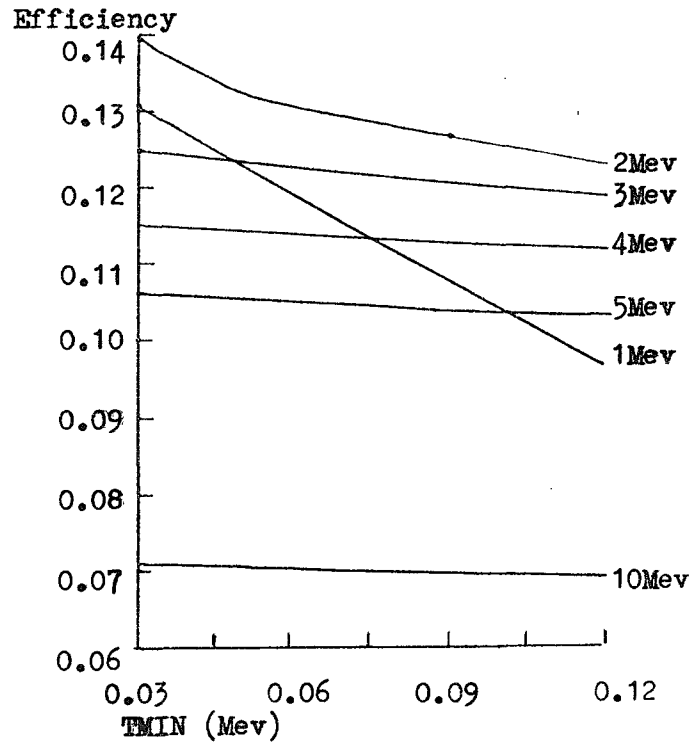


Diagram 7.12
Efficiency versus
TMIN



From the diagram we can see that, as we would expect, as EVO becomes larger and larger compared with these 4 values of TMIN, the difference in efficiencies becomes less, as the part of the integral for T less than TMIN is smaller in proportion when TMIN is smaller compared with TMAX, and TMAX will increase as EVO increases.

The graphs from EVO=6 Mev to 9 Mev have not been included for greater clarity, because it can be seen that the slopes just become smaller and smaller for increasing energy.

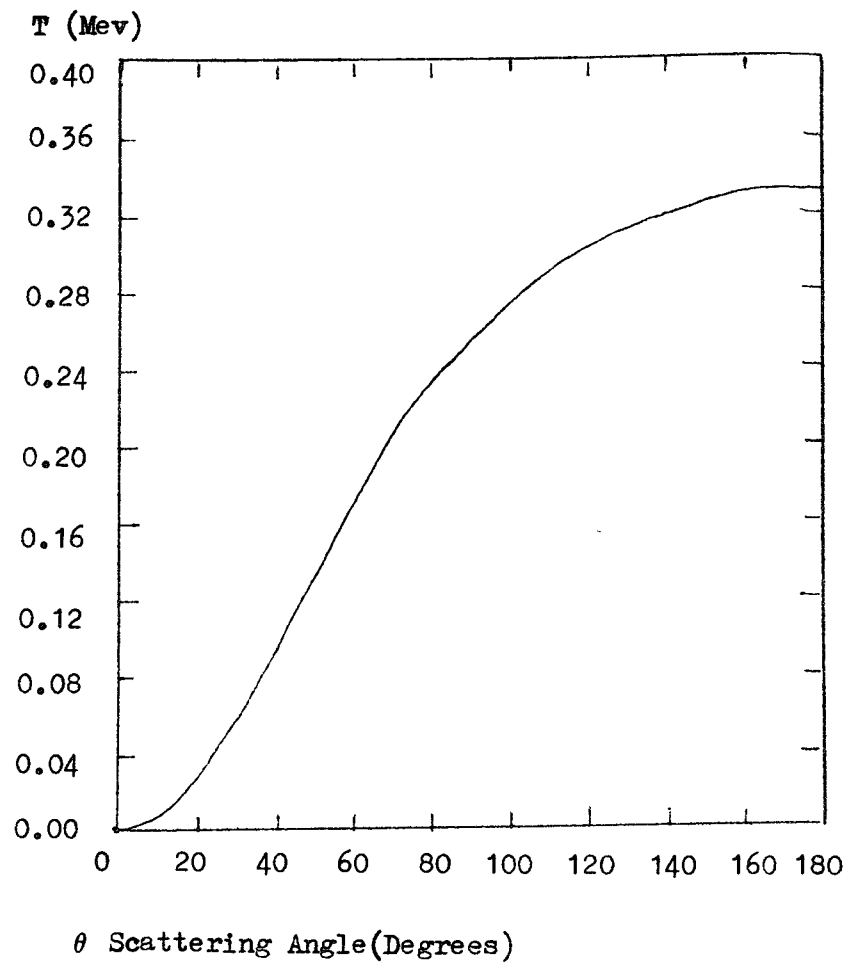
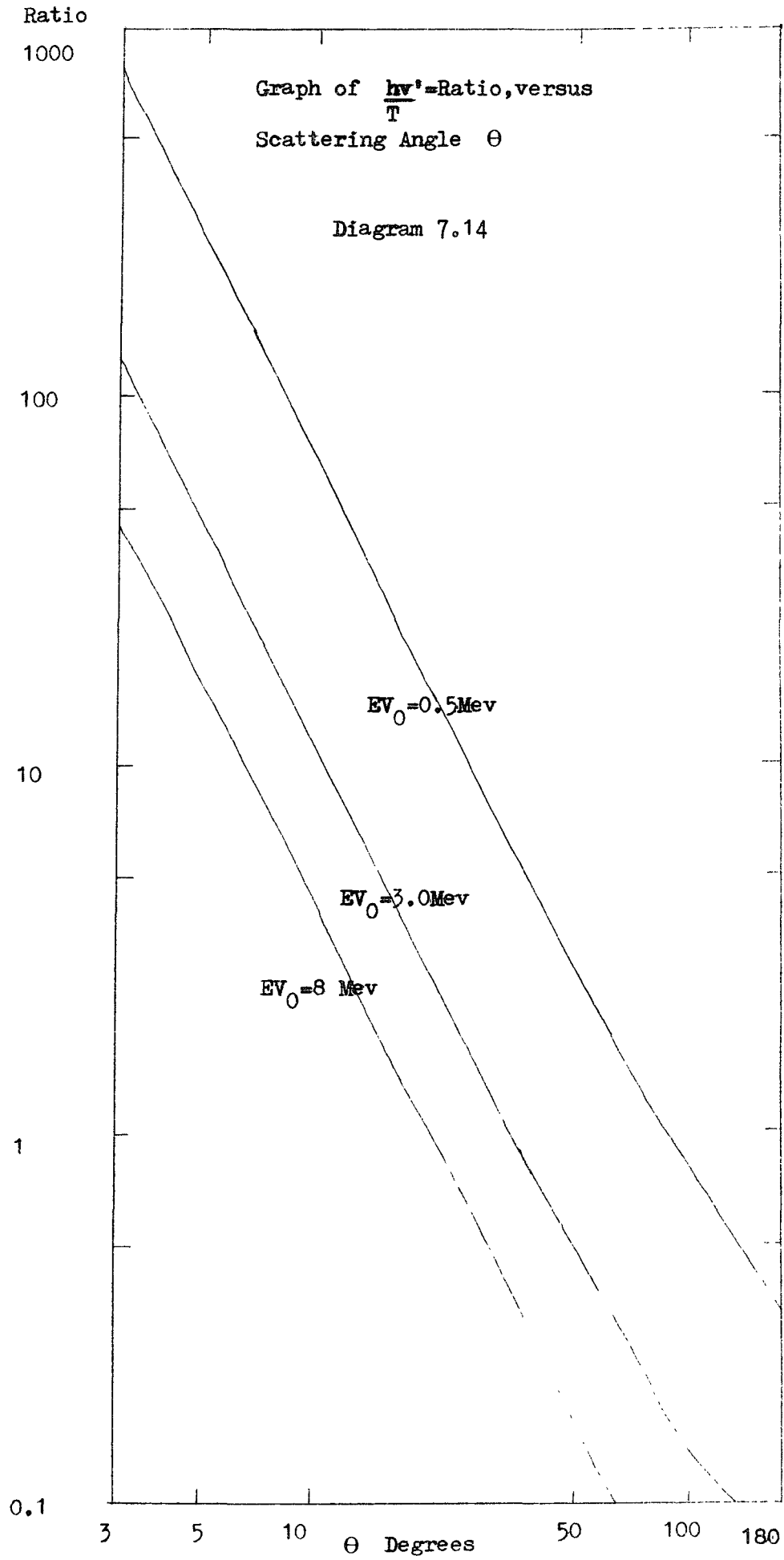


Diagram 7.13 T versus scattering angle θ
for $E_{VO}=0.5\text{Mev}$



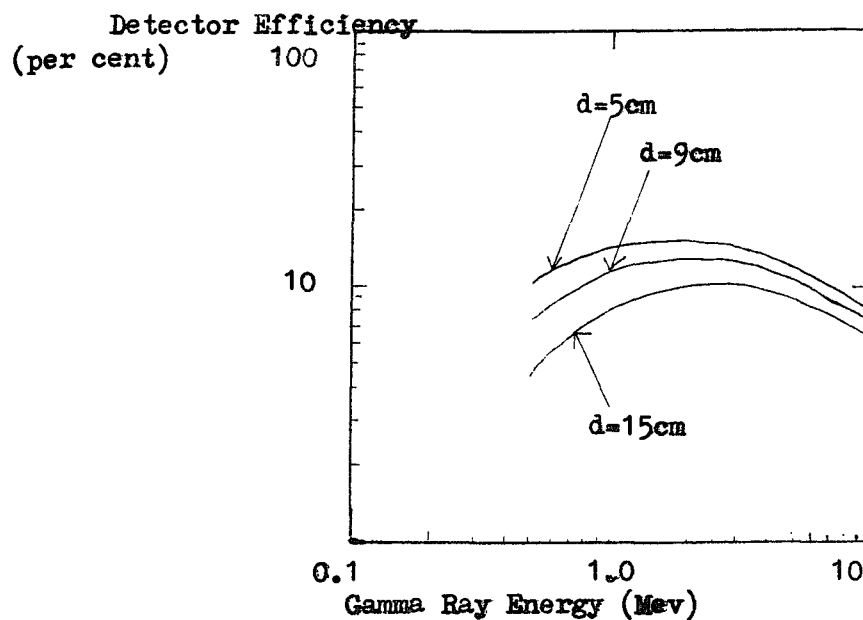


Diagram 7.15 Detector Efficiency of the Compton coincidence unit as a function of incident photon energy for several separations between the two elements S1 and S2. Thickness of S1 $X_0=12\text{cm}$. S1 Threshold=30keV S2 Threshold=300keV

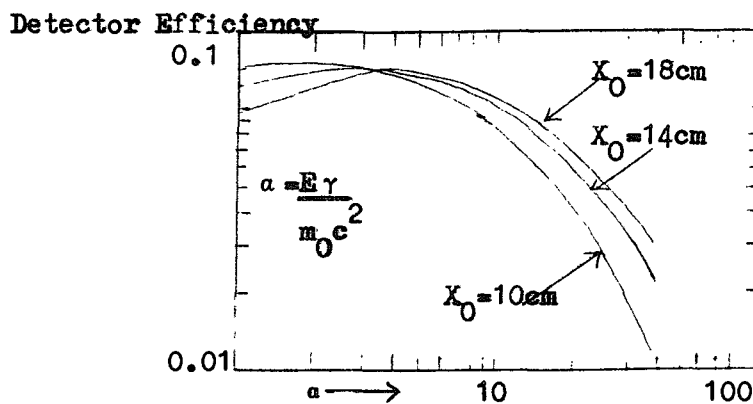
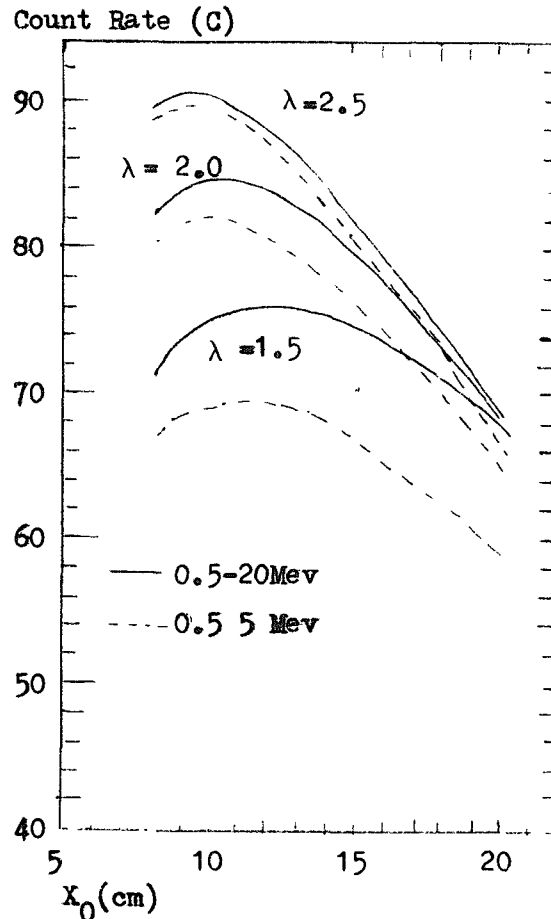


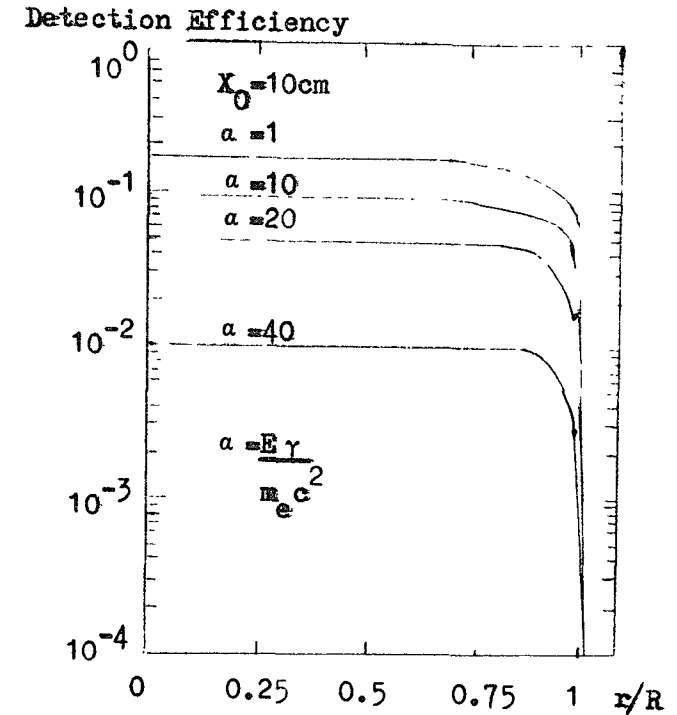
Diagram 7.16 Detection efficiency of the central unit as a function of photon energy for several thicknesses of the upper element S1 (averaged over the sensitive area of the detector)

Diagram 7.18



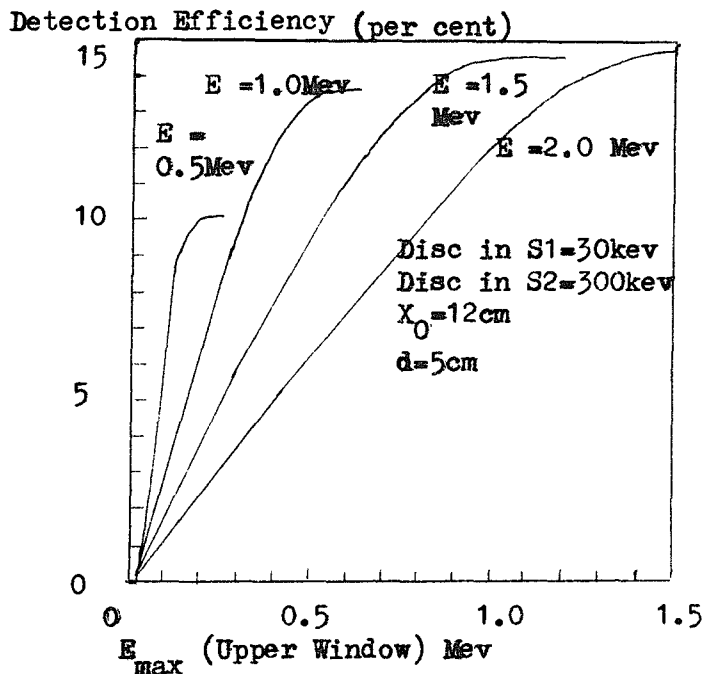
Integral number of photon counts between 0.5 Mev and 20 Mev for various thicknesses of the S1 detector for several slopes of the incident gamma-ray spectrum, λ . The count rate is in arbitrary units i.e. only shows relative count rate.

Diagram 7.17



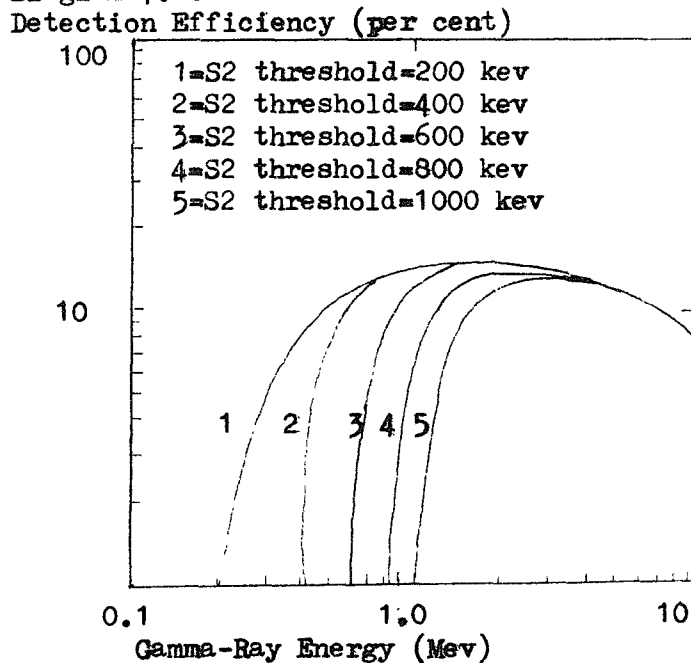
Detection efficiency of the Compton coincidence system as a function of arrival position on the surface of the S1 element for several values of the incident gamma-ray energy.

Diagram 7.19



Detection efficiency of the central unit as a function of the upper threshold level (E_{max}) on the S1 element for several incident photon energies.

Diagram 7.20



Detection efficiency of the Compton coincidence system as a function of the incident photon energy for several values of the lower threshold (E_{min}) of the S2 element.

Compton scattering interaction, it is possible to calculate the detection efficiency, when the requirement of a pulse in S1 and S2 (i.e. S1. S2) is used, as a function of the upper threshold level in the S1 detector, E_{\max} . This is shown in diagram 7.19. It may be noted that even when E_{\max} is set equal to about $0.4 E_{\gamma}$, only 10% of the genuine gamma events are vetoed. The contributions from many sources of background may be significantly reduced by this method, because they deposit energy in quite different proportions between detectors S1 and S2. By requiring that a minimum amount of energy be deposited in the S2 detector, other sources of background may be reduced. The effect of this procedure is shown in diagram 7.20.

Because S1 and S2 are close, the detection efficiency is high, and peaked in the direction of the shield aperture. This enables the rejection of much of the high flux of gamma rays which originate from close to the horizon.

The reason for using sodium iodide for the bottom detector is because it maximises the probability of detecting the photon scattered in S1, and because it reduces the probability of scattering of photons into S1.

7.6 Sources of Background

While the main sources of background are discussed in this section, a more comprehensive examination of the background effects has been accomplished by S.J. Martin (1978) and Baker et al.(1978).

7.6.1 Atmospheric Gamma Ray Induced Background

The cosmic gamma ray background and the gamma rays produced in the atmosphere can induce background gamma ray counts in the detector.

Matteson et al.(1974), Schönfelder et al.(1977) and Ling (1974) have investigated the spectral and angular distribution of the gamma ray background up to 10 MeV. A pronounced zenith dependence, which increases with energy, can be seen in the atmospheric flux per steradian. Baker et al.(1978) have extrapolated Ling's Semi-Empirical Model up to an energy of 30 MeV. This has then been combined with the experimentally

determined values of the detector efficiency and angular response to give the expected detector background at 3.5 mb and geomagnetic latitude $\lambda = 40^\circ$ (figures 7.21 and 7.22).

7.6.2 Neutron Induced Background

Atmospheric neutrons can interact with the nuclei of the detector which may subsequently emit charged particles and/or gamma rays. These emissions may then be registered as counts in the central detectors. In sodium iodide the amount of energy transferred in a neutron elastic scattering reaction (n,n') is small, because it comprises intermediate and heavy nuclei, and consequently this mechanism will generate negligible background in the energy range of interest. A large part of the neutron induced background in the NaI(Tl) crystal will be due to neutron absorption by I^{127} nuclei. For sodium, the absorption cross section is much smaller. Background counts can be produced by not only the gamma rays emitted promptly following a neutron absorption, but also delayed gamma rays produced by the decay of the I^{128} nucleus, which has a half-life of 25 minutes. Inelastic neutron scattering is also present within the NaI(Tl) crystal and can also give rise to background gamma rays.

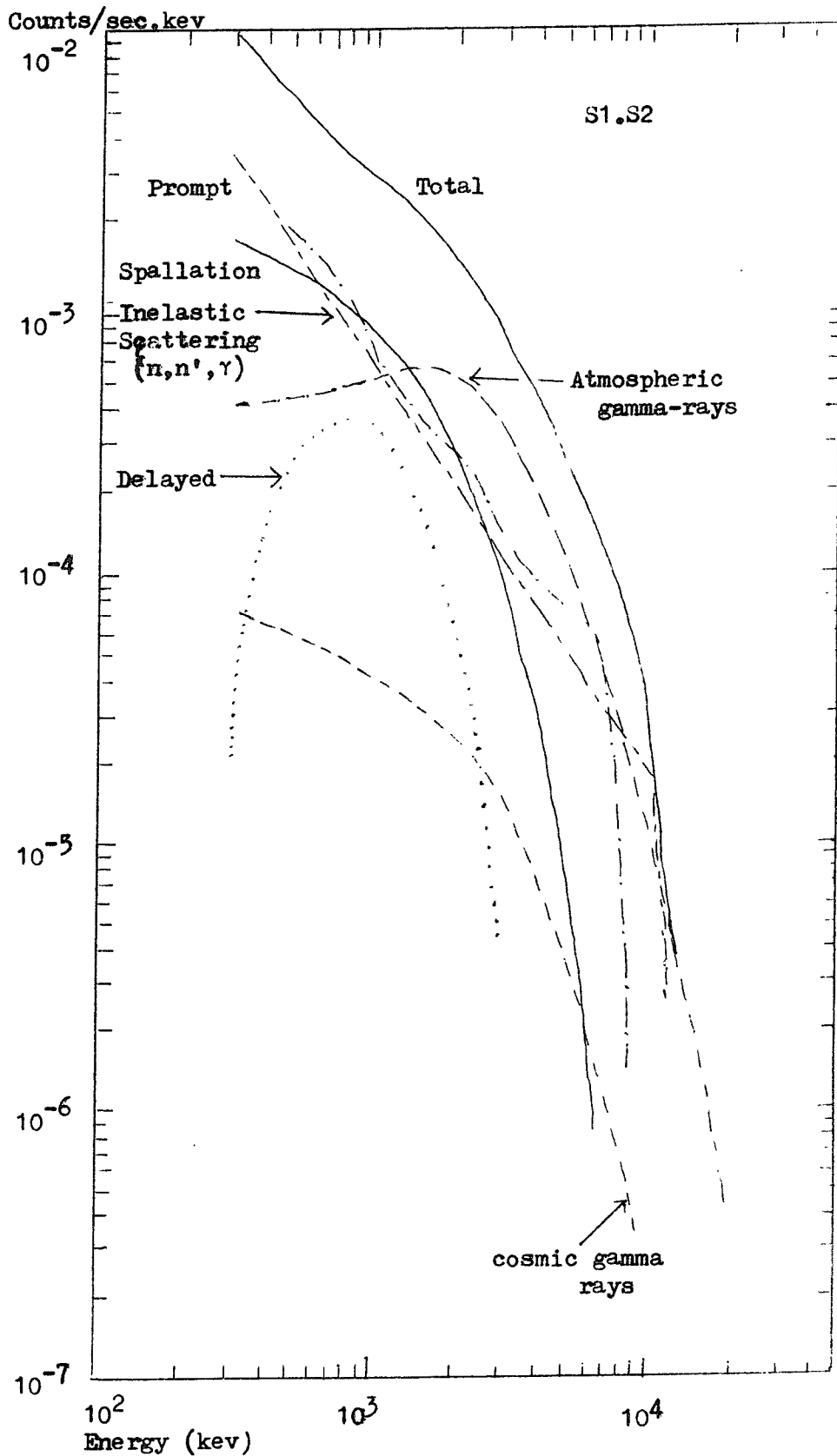
From the work of Ling (1974), it is expected that a power law with an index of -1.5 can be fitted to the expected energy loss spectrum in the energy range 0.2 - 12 MeV.

The expected absorption rate in the NaI(Tl) crystal at 3.5 mb is estimated at 24/sec by the Southampton Group. This includes the effect of the neutron shield which is efficient up to energies greater than 600 eV.

For neutrons of 65 keV, the energy loss spectrum for the prompt and delayed effects in the NaI(Tl) crystal on its own, and in coincidence with the liquid scintillator, can be seen in diagram 7.23. From this it can be deduced that the integral count rate in the coincidence system is less than that in the NaI(Tl) alone by a factor of 13 for the prompt effect, and 60 for the delayed effect.

The 65 keV neutrons were generated via the reaction $Li^7(p,n)Be^7$, at Harwell, England.

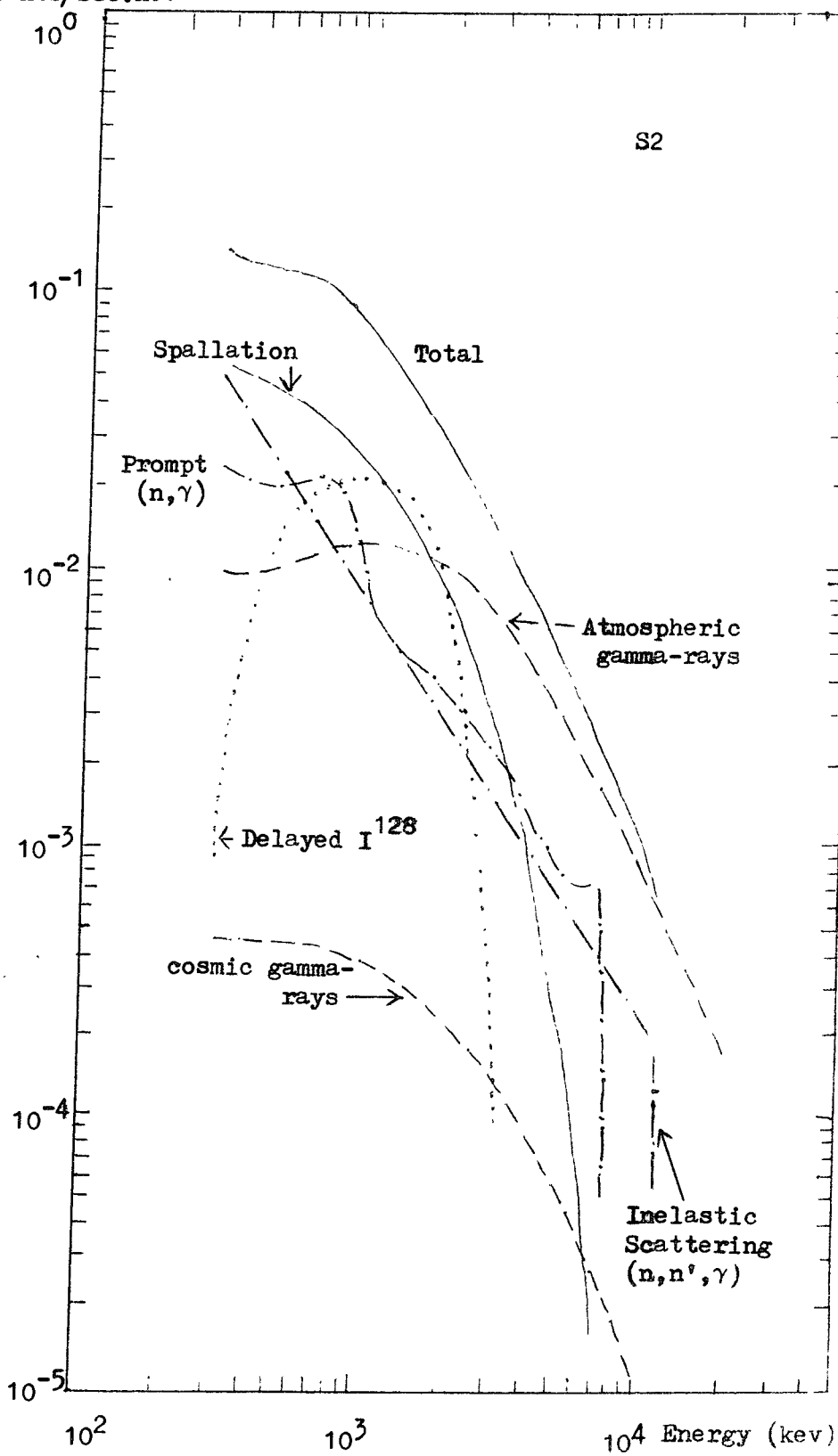
Diagram 7.21



Estimated background counts in the NaI(21) in coincidence with the liquid scintillator.

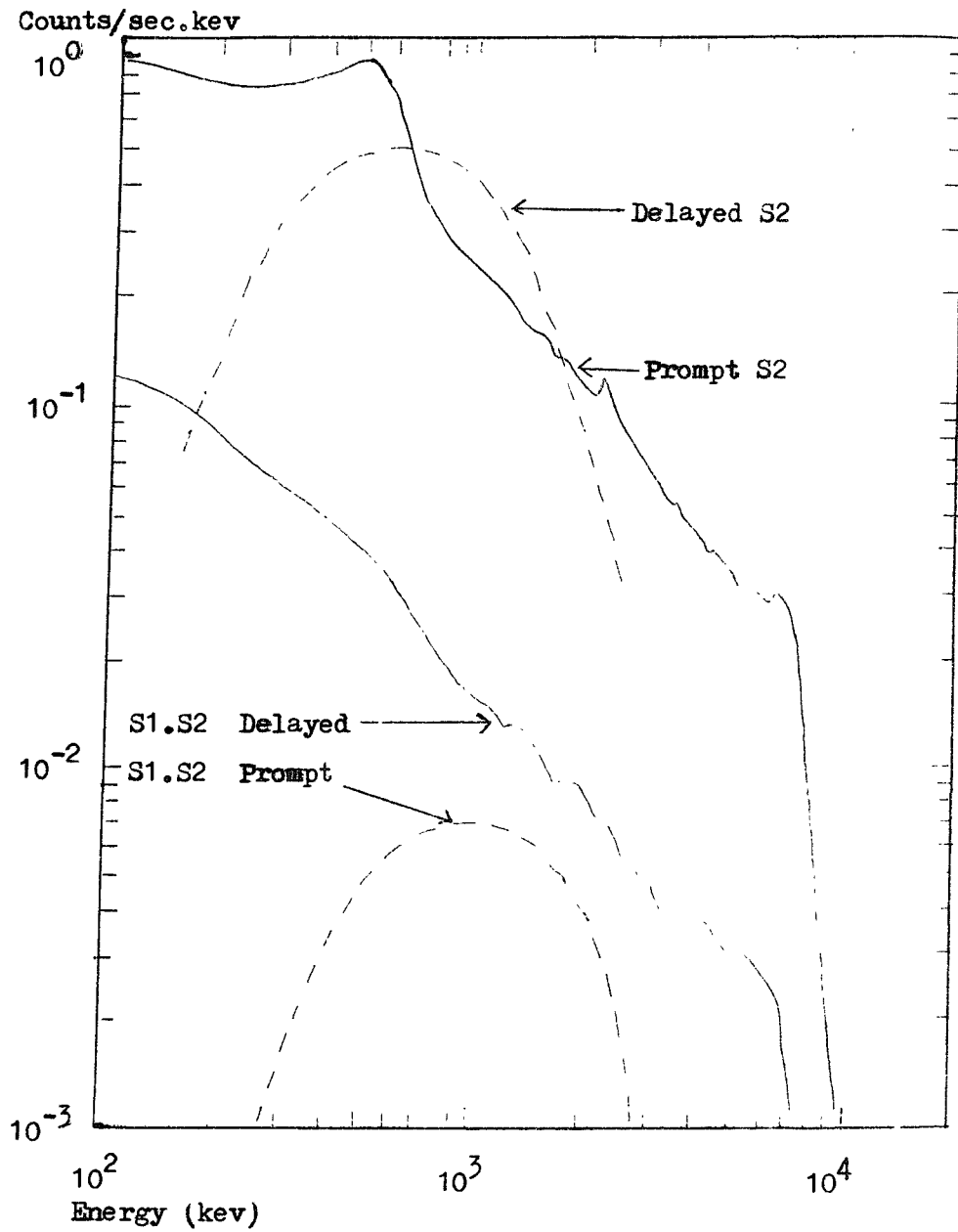
Diagram 7.22

Counts/sec.kev



Estimated background counts in NaI(Tl) alone.

Diagram 7.23



Energy loss spectrum for the prompt and delayed effects in NaI(Tl) given as S1 and S1.S2 , for neutrons of 65 keV.

7.6.3 Spallation

Protons and neutrons may interact with the material of the instrument to give rise to spallation products. The liquid scintillator has only very small spallation effects. The production cross sections of C^{11} and C^{10} are 28 mbarn and 3 mbarn respectively, (White and Schönfelder, 1975) and the formation and decay of these give about 1.6 counts per second.

The detector was exposed to 2.1 GeV/c protons generated by the Nimrod accelerator at the Rutherford Laboratory, U.K., to assess experimentally the effect of the high energy protons.

To simulate the number of protons expected in an entire day's balloon flight at 40° geomagnetic latitude, the NaI(Tl) crystal was irradiated in 2000 second time intervals with 10^7 , 2 GeV/c protons. Baker et al. (1978) found that for balloon flights over Texas, the spallation induced background spectrum in the coincidence system should be represented to a first approximation by the expression :

$$2.2e^{-E/0.9} \text{ count/s MeV.}$$

More details about the instrument response and sensitivity are given by Baker et al. (1978) and Martin (1978). Having discussed the instrument, it is of interest to see the preliminary results of a first flight of this detector, as in the next section.

7.7 Preliminary Results of the MISO Detector

From previous observations by Ariel 5, and UCSD (Ives et al., 1976; Baity et al. 1975; Pacieras et al. 1977) of the Seyfert galaxy NGC 4151, it was decided that the MISO detector should be able to observe this source. In addition the detector observed the Crab Nebula, although the data from this source has not yet been fully analysed (to date). This section describes the results obtained so far for NGC 4151, which have been published by Di Cocco et al. (1977).

Since the original detection of X ray emission from NGC 4151 (Gursky et al. 1971) many questions were raised concerning the connection between X ray emission and the Seyfert phenomenon. One question in

relation to NGC 4151 has been the apparent discrepancy between previous X ray measurement which has been explained by some (Tananbaum et al., 1978) as being due to X ray variability of NGC 4151.

The Seyfert galaxy NGC 4151 was one of the celestial objects observed during a balloon flight from Palestine, Texas, on 22nd and 23rd May, 1977, of the MISO low energy (0.2 to 20 MeV) gamma ray telescope. A hard X ray telescope was also included in the scientific payload, viewing the same region of the sky as the gamma ray detector. The X ray detector had an aperture of $2^\circ \times 5^\circ$ FWHM and was designed around a sodium iodide crystal 3mm thick and having a sensitive area of about 70 cm^2 .

The observations of NGC 4151 were all made within 18° of the zenith at a float altitude of approximately 7 mbar for a period of 3 hours. Background evaluation was made for half of this time. Based on the differences between the "ON" and "OFF" source counting rate, NGC 4151 was detected at the 6.5σ level in the 0.15 to 20 MeV energy band. Spectral information is still being analysed for the MISO detector. The results are shown in diagram 7.24. The hatched area takes into account the statistical fluctuations at 1σ level and the uncertainty of the precise exposure of the source. The full information on the exposure will be incorporated in a future more detailed analysis.

The gamma ray results show good agreement with a power law extension of the X ray spectrum using a spectral index similar to that suggested by Baity et al. (1975), and to the more recent X ray results of Auriemma et al. (April, 1978) and Tananbaum et al. (July, 1978). It is of interest to note that the Uhuru observations of Tananbaum et al. (1978) show as much as a factor of 10 increase in intensity from NGC 4151, on a time scale possibly as short as 730 seconds. Elvis (1976), using the Ariel 5 Sky Survey Instrument, reported a flare with a factor of 1.7 ± 0.2 increase in less than 3 days for NGC 4151.

The observations by Tananbaum et al. of such large flux increases on such short time scales impose significant constraints on the models of X ray emission. The size of the emitting region inferred from the time scale of the variability is $\lesssim 2 \times 10^{13} \text{ cm}$, which (Tananbaum et al., 1978) suggests a compact object in the galactic nucleus as the source.

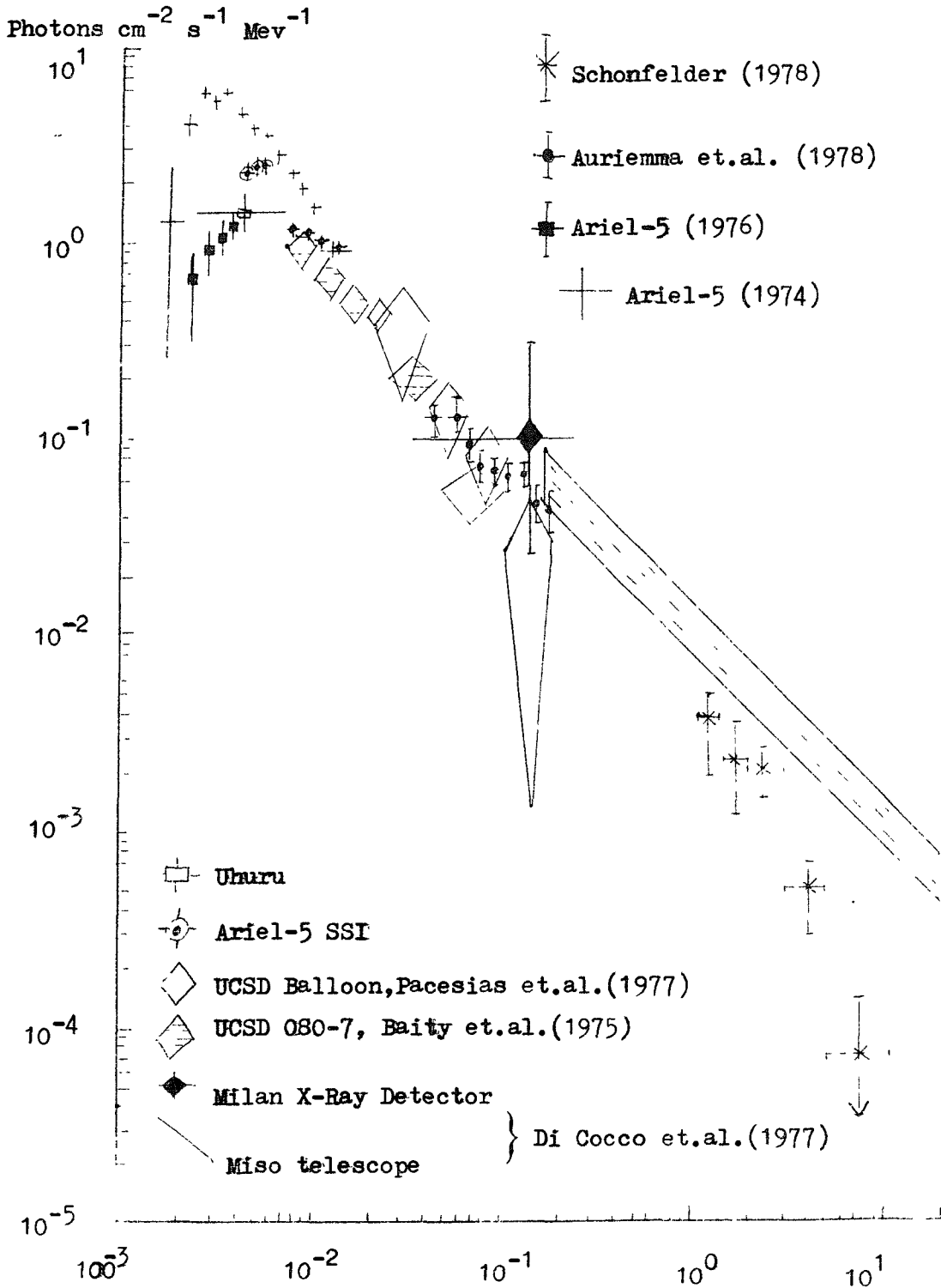
Tananbaum et al. have made preliminary calculations of a model for the emissions of NGC 4151 assuming thermal bremsstrahlung, and following the workings of Blumenthal and Tucker (1974). Tananbaum et al. suggest

Diagram 7.24

Hard X-Ray and low energy gamma ray observations of NGC4151

Uhuru-Gursky et.al.1971,Ulmer et.al.1977,Tananbaum et.al.1977

Ariel-5-Elvis,1976;Ives et.al.1976;Barr et.al. 1977.



(From Martin (1978))

that their observations may be sufficient to rule out multiple pulsar models in which Seyferts derive their energy from supernova explosions (Arons, Kulsnid and Ostriker, 1975). This is because these models imply rather energetic explosions ($\sim 10^{51}$ to 10^{52} ergs), occurring on the order of 1 per year, providing the average luminosity of $\sim 10^{43}$ to 10^{44} ergs s^{-1} for a typical Seyfert. While supernova explosions capable of producing X ray and gamma ray events of 10^{47} ergs over a fraction of a day have been described by, among others, Colgate (1974), Chevalier (1976), and Lasher (1975), the frequency of occurrence of Tananbaum's events would require approximately 1 supernova a day. This would generate at least 10^{46} erg s^{-1} for a time-averaged luminosity for the source, which would be $\gtrsim 20$ times more than the average electromagnetic radiation observed at all wavelengths from NGC 4151 (Stein and Weedman, 1976; Baity et al. 1975). Consequently, it is suggested by Tananbaum et al. (1978) that any multiple pulsar model would have to associate their X ray flares with fluctuation of instabilities in various active pulsars.

An alternative energy source could be accretion onto a massive collapsed object (Black Hole) as described in various details by, among others, Lynden-Bell (1969), Lynden-Bell and Rees (1971), Hills (1975), Frank and Rees (1976), Bahcall and Wolf (1976), Lightman and Shapiro (1977), Meszaros and Silk (1977) and Young (1977). Young (1977) interprets the Seyfert luminosity as due to a black hole in a galactic nucleus which tidally disrupts stars and generates the luminosity by accreting the resultant material.

Mészáros and Silk have also described a model of tidal disruption of stars by a black hole to explain the X ray emission from sources such as NGC 4151. They invoke turbulent dissipation by the accreting gas to generate the high temperatures required for X ray emission, and also predict temporal variability caused by fluctuations in the mass flow.

By contrast, Mushotzky (1976) has produced a synchrotron Self-Compton model (SSC). In this model, the nonthermal radio, X ray and optical emission originate in an extremely small region located in the nucleus of the galaxy. The nonthermal flux causes photoionization of the gas in this nucleus which results in the observed strong emission line optical spectrum. In addition this gas absorbs low energy X rays causing a turnover in the X ray spectrum.

At present, discrimination between various theories, particularly as regards the time scale of the variability of NGC 4151, appears to be

limited by experimental sensitivity. As suggested by Auriemma et al.(1978), simultaneous hard and soft X ray measurements of the spectrum with more sensitive detectors may, in future, produce more constrictions on the theoretical parameters.

Further considerations on the future objectives, and possible future detectors, for gamma ray astronomy are presented in the next chapter.

Chapter 8- The Future of Gamma Ray Astronomy

8.1 Future Detectors

While the MISO low energy gamma ray telescope represents an improvement over many previous detectors, there is still scope for further advances in detector design. Each new design needs to be evaluated in detail using computer analyses. However, even after a comprehensive theoretical prediction of such factors as background counting rate, and even after ground calibration tests, a detector in flight may not match up to its predicted sensitivity. The difference between flight conditions and ground conditions seriously affected, for example, the LEG 1 experiment of Lovett et al.(1973), as previously discussed.

Induced activity in detector materials is another factor which was not predicted to be significant in many detectors at their original design stage.

Observation time is a parameter of major importance in determining the sensitivity of an experiment. Satellite mounted experiments can provide durations of the order of years, compared to balloons which can provide only durations of the order of days to date. However, it may be possible to increase the time at float altitude of conventional zero pressure balloons using extra gas that has been stored in the liquid phase (Ramsden and Baker,1978). Other possibilities in relation to the future use of long duration balloon flights have been reviewed by Ramsden et al. (1977). Flights of up to three months may become possible for small (~ 200 kg) payloads using superpressure balloons. The problem of a telecommunications link to a balloon experiment which may circumnavigate the earth several times may be overcome by communication with existing or future satellites.

There are a variety of new detectors planned or being at present evaluated. Some are of radically new design, others are variations of old designs. The HEAO-C experiment has already been mentioned in section 2.6.

The MISO experiment has flights planned for the future which will include observations of CG(195+4), CG135+1.(COS-B sources) and the BL-Lac objects MK501 and MK421 (Martin, 1978). Graml, Penningsfeld and Schönfelder (1977) have recently described an improved version of

the double Compton telescope originally described by Schönfelder (1973) which should be more suitable for cosmic point source measurements.

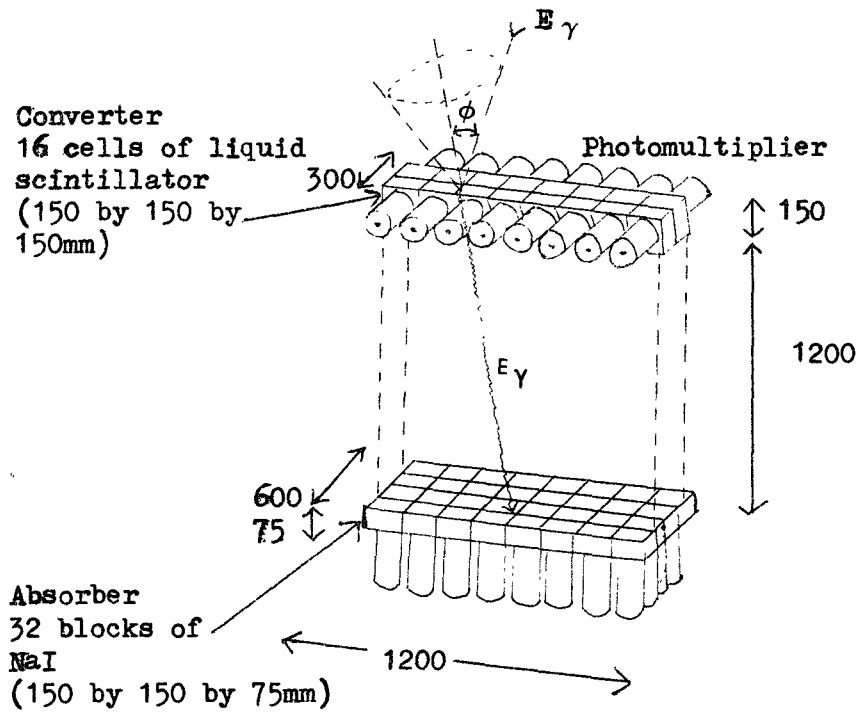
The detector is shown schematically in diagram 8.1. The energy resolution is 10% FWHM at 2 MeV and 8% FWHM at 5 MeV. As an illustration of the sensitivity of the telescope, if the Crab Nebula were viewed for 3 hours balloon flight, and the Crab Nebula spectrum were assumed to be $10^{-3} E^{-2.29}$ photons/cm²sec MeV, then the Crab Nebula would be detected to a significance of 15 standard deviations if the total of the counts in the 1-10 MeV range are considered.

Boclet et al.(1977) describe an alternative system using a larger version of a previously flown Ge(Li) spectrometer actively shielded by NaI. This could be either mounted on a balloon-suspended gondola and used on long duration transmediterranean flights, or else it could be incorporated in a spacelab collaboration. This second alternative would have a sensitivity (for 1 hour source observation) of 2×10^{-5} photons cm⁻² s⁻¹ at 1 MeV, i.e. 5 times better than the HEAO-C Nuclear Gamma experiment.

An interesting variation of the anticollimation approach has been theoretically investigated by Morfill and Pieper (1974). This method uses a battery of parallel cylindrical NaI(Tl) spectrometers which rotate about an axis parallel to that of the detectors, as in diagram 8.2. In the diagram, the axis of rotation is perpendicular to the plane of the paper, and a given detector in position A occults the radiation from the source from reaching the detector at position D. A modulation in intensity of the signals for the detectors D, therefore results, but in only one detector at a time.

This system has been called an "Active Anticollimator" (AAC) by Morfill and Pieper (1974) and they have calculated comparisons between such a system and a normal actively-collimated spectrometer of approximately equal total weight. The comparison assumes that the detectors are used to measure the gamma ray continuum flux from the Crab Nebula whose source strength is $F_s(E) = 9 \times 10^{-3} E^{-2}$ photons cm⁻² s⁻¹ MeV⁻¹, and that the background flux $F_B = 0.026 E^{-2}$ photons cm⁻² s⁻¹ sr⁻¹ MeV⁻¹. In diagram 8.3, the minimum flux sensitivity for a significance $\gg 3$ standard deviations, is shown for six 4 cm radius by 8 cm length spectrometers in the anticollimator geometry with both CsI and NaI as the detector material. The angular resolution is a function of the detector separation and is assumed to be 7° FWHM. The observing time is assumed to be 1 day. It can be seen that, on a weight

Diagram 8.1



Principle of the double Compton telescope. The anticoincidence shields around both detectors are not shown.

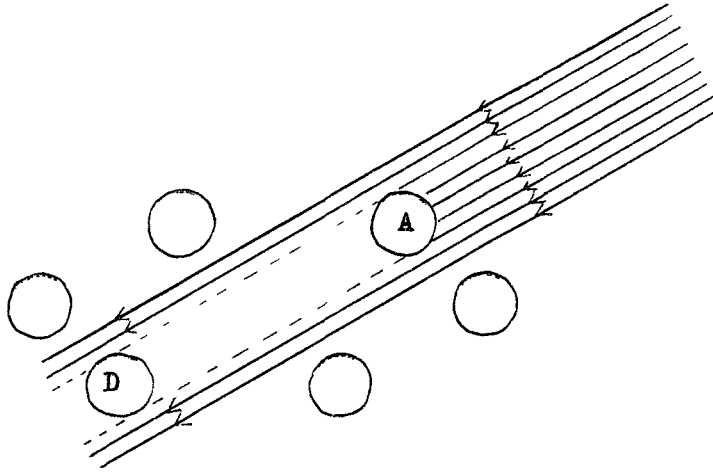
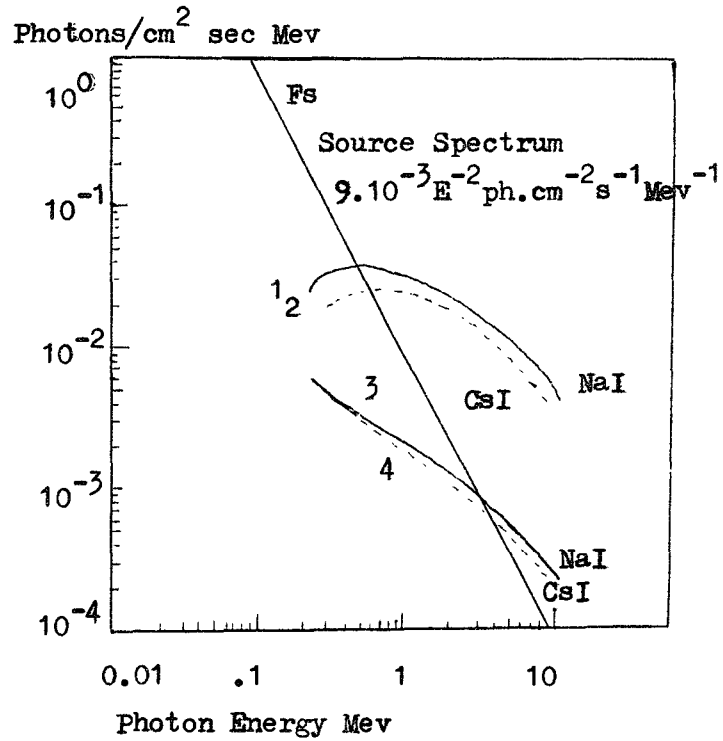


Diagram 8.2

Active Anticollimator. Schematic diagram of the active anticollimator assembly, viewed from an angle above the rotation plane. A is the absorber and D is the detector crystal for the source position shown.

(From Morfill and Pieper, 1974)



1 and 2 Minimum detectable source - active collimation system, vol=1586 cm³.

R=5 cm

3 and 4 Minimum detectable source anticollimation system, vol=1608 cm³

R=4 cm

n=6

Comparison of the sensitivities of an optimum design active anticollimator system consisting of six cylindrical detectors of diameter and length 8 cm. The minimum detectable source strength at 3 is shown for each case as well as the extrapolated Crab X-ray spectrum for comparison. (from G.Morfill and G.F.Pieper, 1974).

Diagram 8.3

for weight basis, the active anticollimator detector can measure a flux more than an order of magnitude lower than the conventional collimated detector. No such active anticollimator has yet been flown, and it may present mechanical development problems. However, it appears that this approach is worth further research to see if the theoretical advantages shown in diagram 8.3 can be fully exploited in practice.

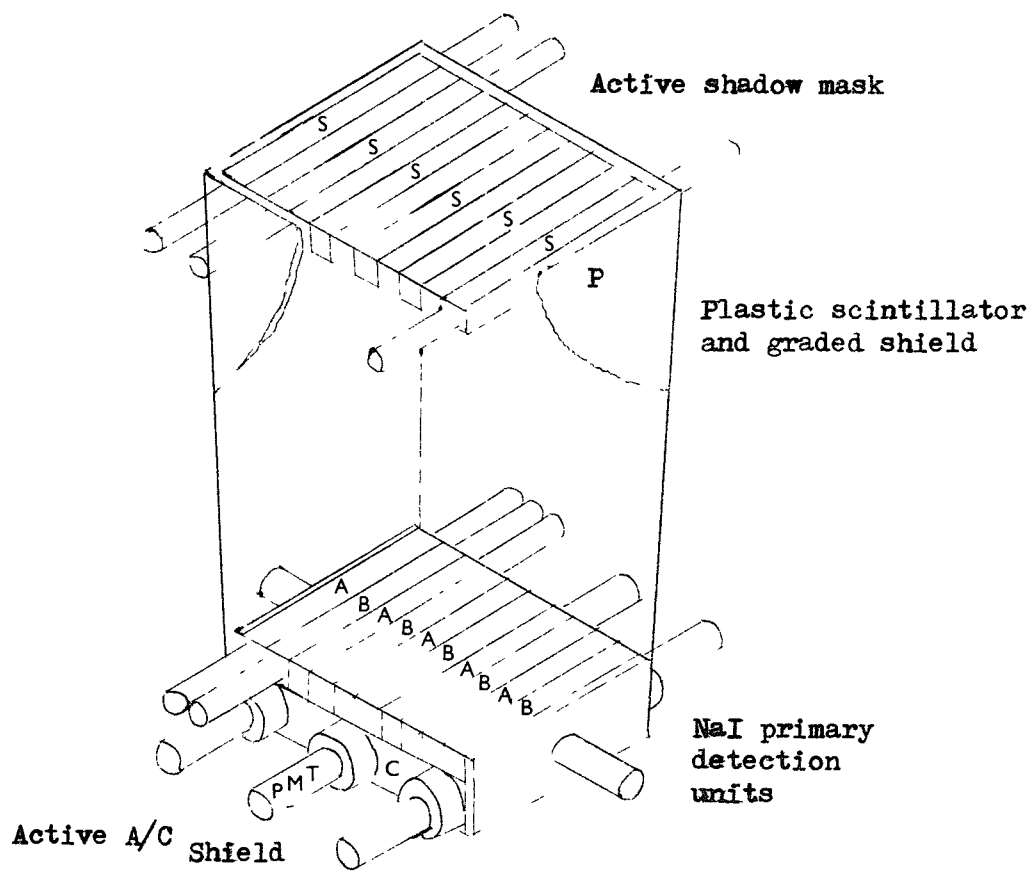
By contrast, another new design has been put forward jointly by the Southampton and Milan University groups. This detector is depicted schematically in diagram 8.4. It is sensitive in the range 10 keV to 10 MeV, and is proposed to fly on spacelab. High sensitivity is attained by using a large ($\sim 2000 \text{ cm}^2$) actively shielded detector. This detector consists of an upper layer of two interleaved sets of detection elements (A and B) beneath which is a large, thick, inorganic anticoincidence shield (C). The upper part of the detector comprises slats of NaI, (s), which provide an active mask, and the overall structure is surrounded by plastic anticoincidence (P).

A source moving across the field of view of the instrument casts a shadow on the elements A and B, giving different count rates R_A and R_B . An element A is shielded by C below and by the elements B on either side. The source and background can thus be measured simultaneously. Angular resolution is obtained by a Fourier analysis of the R_A , R_B and $R_A - R_B$ rates. Using this method of simultaneous background and source measurements, the systematic errors inherent in any experiment due to background variations can be reduced appreciably.

An interesting aspect of gamma ray radiation that has not been investigated in detail, to date, is the polarization, as mentioned by Long and Novick (1978). For the lower energies of X rays, Rees (1978) has investigated the expected polarisation from a number of different types of sources. He comes to the conclusion that polarization studies would give useful information on the geometry of these sources, for example, the orientation of the accretion disc. The experimental difficulties of measuring the polarisation of low energy gamma rays are expected to be great, but the usefulness of polarization studies to the determination of various theoretical parameters indicate that such experimental detection methods are worth investigating further.

From design of future detectors for gamma ray measurements, it is a natural step to consider what sources can be observed in the future. Such sources are considered in the next section.

Diagram 8.4



Newly designed gamma ray detector

8.2 Gamma Ray Sources of Interest

As regards the interest in observing future gamma sources, the astrophysical significance has already been discussed in section 1.2. Future experiments can observe previously detected sources to improve on past accuracy, or to investigate time variability, or its absence, of a source. Alternatively, detectors can randomly search the sky for new sources. A third possibility is to examine sources which have already been observed at other energies, and see if their spectra, extrapolated to low energy gamma ray energies, is compatible with the detection sensitivity of the proposed detector. In the first mentioned category, previously detected gamma ray sources have been reviewed in sections 1.4 to 1.6.

The third category requires careful examination of many other measurements at other energies. Recent X ray measurements of Seyfert galaxies have indicated that there is great promise of a number of Seyfert galaxies detectable in gamma rays. The Uhuru data has been searched (Tananbaum, 1978) for X ray emission from 88 Seyfert galaxies mentioned by Weedman (1978). NGC 4151 has been detected in low energy gamma rays by the MISO detector as described in the last chapter. Weedman (1977) has given a comprehensive review of the general characteristics of Seyfert galaxies. However, Weedman re-emphasises the point made by Baity et al.(1975), that NGC 4151 could not be typical of Seyfert galaxies or else the contribution from Seyferts alone would give a diffuse X ray background 100 times greater than observed. On the basis of this, it seems that Seyferts are not in general strong X ray sources.

The recent observations by Mushotzky et al.(1978) of the BL Lac objects MK501 and MK421 have suggested that many BL-Lac objects may have hard X ray spectra. Their HEAO-1 measurements when compared with those of OSO-8 shows a factor of 6 decrease in flux from MK 421 (2 to 60 keV band). This confirms the strong variability of this source in the X ray band.

Reviews of the general properties of BL Lac objects are given by Stein, O'Dell and Strittmatter (1976) and Miller (1978).

Many theoretical questions are raised by BL-Lac objects. Perhaps the main problem associated with X rays and BL-Lac objects are certain conflicts with conventional distance determinations, as follows:

The absence of distance determinations for BL Lac objects - not

to mention the controversy over the distance-redshift relation for QSOs - has hampered detailed study of source characteristics. If observed redshifts are used to determine distances on the basis of a Hubble constant $H_0 \sim 50 \text{ km sec}^{-1} \text{ Mpc}^{-1}$, there are difficulties with an incoherent synchrotron interpretation for at least some BL Lac objects and QSOs (Jones and Burbidge, 1973; Jones et al. 1974; Burbidge, 1974).

The essence of the problem was first stated by Hoyle, Burbidge and Sargent (1966) (see also Kellerman and Pauliny-Toth, 1969), who pointed out that, in single models, rapid variability of a very bright source implies a small volume containing the high energy electrons and synchrotron radiation. A luminosity confined to a small volume implies a very large energy density of radiation, in which high-energy electrons rapidly lose energy through Compton scattering. This leads to short electron lifetimes and a large flux of Compton scattered photons - some of which would appear as X rays. Since X rays have not been generally observed from BL Lac objects (Morgon et al., 1976; Ulmer and Murray, 1976) limits can be set on physical conditions in the source and lead to a conflict with the distance determination if the emission mechanism is accepted.

Various alternative theories have been proposed to avoid these difficulties (Stein et al. 1976). However, the recent X ray observations of Mushotzky et al. (1978) may well imply that the absence of X ray measurements from BL-Lac objects previously, was due mainly to instrumental factors or the particular choice of BL-Lac objects to be observed. Whatever the true situation, it is clear that X ray measurements, or upper limits, have an important role to play in the theoretical background to BL-Lac objects.

Other possibly observable sources in the 1-10 MeV region are: Scorpius X-1 which has been observed to be a strong source (Davidson et al. 1971) by Uhuru and has been observed by Haynes et al. (1972); Cyg X-3, Her X-1 (notable for its 58 keV X ray line - Trümper (1978), Kendziorra (1977), Voges (1978) and Coe et al. (1977)). These sources are possible candidates from extrapolation from lower X ray energies. By contrast, one can extrapolate from observed higher energy sources to lower energies. For example, COS-B satellite observations (Hermsen et al. 1977) indicate that the high energy sources CG 135+1, CG 195+4, CG 333+0, may have lower energy counterparts.

It seems likely that many more interesting X and gamma ray sources will be discovered in the future.

8.3 An Anticollimated Double Compton Telescope

The LEG 4 anticollimated detector had the disadvantage of a high background count rate. The MISO double Compton telescope was designed to reduce the background. Unfortunately the detection efficiency of the source was also reduced, and the background count rate was not reduced to the expected amount by the relatively heavy shielding material. In addition the large amount of background shielding material made the payload relatively heavy.

An alternative design has been suggested by the Southampton Group for which some initial calculations are presented.

This design makes use of the intrinsic directionality of the Compton coincidence requirement, in order to reduce the background count rate. The finer angular resolution is then provided by an anticollimation system.

In order to find the background counting rate in the detector, the efficiency of the Compton telescope as a function of angle needs to be determined. This is by nature a complex problem. However, some simplifying assumptions enable a preliminary assessment of the capabilities of this type of system to be made.

1 to 10 MeV photons are mainly Compton scattered at a small angle to the incident direction, so the assumption is made that atmospheric background photons interacting in the top element, keep their initial direction after scattering. Next, the two detector elements are assumed to be thin discs situated at their centres, in order to determine the effective area of overlap seen by an incident photon at any particular incident angle. This assumption should be reasonable for separations of the centres of the two elements comparable to, or greater than the diameters of the elements. The geometry is then represented by the equations given in Appendix 1.

Let us assume that we have a Compton telescope as in diagram 8.5. Then the proportion of ~~area of overlap of the two elements~~ seen by a background gamma ray incident at an angle θ to the axis of the telescope is given by

$$R = \frac{2r^2(a - \sin a \cos a)}{\pi r^2}$$

$$R(\theta) = \frac{2}{\pi} (a - \sin a \cos a)$$

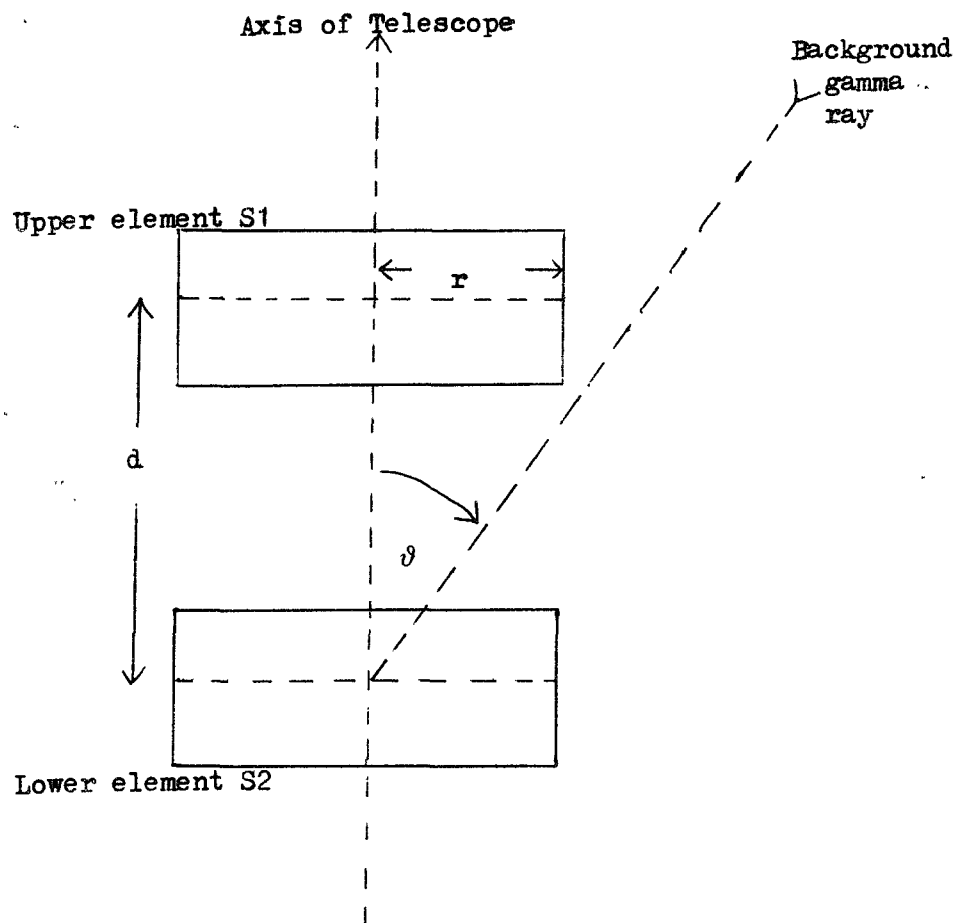


Diagram 8.5

where

$$\cos \alpha = \frac{d \tan \theta}{2r}$$

and θ varies from 0 to a maximum of $\theta_{\max} = \tan^{-1} \frac{2r}{d}$.

$R(\theta)$ is shown as a function of θ in diagram 8.6 for various values of $\frac{2r}{d}$.

Now we assume that the zenith angle distribution of the atmospheric gamma ray background follows that found by Schönfelder (1977) (see diagram 4.18) with a proportional factor at angle θ of $Z(\theta)$.

With regard to the efficiency, we can see from diagram 7.15 that the detection efficiency for 1 to 10 MeV photons along the axis of the Compton telescope is of the order of $\epsilon_{dc} = 10\%$, if the separation of the centres of the detectors elements is about 25 cm, i.e. approximately equal to the diameter of each element (27cm for the MISO experiment), i.e. $\frac{2r}{d} = 1$.

Let us assume that the detection efficiency (except for the area factor $R(\theta)$), is approximately the same at an angle θ for background gamma rays as for gamma rays incident along the axis of the telescope; and assume that this efficiency is $\epsilon_{dc} = 10\%$ for $\frac{2r}{d} = 1$. This may be contrasted with the efficiency, ϵ_s , for a single element, which is approximated by the inverse of the energy loss conversion factors R , in diagram 4.6, and is greater than 30% in the range 1 to 10 MeV.

It can be seen that the ratio of the total background counts in the Compton telescope, to the total background counts in a detector with just one element instead of the two, is given by:

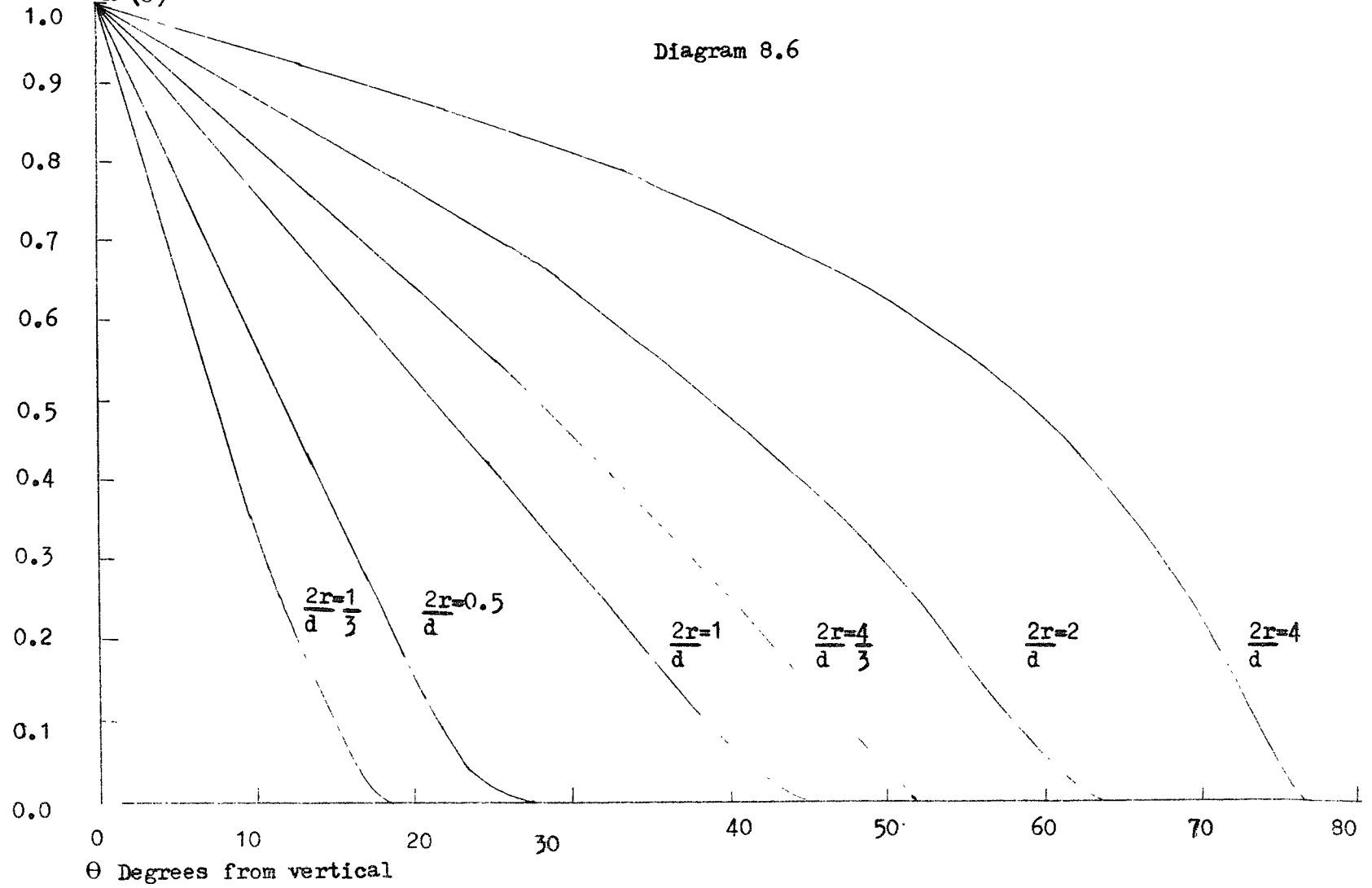
$$\frac{N_{B,dc}}{N_s} = \frac{\epsilon_{dc} \int_{\theta=0}^{\theta=2\pi} R(\theta) Z(\theta) d\theta}{\epsilon_s \int_{\theta=0}^{2\pi} Z(\theta) d\theta}$$

approximately, where subscript dc denotes double Compton, s denotes single element, and ϵ_{dc} is the 10% efficiency discussed, and ϵ_s is the 30% efficiency.

However, in determining the sensitivity of the telescope, we need to take into account the reduction in efficiency for source counts as

Area function R (θ)

Diagram 8.6



well as background counts. Let us compare an anticollimated double Compton telescope observing a source flux of s photons with a single element detector (as in LEG 4 and LEG 2) for the same time. The dimensions of each element of the Compton telescope are assumed to be the same as the dimensions of the single element. Then the sensitivity can be defined as the number of source counts observed, divided by the square root of the background counts, for a particular energy interval. i.e. $\frac{\epsilon S}{\sqrt{B}}$ where ϵ is the efficiency for the on-axis source photons, and ϵS is then the number observed in the energy loss spectrum. B is the number of background energy loss counts for the same energy interval. Then the ratio of this sensitivity quantity for the 2 systems gives a measure of any improvement of an anticollimated double Compton telescope over an anticollimated single element telescope of similar dimensions.

For the example chosen of $\frac{2r}{d} = 1$, it is found by numerical integration that the background count rate should be reduced by a factor of 0.033, while the source count rate is reduced by a factor of a third. Consequently, the ratio of sensitivities is approximately 1.6. In other words, this is an improvement. However, for $\frac{2r}{d} = 0.5$ the ratio could be as high as 2.6. There is scope for placing additional background shielding as in the MISO telescope, but at carefully chosen sites, so that the larger background flux at larger zenith angles, combined with the $R(\theta)$ geometrical factor, is reduced most significantly, for the lowest weight of shielding material. This selective shielding should be much lighter for the same effect, than the all round shielding of the MISO detector. In addition, less shielding is used because the directionality is mainly provided by the anticollimation system. The directionality can be further improved, and the background count rate lowered, by examining the energy deposited in the 2 elements which is dependent on the direction of the incoming photon, as mentioned in section 7.2.2.

Although the MISO telescope had a higher background count rate than was expected, Dean et al. (1973), with a similarly shielded detector, obtained a reduction in background counting rate by a factor of 18 by the anticoincidence veto signal system (Martin, 1978). It is to be hoped that this discrepancy between the background counting rates of the MISO telescope and the flight of Dean et al., will be resolved favourably for this type of semi-active shielding. If it is eventually concluded that semi-active shielding is favourable, then

the natural evolution of the MISO telescope might be in the direction of an anticollimated system with preferential shielding of background at high values of $R(\theta)Z(\theta)$, as in diagram 8.7.

The calculations presented here are approximate. A full analysis would require a Monte-Carlo treatment taking into account the zenith variations in the background. The advantage of less shielding for the same sensitivity is less weight suspended by the balloon, and the reduction of possible induced activity in the shield material itself which can cause an increased background count rate over that expected. In addition, an anticollimated double Compton telescope has the feature of a good gamma ray signature.

8.4 Summary

This work on experimental gamma ray astronomy has described the design, flight and analysis of the LEG 4 anticollimated low energy gamma ray telescope. Results of observations of the atmospheric gamma ray background, and the pulsed and unpulsed fluxes from the Crab Nebula are reported. No significant gamma ray bursts were found.

For future detectors, initial design calculations for the efficiency of a double Compton telescope are described.

It is concluded that the optimisation of design of future gamma ray detectors requires considerable effort in producing a generalised computer program to calculate all the relevant variables involved in deciding which design is best suited to a particular application. It appears that anticollimated detector designs may well prove to be the optimum design configuration for the detection of low energy gamma rays from point sources, although alternative designs still require careful consideration.

While the obstacles in this field are large, the potential of gamma ray astronomy justifies the continued effort to improve techniques. Gamma ray astronomy has a high probability of becoming a very effective tool in probing the universe, because of the unique signature of spectral lines, the relative penetrability of gamma rays, and their origin in high energy astrophysical processes.

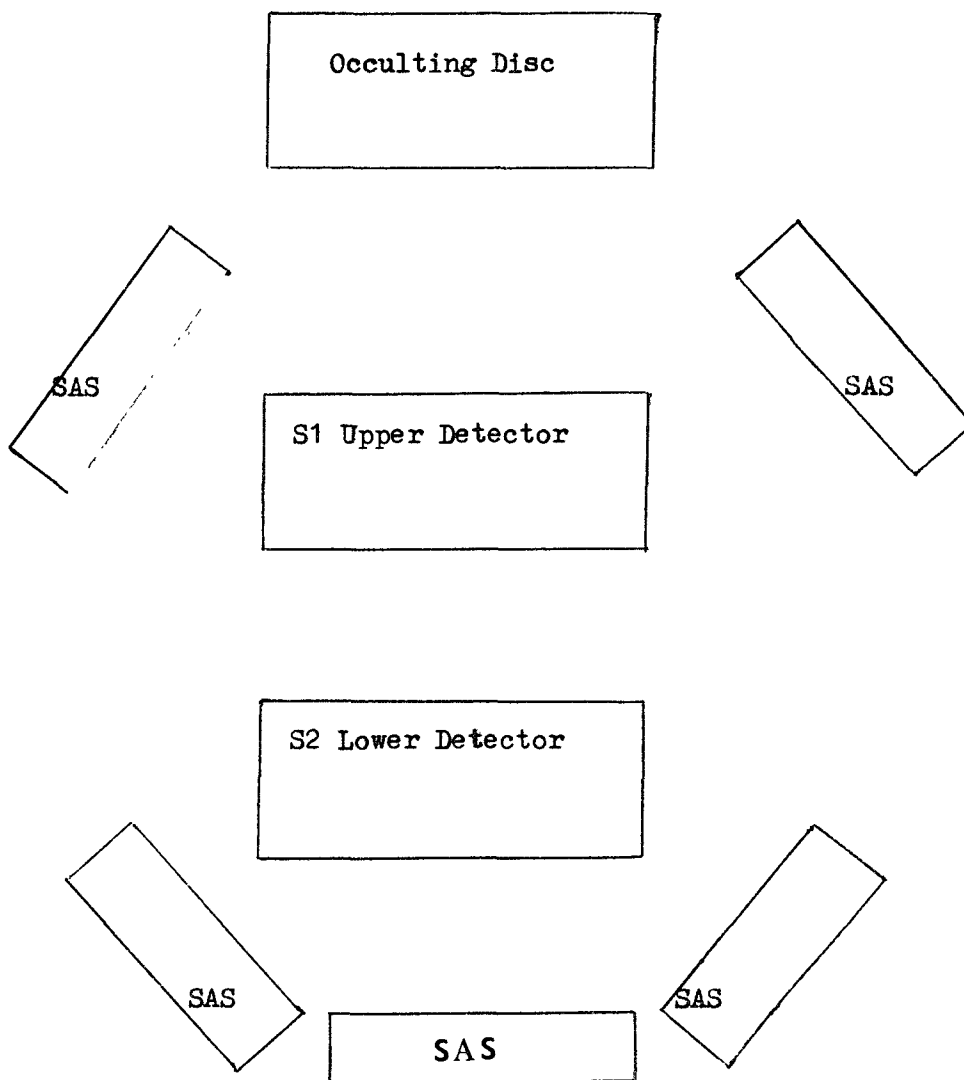


Diagram 8.7 Anticollimated Double Compton Telescope

SAS.....Semi-active shielding placed at high values of $R(\theta)Z(\theta)$ for maximum efficiency.

Appendix

The Thin Disc Approximation

This approximation can be used to find the effective area of occultation for anticollimated telescopes or the effective efficiency of a double Compton telescope as in section 8.3. For the nature of the problem, see diagram A.1.

The thin disc approximation assumes that a disc halfway up the lead occulting disc totally excludes gamma rays of all energies from its projection onto a disc halfway up the detector crystal. The edge effects and variations with energy within the range of interest, are assumed either to cancel each other out, or be negligible.

Let the angle between the true direction of the source and the axis of the detectors be U . See diagrams A.2 and A.3 and A.4 for a view of the situation. Note that the radius of the lead disc is greater than the radius of the detector crystal. Thus there is a minimum angle U_{\min} , up to which the total area is still occulted.

From diagram A.3, we can see that U_{\min} is given by

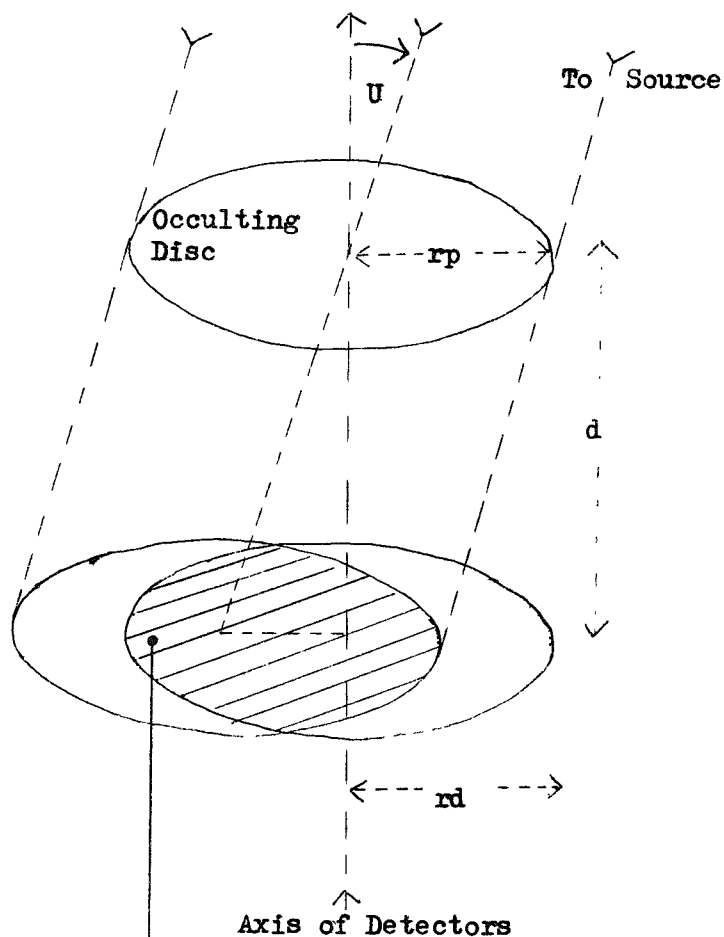
$$U_{\min} = \tan^{-1} \left\{ \frac{r_p - r_d}{d} \right\}$$

where d is height between centre of lead disc and centre of detector crystal. Note also that if the angle is greater than U_{\max} as shown in diagram A.3, then none of the detector crystal is occulted. We can see that this is given by

$$\tan U_{\max} = \frac{2r_d + r_p - r_d}{d} \quad ; \quad U_{\max} = \tan^{-1} \left(\frac{r_p + r_d}{d} \right)$$

Thus we want to find the area occulted for angle U such that

$$\tan^{-1} \left(\frac{r_p - r_d}{d} \right) < U < \tan^{-1} \left(\frac{r_p + r_d}{d} \right)$$



Area Occulted

Diagram A.2

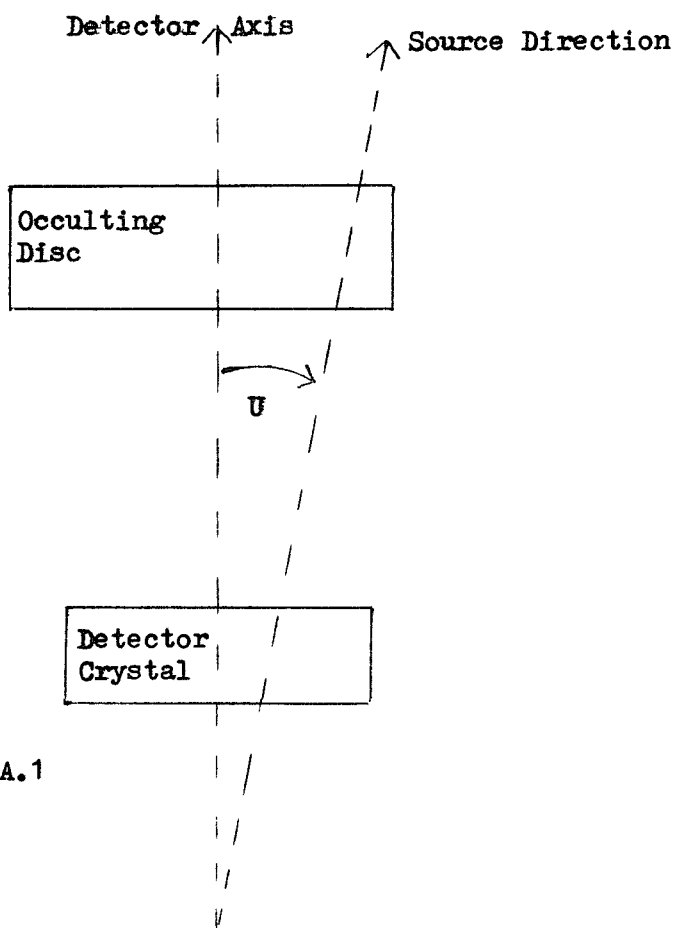


Diagram A.1

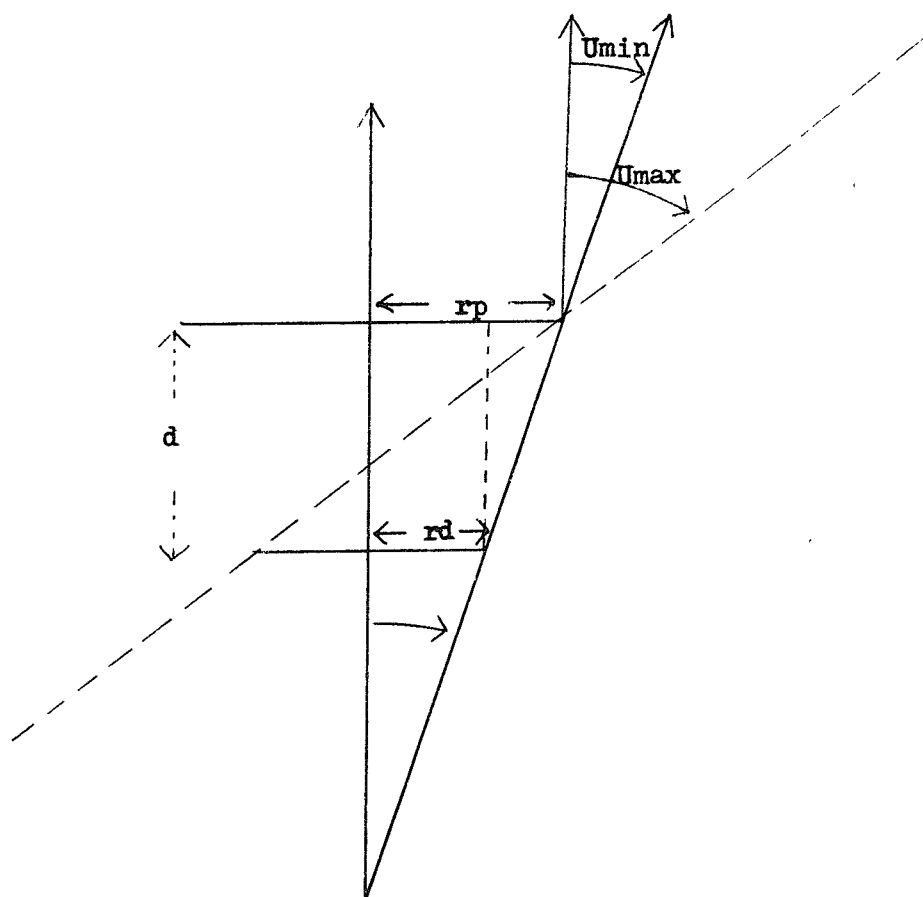
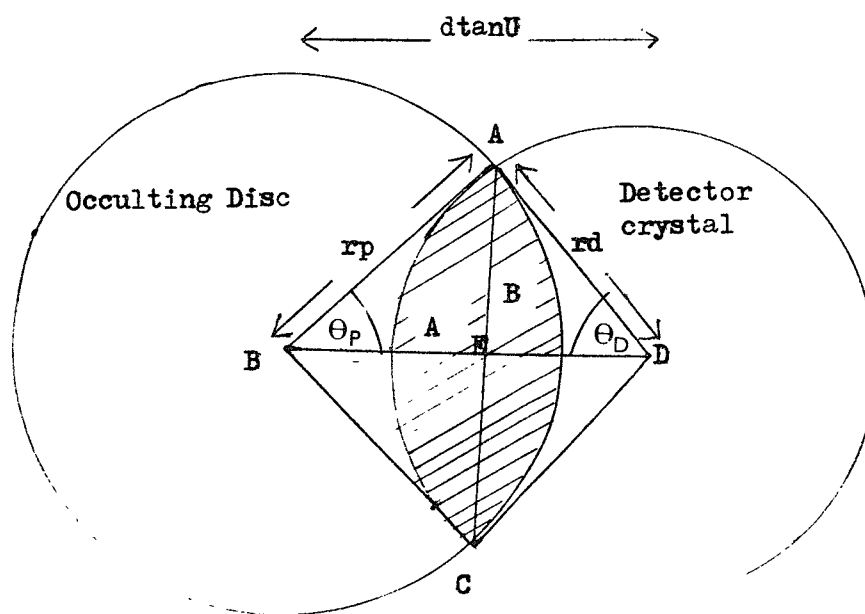


Diagram A.4 Vertical Projection



If $U < \tan^{-1}\left(\frac{r_p - r_d}{d}\right)$, then Area = 0 (All obscured).

If $U > \tan^{-1}\left(\frac{r_p + r_d}{d}\right)$, then Area = 1 (none obscured),

where the Area is the area of the crystal exposed to the source, divided by the total area of the crystal "disc" (πr_d^2).

Using diagram A.4 (the vertical projection), we can see that the area we want is Area A + Area B.

Then the ratio of the exposed area of the detector crystal over the total crystal area is given by:

$$\frac{\pi r_d^2 - \text{Area A} - \text{Area B}}{\pi r_d^2} = 1 - \frac{\text{Area A} + \text{Area B}}{\pi r_d^2}$$

Now Area A = Area of segment ACD = Area of triangle ACD

$$= \frac{2\theta_D}{2\pi} \times \pi r_d^2 - \frac{2(r_d \sin \theta_d)}{2} \cdot r_d \cos \theta_d$$

⏟
⏟
 height of triangle base of triangle

$$\text{Therefore, } A = \theta_d r_d^2 - r_d^2 \sin \theta_d \cos \theta_d$$

$$\text{Therefore, } A = r_D^2 (\theta_D - \frac{1}{2} \sin 2\theta_d)$$

$$\text{Similarly, Area B} = r_p^2 (\theta_p - \frac{1}{2} \sin 2\theta_p)$$

Now it just remains to relate θ_d and θ_p angles to the angle U between the true direction of Crab Nebula and the direction the axis of the detectors was actually pointing.

We can see from diagram A.4 that:

$$AE = r_p \sin \theta_p = r_d \sin \theta_d \quad (1)$$

Also the displacement between the centres, BD, corresponds to displacement of $d \tan U$.

Therefore:

$$d \tan U = BD = BE + ED = r_p \cos \theta_p + r_d \cos \theta_d$$

Therefore

$$d \tan U = r_p \cos \theta_p + r_d \cos \theta_d \quad (2)$$

Therefore from (1) and (2) we can find θ_p and θ_d .

Side Note (1) - A check for $\vartheta_D > 90$ degrees

See diagram A.5. Let $\vartheta_D = 135$ degrees $= \frac{3\Pi}{4}$

$$\text{Then A} = r_d^2 \left(\frac{3\Pi}{4} + \frac{1}{\sqrt{2}} \frac{1}{\sqrt{2}} \right)$$

Then add on Area B.

ϑ_p should always be < 90 degrees.

We can solve for ϑ_D and ϑ_p from equations (1) and (2) or alternatively and equivalently we can use the cosine formula on the triangle ABD (see diagram A.4):

$$\frac{r_d^2 + d^2 \tan^2 U - r_p^2}{(r_d)d \tan U} = \cos \vartheta_d \quad (3)$$

Similarly

$$\frac{r_p^2 + d^2 \tan^2 U - r_d^2}{2dr_p \tan U} = \cos \vartheta_p \quad (4)$$

We must check for $\vartheta_D > 90^\circ$. Does the above give the right sign of the $\cos \vartheta_d$?

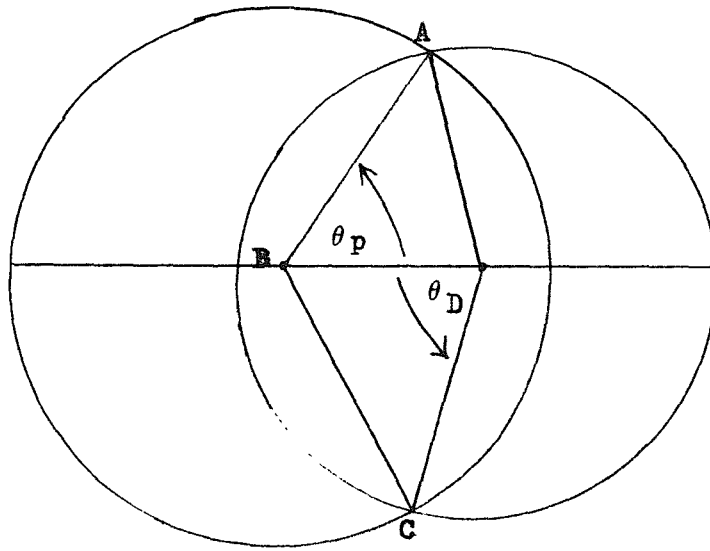


Diagram A.5

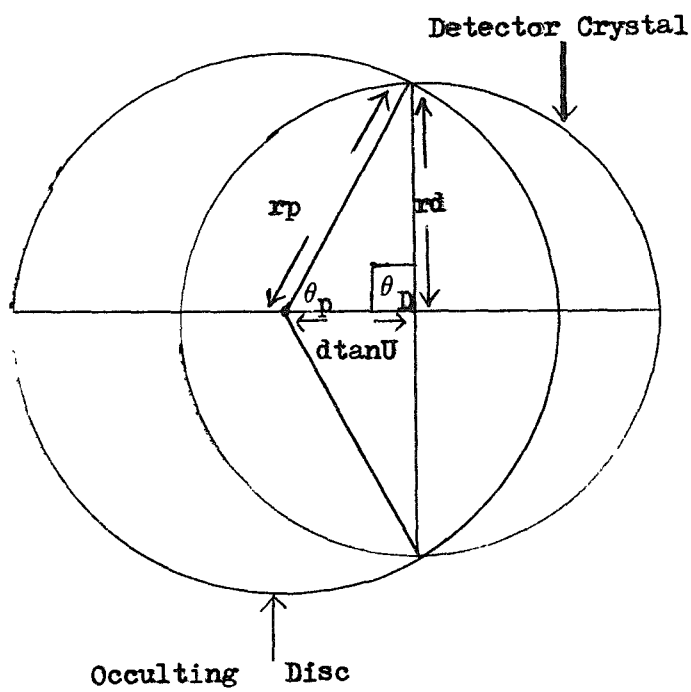


Diagram A.6

The sum of the squares of 2 sides of a triangle is always greater than the square of the third side.

$$r_d^2 + d^2 \tan^2 U > r_p^2$$

and as $\tan U$ is always +ve as $0 < U < 90$ degrees. $\cos \theta_d$ is always +ve when derived from equation (3) above. This is obviously incorrect for when $\theta_d > 90$ degrees. So we need an extra condition to get the right sign for $\cos \theta_d$. $\cos \theta_d$, $\sin \theta_p$, and $\sin \theta_d$ are always +ve anyway, so they don't matter so much.

Condition for when $\theta_d = 90^\circ$ (The "turn over point")

This situation is as in diagram A.6, i.e. when $\theta_d = 90$ degrees.

$$r_p^2 = r_d^2 + d^2 \tan^2 U_T$$

$$\tan U_T = \left(\frac{r_p^2 - r_d^2}{d^2} \right)^{\frac{1}{2}}$$

$$U_T = \tan^{-1} \left(\frac{r_p^2 - r_d^2}{d^2} \right)^{\frac{1}{2}}$$

where U_T is the turn over angle.

So for $U < U_T$, $\cos \theta_d = -\cos \theta_d$ (as $\theta_d > 90^\circ$)

if $U > U_T$, $\cos \theta_d = +\cos \theta_d$

Thus all quantities are determined in terms of the angle U . Since we know the direction, the detector should have been pointing towards the source, and we can find the direction the axis of the detector actually pointed using the magnetometers and pendulum used on LEG 4, we can thus find the angle U , and hence the effective area of occultation of the crystal.

The mathematics of this thin disc approximation were originated by Dr. R.K. Manchanda (private communication). It can be seen that the thin disc approximation can be extended to include the true 3-dimensional situation, by considering gamma rays passing through successive thin

discs of infinitesimal depth, and numerically integrating up to the full depth.

REFERENCES

- Adams et al, 1969, *Astrophys. Lett.*, 3, 51
- Agrinier et al, 1973, *Nat. Phys. Sci*, 242, April 23, 1973
- Agrinier et al, 1973, *Proc. 13th Internat. Cosmic Ray Conf.*, 1, 8
- Albats, Frye et al, 1972, *Nature* 240, 221, 1972
- Apparao, 1973, p. 51 *Denver Conf. (13th Internat. Cosmic Ray Conf.)* vol. 1 OG sessions 17-30 Aug 1973
- Apparao, 1973, *The Crab Nebula, Astrophys. and Space Sci.* 25
- Apparao et al, 1966, *J. Geophys. Res.* 71, 1781
- Argyle, et al, 1972, *Ap. J (Letters)*, 175, 189
- Arons et al, 1971, *Ap. J.* 170, 431
- Arons et al, 1975, *Ap. J.*, 198, 687
- Auriemma et al, 1978, *Astroph. J.*, 221: L7-L111
- Bahcall, J.N., and Wolf, R.A., 1976, *Ap. J.*, 209, 214
- Baity, et al, 1975, *Ap. J. (Letters)*, 199, L5-L8
- Baker RE, Lovett, Orford, 1973, *Nat. Phys. Sci.* vol 245, No. 141 pp 18-19
- Baker RE, 1978, Submitted to *Nuclear Instruments and Methods*, May 1978
- Baker RE, et al, 1973, *Proc. 13th I.C.C.R. Denver*
- Barr et al, 1977, *M.N.R.A.S.* 181, 43P
- Bennett, K et al, 1977, *Astron. Astrophys.* 56, 469
- Berger and Seltzer, 1972, *Nucl. Instr. and Meth.*, 104, 317
- Bertolini, G et al, 1968, "Semiconductor Detectors".
- Bewick A, et al, 1975, *Nature* 258, 686
- Bignami et al, 1978, *Astron. Astrophys.* 67, 149-152
- Blumenthal, GR and Tucker, W, 1974, in *X-Ray Astronomy*, ed. R. Giacconi and H. Gursky (Boston: Reidel), p. 99
- Boclet et al, 1972, *Nat. Phy. Sci.* 235, p. 69
- Boclet et al, 1977, *Proceedings of 12th ESLAB Symposium*, Froscati, Italy, ESA-SP-124
- Boldt et al, 1969, *Nature* vol. 223, July 19th, p. 280
- Boldt et al, 1969, in H. Ogelman and J.R. Wayland (eds), *Lectures in High Energy Astrophysics*, NASA SP-199 p. 49

- Bolton, C.T., 1972, Nat. Phys. Sci. 240, 124
- Bond, H.E., 1977, I.A.U. Circ No. 3085
- Bratolyobova-Tsulukidze, L.I., 1970, Proc. 11th Internat. Cosmic Ray Conf (Budapest, 1969), in Acta Phys. Acad. Sci. Hungarical, 29, Suppl. 1, 123
- Brown, R.L., 1970, Astrophys. J. (Letters) 159, L187
- Burbidge, G.R., 1974, Nature 250: 181
- Burbidge G.R. et al, 1974, Ap. J. 193: 43
- Burbidge G.R. et al, 1957, Rev. Mod. Phys., 29, 547
- Canizares C.R., et al, 1974, Astrophys. J. (letters) 192, L161
- Canizares, C.R., et al, 1976, Astrophys. and Space Sci. 42, 111-122
- Carpenter et al, 1975, Center for Astrophysics, 14th Internat. Cosmic Ray Conf. Munich, 1975.
- Carpenter et al, 1976, Nature, vol 259, Jan 15
- Carter et al, 1976, Nature, 262, 371
- Cheng, A.F., Ruderman, M.A., 1977, Astr. J. 216, 865-872
- Chevalier, R.A., 1976, Ap. J. 207, 872
- Chubb, T.A., et al, 1966, J. Geophys. Res. 71, 3611
- Chupp, E.L., 1976, "Gamma Ray Astronomy", D. Reidel Publishing Co.
- Chupp. E.L., 1973, Nature, 241, 333
- Chupp. E.L., et al, 1973, in R. Ramaty and R.G. Stone (eds), High Energy Phenomena on the Sun, NASA SP-342, p. 285
- Chupp, E.L., et al, 1974, in M.J. Rycroft and R.D. Reasenberg (eds) Space Research XIV, Akademie-Verlag, Berlin, p. 463
- Chupp, E.L., et al, 1974, in C.B. Cosmovici (ed) Supernovae and Supernovae Remnants. D. Reidel Publishing Co., Dordrecht, Holland, p. 311
- Clark, Lewin, and Smith, 1968, Ap. J., 151, 21
- Clark, G.W. and Li. F.K., 1977, IAU Circ No. 3092
- Clayton D.D. and Craddock, W.L. 1965, Ap. J. 142, 189
- Clayton, Colgate and Fishman, 1969, Ap. J., 155, 75
- Clayton and Silk, 1969, Ap. J. 158, L43
- Clayton D.D. and Fowler, W.A., 1969, Comments on Astrophys. and Space Phys., 1, No. 4, 147

- Clayton, D.D. and Worsley, S.E.: 1969, *Astrophys. J.* 157, 1381
- Cline, T.L., and Desai, U.D., 1976, *Ap. Space Sci.*, 42, 17
- Cline, T.L., et al, 1976, GSFC Preprint X-661-76-278
- Cocke, W.J., 1975, *Ast. J.* 202: 773-781
- Coe M.J., et al, 1975, *Nature* Vo. 256, Aug. 21., p. 630
- Coe, M.J. et al, 1977, *Nature*, 268, 508-509
- Colgate, S.A., 1974, *Ap. J.*, 187, 333
- Cowsik, R. et al, 1970, *Ap. and Sp. Sci.* 6, 390
- Daju et al, 1970, *Astrophys. Lett.*, 6, 225
- Daniel, R.R., Gokhale et al, 1971, *J. Geophys. Res.* 76, 3152
- Daniel, 1972, I.A.U. Madrid Conf. "X and Gamma-Ray Astronomy" ed. Bradt and Giacconi (I.A.U., 1973)
- Daniel, R.R., et al, 1967, *Nature* 213, 21
- Daniel, R.R., et al, 1972, *Ap. Space Sci.*, 18, 462
- Daniel, R.R., et al, 1975, *Proc. 14th Internat. Cosmic Ray Conf.*, 1, 23
- Daniel, R.R., et al, 1975, *Pramana*, 5, No. 3, 107
- Davidson, A, 1975, I.A.U. Circ No. 2824
- Davidson, K, et al, 1971, *Ap. J.* 168, 45
- Davison, P.J.N., et al, 1975, *Ap. J. Letters*, 196, L23
- Dean, A, et al, 1973, *Astr. Ap.*, 28, 131
- Delury, J.T., Luscombe, G.W., Ramsden, D., and Baker, R.E., 1976, *ESA-SP*, 115, 265
- Dennis et al, 1973, *Ap. J.*, 186, 97
- Di. Cocco G., 1976, Private Communication
- Di. Cocco G., 1977, *Nature* vol. 270, Nov. 24th
- Drake, F.D., 1971, I.A.U. Symposium No. 46 (New York: Springer-Verlag), 73
- Ducros G., et al, 1970, *Nature* 227, 152
- Dyer C.S., et al, 1972, *Ap. Space Sci.*, 19, 359
- Dyer C.S., et al, 1971, *Astrophys and Space Sci.* 14, 243
- Eardley, D.M., et al, 1978, *Comments on Astrophys.*, Vol. 7, No. 5, p 151
- Elvis, M, et al, 1978, *M.N.R.A.S.*, 183, 129
- Elvis, M, 1976, *M.N.R.A.S.*, 177, 7p-12p
- Evans, W.D., et al, 1976, *Astrophys. J. Lett.*, 207, L91
- Evans, R.D., 1955, *The Atomic Nucleus* (McGraw-Hill)

- Fazio, G.G., 1967, in L. Goldberg (ed) Ann. Rev. of
Astron. and Astrophys., Vol 5
- Fazio, G.G. et al, 1972, Ap. J. 175: L117-L122, Aug. 1
- Fichtel C.E. et al, 1975, Ap. J., 198, 163
- Fichtel C.E. et al, 1973, Ap. J. (Letters), 186, L99
- Fichtel, C.E., 1977, Gamma Ray Astrophysics, Space Sci.
Revs. 20, 191
- Fichtel, C.E., 1975, Physics Today, Sept., p. 42
- Fishman, G.J., et al, 1969, Astrophys. J. Lett, 158, L161
- Fishman G.J., et al, 1972, Ap.J ., 171, 163
- Fishman G.J., and Clayton, D.D., 1972, Ap. J. 178, 337
- Fishman G.J. et al, 1978, Submitted to Ap. J. Letters
- Floyd, Glass, Schnopper, 1969, Nature, 224, 50
- Forman, W, et al, 1974, Ap. J. (Letters) 193, L67-L70,
May 24
- Forman, W. et al, 1976, Astrophys. J. Lett. 207, L177
- Forrest et al, 1975, Proc. Intern. Conf. on X-rays in
Space, Univ. of Calgary, Canada, p. 341
- Forrest et al, 1975, Internal Report, Dept. of Physics,
Univ. of New Hampshire
- Frank J. and Rees M.J., 1976, M.N.R.A.S., 176, 633
- Fritz et al, 1971, Astrophys. J. Letters 164, L55
- Fukuda, Y, et al, 1975, Nature, 254, 398
- Gallagher, J.S. and Ney, E.P., 1976, Ap. J. (Letters),
204, L35
- Giacconi, 1962, Phys. Rev. Lett., 9, 439
- Ginzberg V.L. and Syrovatskii, 1964, "The Origin of Cosmic
Rays" Pergamon Press
- Ginzberg, V.L., 1967, in Hautes Energies En
Astrophysique, Vol. 1 edited by C. Dewitt,
E. Schatzman, and P. Veron, p. 17, Gordon and Breach
Science Publishers Inc. New York
- Ginzberg, V.L., 1969, "Elementary Processes for Cosmic
Ray Astrophysics" Gordon and Breach Publish.Co
- Golenetskii, S.V., et al, 1971, Astrophys. Lett. 9, 69
- Gold, T, 1968, Nature 218, 731
- Gold, T, 1969, Nature 221, 25
- Graml, U, and Schönfelder, B, 1977, J. Geophys. Res., 82,
1055

- Greisen, K, et al, 1975, Ap. J. 197, 471
- Greisen, K, 1971, "The Physics of Cosmic X-Ray, Gamma-Ray and Particle Sources" - Gordon and Breach
- Grindlay, J.E., et al, 1976, Ap. J. 209, 592
- Grindlay, J.E., 1978, Nature, Vol 273, 13 May
- Grindlay, J.E., 1976, Comment Astrophys., 6, 165-175
- Grindlay, J.E., and Gursky, H., 1976, Astrophys. J. Lett. 209, L61
- Grindlay J.E. et al, 1975, Ap. J. 201, 82
- Grindlay J.E., 1978, Astrophys. J. 221, 234, April 1
- Grindlay J.E. et al, 1976 Astrophys. J. 205, L127-L130
- Grindlay J.E. et al, 1978, Nature, vol. 274, Aug
- Gruber, D.E., 1974, Intern. Conf. on X-Rays in Space, Calgary, Canada UCSD-SP-74, 09
- Gruber, D.E., 1974, Ph. D. Thesis UCSD-SP-74-05
- Gruber, D.E. and Ling, J.C., 1977, Astro. J. 213: 802-814
- Gursky, H, et al, 1971, Ap. J. (Letters), 165, L43
- Guthrie P. and Tadamaru, E, 1973, Nature, 241, 77
- Hagedorn, R, 1965, Nuovo Cimento, Suppl. 3, 147-186
- Hall, R.D., et al, 1975, Papers 14th Internat. Cosmic Ray Conf. (Munich), 4, p. 84
- Hardee, P.E., 1977, Ast. J. 216: 873-880
- Hartman, et al, 1976, from "The Structure and Content of the Galaxy and Galactic Gamma Rays", June 1976, Goddard Space Flight Center, Maryland, X-662-76-154, p. 12
- Harwit, M, 1973, Astrophysical Concepts, J. Wiley and Sons, New York
- Hayakawa, S, 1969, Cosmic Ray Physics, J. Wiley and Sons, New York
- Haymes, R.C. et al 1968a Ap. J. 151, L125
 1968b Ap. J. 151, L9
 1970 Ap. J., 159, 1111
 1975, Astrophys. J. 201, 593
- Heiles, C, et al, 1970, Nature, 226, 529
- Heitler W, 1954, The Quantum Theory of Radiation, Oxford Univ. Press, London
- Helmken, et al, 1975, Centre for Astrophys. 14th Intern. Cosmic Ray Conf., Munich

- Hermsen W. et al, 1977, Proc. 12th ESLAB Symposium, 13,
ESA-SP-124
- Herzo, D, et al, 1975, Nucl. Instr. Meth. 123, 583
- Herzo, D, et al, 1976, Ap. J. Letts. 203, L115
- Heterich, W, et al, 1973, Proc. 13th Internat. Cosmic Ray
Conf. I, 8
- Hillier et al, 1970, Ap. J., 162, L177
- Hinata, S, 1977, Ast. J. 216: 101-102
- Hinata, S, 1978, Astrophys. Space Sci. 55, 427-439
- Hirasima, Y, et al, 1969, Acta Phys. Hungaria (Suppl. 2)
29, 683
- Hoffman, J.A. et al, Astrophys. J. Lett. 210, L13, 1976
- Hoffman, J.A. et al, 1977, M.N.R.A.S., 179, 57P
- Hoffman, J.A., et al, Ast. J. Lett, 1977
- Holt, S.S., 1967, J. Geophys. Res., 72, 3507
- Hopper, V.C. et al, 1973, Ap. J. (Letters), 186, L55
- Horstman, H.M., et al, 1975, Riv. Nuovo Cimento, 5, 255
- Hoyle, F, et al, 1966, Nature, 209: 751
- Ives, J.C., et al, 1976, Astrophys. J. Lett. 207, L159
- Jacobson, A.S., et al, 1975, Nucl. Instrum. Methods,
127, 115
- Johnson, H.M., et al, 1978, 222, 664-666
- Johnson, W.N. III and Haynes R.C., 1973, Astrophys. J. 184,
103
- Johnson, et al, 1976, Ap. and Sp. Sci. 42, 35
- Jones, F.C., 1961, J. Geophys. Res., 66, 2029
- Jones, F.C., 1965, Phys. Ref., 137, B1306
- Jones, F.C., 1971, GSFC-X-641-71-372, Goddard Space Flight
Centre, Greenbelt, Maryland
- Jones, T.W., 1974, Ap. J. 191: L15
- Jones, T.W., et al, 1973, Ap. J. 186: 791
- Jones, P.C., 1975, I.A.U. Circ No. 2863
- Kaluzienskii, L.J., et al, Nature Vol. 256, Aug 21, 1975,
p. 633
- Kellermann, K.I., 1974, Ap. J. Letters 194, L135
- Kellermann, K.I., et al, 1969, Ap. J. 155: L71
- Kendziorra, E, et al, 1977, Astrophys. J. Lett. 217,
L93-L96
- Kinzer, R.L., 1974, J. Geophys. Res. 79, 4567

- Kinzer R.L., et al, 1973, Ap. J., 180, 547
- Klebesadel, R.W., et al, 1976, Ap. Space Sci., 42, 3
- Klebesadel, R.W., et al, 1973, Ap. J. (Letters) 182, L85
- Kleinmann, D.E., et al, 1976, Astrophys. J. Lett., 210 L83
- Kniffen, D/A, et al, 1974, Nature, 251, 397
- Kniffen, D.A., et al, 1975, Proc. 14th ICRC, 1, Munich, 100
- Kondo et al, 1969, in C.De Jager and Z. Svestka (eds),
Solar Flares and Space Research, North Holland,
Pub. Co., p. 314
- Kowal, C.T., 1972, IAU Circular No. 2405, Central Bureau
for Astronomical Telegrams, Smithsonian Astrophysical
Observatory, Cambridge, Mass
- Kozlovsky, B, and Ramaty, R, 1974, Astron. and Astrophys.
34, 477
- Kraushaar, W.L., et al, 1972, Ap. J. 177, 341
- Kuo, F, et al, 1973, Ap. J. (Letters), 186, L51
- Kurfess, 1971, Ap. J., 168, L39
- Laros, J.G., et al, 1973, Ap. J. 179, 375
- Laros, J.G., et al, 1973, Nat. Phys. Sci., 246 109
- Leventhal, M, 1973a, Astrophys. J. (Letters) 183, L147
- Leventhal, M, 1973b, Nature (Phys. Sci.) 246, 136
- Leventhal, M, et al, 1977, Ast. J., 216; 491-502
- Lewin, W.M.G., et al, 1977, Ann. N.Y. Acad. Sci. 302, 210
- Lewin, W.H.G., and Joss P.C., 1977, Nature Vol 270,
p211-216
- Lewin, W.H.G., 1977, Proc. 8th Texas Symposium on
Relativistic Astrophys., Ann. N.Y. Acad., Sci., 1977
- Lewin, W.H.G., 1977, M.N.R.A.S., 179, 43
- Lewin, W.H.G., 1977, Nature, 267, 28
- Lewin, W.H.G., et al, 1976, I.A.U. Circ. No. 2994
- Lewin, W.H.G., et al, 1976, Astrophys. J. Lett., 207, L95
- Lewin, W.H.G. et al, 1976, CSR-P-76-14, Submitted to
Nature June 11th, 1976
- Li, F, and Clark, G.W., 1977, IAU Circ. No. 3092
- Li, F.K., and Lewin, W.H.G., 1976, IAU Circ. No. 2983
- Li, F.K., et al, 1977, M.N.R.A.S., 179, 21P
- Lightman, A.P., and Shapiro, S.L., 1977, Ap. J. 211, 244
- Liller, W, 1977, Astrophys. J. Lett., 213, L21
- Ling J.C., 1975, J. Geophys. Res., 80, 3241

- Lingenfelter, R.E., and Ramaty, R., 1978, Physics Today, March
- Long K.S., and Novick R., 1978, Gamma Ray Symposium at Goddard Space Flight Centre, NASA Technical Memorandum 79619
- Lovett R., 1973, Thesis, University of Southampton
- Lüst R., and Linkau K., 1967, in J.G. Emming (ed.), Electromagnetic Radiation in Space, Springer-Verlag, New York, p.231
- Lynden-Bell D., 1969, Nature, 223, 690
- Lynden-Bell D., and Rees M.J., 1971, M.N.R.A.S., 152, 461
- Maccagni et al., 1974, Proc, 9th Eslab. Symposium, Nov.1974
- Maccagni et al., 1975, 14th Int. Cosmic Ray Conf. Munich 9, 3135-3140
- Manchanda R.K. et al., 1978, Ap. and Sp. Sci., 53, 231
- Mandrou P. et al., 1976, Nucl. Instr. Meth., 133, 553
- Mandrou P. et al., 1977, Ast. J. 212, 704-706
- Mandrou P. et al., 1977, Proc. 12th Eslab Symposium, Frascati, Italy, 24-27 May, 1977, (ESA SP-124)
- Maraschi L., and Treves A., 1973, p.43, 13th I.C.R.C., vol.1, Aug.(Denver)
- Maraschi L. and Treves A., 1973, International Conf. on Supernovae, Lecce, May 7-11, 1973
- Margon et al., 1976, Ap. J.207
- Martin S.J., 1978, Thesis, Univ. of Southampton
- Martinis C. Di, 1972, Thesis, Univ. of Milan
- Masnou et al., 1977, Proc. 12th Eslab Symposium, 13, Frascati, Italy, (ESA-SP-124)
- Massaro E. and Salvati, 1977, Proc. 12th Eslab Symposium (ESA-SP-124)
- Matteson J.L., 1971, Ph.D. thesis, Univ. Calif., San Diego

- Matteson J.L. et al., 1974, Proc. 9th Esrlab Symposium, 1974, Frascati, Italy, ESRO SP-106, p.137
- Mazets E.P., et al., 1975, Ap. Space Sci., 33, 347
- McBreen et al., 1973, Ap.J. 184, 571-580, Sept. 1
- McClintock J.E., 1977, IAU Circ. No. 3084
- McClintock J.E., 1977, IAU Circ. No. 3088
- McClintock J.E. et al., 1977, Nature 270, 320-321
- McKechnie S.P., 1976, Thesis, Univ. of Southampton
- McKechnie, Mount, Ramsden, 1976, Ap.J. Lett vol.207, p. L151, Aug.1st
- Menuguzzi M., and Reeves H., 1973, Proc.13th ICCR Vol.1, Denver, Colorado, p.478
- Meszaros P. and Silk J., 1977, Astr. Ap., 55, 289
- Metzger A.E., 1964, Nature 204, 766
- Metzger A.E. et al., 1974, Astro. J. 194, L19 - L25
- Metzger A.E. et al., 1974, Proc. of the 5th Lunar Conference, Volume 2, page 1067
- Michel F.C., 1978, Ast. J. 220, 1101-1106
- Miller J.S., 1978, Comments Astrophys. Vol 7, No.6, p.175-182
- Morfill G., and Piper G.F., 1974, in I.B. Strong (ed.) Proc. Conf. on Transient Cosmic and X-ray Sources LA-55050c, Los Alamos, p.206
- Morrison P., 1958, Nuovo Cimento, 7, 858
- Morrison P., 1966, in R.E. Marshak (ed.) "Perspectives in Modern Physics", John Wiley and Sons, N.Y., p.343
- Morrison P., 1967, in L. Goldberg (Ed.), Ann. Rev. Astron. and Astrophys. Vol.5, Annual Reviews. Inc., Palo Alto, Calif., p.325
- Mushotzky R.F., 1976, Thesis, Univ. of Calif., San Diego

- Mushotzky R.F. et al., 1978, Preprint, Laboratory for High Energy
Astrophysics NASA/Goddard Space Flight Center, Greenbelt, Maryland,
20771
- Oda, M., 1977, SP, Sci. Rev., 20, 759
- Orwig L.E. et al., 1972, Bul.A.P.S., 17, 524
- Orwig L.E., 1971, Doctoral Thesis, Univ. of New Hampshire, Durham, N.H.
- Orwig, L.E., 1971, Nature, 231, 171
- Paciesas W.S. et al., 1977, M.N.R.A.S., 178, Short Communication,
23p-25p
- Page D.N., and Hawking S.W., 1976, Astroph. J., 206, 1-7, May 15
- Pal Y., 1973, IAU Symposium No.55, X and Gamma Ray Astronomy, ed. H. Bradt
and R. Giacomi (Dordrecht, Reidel), p.279
- Parlier et al., 1975, 14th Internat. Cosmic Ray Conf. (Munich), 1, 14
- Parlier et al., 1973, Nat. Phys.Sci., 242, 117
- Parsignault D.R., 1975, Harvard College Observatory, Preprint,
CFA/HEA - 75 - 09 7
- Pehl R.H., 1977, Physics Today, Nov.1977, p.50
- Peterson L.E. et al., 1968, Canad. J. Phys., 46, 5437
- Peterson L.E. et al., 1972, Space Sci. Rev., 13, 320
- Ramaty R. et al., 1975, Space Sci. Rev., 18, 341
- Ramaty R. et al., 1975, in S.R. Kane (ed.), IAU Symposium No.68,
D. Reidel Publish.Co., Dordrecht, Holland, p.363
- Ramaty R. et al., 1977, Astroph. J., 214, 617-631
- Ramsden D. and Baker R.E., 1978, Proc. of Cospar Confer.
- Rangan and Rao, 1972, Astrophys. and Space Sci., 15, 161
- Ricker G.R. et al. 1975, Ap. J. (Letters), 197, L83

- Ricketts M.J. et al., 1975, Nature, 256, p.631
- Roberts D.H. and Sturrock P.A., 1973, Ap. J., 181, 161
- Rocchia R. et al., 1976, Ap. J. 209, 350
- Rosenberg F.D. et al., 1975, Nature, Vol.256, 1975, p.628
- Rothschild R.E. et al., 1974, Ap.J. Letts 189, L13
- Ruderman M., 1969, Nature, 223, 597
- Ryan J.M. et al., 1976, Preprint 1GPP-UCR-76-2, Univ. of Calif. Riverside
- Salvati M. and Massaro E., 1978, Astron. Astrophys., 67, 55-63
- Sargent W.L.W., et al., 1974, in C.B. Cosmovici (ed.), Supernovae and
Supernovae Remnants, D. Reidel Public., 33
- Sartori L. and Morrison P., 1967, Astrophys.J., 150, 385
- Scargle J.D. and Pacini F., 1971, Nat..Phys. Sci. 232, 144
- Schönfelder V., 1973, Nucl.Inst. and Meth., 107, 385
- Schönfelder V., et al., 1975, Nature Vol.257, Oct 2nd, p.375
- Schönfelder V. et al., 1975, ESRO SP-106, 94-97
- Schönfelder V. et al., 1977, Ast. J. 217, 306-319
- Schönfelder V. et al., 1973, Papers 13th Int. Cosmic Ray Conf. (Denver)
4, 2709
- Schönfelder V. et al., 1975, J. Geophys. Res., 80, 3681
- Schönfelder V. et al., 1978, Nature Vol.274, 27th July, p.344
- Schönfelder V. et al., 1975, Papers 14th ICRC(Munich), 1, 8
- Schönhardt R., 1971, IAU Sumposium on the Crab Nebula, eds. R.S. Davies
and F.J. Smith, pp.110-113
- Sersic J.L. et al., 1972, Astrophys. Space Sci., 19, 469

- Share G.H., 1973, p.103, Internat. Sympos. on Gamma Ray Astrophys.,
Goddard Space Flight Centre, 1973
- Share G.H., 1972, IAU Madrid Conf. "X and Gamma Ray Astronomy", ed.
Bradt and Giacconi (IAU, 1973)
- Share G.H. et al., 1974, Ap. J. 187, 511
- Shklovsky I.S., 1960, Cosmic Radio Waves, Harvard Univ. Press, Cambridge,
Mass.
- Shklovsky I.S., 1966, Soviet Astron., A.J., 10, 6
- Shklovsky I.S., 1970, Ap.J. (Letts), 159, L77
- Silk J., 1970, Space Sci. Rev., 11, 671
- Silk J., 1973, Ann. Rev. Astr. Ap., 11, 269
- Sofia and Horn, 1974, Ast. J. 194, 593-595, Dec. 15th
- Staib J.A. et al., 1974, J. Geophys. Res., 79, 929
- Stecker F.W., 1969, Ap.J., 157, 507
- Stecker F.W., 1969, Nature 211, 1229
- Stecker F.W. and Puget J.L., 1974, Proc. Estab. Symposium on the Context
and Status of Gamma Ray Astronomy, Frascati, Italy.
- Stecker F.W. et al., 1971, Phys. Rev. Lett, 27, 1469
- Stecker F.W., 1971, Gamma Ray Astrophysics, form "Origin of Cosmic Rays"
267-334, 1975, D. Reidel
- Stein W.A., and Weedman D.W., 1976, Ap.J., 205, 44
- Stein W.A. et al., 1976, Ann. Rev. Astron. Astrophys., 14, 173
- Strong I.B., et al., 1974, Astrophys. J. (Letters), 188,L1
- Strong I.B., 1974, 9th Eslab Symposium ESRO - SP - 106
- Strong I.B., (ed.), 1974, Proc. Conf. on Transient Cosmic Gamma and X ray
Sources, LA - 5505 - C, Los Alamos Scientific Laboratory

- Sturrock P.A., 1971, Ap.J., 164, 529
- Suri et al., 1975, Solar Phys., 43, 415
- Swank J.H. et al., 1976, IAU Circ. No. 2963
- Tananbaum H. et al., 1978, Astrophys. J., 223, 74-81
- Tananbaum H. et al., 1977 - preprint
- Thompson D.H., 1974, J. Geophys. Res. 79, 1309
- Thompson D.J. et al., 1977, Astro. J., 213, 252-262
- Thorne K.S., Price R.H., 1975, Ap.J. Letts, 195, L101
- Trombka et al., 1977, Ap. J. 212, 925
- Trombka et al., 1973, Ap. J. 181, 737
- Trumper J. et al., 1978, Astrophys. J. Lett. 219, L105-L110
- Truran, 1975, Private Communication to Leventhal et al., 1977
- Ulmer M.P., 1977, Ap. J. (Letters), 218, L1
- Ulmer M.P., Murray S.S., 1976, Ap.J. 207
- Ulmer M.P. et al., 1974, Astrophys. J., 193, 535
- Ulmer M.P. et al., 1977, Astrophys. J. Lett., 214, L11
- Ulmer M.P. et al., 1974, Ap. J., 189, 339
- Valentine et al., 1970, Proc. 11th ICRC (Budapest, 1969) in Acta Phys.
Acad. Sci. Hungarical, 29, Suppl. 1, 101
- Vette J.I. et al., 1970, Ap. J., 160, L161
- Vedrenne, 1971, Astron. and Astrophys., 15, 50
- Voges W. et al., 1978, IAU, Circ. No. 3184
- Walraven G.D. et al., 1975, Ap. J. 202, 502-510
- Webber and Reinert, 1970, Ap. J., 162, 883

- Weedman D.W., 1978, M.N.R.A.S., 184, 11p - 13p
- Weedman D.W., 1977, Ann. Rev. Astron. Astrophys., 69-95
- Weekes T.C., and Porter N.A., 1977, Proc. 12th Eslab Symposium, Frascati, ESA SP-124
- White R.S. and Schönfelder V., 1975, Ap. Space Sci., 38,19
- White R.S. et al., 1978, Nature, 271, 635
- White R.S. et al., 1973, p.7, Denver, 13th ICRC vol.1
- White R.S. et al., 1976, preprint, IGPP-UCR-76-3, Univ. of Calif., Riverside
- White R.S. et al., 1977, Ast. J., 218, 920-927
- Wilson R.B. et al., 1976, Preliminary Report, IGPP-UCR-76-1
- Winkler P.F. and White A.E., 1975, Ap. J. Letters
- Young P.J., 1977, Ap. J. , 215, 36
- Zimmerman, 1974, Astron. and Astrophys., 34, 305-307

Acknowledgements

I would like to thank Dr. D. Ramsden for supervision and guidance.

In addition, many thanks to: Dr. S.J. Burnell, Dr. K.J. Orford, Dr. R. Lovett, Mr. R.E. Baker, Mr. F.H. Coleman, Dr. A. Dean, Mr. R. Martin and Mr. W.R. Spicer, for contributions to design and building of the LEC detectors; the staff of the University of Southampton computing facilities; Dr. J. Rankin for the pulsar phase data; G. Di Cocco, Dr. R.K. Manchanda, Dr. R.C. Butler, J. Carter, N. Dipper and last but not least, S.J. Martin for invaluable suggestions and information.

I am also indebted to Professor G.W. Hutchinson and Professor K. Barnes for the use of the departmental facilities, and to the Science Research Council for the provision of a maintenance grant.